The Scientific World Journal

Toxicology and Disease/Cancer Therapy in Reactive Oxygen Species-Mediated Drugs and Treatments

Guest Editors: Hsueh-Wei Chang, Shao-Yu Chen, Li-Yeh Chuang, and Sanjay Guleria

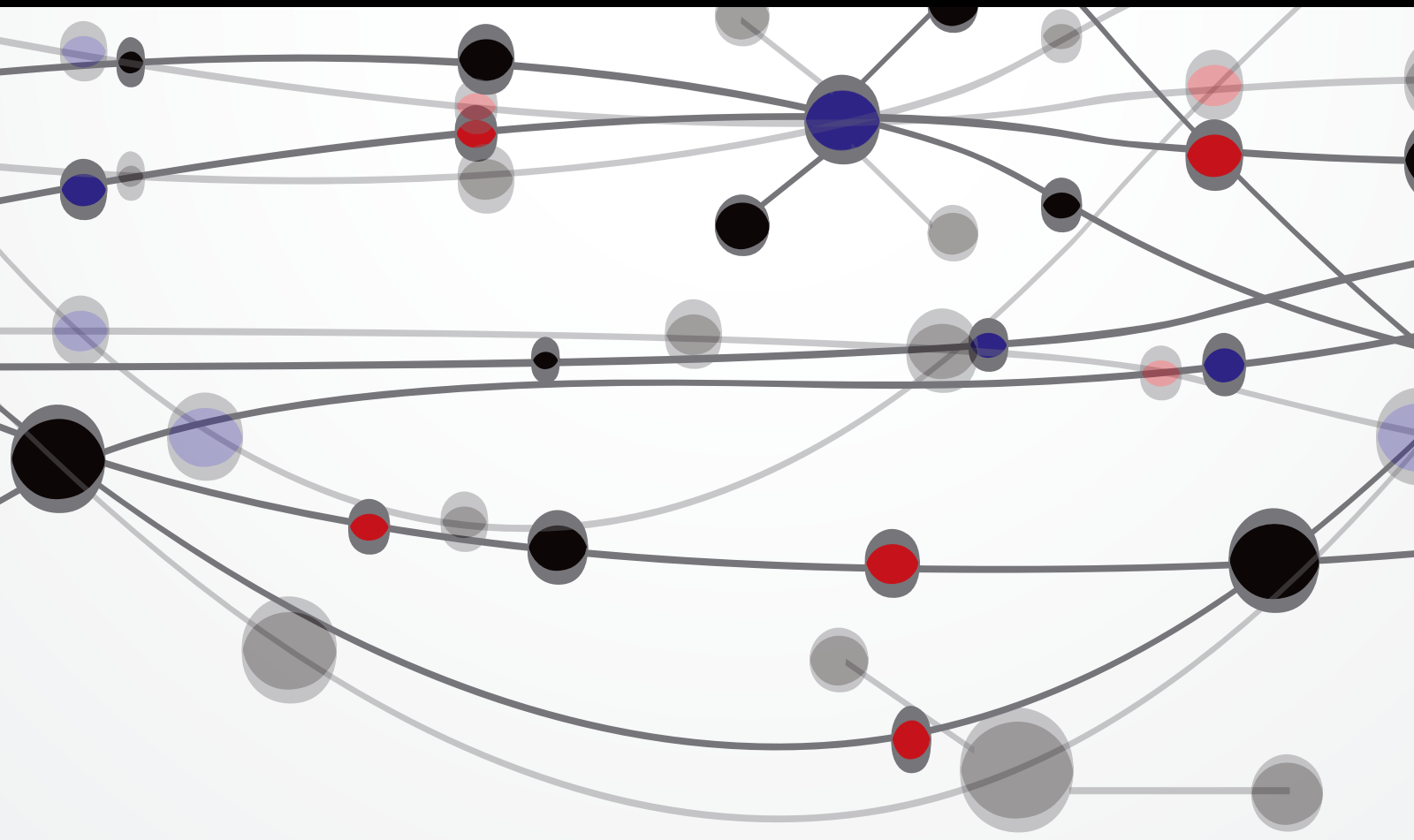

Toxicology and Disease/Cancer Therapy in Reactive Oxygen Species-Mediated Drugs and Treatments

The Scientific World Journal

Toxicology and Disease/Cancer Therapy in Reactive Oxygen Species-Mediated Drugs and Treatments

Guest Editors: Hsueh-Wei Chang, Shao-Yu Chen, Li-Yeh Chuang, and Sanjay Guleria

Contents

Hindawi Publishing Corporation
The Scientific World Journal
Volume 2015, Article ID 860563, 1 page
http://dx.doi.org/10.1155/2015/860563

Editorial

Toxicology and Disease/Cancer Therapy in Reactive Oxygen Species-Mediated Drugs and Treatments

Hsueh-Wei Chang,[1] Shao-Yu Chen,[2] Li-Yeh Chuang,[3] and Sanjay Guleria[4]

[1]*Department of Biomedical Science and Environmental Biology, Research Center of Excellence for Environmental Medicine, Cancer Center, Kaohsiung Medical University Hospital, Kaohsiung Medical University, Kaohsiung 80708, Taiwan*
[2]*Department of Pharmacology and Toxicology, University of Louisville, Health Sciences Center, Louisville, KY 40292, USA*
[3]*Department of Chemical Engineering and Institute of Biotechnology and Chemical Engineering, I-Shou University, Kaohsiung 84001, Taiwan*
[4]*Division of Biochemistry and Plant Physiology, SK University of Agricultural Sciences and Technology, Chatha, Jammu 180009, India*

Correspondence should be addressed to Hsueh-Wei Chang; changhw@kmu.edu.tw

Received 17 November 2014; Accepted 17 November 2014

Reactive oxygen species (ROS) induce or protect cellular oxidative damage. ROS are also known to play an important role in apoptosis, autophagy, endoplasmic reticulum stress, mitochondrial dysfunction, cell migration, and invasion. This special issue presents the recent advances in basic research and association studies of some natural products and chemical drugs for cancer and disease treatments.

The papers by M.-G. Lee et al. and H.-W. Huang et al. reported the antioxidant/tyrosinase suppression/wound repair properties and antiproliferative effect on oral cancer of *Cinnamomum osmophloeum* Kanehiraand *Cryptocarya concinna* Hance root extracts, respectively. Similarly, S.-C. Chien et al. reported the protective effect of Chinese herbal medicine "Jia-wei-xiao-yao-san" against chemical-induced hepatic fibrosis in rats.

Y. Fong et al. reported the antiproliferative and antiapoptotic effects on lung cancer cell lines of sirtinol, a sirtuin inhibitor. W.-C. Lee et al. reported that indoxyl sulfate (IS) induced oxidative stress and endothelial dysfunction in chronic kidney disease patients can be due to mitochondrial dysfunction and impaired biogenesis which can be reverted by treatment with antioxidants.

The papers by B. Huang et al. and P.-H. Chen et al. provided the findings on the upstream role of H_2S and arsenic in modulating protein S-nitrosylation in endothelial cells and keratinocytes, respectively. W.-T. Chang et al. reported that epirubicin/progesterone combination is effective in increasing apoptosis and inversely decreasing autophagy on HA22T/VGH cells and can potentially be used to treat hepatocellular carcinoma.

The papers by S.-J. Wu et al. and P.-H. Chen et al. provided the cancer association studies of betel quid-consuming patients in terms of oxidative stress response genes such as polymorphisms for the human retinoic acid (RA) 4-hydroxylase (CYP26), the monoamine oxidase, and the cytochrome P450, family 26, subfamily B, polypeptide 1 (CYP26B1) genes.

Finally, the paper by Y.-R. Lin et al. introduced the proteomics technique for evaluating cytotoxicity of unmodified nano-Fe_3O_4 based on tandem mass spectrometry (LC-MS/MS) and T.-C. Cheng et al. provided the *in silico* virtual screening to discover specific inhibitors for intestinal *E. coli* β-glucuronidase.

Hsueh-Wei Chang
Shao-Yu Chen
Li-Yeh Chuang
Sanjay Guleria

Hindawi Publishing Corporation
The Scientific World Journal
Volume 2015, Article ID 740815, 8 pages
http://dx.doi.org/10.1155/2015/740815

Research Article

Discovery of Specific Inhibitors for Intestinal *E. coli* β-Glucuronidase through *In Silico* Virtual Screening

Ta-Chun Cheng,[1] Kuo-Hsiang Chuang,[1] Steve R. Roffler,[2] Kai-Wen Cheng,[3] Yu-Lin Leu,[4] Chih-Hung Chuang,[5] Chien-Chaio Huang,[5] Chien-Han Kao,[6] Yuan-Chin Hsieh,[6] Long-Sen Chang,[3] Tian-Lu Cheng,[5,6,7] and Chien-Shu Chen[8]

[1]*Graduate Institute of Pharmacognosy, Taipei Medical University, 252 Wu Hsing Street, Taipei 11031, Taiwan*
[2]*Institute of Biomedical Sciences, Academia Sinica, 128 Section 2, Academia Road, Nankang, Taipei 11529, Taiwan*
[3]*Institute of Biomedical Science, National Sun Yat-Sen University, 70 Lienhai Road, Kaohsiung 80424, Taiwan*
[4]*Department of Pharmacy, Chia Nan University of Pharmacy and Science, 60 Section 1, Erh-Ren Road, Tainan 71710, Taiwan*
[5]*Department of Biomedical and Environmental Biology, Kaohsiung Medical University, 100 Shih-Chuan 1st Road, Kaohsiung 80708, Taiwan*
[6]*Graduate Institute of Medicine, Kaohsiung Medical University, 100 Shih-Chuan 1st Road, Kaohsiung 80708, Taiwan*
[7]*Center for Biomarkers and Biotech Drugs, Kaohsiung Medical University, 100 Shih-Chuan 1st Road, Kaohsiung 80708, Taiwan*
[8]*School of Pharmacy, China Medical University, 91 Hsueh-Shih Road, Taichung 40402, Taiwan*

Correspondence should be addressed to Tian-Lu Cheng; tlcheng@kmu.edu.tw and Chien-Shu Chen; cschen7@mail.cmu.edu.tw

Received 15 August 2014; Accepted 27 August 2014

Academic Editor: Li-Yeh Chuang

Glucuronidation is a major metabolism process of detoxification for carcinogens, 4-(methylnitrosamino)-1-(3-pyridy)-1-butanone (NNK) and 1,2-dimethylhydrazine (DMH), of reactive oxygen species (ROS). However, intestinal *E. coli* β-glucuronidase (eβG) has been considered pivotal to colorectal carcinogenesis. Specific inhibition of eβG may prevent reactivating the glucuronide-carcinogen and protect the intestine from ROS-mediated carcinogenesis. In order to develop specific eβG inhibitors, we found that 59 candidate compounds obtained from the initial virtual screening had high inhibition specificity against eβG but not human βG. In particular, we found that compounds **7145** and **4041** with naphthalenylidene-benzenesulfonamide (NYBS) are highly effective and selective to inhibit eβG activity. Compound **4041** (IC_{50} = 2.8 μM) shows a higher inhibiting ability than compound **7145** (IC_{50} = 31.6 μM) against eβG. Furthermore, the molecular docking analysis indicates that compound **4041** has two hydrophobic contacts to residues L361 and I363 in the bacterial loop, but **7145** has one contact to L361. Only compound **4041** can bind to key residue (E413) at active site of eβG via hydrogen-bonding interactions. These novel NYBS-based eβG specific inhibitors may provide as novel candidate compounds, which specifically inhibit eβG to reduce eβG-based carcinogenesis and intestinal injury.

1. Introduction

Glucuronidation represents a major route of drug metabolism in the liver [1–3]. Many carcinogens and xenobiotics are detoxified by conjugation with a glucuronide acid to increase their water solubility, thus facilitating their excretion [4, 5]. For example, the 4-(methylnitrosamino)-1-(3-pyridy1)-1-butanone (NNK) and 1,2-dimethylhydrazine (DMH), which lead to reactive oxygen species- (ROS-) mediated DNA damage, mutagenesis, and carcinogenesis, can be metabolized and detoxified to glucuronide form by UDP-glucuronosyltransferases (UGTs) [6–8]. However, when the glucuronide conjugates enter the intestine through enterohepatic circulation, they can be hydrolyzed and their toxicity can be reversed by *E. coli* β-glucuronidase (eβG) [9–11], which would induce intestinal injury [5, 12–14] and colon carcinogenesis. In addition, chemotherapy-induced diarrhea (CID) and intestinal damage have been clinically demonstrated in several chemotherapeutic drugs such as CPT-11 [15–17], 5-FU [18], and oxaliplatin [19]. There is a specific

βG inhibitor, glucaro-1,5-lactone, which has been shown to alleviate CPT-11-induced mucosal damage in the small intestine *in vivo* [5]. However, glucaro-1, 5-lactone of the current treatments against CID is limited and not effective, since it preferentially inhibits human βG (hβG) activity [20], which may induce mucopolysaccharidoses (MPS) [21, 22]. The current treatments against CID are limited and not effective. Therefore, it is crucial to develop an eβG specific inhibitor, which cannot affect hβG activity, as an effective treatment against carcinogenesis and CID.

The crystal structures of hβG and eβG have been reported [16, 17]. In addition, eβG has a unique "bacteria loop" (LGIGFEAGNKPKELYSE) [16] which is absent in hβG. Some known drugs such as Amoxapine [23, 24] and Loxapine [23] and eβG inhibitors [16] have been also demonstrated to interact with the residues of bacterial loop and active sites of eβG [16, 24]. Those reports indicate that the area around the unique loop and the active site is an important target for eβG inhibitor selection.

For the development of specific eβG inhibitors, we demonstrated a crystal structure of recombinant eβG (provided by Steve R. Roffler, Institute of Biomedical Sciences, Academia Sinica, Taipei, Taiwan) in complex with D-glucaro-1, 5-lactone which revealed that the inhibitor was bound at the residues (E413, E504) of active site. And, we further compared the active center between eβG and hβG though overleap. We obtained candidate compounds that selectively inhibit eβG via computational screening by DOCK 4.0 program [25, 26] and X-ray crystal structure of eβG. A chemical database (SPECS) containing ~300,000 commercially available compounds was computationally screened against a grid box enclosing the unique bacterial loop at eβG active site. To prove whether the candidate compounds can effectively inhibit eβG without affecting hβG activity, compounds were examined based on their specific inhibition for eβG versus hβG by *in vitro* βG activity-based assays. The binding motifs of eβG specific inhibitors were determined by molecular docking studies. The novel eβG specific inhibitor may provide a highly effective and selective agent to prevent eβG-based carcinogenesis and CID.

2. Materials and Methods

2.1. Expression and Purification of βG Protein. Plasmid pRESTB containing βG gene and a histidine tag at the N-terminus was constructed as described [27]. Recombinant βG (human and *E. coli*) was produced by isopropyl β-D-thiogalactopyranoside (IPTG) induction of BL21 (DE3) bacteria. βG was purified from bacterial supernatants by affinity chromatography on nickels Sepharose 6 Fast Flow (GE Healthcare). The column was washed by phosphate-buffered saline (PBS), with 50 mM imidazole, and βG was eluted by PBS with 250 mM imidazole. The purified βG was desalted on a Sephadex G-25 column equilibrated with PBS and stored at −80°C.

2.2. Virtual Screening of eβG Specific Inhibitors. The virtual screening was performed using the DOCK 4.0 program and the X-ray crystal structure of eβG (provide by Steve R. Roffler). The B-chain structure of protein, water molecules, and the cocrystallized inhibitor D-glucaro-1,5-lactone were removed. The remaining A-chain protein structure was used to prepare the target site for docking simulations. The active-site region of eβG was specified as the target site for ligand docking in virtual screening. Briefly, a molecular surface around the target site was generated with the MS program using a 1.4 Å probe radius and this surface was used to generate with the SPHGEN program 43 overlapping spheres to fill the target site. A grid box enclosing the target site was created for grid calculations with dimensions 19.3 × 22.4 × 15.6 Å. The force filled scoring grids were calculated with the GRID program using a distance-dependent dielectric constant of 4r, an energy cutoff distance of 10 Å, and a grid spacing of 0.3 Å. The database for virtual screening was the SPECS compound collection, which included ~300,000 commercially available compounds (downloaded from the ZINC database web site). The DOCK 4.0 program performs docking simulations using a distance-matching algorithm. The matching parameters used to run virtual screening were set as follows: distance tolerance = 0.5, distance minimum = 2.5, nodes maximum = 10, and nodes minimum = 4. The SPECS database was computationally screened against the active site of eβG using the force field scoring function based on interaction energy. Virtual screening was performed on a Silicon Graphics Octane workstation with dual 270 MHz MIPS R12000 processors.

For compound selection, the docking models of the 4724 top-ranked compounds (energy score values ≤ −42.00 kcal/mol) were visually inspected using the software PyMOL. Together with consideration of chemical diversity, the selection of compounds was assisted by analysis of the docking models with respect to shape fitting and hydrogen-bonding and hydrophobic interactions. Finally, we selected 59 compounds for enzyme inhibition assays against *E. coli* and human βGs. The compounds for testing were purchased from the SPECS Company. The SPECS ID number and docking energy score for compounds are listed in the supporting information.

2.3. In Vitro βG-Activity Assay of eβG Specific Inhibitors. The candidate compounds were purchased from SPECS (The Netherlands). Each candidate was provided as a solid power and dissolved in 100% DMSO (Sigma-Aldrich) to 10 mM as stock. Candidates were screened for their inhibition specificity of eβG versus hβG, which were conducted at pH 7.3 or pH 5.4, in triplicate, respectively. 40 μL purified βG was treated with 10 μL compound solution at 37°C for 30 min and sequentially incubated with 50 μL of pNPG (Sigma-Aldrich) at 37°C for 30 min. Reactions were quenched with 5 μL of 2 N sodium hydroxide (Sigma-Aldrich). Each reaction consisted of 3.75 ng purified βG, 50 μM compound, and 5 mM pNPG in PBS containing 10% DMSO and 0.05% BSA (Sigma-Aldrich). βG-activities were measured by color development of pNP detected on a microplate reader at OD 405 nm. Results are displayed as percent of βG activity compared with

the untreated control. For IC_{50} determination, compounds at various concentrations (100 μM to 0.001 μM) were added.

2.4. Molecular Docking Studies of eβG Specific Inhibitors. The crystal structure of eβG for the virtual screening was also utilized in the docking studies of compounds **7145** and **4041**. Hydrogen atoms were added to the A-chain protein structure, and the resulting structure was used in the docking simulations. The 3D structures of compounds were built and optimized by energy minimization using the MM2 force field and a minimum RMS gradient of 0.05 in the software Chem3D 6.0 (CambridgeSoft Corp., Cambridge, MA). Docking simulations were performed using the GOLD 5.0 program [28] on an HP xw6600 workstation with Intel Xeon E5450/3.0 GHz Quadcores as the processors. The GOLD program utilizes a genetic algorithm (GA) to perform flexible ligand docking simulations. In the present study, for each of the 30 independent GA runs, a maximum number of 100000 GA operations was performed on a single population of 100 individuals. Operator weights for crossover, mutation, and migration were set to 95, 95, and 10, respectively. The GoldScore fitness function was applied for scoring the docking poses of compounds. The docking region was defined to encompass the active site of eβG. The best docking solution (with the highest GOLD fitness score) for a compound was chosen to represent the most favorable predicted binding mode to eβG.

3. Results

3.1. Comparison of the Active Site Structures of eβG and hβG. To identify the active site of eβG, recombinant full-length eβG was purified and shown to hydrolyze pNPG to PNP for detecting βG activity. The enzyme was crystallized in complex with an established inhibitor, D-glucaro-1, 5-lactone. Crystal structure of eβG (provided by Steve R. Roffler) in complex with D-glucaro-1, 5-lactone revealed that the inhibitor was bound at residues (E413 and E504) of the active site (Figure 1(a)). To compare the structures of the active centers between eβG and hβG (PDB ID 1BHG), βGs were analyzed by computer simulation technology. After superimposition, the crystallized structure of eβG is 45% similar to hβG. Moreover, there is a "bacterial loop" within eβG which is absent in hβG (Figure 1(b)). Similar results have been also shown in other reports [16]. This eβG unique loop of the active center is an ideal target site for screening compounds that can selectively inhibit eβG activity.

3.2. In Silico Virtual Screening of eβG Inhibitor Candidates. To identify potential eβG inhibitors that can selectively block eβG activity, but not hβG, the virtual screening proceeded based on the different structures of the active center between eβG and hβG. The SPECS database (~300,000 commercially available compounds) was computationally screened against the "grid box" which contains the bacterial loop of eβG and active site using the DOCK program (version 4.0). Fifty-nine candidate compounds were acquired from the initial virtual screening which was designed to target the bacterial loop of eβG and its active site. The docking energy scores of 59 candidate compounds measured by the DOCK program are −43 to −55 kcal/mol (Table S1 in the Supplementary Material available online at http://dx.doi.org/10.1155/2014/740815).

3.3. Screening of eβG Inhibitor Candidates by In Vitro βG Activity Assay. To prove whether these 59 candidate compounds can effectively inhibit eβG without affecting hβG activity, 50 μM compounds were examined for their specific inhibition for eβG versus hβG by *in vitro* βG-based activity assays, in which the conversion of pNPG to PNP was detected by measuring the increases in PNP absorbance at OD 405 nm. The result showed that all the 59 candidate compounds displayed selective inhibition against eβG activity. The inhibiting ability against eβG activity, especially, was >95% in 7 candidates of eβG specific inhibitors (Table S1). Based on these results, we concluded that the pocket site in the unique loop and active site of eβG are an ideal site to screen eβG specific inhibitors through virtual screening. We found that compound **7145** (4-tert-butyl-N-(4-oxo-1(4H)-naphthalenylidene-benzenesulfonamide) can inhibit >95% eβG activity and does not hamper hβG activity at 50 μM condition (Table S1). The result indicated that the derivatives of naphthalenylidene-benzenesulfonamide (NYBS) might effectively and specifically inhibit the eβG activity. Based on the NYBS structure, we performed the substructure search and then found compound **4041** (4-methyl-N-(4-oxo-3-(1H-1,2,4-triazol-5ylsulfanyl)-1(4H)-naphthalenylidene)benzenesulfonamide). In particular, compound **4041** has been shown to be a more potent eβG antagonist than compound **7145**. Figure 2 and Table 1 show that while compound **4041** (IC_{50} = 2.8 μM) can selectively inhibit >80% eβG activity, at 10 μM, the inhibition of compound **7145** (IC_{50} = 31.6 μM) is 55% inhibition. Compared to D-saccharic acid 1,4-lactone (saccharolactone), which showed higher inhibition on hβG, our candidate compounds displayed specificity against eβG activity (Figure 2). Based on these results, we concluded that the derivatives of NYBS may provide a novel specific inhibitor to reduce eβG-based intestinal injury and CID.

3.4. Molecular Docking Studies of eβG Specific Inhibitors. To predict the binding modes of compounds **7145** and **4041** in the active site of eβG, we performed molecular docking studies using the GOLD 5.0 program. As depicted in Figure 3, the docking model revealed that compound **7145** forms four hydrogen bonds to eβG. Three of the hydrogen bonds, to residues Y468, Y472, and R562, arise from the SO_2 group of compound **7145**. The carbonyl group on the bicyclic 4-oxo-1(4H)-naphthalenylidene ring can form one hydrogen bond with H296. Compound **7145** makeshydrophobic interactions with the surrounding residues, including W549, F554, F164, V355, V446, M447, F448, Y468, and Y472. The residue L361 in the bacterial loop makes hydrophobic contact with compound **7145**. Compound **7145** showed a GOLD fitness score of 62.09.

The docked orientation of compound **4041** is considerably different from that of compound **7145**

Table 1: The structure, IC_{50}, and GOLD fitness scores of compound **7145** and compound **4041** docked into the active site of eβG.

Compound	Structure	GOLD fitness score[a]	IC_{50} (μM)
7145	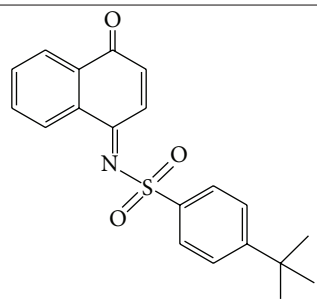	62.09	31.6
4041	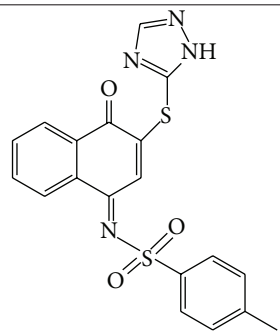	64.91	2.8

[a]Docking simulations were performed using the GOLD 5.0 program.

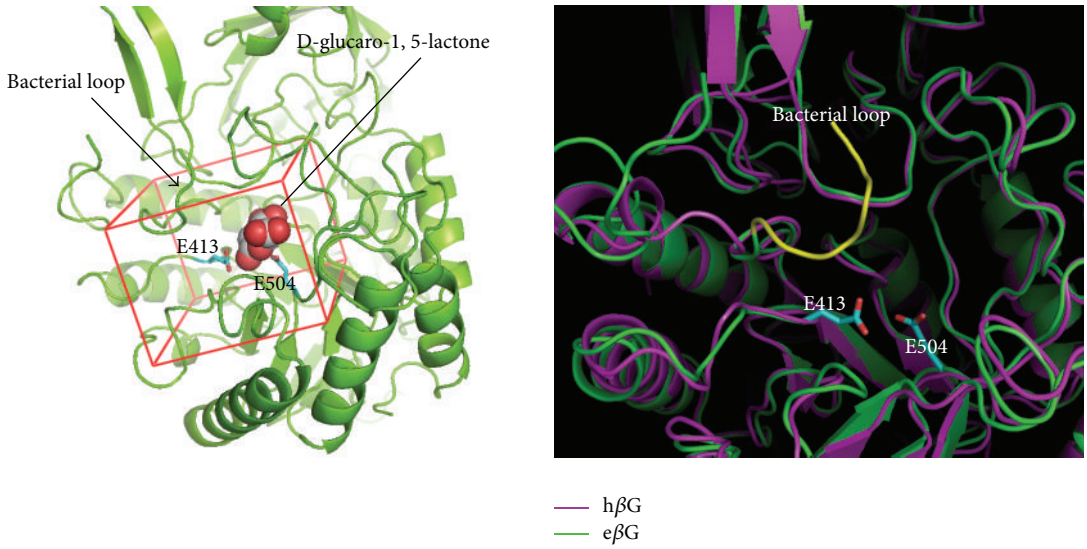

Figure 1: The crystal structure of eβG and hβG. (a) The crystal structure of eβG bound with the inhibitor D-glucaro-1,5-lactone in the active site was used in the virtual screening. A docking box (red line) was defined to enclose the active site for virtual compound screening. (b) The eβG (green) and hβG (purple) were modeled by superimposing. The eβG contains a "bacterial loop" (yellow) not found in the hβG. The E413 and E504 are two catalytic residues in the active site of eβG.

(Figure 3). For compound **4041**, the bicyclic 4-oxo-1(4H)-naphthalenylidene ring points towards M447 and makes a π-π stacking interaction with Y472. In contrast, the bicyclic ring of compound **7145** is oriented in the opposite direction to M447 and located very close to the experimental binding position of the inhibitor D-glucaro-1,5-lactone. Compound **4041** is hydrogen bonded to residues Y472 and R562 through the SO_2 group and to E413 through the 1,2,4-triazole moiety. Compound **4041** makes hydrophobic interactions with the surrounding residues, including V446, M447, Y472, and L561. The residues L361 and I363 in the bacterial loop make hydrophobic contact with compound **4041** (Figure 4). Compound **4041** has a GOLD fitness score of 64.91 higher than that of compound **7145**. Figure 5 shows

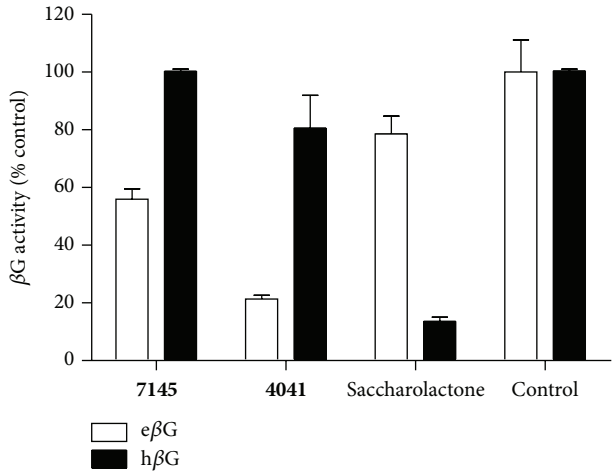

Figure 2: Specific inhibition of compounds **7145** and **4041** against eβG. Compound **7145** and compound **4041** acquired from ligand docking in virtual screening were evaluated based on their selective inhibition for recombinant eβG versus hβG. 10 μM of compound **7145**, compound **4041**, saccharolactone, and 10% DMSO (control) was incubated with purified eβG (□) and hβG (■), respectively. βG activity was determined by hydrolysis of the pNPG substrate. Error bars represent SD; $N = 3$.

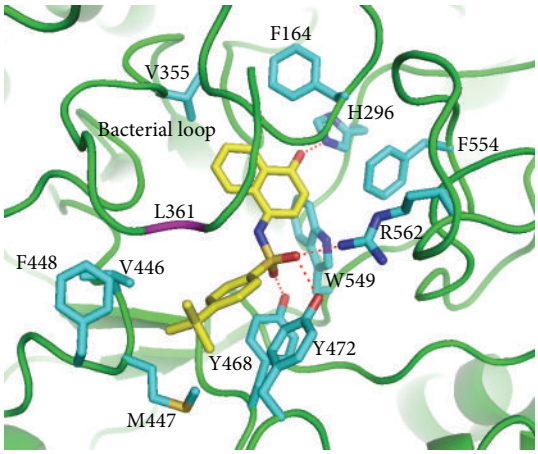

Figure 3: Binding model of compound **7145**. Predicted binding mode of compound **7145** in the active site of eβG from the docking study. Compound **7145** (yellow) and some amino acid residues (cyan) interacting with the inhibitor are shown as stick structures. The red dashed lines indicate hydrogen-bonding interactions. The residue L361 (purple) in the bacterial loop makes hydrophobic contact with compound **7145**.

an overlay of the docking pose of compound **4041** with the bound orientation of an eβG-specific inhibitor [16] observed in the cocrystal structure of eβG. In comparison to the cocrystallized inhibitor, compound **4041** has similar binding interactions with eβG, including hydrogen bonding to the catalytic residue E413 and close contact with the bacterial loop. Based on these results, we suggest that binding to the active site and the bacterial loop of eβG may provide selective abilities of inhibitors against eβG.

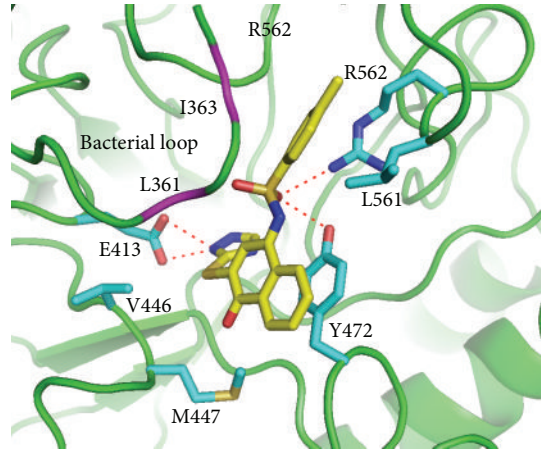

Figure 4: Binding model of compound **4041**. Predicted binding mode of compound **4041** in the active site of eβG from the docking study. Compound **4041** (yellow) and some amino acid residues (cyan) interacting with the inhibitor are shown as stick structures. The red dashed lines indicate hydrogen-bonding interactions. The residues L361 and I363 (purple) in the bacterial loop make hydrophobic contact with compound **4041**.

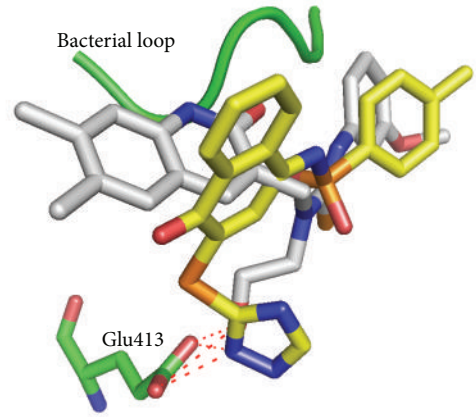

Figure 5: Binding model of compound **4041** in the crystal structure. Overlay of the docking pose of compound **4041** (yellow) with the bound orientation of an eβG-specific inhibitor (gray) observed in the cocrystal structure of eβG.

4. Discussion

In this study, we have obtained potent and selective eβG inhibitors from *in silico* virtually screening and further confirmed their inhibition specificity by *in vitro* βG activity-based assay. All the 59 candidate compounds from the initial screening showed high effective and selective inhibition against eβG. We identified the two most promising compounds, compound **7145** and its derivate compound **4041**, showing IC_{50} values of 31.6 μM and 2.8 μM, respectively. Importantly, compound **4041** with naphthalenylidene-benzenesulfonamide displayed inhibition selectivity against eβG by binding to the active site at E413 and the unique loop of eβG at L361 and I363.

High-throughput screening (HTS) allows researchers to screen millions of compounds for lead identification in drug discovery. However, this method is limited by the size of compound library. Generally, a compound library is quite costly, and the screening process is time-consuming; thus, the limitations have become more apparent. Hence, virtual screening has become an important tool to access novel drugs for lead indentation [29]. The hit rate of virtual screening can reach up to 2–24% which is much higher than HTS with 0.01–0.001% [30]. In our study, we obtained 59 potential eβG inhibitors via virtual screening of a library which consisted of ~300,000 compounds. All candidate compounds showed specific inhibition against eβG, but not hβG, and met the criteria as virtual screening. The structure-based virtual screening can select compounds with no range limitation and narrow down the candidates for further evaluation, which saves both money and time.

hβG is a lysosomal enzyme of normal tissues, and quite low levels of hβG are found in serum [31, 32]. In contrast, eβG is mainly found in the intestine. Both hβG and eβG catalyze hydrolysis of β-D-glucuronic acid residues from the nonreducing end of glycosaminoglycans [33, 34], but the enzyme has a unique acidic optimum pH. While hβG displays maximal catalytic activity at pH 4–4.5 [32, 35], eβG exhibits optimal activity at neutral pH. Inhibiting hβG may cause MPS [21, 22], a lysosomal storage disease that can affect appearance, physical abilities, organ and system functioning, and, in most cases, mental development. It is crucial to screen compounds that can only block eβG activity but not affect hβG.

A unique loop structure was found in eβG which lacked hβG after superimposition of two βGs, which provides a target site to screen compounds that can distinguish the two βGs [16]. We found 59 candidate compounds which can selectively inhibit eβG activity through molecular docking against the grid box enclosing the bacterial loop and active site of eβG. Some known drugs, such as Amoxapine and Loxapine, have been demonstrated to interact with the residues of bacterial loop and active site of eβG and inhibit variant bacterial βG activity [24]. Wallace and colleagues indicated that the key residues of bacterial loop are L361 and F365 [16], indicating that we can develop the eβG specific inhibitor by targeting the unique loop of eβG. In this report, compound **4041** can bind to E413 (key residue in active site of eβG) through the 1,2,4-triazole moiety but not show in the compound **7145**. Furthermore, compound **4041** has twohydrophobic contacts to residues L361 and I363 in the bacterial loop. But, compound **7145** shows one hydrophobic contact withresidue L361. In eβG activity assay, compound **4041** (IC_{50} = 2.8 μM) also shows a higher inhibiting ability than compound **7145** (IC_{50} = 31.6 μM). We concluded that the inhibiting ability of eβG has positive correlation with the interacting quantities to the active site and the unique loop of eβG.

eβG inhibitors can be developed as a chemotherapy adjuvant to reduce CID [16, 24]. CID is a main side effect that occurs in up to 50–80% of patients depending on chemotherapy regimen [36]. There are several studies indicating that inhibiting βG activity can reduce CID and intestinal injury [37]. Inhibition of intestinal βG by antibiotics could reduce CPT-11-induced diarrhea *in vivo*. But, antibiotics will kill all native gut floras, including probiotics within the digestive tract, which is not recommended for chemotherapeutic patients. Moreover, the eβG has also been considered to play a pivotal role in the development of colon carcinogenesis. For example, the DMH and NNK (ROS based carcinogen) have been report that their glucuronide metabolite may be re-toxic by eβG and induce intestinal damage and colon tumor *in vivo* [6–8, 12–14]. eβG specific inhibitors may act as colon cancer chemoprevention agents by reducing the generation of xenobiotics from glucuronide metabolites. Thus, the specific eβG inhibitor can be applied in nutrient supplement for cancer prevention.

5. Conclusions

In conclusion, we have identified that two compounds, compound **7145** and compound **4041**, can selectively inhibit eβG activity without disrupting hβG activity by binding to the active site and the unique loop within eβG. Because of their high specificity and efficacy against eβG, they have great potential to be developed as a chemotherapy adjuvant for antidiarrhea treatment and cancer chemoprevention agent. Moreover, we proved that inhibitors for the desire enzymes can be selected from virtual screening based on the structure docking showing a high hit rate, which may provide a fast and inexpensive approach for new drug discovery.

Conflict of Interests

The authors declare that there is no conflict of interests regarding the publication of this paper.

Authors' Contribution

Ta-Chun Cheng and Kuo-Hsiang Chuang contributed equally.

Acknowledgments

This work was supported by grants from the National Research Program for Biopharmaceuticals, Ministry of Science and Technology, Taipei, Taiwan (MOST 103-2325-B-037-007, MOST 103-2325-B-041-001, NSC 101-2320-B-041-001-MY2, and NSC 102-2320-B-038-043-MY2), the Ministry of Health and Welfare, Taiwan (MOHW103-TD-B-111-05), the National Health Research Institutes, Taiwan (NHRI-EX103-10238SC), the China Medical University, Taichung, Taiwan (CMU99-N1-19-1 and CMU99-N1-19-2), 103NSYSU-KMU Joint Research Project (NSYSUKMU103 I-003), Comprehensive Cancer Center of Taipei Medical University/Health and Welfare Surcharge of Tobacco Products (MOHW103-TD-B-111-01), and the Grant of Biosignature in Colorectal Cancers, Academia Sinica, Taiwan. This study is also supported partially by Kaohsiung Medical University "Aim for the Top 500

Universities Grant" (Grants nos. KMU-TP103C00, KMU-TP103C01, KMU-TP103C11, KMU-TP103H10, and KMU-DT103005).

References

[1] G. M. Nelson, A. E. Swank, L. R. Brooks, K. C. Bailey, and S. E. George, "Metabolism, microflora effects, and genotoxicity in haloacetic acid-treated cultures of rat cecal microbiota," *Toxicological Sciences*, vol. 60, no. 2, pp. 232–241, 2001.

[2] I. Rowland, "The influence of the gut microflora on food toxicity," *Proceedings of the Nutrition Society*, vol. 40, no. 1, pp. 67–74, 1981.

[3] C. Humblot, M. Murkovic, L. Rigottier-Gois et al., "β-glucuronidase in human intestinal microbiota is necessary for the colonic genotoxicity of the food-borne carcinogen 2-amino-3-methylimidazo[4,5-f]quinoline in rats," *Carcinogenesis*, vol. 28, no. 11, pp. 2419–2425, 2007.

[4] A. Rowland, J. O. Miners, and P. I. Mackenzie, "The UDP-glucuronosyltransferases: their role in drug metabolism and detoxification," *International Journal of Biochemistry and Cell Biology*, vol. 45, no. 6, pp. 1121–1132, 2013.

[5] K. Takasuna, T. Hagiwara, K. Watanabe et al., "Optimal antidiarrhea treatment for antitumor agent irinotecan hydrochloride (CPT-11)-induced delayed diarrhea," *Cancer Chemotherapy and Pharmacology*, vol. 58, no. 4, pp. 494–503, 2006.

[6] T. Chihara, K. Shimpo, T. Kaneko et al., "Inhibition of 1, 2-dimethylhydrazine-induced mucin-depleted foci and O^6-methylguanine DNA adducts in the rat colorectum by boiled garlic powder," *Asian Pacific Journal of Cancer Prevention*, vol. 11, no. 5, pp. 1301–1304, 2010.

[7] P. M. Kim and P. G. Wells, "Genoprotection by UDP-glucuronosyltransferases in peroxidase-dependent, reactive oxygen species-mediated micronucleus initiation by the carcinogens 4-(methylnitrosamino)-1-(3-pyridyl)-1-butanone and benzo[a]pyrene," *Cancer Research*, vol. 56, no. 7, pp. 1526–1532, 1996.

[8] M. Kim, S. Miyamoto, S. Sugie et al., "A tobacco-specific carcinogen, NNK, enhances AOM/DSS-induced colon carcinogenesis in male A/J mice," *In Vivo*, vol. 22, no. 5, pp. 557–564, 2008.

[9] K. R. Kaderlik, R. F. Minchin, G. J. Mulder et al., "Metabolic activation pathway for the formation of DNA adducts of the carcinogen 2-amino-1-methyl-6-phenylimidazo[4,5-b]pyridine (PhIP) in rat extrahepatic tissues," *Carcinogenesis*, vol. 15, no. 8, pp. 1703–1709, 1994.

[10] N. Nalini, V. Manju, and V. P. Menon, "Effect of coconut cake on the bacterial enzyme activity in 1,2-dimethyl hydrazine induced colon cancer," *Clinica Chimica Acta*, vol. 342, no. 1-2, pp. 203–210, 2004.

[11] N. Nalini, K. Sabitha, P. Viswanathan, and V. P. Menon, "Influence of spices on the bacterial (enzyme) activity in experimental colon cancer," *Journal of Ethnopharmacology*, vol. 62, no. 1, pp. 15–24, 1998.

[12] A. Likhachev, V. Anisimov, L. Paranova, and K. Pozharisski, "Effect of exogenous β-glucuronidase on the carcinogenicity of 1,2-dimethylhydrazine in rats: evidence that carcinogenic intermediates form conjugates and act through their subsequent enzymatic release," *Carcinogenesis*, vol. 6, no. 5, pp. 679–681, 1985.

[13] S. N. Newaz, W. F. Fang, and H. W. Strobel, "Metabolism of the carcinogen 1,2-dimethylhydrazine by isolated human colon microsomes and human colon tumor cells in culture," *Cancer*, vol. 52, no. 5, pp. 794–798, 1983.

[14] S. Wolter and N. Frank, "Metabolism of 1,2-dimethylhydrazine in isolated perfused rat liver," *Chemico-Biological Interactions*, vol. 42, no. 3, pp. 335–344, 1982.

[15] K. Kobayashi, "Chemotherapy-induced diarrhea," *Gan To Kagaku Ryoho*, vol. 30, no. 6, pp. 765–771, 2003.

[16] B. D. Wallace, H. Wang, K. T. Lane et al., "Alleviating cancer drug toxicity by inhibiting a bacterial enzyme," *Science*, vol. 330, no. 6005, pp. 831–835, 2010.

[17] A. B. Roberts, B. D. Wallace, M. K. Venkatesh, S. Mani, and M. R. Redinbo, "Molecular insights into microbial β-glucuronidase inhibition to abrogate CPT-11 toxicity," *Molecular Pharmacology*, vol. 84, no. 2, pp. 208–217, 2013.

[18] S. Cascinu, E. Bichisao, D. Amadori et al., "High-dose loperamide in the treatment of 5-fluorouracil-induced diarrhea in colorectal cancer patients," *Supportive Care in Cancer*, vol. 8, no. 1, pp. 65–67, 2000.

[19] G. Dranitsaris, J. Maroun, and A. Shah, "Severe chemotherapy-induced diarrhea in patients with colorectal cancer: a cost of illness analysis," *Supportive Care in Cancer*, vol. 13, no. 5, pp. 318–324, 2005.

[20] M. Fittkau, W. Voigt, H.-J. Holzhausen, and H.-J. Schmoll, "Saccharic acid 1.4-lactone protects against CPT-11-induced mucosa damage in rats," *Journal of Cancer Research and Clinical Oncology*, vol. 130, no. 7, pp. 388–394, 2004.

[21] G. Constantopoulos, S. Rees, B. G. Cragg, J. A. Barranger, and R. O. Brady, "Experimental animal model for mucopolysaccharidosis: suramin-induced glycosaminoglycan and sphingolipid accumulation in the rat," *Proceedings of the National Academy of Sciences of the United States of America*, vol. 77, no. 6, pp. 3700–3704, 1980.

[22] P. M. Gillett, R. A. Schreiber, G. P. Jevon et al., "Mucopolysaccharidosis type VII (Sly syndrome) presenting as neonatal cholestasis with hepatosplenomegaly," *Journal of Pediatric Gastroenterology and Nutrition*, vol. 33, no. 2, pp. 216–220, 2001.

[23] S. Ahmad, M. A. Hughes, L.-A. Yeh, and J. E. Scott, "Potential repurposing of known drugs as potent bacterial β-glucuronidase inhibitors," *Journal of Biomolecular Screening*, vol. 17, no. 7, pp. 957–965, 2012.

[24] R. Kong, T. Liu, X. Zhu et al., "Old drug new use—amoxapine and its metabolites as potent bacterial β-glucuronidase inhibitors for alleviating cancer drug toxicity," *Clinical Cancer Research*, vol. 20, no. 13, pp. 3521–3530, 2014.

[25] I. D. Kuntz, "Structure-based strategies for drug design and discovery," *Science*, vol. 257, no. 5073, pp. 1078–1082, 1992.

[26] E. C. Meng, B. K. Shoichet, and I. D. Kuntz, "Automated docking with grid-based energy evaluation," *Journal of Computational Chemistry*, vol. 13, no. 4, pp. 505–524, 1992.

[27] T.-L. Cheng, B.-M. Chen, L.-Y. Chan, P.-Y. Wu, J.-W. Chern, and S. R. Roffler, "Poly(ethylene glycol) modification of β-glucuronidase-antibody conjugates for solid-tumor therapy by targeted activation of glucuronide prodrugs," *Cancer Immunology Immunotherapy*, vol. 44, no. 6, pp. 305–315, 1997.

[28] G. Jones, P. Willett, R. C. Glen, A. R. Leach, and R. Taylor, "Development and validation of a genetic algorithm for flexible docking," *Journal of Molecular Biology*, vol. 267, no. 3, pp. 727–748, 1997.

[29] N. C. Cohen, J. M. Blaney, C. Humblet, P. Gund, and D. C. Barry, "Molecular modeling software and methods for medicinal chemistry," *Journal of Medicinal Chemistry*, vol. 33, no. 3, pp. 883–894, 1990.

[30] E. T. Maggio and K. Ramnarayan, "Recent developments in computational proteomics," *Drug Discovery Today*, vol. 6, no. 19, pp. 996–1004, 2001.

[31] Y.-C. Su, K.-H. Chuang, Y.-M. Wang et al., "Gene expression imaging by enzymatic catalysis of a fluorescent probe via membrane-anchored β-glucuronidase," *Gene Therapy*, vol. 14, no. 7, pp. 565–574, 2007.

[32] Y.-L. Leu, S. R. Roffler, and J.-W. Chern, "Design and synthesis of water-soluble glucuronide derivatives of camptothecin for cancer prodrug monotherapy and antibody-directed enzyme prodrug therapy (ADEPT)," *Journal of Medicinal Chemistry*, vol. 42, no. 18, pp. 3623–3628, 1999.

[33] A. W. Wong, S. He, J. H. Grubb, W. S. Sly, and S. G. Withers, "Identification of Glu-540 as the catalytic nucleophile of human β- glucuronidase using electrospray mass spectrometry," *The Journal of Biological Chemistry*, vol. 273, no. 51, pp. 34057–34062, 1998.

[34] T. Legigan, J. Clarhaut, B. Renoux et al., "Synthesis and antitumor efficacy of a β-glucuronidase-responsive albumin-binding prodrug of doxorubicin," *Journal of Medicinal Chemistry*, vol. 55, no. 9, pp. 4516–4520, 2012.

[35] T.-C. Cheng, S. R. Roffler, S.-C. Tzou et al., "An activity-based near-infrared glucuronide trapping probe for imaging β-glucuronidase expression in deep tissues," *Journal of the American Chemical Society*, vol. 134, no. 6, pp. 3103–3110, 2012.

[36] A. Stein, W. Voigt, and K. Jordan, "Chemotherapy-induced diarrhea: pathophysiology, frequency and guideline-based management," *Therapeutic Advances in Medical Oncology*, vol. 2, no. 1, pp. 51–63, 2010.

[37] D.-H. Kim and Y.-H. Jin, "Intestinal bacterial β-glucuronidase activity of patients with colon cancer," *Archives of Pharmacal Research*, vol. 24, no. 6, pp. 564–567, 2001.

Hindawi Publishing Corporation
The Scientific World Journal
Volume 2015, Article ID 303415, 7 pages
http://dx.doi.org/10.1155/2015/303415

Research Article

Evaluation of *Cinnamomum osmophloeum* Kanehira Extracts on Tyrosinase Suppressor, Wound Repair Promoter, and Antioxidant

Man-Gang Lee,[1,2] Su-Yu Kuo,[3] Shih-Yu Yen,[4] Hsia-Fen Hsu,[5] Chung-Hang Leung,[6] Dik-Lung Ma,[7] Zhi-Hong Wen,[1,8] and Hui-Min David Wang[3]

[1]*Department of Marine Biotechnology and Resources, National Sun Yat-sen University, Kaohsiung 804, Taiwan*
[2]*Division of Urology, Department of Surgery, Zuoying Branch of Kaohsiung Armed Forces General Hospital, Kaohsiung 813, Taiwan*
[3]*Department of Fragrance and Cosmetic Science, Graduate Institute of Natural Products, Center for Stem Cell Research, Kaohsiung Medical University, No. 100, Shih-Chuan 1st Road, San-Ming District, Kaohsiung 80708, Taiwan*
[4]*Department of Bioscience Technology, Chang Jung Christian University, Tainan 711, Taiwan*
[5]*Metal Industries Research & Development Centre, Kaohsiung 812, Taiwan*
[6]*State Key Laboratory of Quality Research in Chinese Medicine, Institute of Chinese Medical Sciences, University of Macau, Macau*
[7]*Department of Chemistry, Hong Kong Baptist University, Kowloon Tong, Hong Kong*
[8]*Marine Biomedical Laboratory & Center for Translational Biopharmaceuticals, Department of Marine Biotechnology and Resources, National Sun Yat-sen University, 70 Lien-Hai Road, Kaohsiung 804, Taiwan*

Correspondence should be addressed to Zhi-Hong Wen; wzh@mail.nsysu.edu.tw and Hui-Min David Wang; davidw@kmu.edu.tw

Received 28 May 2014; Revised 30 July 2014; Accepted 2 August 2014

Academic Editor: Li-Yeh Chuang

Cinnamomum osmophloeum Kanehira belongs to the Lauraceae family of Taiwan's endemic plants. In this study, *C. osmophloeum* Kanehira extract has shown inhibition of tyrosinase activity on B16-F10 cellular system first. Whether extracts inhibited mushroom tyrosinase activity was tested, and a considerable inhibition of mushroom tyrosinase activity by *in vitro* assays was presented. Animal experiments of *C. osmophloeum* Kanehira were carried out by observing animal wound repair, and the extracts had greater wound healing power than the vehicle control group (petroleum jelly with 8% DMSO, w/v). In addition, the antioxidant capacity of *C. osmophloeum* Kanehira extracts *in vitro* was evaluated. We measured *C. osmophloeum* Kanehira extract's free radical scavenging capability, metal chelating, and reduction power, such as biochemical activity analysis. The results showed that a high concentration of *C. osmophloeum* Kanehira extract had a significant scavenging capability of free radical, a minor effect of chelating ability, and moderate reducing power. Further exploration of the possible physiological mechanisms and the ingredient components of skincare product for skin-whitening, wound repair, or antioxidative agents are to be done.

1. Introduction

Skin, made up of three layer cells including, epidermis, dermis, and hypodermis, is the largest vertebrates organ in the human body. Human skin is commonly exposed to oxidative stresses from solar ultraviolet (UV) radiation and free radicals as well as its induced cellular reactive oxygen species (ROS) [1, 2], which are the common reasons for tumor genesis or skin aging. To protect skin from UV radiation, skin operates complex defense system including skin thickening, pigment synthesis, and a network of nonenzymatic and enzymatic antioxidative mechanisms [2]. In addition to a significant responsibility, in the prevention of human skin UV-caused damage, which increases melanocytes transfer of melanosomes to keratinocytes, melanin determines skin color [3]. Hyperpigmentation is commonly cared with therapeutic drugs or cosmetics of pigment-reducing or skin-whiten abilities. During the melanin synthesis processes, tyrosinase is classified to be the rate-limiting oxidase at first two steps [4]. It catalyzes the pigments production such as

(a) (b)

Figure 1: The photos of *Cinnamomum osmophloeum* Kanehira. (a) Leaves. (b) A whole plant.

eumelanin and phenomelanin. Two types of pigments production were reported, including the L-tyrosine hydroxylation to 3,4-dihydroxy-L-phenylalanine (L-DOPA) and then the L-DOPA oxidation to dopaquinone (a biochemical precursor to pigments) [5]. In the active site for tyrosinase, two copper ions are essential to catalyze colorful pigments or melanin by oxidative stress. To antagonize tyrosinase activity can reduce the syndrome of hyperpigmentation and dermatological disorders.

Skin as the first immune defense line of human plays a noteworthy role in avoiding various biological, chemical, mechanical, and physical damages [1, 2]. Chronic or acute severe injuries on the skin, such as abrasions, burns, leg ulcers, or lesions, in consequence considerable losses of dermal tissues pose huge challenges to the therapeutic processes. Keratinocytes in epidermis and fibroblasts in dermis are the first stop for body protection against external stimulus or for the skin wound healing [6]. In terms of wound healing, wound closure is known to be initiated by fibroblast migration from its margins. Based on the migratory force, resistance from the regenerated tissue may lead to fibroblast differentiation [7], which is featured by the local expression profiles of skin cells, such as several growth factors and the extracellular matrix. Skin wound healing is a cutting edge study for many medicine fields [8].

Smoking factors, salted food, or environmental toxicants bring about various oxidative stresses to human being [9]. The level of excessive free radicals produces a high oxidative stress which is a negative effect against the normal skin and results in aging or some diseases. Through biochemical processes, the intracellular physiological oxidants are engendered from nonenzymatic systems such as those involving enzymatic catalysis, transition metals, various oxidases that transformed them into the reactive nitrogen species, or reactive oxygen species [1]. If antioxidants are invigorated, they can significantly prevent or reduce the oxidative pressure damages [10]. There are several important components constructed to cellular membrane lipids from the phospholipids, membrane proteins, polyunsaturated fatty acids, cholesterol, and nucleic acids [11]. Excessive free radicals and ROS cause oxidative pressure injury on lipids, proteins, and DNA, and the damage eventually induced cellular damage, aging, neural disorders, diabetes, atherosclerosis, inflammatory, cancer, and cardiovascular disease, especially unwanted pigment accumulation [12].

Cinnamomum osmophloeum Kanehira is commonly recognized as indigenous cinnamon or pseudocinnamomum. The natural plant is native to broad-leaved forests of Taiwan's endemic plants (Figure 1) and lots of exercises as a Chinese herbal medicine, including tannin, resin, mucilage, sugar, and essential oil, among which essential oils had excellent inhibitions on bacterial pharmacological characteristics [13]. This plant contains many nutrients such as manganese, dietary fiber, iron, and calcium, commonly used as a spice and flavoring agent for many foods [14]. Various biofunctional applications have been found that *C. osmophloeum* Kanehira has high anti-inflammatory and antioxidative properties which plays a key role in tissue repair of traditional medicine [15]. Moreover, *C. osmophloeum* Kanehira could be used as a xanthine oxidase inhibitor for management of hyperuricemia and related medicinal situations including gout, hence a potential drug [16].

2. Materials and Methods

2.1. Reagents and Materials. All the reagents were purchased from Sigma Chemical (St. Louis, MO), including dimethyl sulfoxide (DMSO), 1,1-diphenyl-2-picrylhydrazyl (DPPH), 3-(4,5-dimetylthiazol-2-yl)-2,5-diphenyl, tetrazolium bromide (MTT), 3-*tert*-butyl-4-hydroxyanisole (BHA), ethylenediaminetetraacetic acid (EDTA), $FeCl_3$, $FeCl_2{\cdot}4H_2O$, kojic acid, L-tyrosine, mushroom tyrosinase, potassium ferricyanide [$K_3Fe(CN)_6$], trichloroacetic acid and vitamin C, and other highest purity chemical buffers and reagents. Cell culture reagents were purchased from GIBCO BRL (Gaithersburg, MD), including fetal bovine serum (FBS) and Dulbecco's modified Eagle medium (DMEM).

2.2. Extraction of C. osmophloeum Kanehira Leaves. The plant specimen was authenticated by Ladies Biotech Co., LTD, where voucher specimens were kept. Dry leaves of *C. osmophloeum* Kanehira (0.6 kg) were sliced and soaked in 3 L ethyl alcohol for one day before further three ethyl alcohol extractions. After filtration, the extracts were evaporated to final weight of 8.49 g.

2.3. B16-F10 Melanoma Cell Cultures. The melanoma B16-F10 cells (BCRC 60031 in ATCC) were maintained at 37°C under 5% CO_2 atmosphere by feeding the medium (10 mM

HEPES, 13.4 mg/mL DMEM, 100 μg/mL streptomycin sulfate, 143 U/mL benzylpenicillin potassium, and 24 mM $NaHCO_3$, pH 7.1) with 10% FBS [17].

2.4. B16-F10 Cell Viability. MTT assay was used to evaluate the effects of cell viabilities for the treatments of *C. osmophloeum* Kanehira extracts [17]. Briefly, cells (6×10^3 cells/well) were plated in 96-well plates for overnight. Cells were treated with either vehicle (DMSO) or indicated concentrations of eachsample for 24 h. Subsequently, 0.5 mg/mL MTT in 100 μL of fresh medium was used to replace the medium and the reaction was performed in a 37°C cell culture incubator for 2 h. The generating crystals were dissolved in 100 μL of DMSO with smooth shaking for 10 min in darkness. Finally, the absorbance (A) value of this reaction was detected at 595 nm by multiplate reader (UV-vis, BioTek, Winooski, VT). Cell viability (%) was formulated as follows:

$$\text{Cell viability (\%)} = 100 \times \frac{\text{OD}_{\text{sample}}}{\text{OD}_{\text{control}}}. \quad (1)$$

2.5. B16-F10 Cellular Tyrosinase Activity. The tyrosinase activity was dependent on the dopachrome formation rate as previously described [17]. Melanoma B16-F10 cells (10^5 cells/well) were seeded in a 12-well plate with 1,000 μL of medium, and they were treated with indicated concentrations of extracts for 48 h. After PBS washing, B16-F10 cells lysed with 1% triton X-100/PBS and 50 μL of 2 mM L-tyrosine were added. Standing for 3 h at 37°C in darkness, its absorbance at 490 nm was examined spectrophotometrically, where the tyrosinase activity evaluation formula was similar to (2).

2.6. B16-F10 Cellular Melanin Contents. The cellular melanin contents were measured with minor modifications as previously described [17]. Briefly, B16-F10 melanoma cells (2.5×10^5 cells/well/1500 μL of medium) plated in 6-well plates were treated with extracts and incubated for 48 h. After dissolving in 10% DMSO with 50 μL of 2.0 N NaOH for 1 h at 90°C, cell lysates were centrifuged at 10,000 ×g for 10 min to collect the supernatants for melanin determination using spectrophotometer at 475 nm with similar formula to (2).

2.7. Mushroom Tyrosinase Activity. The mushroom tyrosinase activity was measured with minor modifications as previously described [18, 19]. The various concentrations of extracts were added: 2 μL with 68 μL of 50 mM phosphate buffer (pH 6.8), 10 μL of 0.5 units/mL of mushroom tyrosinase, and 10 μL of the mixture. The absorbance of the mushroom tyrosinase inhibition assay at 490 nm was determined at 5 min per interval until 30 minutes with a 96-well plate spectrophotometer, where kojic acid was regarded as a positive control. Mushroom tyrosinase activity (%) was formulated as follows:

$$\text{Mushroom tyrosinase activity (\%)} = 100 - \left[100 \times \frac{(A-B)-(C-D)}{(A-B)}\right], \quad (2)$$

where A is the OD value under no sample; B is the OD value under no sample and tyrosinase; C is the OD value under sample; and D is the OD value under sample but no tyrosinase.

2.8. Animal Experiments. Six-week-old male Wistar rats are used. These rats are kept on standard rat chow and water ad libitum for 1 week before challenging. The animal studies were performed under authorization from the Animal Use Committee of Kaohsiung Medical University. The experimental rats were housed on a 12/12-hour light-dark cycle with the air conditioner and adequate supply of food and water. Twelve rats were grouped into two sets, that is, petroleum jelly and *C. osmophloeum* Kanehira extracts (experimental groups). The wound healing of skin was measured with minor modifications as previously described [20]. After rats were anesthetized, its dorsal hair was shaved and the wounds of 1 cm in diameter were generated. After a back skin excising, the wounds of all experimental rats were quickly covered with the petroleum jelly (8% DMSO, w/v) or 0.8 mg extracts, where the petroleum jelly was used as a reference.

2.9. Measurement of the Wound Area. Digital camera (Coolpix P6000, Nikon, Japan) was used to record the progression of skin wound after 0, 1, 3, and 5 days with protocol parameters (aperture: F/7.2, shutter speed: 1/60). The wound dressing was not removed under healing period unless the substance was easy to detach manually. The area of each skin wound was determined by SPOT software (Diagnostic Instruments, Inc., Sterling Heights, MI, USA). Some random Sani-Chips were visualized on wound sites; however, wound size measurements were not interfered. The wound healing index was formulated as follows:

$$\frac{\text{Wound area of day } N}{\text{Wound area of day 0}} \times 100\%. \quad (3)$$

2.10. Determination Antioxidation Ability by DPPH$^\bullet$ Radical Scavenging. The principle of antioxidation determination is based on the color change of DPPH to light yellow if free radicals are scavenged [21]. The more the light color rendered, the higher the antioxidant capacity from the component. Suitable concentration doses of *C. osmophloeum* Kanehira extracts were added to 1 μL and with 99 μL of DPPH solution. When DPPH reacted with antioxidants or vitamin C (positive control), it changed to reduced form and led to a lower absorbance at 517 nm. The scavenging activity (%) of DPPH radical was formulated as follows:

$$\text{Scavenging activity (\%)} = 100 \times \frac{\left(\text{OD}_{\text{control}} - \text{OD}_{\text{sample}}\right)}{\text{OD}_{\text{control}}}. \quad (4)$$

2.11. Metal Chelating Activity. Metal chelating activity was measured with slight modifications as previously described [5]. Briefly, *C. osmophloeum* Kanehira extracts dissolved in DMSO were mixed with a reagent containing 10 μL of 2 mM $FeCl_2 \cdot 4H_2O$. To initiate the reaction with the addition of

20 μL of 5 mM ferrozine, the solution was vigorously shaken and then it was stood for 10 min at room temperature. EDTA was regarded to be a positive control. Its absorbance at 562 nm was calculated as the chelating activity (%) and its method was alike to (4).

2.12. Reducing Power. The reducing power of *C. osmophloeum* Kanehira extracts was determined according to the previous method [21]. The extracts were incubated with 85 μL of 67 mM phosphate buffer (pH 6.8) and 2.5 μL of 20% $K_3Fe(CN)_6$ at 50°C for 20 min. After the addition of 160 μL of trichloroacetic acid (10%), it was centrifuged at 3,000 ×g for 10 min to collect the supernatant (75 μL) for reacting with 2% $FeCl_3$ (25 μL). BHA was regarded to be a positive control. Finally, its absorbance at 700 nm was measured by spectrophotometer.

2.13. Statistics. Data are indicated as a mean and standard deviation in triplicate at least. Its difference significance was evaluated by Student's *t*-test.

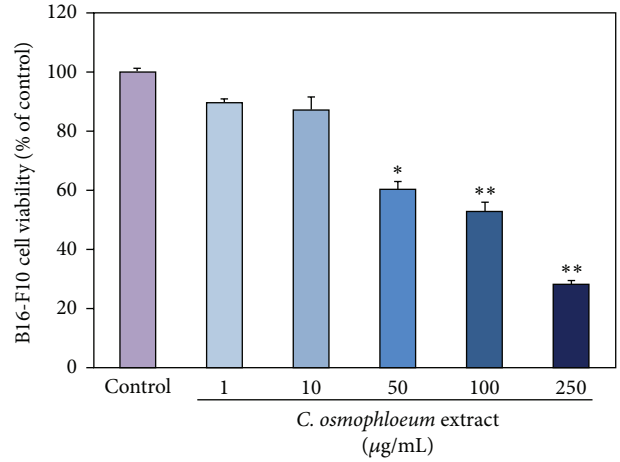

Figure 2: The cytotoxicity of *C. osmophloeum* Kanehira extracts on marine melanoma B16-F10 cells. Data: the mean value ± SD (triplicate values for three independent experiments); $* < 0.01$, $** < 0.001$.

3. Results and Discussion

3.1. B16-F10 Cytotoxicity of C. osmophloeum Kanehira Extracts. Melanoma B16-F10 cells were cultured in the indicated doses of tested extracts (10, 25, 50, 100, and 200 μg/mL). In Figure 2, the cell viability was determined by MTT assay. The proliferation of B16-F10 cell was inhibited by extracts in a dose-responsive manner ranging from 10 to 200 μg/mL. When the mouse melanoma cells were incubated in a higher assay surrounding 100 μg/mL, the viabilities of extract-treated B16-F10 cells were more than 50% at 48 h treatment, suggesting that extracts had discernable cytotoxic effect on mouse melanoma cells.

3.2. C. osmophloeum Kanehira Extracts on B16-F10 Cellular Tyrosinase Activity and Melanin Content. We further investigated the *in situ* cellular tyrosinase and melanin suppressions of extracts. The melanin generation mechanisms contain the L-tyrosine hydroxylation and the L-DOPA oxidation to its corresponding dopaquinone to form pigment by additional multiple biosynthesis steps through the enzymatic tyrosinase. We verified that the extracts had the tyrosinase-inhibiting ability and melanin content effectiveness in mouse melanoma cell, B16-F10. In Figure 3(a), the extracts had revealed superior obvious suppressions even at a moderate quantity concentration to both tyrosinase activity and melanin content. Additionally, Figure 3(b) shows that melanin contents and tyrosinase activities were highly correlated under the same dose-responsive manner upon *C. osmophloeum* Kanehira treatments. Both tyrosinase activity and melanin content decreased in a similar dose-dependent tendency, when we increased dosages of extracts, indicating that the inhibition of cellular tyrosinase activity might induce the epidermal melanin reduction. But interestingly, extracts at the concentration 100 μg/mL, the cell viability remained 52% (Figure 2), and the tyrosinase activity was 18% lower than cell viability (Figure 3(a)). Melanin content did not show evident reduction. On the contrary, with highest concentration of *C. osmophloeum* Kanehira extracts at 50 μg/mL, the melanin content was decreased for low cell viability. As the tendency of tyrosinase activity was lower than cell viability, the melanin content was a bit higher than cell viability.

3.3. Measurement of C. osmophloeum Kanehira Extracts on Mushroom Tyrosinase Activity. We previously reported that UV exposure may induce the oxidative stress which is prone to be skin darkening and ROS generation for tumor progression [22, 23]. For the prevention of skin darkening and the hyperpigmentation, we evaluated the inhibitory effects of *C. osmophloeum* Kanehira extracts using *in vitro* mushroom tyrosinase inhibitory assay. The inhibition effectiveness of *C. osmophloeum* Kanehira extracts demonstrates moderate suppression to the activity of mushroom tyrosinase at 200 μM (Figure 4). Accordingly, these compounds have the potential use for supplements in industry of cosmetics and pharmaceuticals.

3.4. Evaluation of the In Vivo Wound Size Assay. In order for *C. osmophloeum* Kanehira extracts to be utilized as a dermal agent, they should exhibit minimal toxicity towards normal tissues. The wound-healing performance of the *C. osmophloeum* Kanehira extracts was measured by an animal model in terms of the full thickness wound assay and monitored by image analysis of excision wound area. We discovered that the mice displayed no obvious evidences of gross toxicity during the course of the treatment period. The body weight of the mice was also monitored at an interval of every other day over the course of this study. The results showed that the body weight of mice in the treatment and the control groups was not significantly different over the duration of the experiment (data not shown). Additionally, the mean values of the heart, liver, and kidney weights after sacrifice between these two groups of mice were not significantly changed.

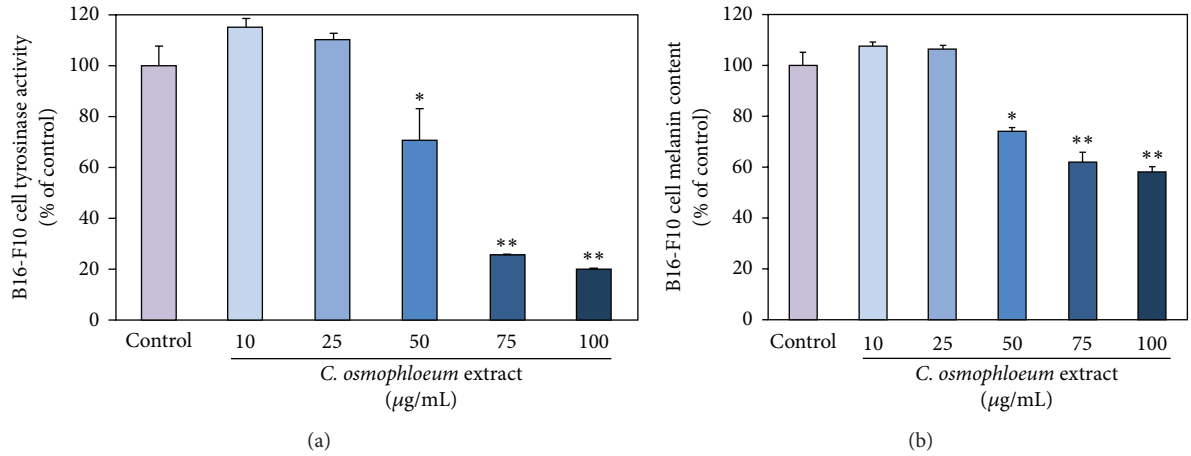

Figure 3: The inhibitory effects of various concentrations of *C. osmophloeum* extracts on B16-F10 cells. (a) The tyrosinase activity and (b) the melanin content of B16-F10 cells were incubated with indicated concentrations of *C. osmophloeum* extracts. Data: the mean value ± SD (triplicate values for three independent experiments); ∗ < 0.01, ∗∗ < 0.001.

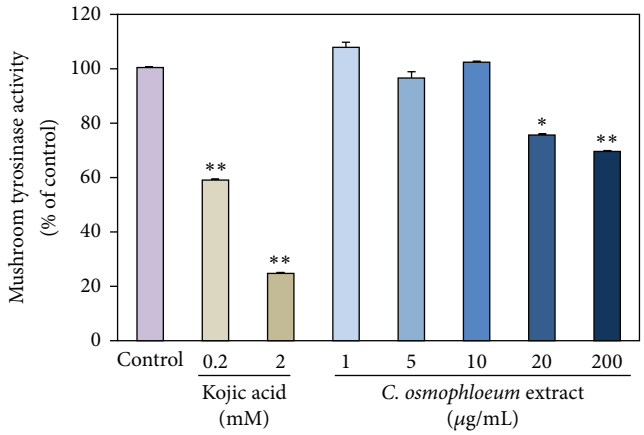

Figure 4: The inhibitory effects of various concentrations of *C. osmophloeum* extracts and kojic acid on mushroom tyrosinase for 5 minutes. Data: the mean value ± SD (triplicate values in three independent experiments); ∗ < 0.01, ∗∗ < 0.001.

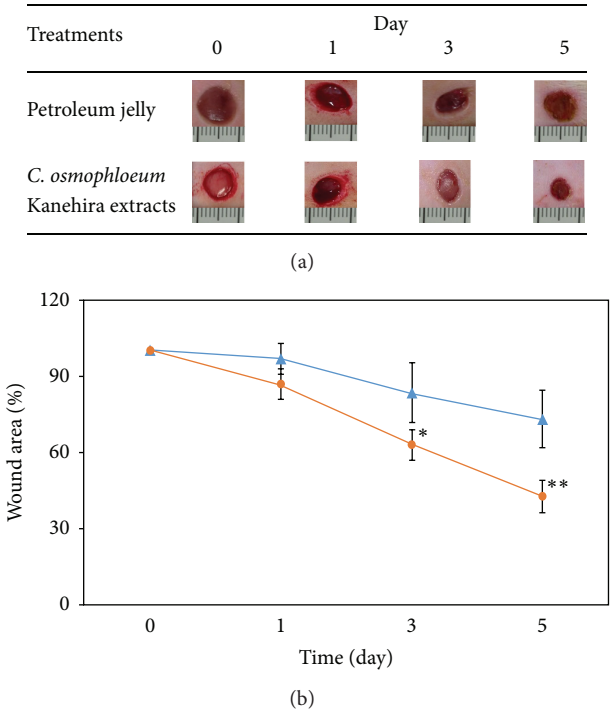

Figure 5: The wound healing of *C. osmophloeum* extracts on animal model. (a) Wound healing after 0, 1, 3, and 5 days after injury. After the full thickness excisions of 1 cm in diameter were made, the petroleum jelly (8% DMSO, w/v) or 0.8 mg *C. osmophloeum* extracts covered on the hurt. For injury group, wounds were not covered for control. At the first day, the wound healing area from petroleum jelly (8% DMSO) group was smaller than that of *C. osmophloeum* group until 5 days. (b) The differences between wounds of petroleum jelly (8% DMSO, w/v, blue solid triangle) and 0.8 mg *C. osmophloeum* group (orange solid circle) were statistically significant at day 5. Data: the mean value ± SD (triplicate values in two independent experiments); ∗ < 0.01, ∗∗ < 0.001.

The wound areas of both petroleum jelly (8% DMSO, w/v) and 0.8 mg extract treatment groups were decreased in a time-dependent manner (Figure 5). Wound areas of extract-treatment groups at days 0, 1, 3, and 5 were 100 ± 0.1%, 86.7 ± 5.8%, 63.0 ± 6.1%, and 42.7 ± 6.4%, respectively, which were smaller than those of petroleum jelly group (100 ± 0.4%, 96.7 ± 5.8%, 83.3 ± 11.5%, and 73.0 ± 11.3%) (Figure 5(a)). In the beginning of the wound creation, the experimental group displayed smaller area than that of petroleum jelly group which showed a constant repair trend after 3 days. The *C. osmophloeum* Kanehira-treated wound healing displayed over 30% and 50% wound area closure after 3 and 5 days, respectively (Figure 5(b)). Therefore, the repairing ability and the wound shrinking ratio of the extract experimental group were higher and more effective.

3.5. Antioxidative Properties of C. osmophloeum Kanehira Extracts. Accumulating evidence shows that free radical increases can lead to skin melanin overexpression and speed up the variety of oxidations of lipids in manufactured food

Table 1: Measurement of *C. osmophloeum* extracts on antioxidant experiments. The data were expressed as a mean value in three independent experiments.

C. osmophloeum extract (μg/mL)	DPPH scavenging (%)	Metal chelating ability (%)	Reducing power (OD 700)
1	≤10.0	≤10.0	0.09 ± 0.00
10	≤10.0	≤10.0	0.10 ± 0.00
50	≤10.01	≤10.0	0.18 ± 0.02
100	13.23 ± 0.01	≤10.0	0.27 ± 0.03
250	38.97 ± 0.02	≤10.0	0.48 ± 0.02
Vitamin C[a]	80.82 ± 0.00	—	—
EDTA[b]	—	80.76 ± 0.01	—
BHA[c]	—	—	0.56 ± 0.03

"—" is no testing.
[a]Vitamin C was used as a positive control on DPPH assay at 100 μM.
[b]EDTA was used as a positive control on metal chelating ability at 100 μM.
[c]BHA was used as a positive control on reducing power at 100 μM.

and cosmetics [1]. Natural antioxidants, particularly free radical eliminating abilities, are essential to skin caring. In Table 1, the inhibitory data for extracts to DPPH from 0 to 250 μg/mL were found. Based on this information, extracts showed a dose-dependent manner in our testing conditions and might function as chain-breaking agents or radical ion neutralizers inhibiting the generation of excess free radicals in reference to control of 100 μM vitamin C.

Several literatures reported that reducing power and metal ions-chelating ability from a reagent are commonly displayed through antioxidative effect [18, 19]. In Table 1, the ferrous ion chelating data of *C. osmophloeum* Kanehira extracts were found. When the complex formation of ferrozine and Fe(II) is interfered, it was detectable spectrophotometrically. Therefore, *C. osmophloeum* Kanehira extracts were demonstrated to have few Fe(II) chelating belongings.

The measurement of reducing power is one of the easy and effective methods by reacting with a Fe(III) ferricyanide complex [18, 19]. The solution color changes from light yellow to dark green and blue depended on the level of antioxidants within samples. As shown in Table 1, *C. osmophloeum* Kanehira extracts reducing powers were compared to similar antioxidative power with 3-*tert*-butyl-4-hydroxyanisole (BHA) at 100 μM.

4. Conclusion

Various biochemical characterization properties of *C. osmophloeum* Kanehira extracts were explored within this study. In the cellular experiments, extracts had tyrosinase inhibition effect and melanin content diminution but were cytotoxic. The extracts might have lower cell viabilities to contribute to the results in both inhibited tyrosinase activity and reduced melanin content. In the animal model, we found that the extracts could repair the wound. The antioxidative assays suggested that high concentration of extracts had moderate antioxidative abilities in terms of DPPH scavenging capacity and reducing power ability except metal chelating. In the future, we will analyze purification from *C. osmophloeum* Kanehira extracts to find an effective antioxidant and tyrosinase inhibitor.

Conflict of Interests

The authors had no conflict of interests.

Acknowledgments

This study was supported by grants from the National Science Council, Taiwan (NSC 99-2221-E-037-006-MY3 and NSC 102-2221-E-037-005). The authors also thank Ladies Biotech Co., LTD, for providing the testing sample plant materials, *C. osmophloeum* Kanehira extracts. They also thank the support from Center for Stem Cell Research, Kaohsiung Medical University, Kaohsiung, Taiwan (KMU-TP103G00 and KMU-TP103G02-05).

References

[1] S. Malireddy, S. R. Kotha, J. D. Secor et al., "Phytochemical antioxidants modulate mammalian cellular epigenome: implications in health and disease," *Antioxidants & Redox Signaling*, vol. 17, no. 2, pp. 327–339, 2012.

[2] J. P. S. Silveira, L. N. Seito, S. Eberlin et al., "Photoprotective and antioxidant effects of Rhubarb: inhibitory action on tyrosinase and tyrosine kinase activities and TNF-α, IL-1α and α-MSH production in human melanocytes," *BMC Complementary and Alternative Medicine*, vol. 13, article 49, 2013.

[3] K. Sato and M. Toriyama, "The inhibitory effect of non-steroidal anti-inflammatory drugs (NSAIDs) on the monophenolase and diphenolase activities of mushroom tyrosinase," *International Journal of Molecular Sciences*, vol. 12, no. 6, pp. 3998–4008, 2011.

[4] H.-H. Ko, Y.-T. Tsai, M.-H. Yen et al., "Norartocarpetin from a folk medicine *Artocarpus communis* plays a melanogenesis inhibitor without cytotoxicity in B16F10 cell and skin irritation in mice," *BMC Complementary and Alternative Medicine*, vol. 13, article 348, 2013.

[5] C.-C. Lee, C.-C. Chiu, W.-T. Liao et al., "*Alpinia oxyphylla* Miq. bioactive extracts from supercritical fluid carbon dioxide extraction," *Biochemical Engineering Journal*, vol. 78, pp. 101–107, 2013.

[6] H.-M. Wang, Y.-T. Chou, Z.-H. Wen, Z.-R. Wang, C.-H. Chen, and M.-L. Ho, "Novel biodegradable porous scaffold applied to skin regeneration," *PLoS ONE*, vol. 8, no. 6, Article ID e56330, 2013.

[7] H.-M. Wang, Y.-T. Chou, C.-S. Wu, and J.-T. Yeh, "Polyester/cellulose acetate composites: preparation, characterization and biocompatible," *Journal of Applied Polymer Science*, vol. 126, no. 2, pp. E242–E251, 2012.

[8] H.-M. D. Wang, C.-Y. Chen, and P.-F. Wu, "Isophilippinolide a arrests cell cycle progression and induces apoptosis for anticancer inhibitory agents in human melanoma cells," *Journal of Agricultural and Food Chemistry*, vol. 62, no. 5, pp. 1057–1065, 2014.

[9] A. C. Kulkarni, P. Kuppusamy, and N. Parinandi, "Oxygen, the lead actor in the pathophysiologic drama: enactment of the trinity of normoxia, hypoxia, and hyperoxia in disease and

therapy," *Antioxidants & Redox Signaling*, vol. 9, no. 10, pp. 1717–1730, 2007.

[10] O. R. Temneanu, C. Zamfir, F. Eloaie Zugun, E. Cojocaru, and L. Tocan, "Oxidants and antioxidants relevance in rats' pulmonary induced oxidative stress," *Journal of Medicine and Life*, vol. 4, no. 3, pp. 244–249, 2011.

[11] K. H. Cheeseman, "Mechanisms and effects of lipid peroxidation," *Molecular Aspects of Medicine*, vol. 14, no. 3, pp. 191–197, 1993.

[12] M. Z. Gul, L. M. Bhakshu, F. Ahmad, A. K. Kondapi, I. A. Qureshi, and I. A. Ghazi, "Evaluation of *Abelmoschus moschatus* extracts for antioxidant, free radical scavenging, antimicrobial and antiproliferative activities using in vitro assays," *BMC Complementary and Alternative Medicine*, vol. 11, article 64, 2011.

[13] T. Nuryastuti, H. C. van der Mei, H. J. Busscher, S. Iravati, A. T. Aman, and B. P. Krom, "Effect of cinnamon oil on *icaA* expression and biofilm formation by *Staphylococcus epidermidis*," *Applied and Environmental Microbiology*, vol. 75, no. 21, pp. 6850–6855, 2009.

[14] G. R. Mashhadi NS, G. Askari, A. Feizi et al., "Influence of ginger and cinnamon intake on inflammation and muscle soreness endued by exercise in Iranian female athletes," *International Journal of Preventive Medicine*, vol. 4, pp. S11–S15, 2013.

[15] T. Molania, A. A. Moghadamnia, M. Pouramir et al., "The effect of Cinnamaldehyde on mucositis and salivary antioxidant capacity in gamma-irradiated rats (a preliminary study)," *DARU Journal of Pharmaceutical Sciences*, vol. 20, no. 1, article 89, 2012.

[16] S. Y. Wang, C. W. Yang, J. W. Liao, W. W. Zhen, F. H. Chu, and S. T. Chang, "Essential oil from leaves of *Cinnamomum osmophloeum* acts as a xanthine oxidase inhibitor and reduces the serum uric acid levels in oxonate-induced mice," *Phytomedicine*, vol. 15, no. 11, pp. 940–945, 2008.

[17] R. Halaban, R. S. Patton, E. Cheng et al., "Abnormal acidification of melanoma cells induces tyrosinase retention in the early secretory pathway," *The Journal of Biological Chemistry*, vol. 277, no. 17, pp. 14821–14828, 2002.

[18] H.-M. Wang, C.-Y. Chen, and Z.-H. Wen, "Identifying melanogenesis inhibitors from Cinnamomum subavenium with in vitro and in vivo screening systems by targeting the human tyrosinase," *Experimental Dermatology*, vol. 20, no. 3, pp. 242–248, 2011.

[19] H.-M. Wang, Y.-T. Chou, Z.-L. Hong et al., "Bioconstituents from stems of *Synsepalum dulcificum* Daniell (Sapotaceae) inhibit human melanoma proliferation, reduce mushroom tyrosinase activity and have antioxidant properties," *Journal of the Taiwan Institute of Chemical Engineers*, vol. 42, no. 2, pp. 204–211, 2011.

[20] M.-H. Huang and M.-C. Yang, "Evaluation of glucan/poly(vinyl alcohol) blend wound dressing using rat models," *International Journal of Pharmaceutics*, vol. 346, no. 1-2, pp. 38–46, 2008.

[21] H.-M. Wang, C.-Y. Chen, M.-L. Ho et al., "(-)-*N*-formylanonaine from *Michelia alba* as a human tyrosinase inhibitor and antioxidant," *Bioorganic & Medicinal Chemistry*, vol. 18, no. 14, pp. 5241–5247, 2010.

[22] N. L. Wicks, J. W. Chan, J. A. Najera, J. M. Ciriello, and E. Oancea, "UVA phototransduction drives early melanin synthesis in human melanocytes," *Current Biology*, vol. 21, no. 22, pp. 1906–1911, 2011.

[23] M. S. Eller, K. Ostrom, and B. A. Gilchrest, "DNA damage enhances melanogenesis," *Proceedings of the National Academy of Sciences of the United States of America*, vol. 93, no. 3, pp. 1087–1092, 1996.

Hindawi Publishing Corporation
The Scientific World Journal
Volume 2015, Article ID 620826, 6 pages
http://dx.doi.org/10.1155/2015/620826

Research Article

Indoxyl Sulfate-Induced Oxidative Stress, Mitochondrial Dysfunction, and Impaired Biogenesis Are Partly Protected by Vitamin C and N-Acetylcysteine

Wen-Chin Lee,[1] Lung-Chih Li,[1] Jin-Bor Chen,[1] and Hsueh-Wei Chang[2,3,4,5]

[1]*Division of Nephrology, Department of Internal Medicine, Kaohsiung Chang Gung Memorial Hospital and Chang Gung University College of Medicine, Kaohsiung 83301, Taiwan*
[2]*Institute of Medical Science and Technology, National Sun Yat-Sen University, Kaohsiung 80424, Taiwan*
[3]*Center of Environmental Medicine, Kaohsiung Medical University, Kaohsiung 80708, Taiwan*
[4]*Cancer Center, Kaohsiung Medical University Hospital, Kaohsiung Medical University, Kaohsiung 80708, Taiwan*
[5]*Department of Biomedical Science and Environmental Biology, Kaohsiung Medical University, Kaohsiung 80708, Taiwan*

Correspondence should be addressed to Jin-Bor Chen; chenjb1019@gmail.com and Hsueh-Wei Chang; changhw@kmu.edu.tw

Received 22 August 2014; Revised 14 September 2014; Accepted 15 September 2014

Academic Editor: Li-Yeh Chuang

Indoxyl sulfate (IS) contributes to oxidative stress and endothelial dysfunction in chronic kidney disease patients. However, the role of mitochondria in IS-induced oxidative stress is not very clear. In this study, we examined whether mitochondria play a pivotal role in modulating the effects of antioxidants during IS treatment. In the context of human umbilical vein endothelial cells, we found that IS had a dose-dependent antiproliferative effect. In addition, we used flow cytometry to demonstrate that the level of reactive oxygen species increased in a dose-dependent manner after treatment with IS. High doses of IS also corresponded to increased mitochondrial depolarization and decreased mitochondrial DNA copy number and mitochondrial mass. However, these effects could be reversed by the addition of antioxidants, namely, vitamin C and N-acetylcysteine. Thus, our results suggest that IS-induced oxidative stress and antiproliferative effect can be attributed to mitochondrial dysfunction and impaired biogenesis and that these processes can be protected by treatment with antioxidants.

1. Introduction

Indoxyl sulfate (IS) is a uremic toxin associated with vascular disease and mortality in chronic kidney disease (CKD) patients [1]. Increased reactive oxygen species (ROS) generation contributes to tissue dysfunction [2]. Moreover, IS is a known cause of oxidative stress in endothelial cells [3–5], and it has been shown to strongly decrease the levels of cellular antioxidants such as glutathione (GSH) [3] and increase the production of mitochondrial superoxide [6]. Additionally, IS has been reported to inhibit nitric oxide generation and cell proliferation in vascular endothelial cells [4].

Recently, many studies have investigated compounds that may be capable of regulating IS levels. For example, Kremezin (AST-120), an oral clinical drug with spherical adsorptive carbon, was reported to absorb IS in the gut, decreasing the IS levels in circulation in CKD patients [7]; this improved endothelial function and restored GSH levels [5]. This research provides evidence of the significant role of IS modulators in CKD patients.

Since IS is known to induce oxidative stress, it is reasonable to hypothesize that antioxidants could counteract IS-induced ROS production. Antioxidants such as vitamin E, vitamin C, and N-acetylcysteine (NAC) were reported to inhibit IS-induced ROS generation and antiproliferative effect in human umbilical vein endothelial cells (HUVECs) [3, 4]. Furthermore, several signaling pathways appear to be regulated in IS-treated cells. For example, IS inhibits nitric oxide generation and cell proliferation through ROS-mediated Nox4 overexpression in HUVECs [4]. In addition,

IS upregulates intercellular adhesion molecule-1 (ICAM-1) and monocyte chemotactic protein-1 (MCP-1) expression via ROS-activated NF-κB signaling [8, 9].

Mitochondria are the major ROS-generating organelles [10, 11], and mounting evidence shows that mitochondrial dysfunction may lead to many diseases [12–14]. Although IS-induced ROS generation and antiproliferative effects were reported, the role of mitochondria in this process has not been elucidated yet.

We hypothesized that IS-induced oxidative stress results in mitochondrial dysfunction and impaired mitochondrial biogenesis. To address this hypothesis, we assessed cell viability, ROS generation, mitochondrial membrane potential, mitochondrial DNA copy number, and mitochondrial mass in IS-treated HUVECs and investigated the effects of antioxidants (vitamin C and NAC) on mitochondrial function and biogenesis.

2. Materials and Methods

2.1. Cell Lines and Chemical Information. HUVECs were incubated in a humidified atmosphere with 5% CO_2 at 37°C. Culture medium was prepared as follows: 400 mL of M199 medium (Gibco, Grand Island, NY), 100 mL of fetal bovine serum (Sigma-Aldrich, St. Louis, MO), 25000 U/vial heparin (China Chemical & Pharmaceutical, Tainan, Taiwan), 5 mL of penicillin/streptomycin (Gibco), and 7.5 mg of endothelial cell growth supplement (ECGS) (Millipore, Billerica, MA). IS, ascorbic acid, NAC, crystal violet, and dimethyl sulfoxide (DMSO) were purchased from Sigma-Aldrich, and IS, ascorbic acid, and NAC were further reconstituted to 0–250 μg/mL, 200 μM, and 10 mM for use in experiments, respectively.

2.2. Cell Viability Assay. Cell viability was measured by crystal violet assay [15]. Cells were seeded in 96-well plates (5×10^3 cells/well), treated with IS at indicated concentrations (0, 50, 125, and 250 μg/mL) for 48 h, and washed thrice with phosphate-buffered saline (PBS). Crystal violet reagent (0.05% in PBS) was added to these cells and the mix was incubated for 2 h at 37°C; the cells were then washed 10 times with PBS and air-dried. The cells were incubated with 100 μL of DMSO for 1-2 h to completely dissolve the dye. Finally, the absorbance of these plates was read at 570 nm on a microplate reader.

2.3. Intracellular ROS Detection. Intracellular ROS was detected using 2′,7′-dichlorodihydrofluorescein diacetate (DCFH-DA) [16]. For this purpose, HUVECs (2×10^5 cells) were incubated with different concentrations of IS (0, 50, 125, and 250 μg/mL) for 48 h. Cells were then stained with 10 μM DCFH-DA (Molecular Probes, Life Technologies, Carlsbad, CA) for 30 min at 37°C and detached with trypsin/EDTA. Cells were collected in PBS, washed twice by centrifugation (1500 rpm for 5 min), and resuspended in 0.5 mL of PBS. ROS production was measured by flow cytometry utilizing a fluorescence-activated cell scanner machine (BD Biosciences FACScan system). It was expressed as the mean fluorescence intensity (MFI), which was calculated by CellQuest software.

2.4. Measurement of Mitochondrial Membrane Potential (MMP). Rhodamine 123 (Invitrogen, Life Technologies, Carlsbad, CA) was used to measure MMP, as described previously [17]. In brief, 2×10^5 cells were plated in each well of six-well plates and they were allowed to attach for 16–18 h. After being treated with drugs for 48 h, the cells were harvested by trypsinization, washed in PBS, and resuspended in 200 ng/mL Rhodamine 123. After incubation for 30 min at 37°C, the cells were washed three times and resuspended in 500 mL of PBS. Cytofluorimetric analysis was performed using a BD Biosciences FACScan system. The fluorescence intensity of IS-treated cells was adjusted to that of the untreated control.

2.5. RNA Extraction and Mitochondrial DNA Copy Number. After drug treatment for 48 h, cellular RNA was extracted by PureLink RNA Mini Kit (Ambion, Life Technologies, Carlsbad, CA) and reverse-transcribed to cDNA using SuperScript First-Strand Synthesis System (Invitrogen, Life Technologies, Carlsbad, CA). Mitochondrial DNA (mtDNA) copy number was assessed using real-time polymerase chain reaction (PCR) and adjusted with nuclear DNA (β-actin gene) by using primers against MT-ND1 (forward: 5′-TGGGTACAATGAGGAGTAGG-3′ and reverse: 5′-GGAGTAATCCAGGTCGGT-3′) and actin (forward: 5′-TCACCCACACTGTGCCCATCTACGA-3′ and reverse: 5′-CAGCGGAACCGCTCATTGCCAATGG-3′), as described previously [18, 19]. The threshold cycle number (Ct) values of β-actin and ND1 genes were calculated using the following formula: relative copy number (Rc) = $2^{\Delta Ct}$, where ΔCt = Ct β-actin − Ct ND1.

2.6. Mitochondrial Mass. Mitochondrial mass was determined as described previously with slight modification [20]. In brief, the mitochondria and cytoskeleton (F-actin) were stained by MitoTracker red (Invitrogen, Life Technologies, Carlsbad, CA) and phalloidin (Molecular Probes, Life Technologies, Carlsbad, CA), respectively, and observed using a fluorescence microscope (Olympus BX-UCDB-2; Olympus Corporation, Tokyo, Japan). Image area was analyzed by the Image Pro-Plus version 7.0 (Media Cybernetics, Rockville, MD) system. Only cells with intact cytoplasmic phalloidin staining were counted. Mitochondrial mass was calculated as follows:

$$\text{mitochondrial mass} = \frac{\text{mitochondrial area}}{\text{cytoskeleton area}} \times 100. \quad (1)$$

3. Results

3.1. Cell Viability of IS-Treated HUVECs. The viability of HUVECs treated with the indicated concentrations of IS for 48 h is shown in Figure 1. Cell viability was found to be inversely correlated with IS dose ranging from 0 to 250 μg/mL. In addition, the antiproliferative effect of IS

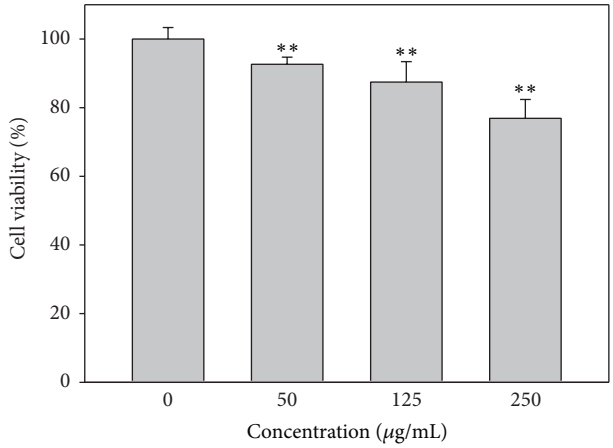

Figure 1: Cell viability of IS-treated HUVECs. Cells were treated with 0, 50, 125, and 250 μg/mL of IS for 48 h and subjected to crystal violet assay. Data, mean ± SD ($n = 12$). $^{**}P < 0.0001$.

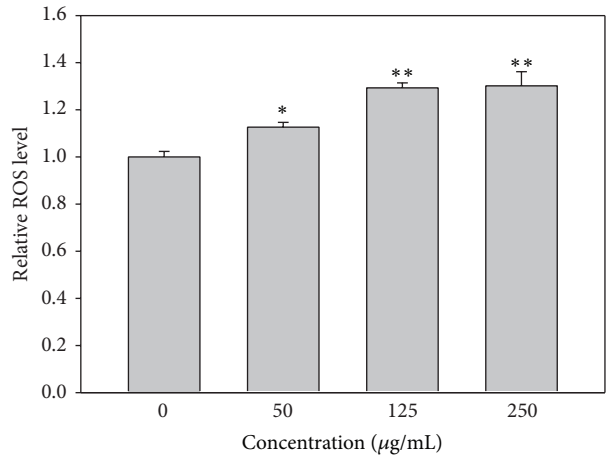

Figure 2: ROS generation of IS-treated HUVECs. Quantification analysis of relative ROS mean intensity of DCFH-DA (% of control). Cells were treated with 0, 50, 125, and 250 μg/mL of IS for 24 h. Data, mean ± SD ($n = 3$). $^{*}P < 0.01$; $^{**}P < 0.001$ compared to the control.

on HUVECs significantly increased in a dose-dependent manner (Figure 1).

3.2. ROS Generation of IS-Treated HUVECs. The mean fluorescence intensity of DCFH-DA was used to measure the relative ROS content (% of control) in IS-treated HUVECs. The results indicated that increasing doses of IS corresponded to higher levels of ROS (Figure 2).

3.3. MMP of IS-Treated HUVECs. The mean fluorescence intensity of Rhodamine 123 was used to measure the relative MMP levels (% of control) in IS-treated HUVECs. Figure 3 shows that MMP was reduced in IS-treated HUVECs. However, the addition of antioxidants such as vitamin C or NAC was able to counteract the effect of IS with regard to MMP (Figure 3).

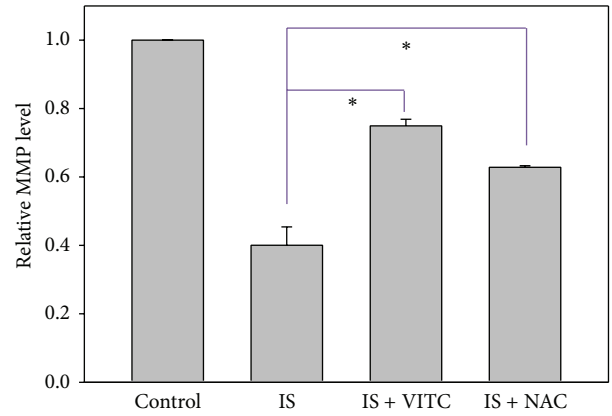

Figure 3: Role of antioxidants in IS-induced mitochondrial depolarization in HUVECs. Quantification analysis of relative MMP mean intensity (% of control) of Rhodamine 123. Cells were treated with IS 125 μg/mL alone as the positive control, cotreated with IS 125 μg/mL and vitamin C 200 μM or NAC 10 mM for 48 h. Cells without IS treatment were regarded as the negative control. Data, mean ± SD ($n = 2$). $^{*}P < 0.05$ compared to the control.

3.4. Mitochondrial Function in IS-Treated HUVECs. Mitochondrial DNA (mtDNA) expression was measured to quantify mitochondrial function in HUVECs treated with IS. In accordance with our previous findings, we saw that mtDNA copy number was dramatically reduced in IS-treated HUVECs, compared to untreated controls. Moreover, these effects could be reversed by the addition of either vitamin C or NAC.

3.5. Mitochondrial Biogenesis in IS-Treated HUVECs. We assessed the effect of IS treatment on mitochondrial biogenesis by measuring mitochondrial mass in IS-treated HUVECs. To this end, we stained the mitochondria, cytoskeletal networks, and nuclei by using MitoTracker red, phalloidin, and DAPI, respectively. Using imaging software, we were able to quantify the mitochondrial mass relative to that of the entire cell (Figure 5(b)); increase in the number of loci of red fluorescent staining indicates increased mitochondrial mass in the cytoplasm. Our results show that mitochondrial mass was dramatically reduced in IS-treated HUVECs compared to controls and that we could counteract these effects with the addition of vitamin C or NAC.

4. Discussion

IS is a known risk factor for cardiovascular disease in CKD patients [1, 21]. Findings from the present and previous studies [3–5] supported the idea that IS can induce antiproliferative effects and ROS generation in a dose-dependent manner. ROS generation was commonly reported, along with mitochondrial depolarization and apoptosis, for example, cancer cells treatment with natural products [22–24]. Similarly, we found that IS induced mitochondrial depolarization and cell death, although the cause of death was not verified

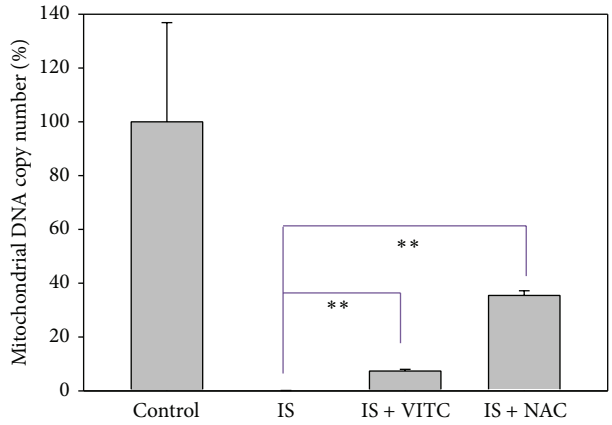

Figure 4: Role of antioxidants in IS-induced mtDNA copy number changes in HUVECs. Quantification analysis of relative mtDNA copy number (% of control) was shown. Cells were treated with IS 125 μg/mL alone as the positive control, cotreated with IS 125 μg/mL and vitamin C 200 μM or NAC 10 mM for 48 h. Cells without IS treatment were regarded as the negative control. Data, mean ± SD ($n = 2$). $^{**}P < 0.005$ compared to the IS only. VITC: vitamin C.

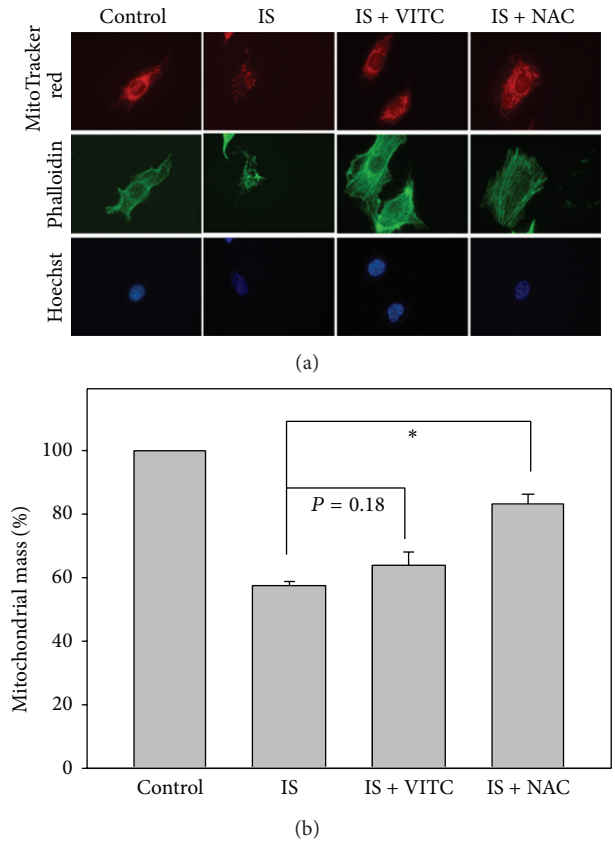

Figure 5: Role of antioxidants in IS-induced mitochondrial mass changes in HUVECs. Cells were treated with IS 125 μg/mL alone as the positive control, cotreated with IS 125 μg/mL and vitamin C 200 μM or NAC 10 mM for 48 h. Cells without IS treatment were regarded as the negative control. The fluorescent dyes and colors were MitoTracker (red), phalloidin (green), and Hoechst 33258 (blue). (a) Representative confocal microscopy. (b) Quantification analysis of relative mitochondrial mass (% of control). Data, mean ± SD ($n = 2$). $^{*}P < 0.01$ compared to the IS only.

to be apoptosis. Moreover, the sensitivity of mitochondria-based methods for cell viability detection like MTT or MTS [23, 24] is better than the crystal violet assay used in the current study. For small dosage effect of IS, the MTT/MTS assays can be considered.

Vitamin C [25] and NAC [26] are both well-known scavengers of free radicals. Interestingly, oxidative stress associated with other ROS-generating drugs such as imidacloprid [27] and melamine [28] was shown to be thwarted by treatment with vitamin C. In addition, liver carcinogenesis induced by diethylnitrosamine was mediated by ROS generation and was reversed by NAC in animal models [29]. Furthermore, pretreatment with NAC partly rescued IS-induced antiproliferative effects and nitric oxide generation in HUVECs at 48 h IS treatment [5]. In our study, we focused on the effect of IS on mitochondrial dysfunction and found that both vitamin C and NAC significantly protected HUVECs from IS-induced mitochondrial dysfunction.

The ROS production of HUVECs stimulated by IS was dose dependent. However, IS could activate NADPH oxidase (NOX) to increase ROS production [3]. It could also relate to mitochondria dysfunction. Accordingly, the origin of ROS production (NOX or mitochondria) after adding IS to HUVECs remains unclear. Using NOX inhibitors [3] or p22phox siRNA [30] for NOX and monitoring cytochrome C oxidase activity may further address this issue.

Many researchers have quantified mitochondrial biogenesis in terms of mitochondrial DNA copy number and mitochondrial mass. For example, knockdown of manganese superoxide dismutase (MnSOD) was reported to increase mtDNA copy number and mitochondrial mass in normal rat kidney cells [31], and overexpression of mitochondrial transcription factor A (TFAM) increased mtDNA copy number and preserved transformation-induced oxidative stress in lymphoblastoid cells [32]. Here, we have shown that IS reduced mtDNA copy number and mitochondrial mass in HUVECs and that these results could be reversed with the addition of vitamin C and NAC. However, some valuable assays including mtDNA deletion assay [33, 34], may offer complementary information on how much effect that IS had on mtDNA reduction. Moreover, the possible presence of the large mtDNA deletions may partly explain that IS-induced marked reduction of PCR-based mtDNA copy number to low level (Figure 4) while the IS-induced mitochondrial mass seems to maintain stable level (Figure 5).

Other antioxidants may have the potential to improve mitochondrial function and biogenesis. For example, red wine polyphenols such as resveratrol enhance mitochondrial biogenesis in coronary arterial endothelial cells via sirtuin 1 activation [20]. Interestingly, other members of the sirtuin family are linked to ROS generation [35]; sirtuin 2 overexpression induced ROS generation in non-small-cell lung cancer [36], and sirtuin 2 was reported to induce alveolar mitochondrial biogenesis in the animal model of *Staphylococcus aureus* pneumonia [37]. These findings indicate the

potential roles of ROS-signaling proteins in the regulation of mitochondrial biogenesis.

Recently, many mitochondrial biogenesis-related transcription factors have been identified. These include peroxisome proliferator-activated receptor gamma coactivator 1-alpha (PGC-1α; PPARGC1A) [38], mitochondrial transcription factors A (TFAM), B1 (TFB1M), and B2 (TFB2M) [39], nuclear respiratory factor 1 (NRF1) [40], nuclear factor, erythroid 2-like 2 (NRF2; NFE2L2) [37], and estrogen-related receptor-α (ESRRA) [41]. Further research is necessary to examine alterations in the expression of these transcription factors in IS-treated cells. This will offer better understanding of the molecular networks that are involved in helping human endothelial cells cope with IS-mediated injuries.

Conflict of Interests

The authors declare that there is no conflict of interests regarding the publication of this paper.

Acknowledgments

This work was supported by the National Science Council, Taiwan (MOST 103-2320-B-037-008); the Center of Environmental Medicine, Kaohsiung Medical University (KMU-TP103A33); the Kaohsiung Chang Gung Memorial Hospital (CMRPG850271, CMRPG850272, CMRPG850273, CMRPG890671, and CMRPG890672); the National Sun Yat-Sen University-KMU Joint Research Project (#NSYSU-KMU 103-p014); the Health and Welfare Surcharge of Tobacco Products, the Ministry of Health and Welfare, Taiwan, China (MOHW103-TD-B-111-05).

References

[1] F. C. Barreto, D. V. Barreto, S. Liabeuf et al., "Serum indoxyl sulfate is associated with vascular disease and mortality in chronic kidney disease patients," *Clinical Journal of the American Society of Nephrology*, vol. 4, no. 10, pp. 1551–1558, 2009.

[2] X. Z. Ruan, Z. Varghese, and J. F. Moorhead, "An update on the lipid nephrotoxicity hypothesis," *Nature Reviews Nephrology*, vol. 5, no. 12, pp. 713–721, 2009.

[3] L. Dou, N. Jourde-Chiche, V. Faure et al., "The uremic solute indoxyl sulfate induces oxidative stress in endothelial cells," *Journal of Thrombosis and Haemostasis*, vol. 5, no. 6, pp. 1302–1308, 2007.

[4] Z. Tumur and T. Niwa, "Indoxyl sulfate inhibits nitric oxide production and cell viability by inducing oxidative stress in vascular endothelial cells," *American Journal of Nephrology*, vol. 29, no. 6, pp. 551–557, 2009.

[5] M. Yu, Y. J. Kim, and D. H. Kang, "Indoxyl sulfate-induced endothelial dysfunction in patients with chronic kidney disease via an induction of oxidative stress," *Clinical Journal of the American Society of Nephrology*, vol. 6, no. 1, pp. 30–39, 2011.

[6] S. Owada, T. Maeba, Y. Sugano et al., "Spherical carbon adsorbent (AST-120) protects deterioration of renal function in chronic kidney disease rats through inhibition of reactive oxygen species production from mitochondria and reduction of serum lipid peroxidation," *Nephron Experimental Nephrology*, vol. 115, no. 4, pp. e101–e111, 2010.

[7] K. Shimoishi, M. Anraku, K. Kitamura et al., "An oral adsorbent, AST-120 protects against the progression of oxidative stress by reducing the accumulation of indoxyl sulfate in the systemic circulation in renal failure," *Pharmaceutical Research*, vol. 24, no. 7, pp. 1283–1289, 2007.

[8] Z. Tumur, H. Shimizu, A. Enomoto, H. Miyazaki, and T. Niwa, "Indoxyl sulfate upregulates expression of ICAM-1 and MCP-1 by oxidative stress-induced NF-κB activation," *American Journal of Nephrology*, vol. 31, no. 5, pp. 435–441, 2010.

[9] H. Shimizu, M. Yisireyili, Y. Higashiyama, F. Nishijima, and T. Niwa, "Indoxyl sulfate upregulates renal expression of ICAM-1 via production of ROS and activation of NF-κB and p53 in proximal tubular cells," *Life Sciences*, vol. 92, no. 2, pp. 143–148, 2013.

[10] Q. Chen, E. J. Vazquez, S. Moghaddas, C. L. Hoppel, and E. J. Lesnefsky, "Production of reactive oxygen species by mitochondria: central role of complex III," *Journal of Biological Chemistry*, vol. 278, no. 38, pp. 36027–36031, 2003.

[11] M. P. Murphy, "How mitochondria produce reactive oxygen species," *Biochemical Journal*, vol. 417, no. 1, pp. 1–13, 2009.

[12] R. Che, Y. Yuan, S. Huang, and A. Zhang, "Mitochondrial dysfunction in the pathophysiology of renal diseases," *American Journal of Physiology—Renal Physiology*, vol. 306, no. 4, pp. F367–F378, 2014.

[13] X. Tang, Y. X. Luo, H. Z. Chen, and D. P. Liu, "Mitochondria, endothelial cell function, and vascular diseases," *Frontiers in Physiology*, vol. 5, article 175, 2014.

[14] J. Hroudová, N. Singh, and Z. Fišar, "Mitochondrial dysfunctions in neurodegenerative diseases: relevance to alzheimer's disease," *BioMed Research International*, vol. 2014, Article ID 175062, 9 pages, 2014.

[15] W. Au, S. Pathak, C. J. Collie, and T. C. Hsu, "Cytogenetic toxicity of gentian violet and crystal violet on mammalian cells in vitro," *Mutation Research*, vol. 58, no. 2-3, pp. 269–276, 1978.

[16] C.-C. Yeh, J.-I. Yang, J.-C. Lee et al., "Anti-proliferative effect of methanolic extract of *Gracilaria tenuistipitata* on oral cancer cells involves apoptosis, DNA damage, and oxidative stress," *BMC Complementary and Alternative Medicine*, vol. 12, no. 1, article 142, 2012.

[17] J. S. Lewis-Wambi, H. R. Kim, C. Wambi et al., "Buthionine sulfoximine sensitizes antihormone-resistant human breast cancer cells to estrogen-induced apoptosis," *Breast Cancer Research*, vol. 10, no. 6, article R104, 2008.

[18] S.-W. Weng, T.-K. Lin, C.-W. Liou et al., "Peripheral blood mitochondrial DNA content and dysregulation of glucose metabolism," *Diabetes Research and Clinical Practice*, vol. 83, no. 1, pp. 94–99, 2009.

[19] C.-W. Liou, T.-K. Lin, J.-B. Chen et al., "Association between a common mitochondrial DNA D-loop polycytosine variant and alteration of mitochondrial copy number in human peripheral blood cells," *Journal of Medical Genetics*, vol. 47, no. 11, pp. 723–728, 2010.

[20] A. Csiszar, N. Labinskyy, J. T. Pinto et al., "Resveratrol induces mitochondrial biogenesis in endothelial cells," *American Journal of Physiology—Heart and Circulatory Physiology*, vol. 297, no. 1, pp. H13–H20, 2009.

[21] V. Menon, A. Gul, and M. J. Sarnak, "Cardiovascular risk factors in chronic kidney disease," *Kidney International*, vol. 68, no. 4, pp. 1413–1418, 2005.

[22] C.-Y. Yen, C.-C. Chiu, R.-W. Haung et al., "Antiproliferative effects of goniothalamin on Ca9-22 oral cancer cells

through apoptosis, DNA damage and ROS induction," *Mutation Research: Genetic Toxicology and Environmental Mutagenesis*, vol. 747, no. 2, pp. 253–258, 2012.

[23] C. C. Yeh, C. N. Tseng, J. I. Yang et al., "Antiproliferation and induction of apoptosis in Ca9-22 oral cancer cells by ethanolic extract of Gracilaria tenuistipitata," *Molecules*, vol. 17, no. 9, pp. 10916–10927, 2012.

[24] C.-C. Chiu, J.-W. Haung, F.-R. Chang et al., "Golden berry-derived 4β-hydroxywithanolide E for selectively killing oral cancer cells by generating ROS, DNA damage, and apoptotic pathways," *PLoS ONE*, vol. 8, no. 5, Article ID e64739, 2013.

[25] D. Bagchi, A. Garg, R. L. Krohn, M. Bagchi, M. X. Tran, and S. J. Stohs, "Oxygen free radical scavenging abilities of vitamins C and E, and a grape seed proanthocyanidin extract in vitro," *Research Communications in Molecular Pathology and Pharmacology*, vol. 95, no. 2, pp. 179–189, 1997.

[26] M. Zafarullah, W. Q. Li, J. Sylvester, and M. Ahmad, "Molecular mechanisms of *N*-acetylcysteine actions," *Cellular and Molecular Life Sciences*, vol. 60, no. 1, pp. 6–20, 2003.

[27] K. S. EL-Gendy, N. M. Aly, F. H. Mahmoud, A. Kenawy, and A. K. H. El-Sebae, "The role of vitamin C as antioxidant in protection of oxidative stress induced by imidacloprid," *Food and Chemical Toxicology*, vol. 48, no. 1, pp. 215–221, 2010.

[28] L. An, Z. Li, and T. Zhang, "Reversible effects of vitamins C and E combination on oxidative stress-induced apoptosis in melamine-treated PC12 cells," *Free Radical Research*, vol. 48, no. 2, pp. 239–250, 2014.

[29] H. Lin, X.-B. Liu, J.-J. Yu, F. Hua, and Z.-W. Hu, "Antioxidant N-acetylcysteine attenuates hepatocarcinogenesis by inhibiting ROS/ER stress in TLR2 deficient mouse," *PLoS ONE*, vol. 8, no. 10, Article ID e74130, 2013.

[30] J. L. Sardina, G. López-Ruano, L. I. Sánchez-Abarca et al., "P22phox-dependent NADPH oxidase activity is required for megakaryocytic differentiation," *Cell Death and Differentiation*, vol. 17, no. 12, pp. 1842–1854, 2010.

[31] A. Marine, K. J. Krager, N. Aykin-Burns, and L. A. MacMillan-Crow, "Peroxynitrite induced mitochondrial biogenesis following MnSOD knockdown in normal rat kidney (NRK) cells," *Redox Biology*, vol. 2, no. 1, pp. 348–357, 2014.

[32] S. Chakrabarty, R. R. D'Souza, S. P. Kabekkodu, P. M. Gopinath, R. Rossignol, and K. Satyamoorthy, "Upregulation of TFAM and mitochondria copy number in human lymphoblastoid cells," *Mitochondrion*, vol. 15, no. 1, pp. 52–58, 2014.

[33] Y. Kraytsberg, E. Kudryavtseva, A. C. McKee, C. Geula, N. W. Kowall, and K. Khrapko, "Mitochondrial DNA deletions are abundant and cause functional impairment in aged human substantia nigra neurons," *Nature Genetics*, vol. 38, no. 5, pp. 518–520, 2006.

[34] M. Majora, T. Wittkampf, B. Schuermann et al., "Functional consequences of mitochondrial DNA deletions in human skin fibroblasts: increased contractile strength in collagen lattices is due to oxidative stress-induced lysyl oxidase activity," *American Journal of Pathology*, vol. 175, no. 3, pp. 1019–1029, 2009.

[35] P. I. Merksamer, Y. Liu, W. He, M. D. Hirschey, D. Chen, and E. Verdin, "The sirtuins, oxidative stress and aging: an emerging link," *Aging*, vol. 5, no. 3, pp. 144–150, 2013.

[36] Z. Li, Q. R. Xie, Z. Chen, S. Lu, and W. Xia, "Regulation of SIRT2 levels for human non-small cell lung cancer therapy," *Lung Cancer*, vol. 82, no. 1, pp. 9–15, 2013.

[37] J. Athale, A. Ulrich, N. Chou MacGarvey et al., "Nrf2 promotes alveolar mitochondrial biogenesis and resolution of lung injury in Staphylococcus aureus pneumonia in mice," *Free Radical Biology and Medicine*, vol. 53, no. 8, pp. 1584–1594, 2012.

[38] R. Ventura-Clapier, A. Garnier, and V. Veksler, "Transcriptional control of mitochondrial biogenesis: the central role of PGC-1α," *Cardiovascular Research*, vol. 79, no. 2, pp. 208–217, 2008.

[39] M. Falkenberg, M. Gaspari, A. Rantanen, A. Trifunovic, N.-G. Larsson, and C. M. Gustafsson, "Mitochondrial transcription factors B1 and B2 activate transcription of human mtDNA," *Nature Genetics*, vol. 31, no. 3, pp. 289–294, 2002.

[40] V. Tiranti, E. Rossi, M. Rocchi, S. DiDonato, O. Zuffardi, and M. Zeviani, "The gene (NFE2L1) for human NRF-1, an activator involved in nuclear-mitochondrial interactions, maps to 7q32," *Genomics*, vol. 27, no. 3, pp. 555–557, 1995.

[41] S. N. Schreiber, R. Emter, M. B. Hock et al., "The estrogen-related receptor α (ERRα) functions in PPARγ coactivator 1α (PGC-1α)-induced mitochondrial biogenesis," *Proceedings of the National Academy of Sciences of the United States of America*, vol. 101, no. 17, pp. 6472–6477, 2004.

Hindawi Publishing Corporation
The Scientific World Journal
Volume 2015, Article ID 160185, 9 pages
http://dx.doi.org/10.1155/2015/160185

Research Article

Association Study between Novel CYP26 Polymorphisms and the Risk of Betel Quid-Related Malignant Oral Disorders

Shyh-Jong Wu,[1] Yun-Ju Chen,[2,3] Tien-Yu Shieh,[4] Chun-Ming Chen,[5,6] Yen-Yun Wang,[7] Kun-Tsung Lee,[8] Yueh-Ming Lin,[9] Pei-Hsuan Chien,[3] and Ping-Ho Chen[5]

[1] *Department of Medical Laboratory Science and Biotechnology, Kaohsiung Medical University, No. 100, Shih-Chuan 1st Road, Kaohsiung 80708, Taiwan*
[2] *Department of Biological Science & Technology, I-Shou University, No. 1, Section 1, Syuecheng Road, Kaohsiung 84001, Taiwan*
[3] *Department of Medical Research, E-Da Hospital, No. 1, Yida Road, Kaohsiung 82445, Taiwan*
[4] *School of Oral Hygiene, Taipei Medical University, No. 250, Wuxing Street, Taipei 11031, Taiwan*
[5] *School of Dentistry, College of Dental Medicine, Kaohsiung Medical University, No. 100, Shih-Chuan 1st Road, Kaohsiung 807, Taiwan*
[6] *Department of Oral and Maxillofacial Surgery, Kaohsiung Medical University Hospital, Kaohsiung Medical University, No. 100, Shih-Chuan 1st Road, Kaohsiung 80708, Taiwan*
[7] *Department of Clinical Research, Kaohsiung Medical University Hospital, No. 100, Shih-Chuan 1st Road, Kaohsiung 80708, Taiwan*
[8] *Department of Oral Hygiene, College of Dental Medicine, Kaohsiung Medical University, No. 100, Shih-Chuan 1st Road, Kaohsiung 80708, Taiwan*
[9] *Division of Colorectal Surgery, Department of Surgery, Kaohsiung Chang Gung Memorial Hospital and Chang Gung University College of Medicine, No. 123, Dapi Road, Kaohsiung 83301, Taiwan*

Correspondence should be addressed to Ping-Ho Chen; phchen@kmu.edu.tw

Received 13 June 2014; Accepted 26 June 2014

Academic Editor: Li-Yeh Chuang

BQ chewing may produce significant amounts of reactive oxygen species (ROS), resulting in oral mucosa damage, and ROS may be metabolized by CYP26 families. Because the CYP26 polymorphisms associated with malignant oral disorders are not well known, we conducted an association study on the associations between the single nucleotide polymorphisms (SNP) of CYP26 families and the risks of malignant oral disorders. BQ chewers with the CYP26A1 rs4411227 C/C+C/G genotype and C allele showed an increased risk of oral and pharyngeal cancer (adjusted odds ratio (aOR) = 2.30 and 1.93, respectively). The CYP26B1 rs3768647 G allele may be associated with oral and pharyngeal cancer (aOR = 3.12) and OPMDs (aOR = 2.23). Subjects with the rs9309462 CT genotype and C allele had an increased risk of oral and pharyngeal cancer (aOR = 9.24 and 8.86, respectively) and OPMDs (aOR = 8.17 and 7.87, respectively). The analysis of joint effects between the CYP26A1 rs4411227 and CYP26B1 rs3768647/rs9309462 polymorphisms revealed statistical significance (aOR = 29.91 and 10.03, respectively). Additionally, we observed a significant mRNA expression of CY26A1 and CYP26B1 in cancerous tissues compared with adjacent noncancerous tissues. Our findings suggest that novel CYP26 polymorphisms are associated with an increased risk of malignant oral disorders, particularly among BQ chewers.

1. Introduction

Approximately 600 million people chew betel quid (BQ) in the world [1], primarily in South/Southeast Asia and the South Pacific islands [2]. BQ without tobacco is an addictive and psychostimulant substance and is a group I human carcinogen, as stated in an evaluation by the International Agency for Research on Cancer (IARC) [3, 4]. Additionally, areca nut (AN) is the primary component in BQ, which has also been categorized as a group I human carcinogen by the IARC [4]. BQ usage is increasingly recognized for its association with malignant oral disorders [4–10]. The malignant oral disorders include oral potentially malignant disorders (OPMDs) (i.e., oral submucous fibrosis (OSF), leukoplakia, erythroplakia, and lichen planus) and cancers of the oral cavity and pharynx. Epidemiological studies have indicated that

BQ chewing can elevate the risk of malignant oral diseases [4–10]. A recent study found that the percentage of male BQ chewers was more than 85% among oral cancer patients [9].

A previous study suggested that chewing BQ may produce significant reactive oxygen species (ROS), such as the hydroxyl radical, which may induce the oxidative damage of oral tissue [11]. ROS are capable of inducing nucleotide modification and the generation of DNA double stranded breaks [12] and cellular 8-hydroxy-2′-deoxyguanosine (8-OH-dG) induced DNA oxidative damage [13]. In granulocyte-differentiated HL60 cells, a previous report indicated that all-trans retinoid acid (at-RA) induces NADPH oxidase-mediated ROS generation [14].

The cytochrome P450 (CYP) 26 family via oxidative metabolism to partially regulate intracellular RA compounds (such as the concentration of at-RA) affected the balance of retinoic acid (RA) in homeostasis as well as their related signal transduction [15]. RA is a vitamin A-activated metabolite that primarily regulates cell growth, differentiation, and apoptosis in the important mechanism of fetal development as well as adult life activities [16]. RA exhibits its cardioprotective effects by preventing cardiomyocyte apoptosis and ROS generation [17]. The at-RA can produce apoptosis [18] by inducing ROS formation in rat Sertoli cells [18, 19]. In granulocyte-differentiated HL60 cells, at-RA produces NADPH oxidase-mediated ROS formation [14].

In this CYP26 family, there are two major isoforms, CYP26A1 and CYP26B1, that can be induced by RA [15]. RA compounds usually control their content through a precise balancing mechanism. We speculated that BQ use would change RA metabolism via the stimulation of CYP26B1 in the oral mucosa, and the metabolism of RA is crucial for the occurrence of oral cancer [9]. This *in vivo* regulation was primarily through CYP26A1 and CYP26B1 metabolism [20], and we speculated that this regulation may be associated with ROS. Thus, the specific aim of this association study was to investigate the role of CYP26 family (CYP26A1 and CYP26B1) single nucleotide polymorphisms (SNPs) in the risk of OPMDs and oral and pharyngeal cancers.

2. Methods

2.1. Participants and Data Collection. Patients with oral/pharyngeal cancers ($N = 211$) and OPMDs ($N = 218$) were identified from the Department of Oral and Maxillofacial Surgery, Kaohsiung Medical University Hospital in Taiwan, between 2006 and 2010. Healthy controls ($N = 218$) were recruited from a community oral health survey. All volunteers signed written informed consent and provided whole blood. The study was approved by the Institutional Review Board of Kaohsiung Medical University Hospital (KMUH-IRB-970413, KMUH-IRB-950315, and KMUH-IRB-950094). The characteristics of the demographic variable and the status of substance use (such as alcohol, BQ, and cigarette use) were investigated by trained interviewers. Alcohol drinkers included current and former drinkers. Smokers included current and former smokers. Alcohol users, BQ chewers, and cigarette smokers were defined as alcoholic beverage consumption (irrespective of quantity) at least once per week for longer than 6 months, at least one quid of BQ chewed per day for longer than 6 months, and at least 10 cigarettes smoked per week for longer than 6 months, respectively. A cumulative lifetime BQ exposure (pack-years) was defined as the number of packs consumed multiplied by chewing years. One pack was defined as chewing 10 quids per day. Eight subjects with oral cancerous tissue and adjacent noncancerous oral tissue were collected during necessary surgery resection. These tissue specimens without chemotherapy or radiation therapy were analyzed. Informed consents was also signed by eight oral and pharyngeal patients.

2.2. DNA Extraction and Genotyping. Eight c.c. of peripheral blood was collected in tubes containing ethylenediaminetetraacetic acid (EDTA). Genomic DNA was extracted from the peripheral blood samples using the QIAamp DNA Mini Kit (Qiagen) according to the manufacturer's instructions. The extracted DNA samples were stored at −80°C until examination. DNA concentrations were checked via optical density at 260–280 nm (Nano Drop ND-2000; Thermo Fisher Scientific Inc.).

Single-nucleotide polymorphisms (SNPs) of CYP26A1 and CYP26B1 were selected with minor allele frequency from a public reference database in the Chinese HapMap-CHB. SNP Genotyping was performed using a Taqman Genotyping Assay according to the manufacturer's instructions. All assays and gDNA were conducted in 384-well plates, and PCR was performed. After PCR amplification, an endpoint plate read was performed using an Applied Biosystems ViiA7 Real-Time PCR System. The Sequence Detection System (SDS) Software analyzed the fluorescence measurements made during the plate read to plot fluorescence (Rn) values based on the signals from each well. The plotted fluorescence signals indicate which alleles are in each sample.

2.3. Real-Time qRT-PCR Analysis. The total RNA was extracted from oral cancerous tissues, as well as their adjacent noncancerous tissue using TRIzol (Invitrogen, Carlsbad, CA, USA) and the commercial protocol of the manufacturer as described [21]. Before further real-time qRT-PCR PCR analysis, each cDNA pool was prepared at −20°C. For real-time PCR assays, specific oligonucleotide primer pairs were purchased from Roche Universal ProbeLibrary. The reactions of real-time qRT-PCR were analyzed using the Roche LightCycler Instrument 1.5 with a LightCycler FastStart DNA Master^{PLUS} SYBR Green I kit (Roche Cat. 03 515 885 001, Castle Hill, Australia). The fold change of the expression of the target gene relative to the internal control gene GAPDH in each sample was calculated using the following formula: $2^{-\Delta\Delta Ct}$ where $\Delta Ct = Ct_{\text{target gene}} - Ct_{\text{internal control}}$ and $\Delta\Delta Ct = \Delta Ct_{\text{test sample}} - \Delta Ct_{\text{control sample}}$.

2.4. Statistical Analysis. The control genotype distribution complied with the Hardy-Weinberg equilibrium ($P \geq 0.05$). In this statistical analysis, the questionnaire data included the demographic information, substance use (alcohol, betel quid, and cigarette use), and history and disease status (normal controls, OPMDs, and oral/pharynx cancer). General linear model (GLM) analysis was used for comparing the

Table 1: Distribution of male betel quid chewers associated with characteristics of selected demographic factors.

BQ chewers	Oral and pharyngeal cancer (N = 211) N (%)[a]	OPMDs (N = 56) N (%)	Control (N = 218) N (%)	P value
Age (mean ± S.D., years)	50.12 ± 9.15	49.19 ± 11.18	43.57 ± 8.58	<0.05
Ethnicity				
Hokkien	181 (85.78)	44 (78.57)	174 (79.82)	0.20
Others	30 (14.22)	12 (21.43)	44 (20.18)	
Education (years)				
≤9	127 (60.19)	29 (51.79)	141 (64.68)	0.19
>9	84 (39.81)	27 (48.21)	77 (35.32)	
Alcohol drinking status				
Nondrinkers	68 (31.28)	16 (28.57)	55 (25.23)	0.38
Drinkers	145 (68.72)	40 (71.43)	163 (74.77)	
Age at starting drinking (mean ± S.D., years)	22.58 ± 6.89	20.14 ± 4.85	18.60 ± 4.73	<0.05
Years of alcohol drinking	24.32 ± 8.63	26.94 ± 10.23	19.21 ± 8.29	<0.05
Cigarette smoking status				
Nonsmokers	16 (7.58)	4 (7.14)	8 (3.67)	0.20
Smokers	195 (92.42)	52 (92.86)	210 (96.33)	
Age at starting smoking (mean ± S.D., years)	19.01 ± 4.06	19.35 ± 5.08	17.38 ± 9.77	0.05
Average amount of smoking (cigarette/day)	26.12 ± 14.47	27.10 ± 15.18	16.06 ± 11.03	<0.05
Years of cigarette smoking	27.89 ± 9.20	28.96 ± 9.12	26.19 ± 7.22	0.05
BQ chewing status				
Age at starting chewing (mean ± S.D., years)	22.17 ± 6.53	22.66 ± 8.23	18.99 ± 5.07	<0.05
Years of BQ chewing	21.96 ± 8.55	21.39 ± 9.44	18.60 ± 9.16	<0.05
Average amount of chewing (quids/day)	34.01 ± 35.39	34.66 ± 27.10	30.83 ± 34.99	0.59
Cumulative lifetime BQ use (pack-years)[a]	73.91 ± 73.58	69.78 ± 53.28	58.73 ± 72.09	0.10

The $P < 0.05$ indicated statistical significance, and it was calculated via the Chi-square or GLM test (post hoc was compared using the Bonferroni test). Means within each row (in capital letter) followed by the different letter are statistically significant differences (via the Bonferroni test ($P < 0.05$)).
[a]One chewed pack corresponds to 10 betel quids.

differences in the means between three groups, and post hoc comparisons were analyzed using the Bonferroni test. Using a multinomial logistic regression model to control for potential confounders, such as demographic factors (continuous age, ethnicity, and education levels) and substance use (cigarette and alcohol use), an exact P value, adjusted odds ratio (aOR), and 95% confidence interval (CI) were produced for our tables. All statistical analyses were performed using the SAS Statistical Package (Version 9.1.3, SAS Institute Inc.).

3. Results

All subjects (N = 485) were BQ chewers. Among these, 56 OPMDs patients, 211 oral and pharyngeal cancer patients, and 218 healthy controls were recruited in this case-control study. The demographic characteristics, alcohol use status, and cigarette use status are shown in Table 1. There was statistical significance in the average ages among oral and pharyngeal cancer patients, OPMDs patients, and healthy controls (50.12 ± 9.15, 49.19 ± 11.18, and 43.57 ± 8.58 years old, respectively). The distribution of ethnicity, education levels, alcohol drinking status, and cigarette smoking status showed no statistically significant differences. Oral and pharyngeal cancer patients exhibited significantly older age at drinking initiation compared with controls ($P < 0.05$). The oral and pharyngeal cancer and OPMDs patients showed a significantly higher average amount of smoking than the controls ($P < 0.05$). In terms of BQ chewing, we observed that oral and pharyngeal cancer and OPMDs patients had a significantly longer duration of chewing and older age at chewing initiation than the controls ($P < 0.05$). Additionally, oral and pharyngeal cancer and OPMDs patients had higher cumulative lifetime BQ use compared with the controls.

3.1. The Distribution of Genetic Polymorphisms between Oral and Pharyngeal Patients and Control Groups. Between the oral and pharyngeal patients and control groups, the difference in genotype frequency distribution was statistically significant for CYP26A1 rs4411227 (Table 2). After adjusting for covariates (age, ethnicity, education, alcohol drinking, and cigarette smoking), the results showed that BQ chewers with the rs4411227 C/G genotype or C/C+C/G combined

Table 2: Distribution of CYP26 families genotype and allele frequency among malignant oral disorders patients and control groups.

	Oral and pharyngeal cancer (N = 211)	OPMDs (N = 56)	Controls (N = 218)	Oral and pharyngeal cancer versus controls		OPMDs versus controls	
BQ chewers	N (%)	N (%)	N (%)	aOR (95% CI)	P	aOR (95% CI)	P
CYP26A1							
rs4411227							
Genotype							
G/G	130 (61.61)	40 (71.43)	170 (77.98)	1.00		1.00	
C/G	74 (35.07)	14 (25.00)	43 (19.72)	2.38 (1.48–3.84)[b*]	0.0004	1.39 (0.67–2.90)	0.3792
C/C	7 (3.32)	2 (3.57)	5 (2.29)	1.65 (0.46–5.95)	0.4417	0.80 (0.09–7.46)	0.8430
Combined genotype							
G/G	130 (61.61)	40 (71.43)	170 (77.98)	1.00		1.00	
C/C + C/G	81 (38.39)	16 (28.57)	48 (22.02)	2.30 (1.45–3.64)*	0.0004	1.33 (0.65–2.70)	0.4389
Allele							
G	334 (79.15)	94 (83.93)	383 (87.84)	1.00		1.00	
C	88 (20.85)	18 (16.07)	53 (12.16)	1.93 (1.30–2.88)*	0.0012	1.22 (0.65–2.29)	0.5447
CYP26B1							
rs887844							
Genotype							
G/G	115 (54.50)	25 (44.64)	133 (61.01)	1.00		1.00	
A/G	96 (45.50)	31 (55.36)	85 (38.99)	1.38 (0.91–2.09)	0.1273	1.87 (1.01–3.49)*	0.0482
Allele							
G	326 (77.25)	81 (72.32)	351 (80.50)	1.00		1.00	
A	96 (22.75)	31 (27.68)	85 (19.50)	1.26 (0.89–1.80)	0.1941	1.55 (0.93–2.57)	0.0898
rs3768647							
C/G	103 (48.82)	34 (60.71)	218 (100.00)	1.00		1.00	
G/G	108 (51.18)	22 (39.29)	0 (0.00)	—[a]		—[a]	
Allele							
C	103 (24.41)	34 (30.36)	218 (50.00)	1.00		1.00	
G	319 (75.59)	78 (69.64)	218 (50.00)	3.12 (2.28–4.27)*	<0.0001	2.23 (1.40–3.54)*	0.0007
rs9309462							
T/T	198 (93.84)	52 (92.86)	216 (99.08)	1.00		1.00	
C/T	13 (6.16)	4 (7.14)	2 (0.92)	9.24 (1.90–45.00)*	0.0059	8.17 (1.25–53.52)*	0.0285
Allele							
T	409 (96.92)	108 (96.43)	434 (99.54)	1.00		1.00	
C	13 (3.08)	4 (3.57)	2 (0.46)	8.86 (1.84–42.59)*	0.0065	7.87 (1.22–50.54)*	0.0298

aOR was adjusted by continuous age, ethnicity, education level, alcohol drinking, and cigarette smoking habits.
[a]Nonestimated: because the number of samples is equal to zero.
[b*]$P < 0.05$.

genotype had an approximately 2-fold increased risk for the development of oral and pharyngeal cancer relative to those with the G/G genotype. The subjects with the C allele had a significantly higher risk of oral and pharyngeal cancer than those in the control groups (aOR = 1.93; 95% CI = 1.30–2.88). There were no significant differences in the genotype distribution of CYP26B1 rs887844 between the oral and pharyngeal patients and the controls (P values >0.05). Compared with the control groups, the subjects with the rs3768647 G allele had a significantly higher independent risk for oral and pharyngeal cancer (aOR = 3.12; 95% CI = 2.28–4.27). After adjusting for covariates, the subjects with the rs9309462 C/T genotype (aOR = 9.24; 95% CI = 1.90–45.00) or C allele (aOR = 8.86; 95% CI = 1.84–42.59) had a significantly higher independent risk for oral and pharyngeal cancer compared with the control groups.

Table 3: Joint effects between CYP26A1 and CYP26B1 polymorphisms among malignant oral disorders patients and control groups.

		Oral and pharyngeal cancer (N = 211)	OPMDs (N = 56)	Controls (N = 218)	Oral and pharyngeal cancer versus controls	OPMDs versus controls
BQ chewers		N (%)	N (%)	N (%)	aOR (95% CI)	aOR (95% CI)
CYP26A1 rs4411227	CYP26B1 rs887844					
Allele	Allele					
G	G	272 (64.45)	75 (66.96)	298 (68.35)	1.00	
C	G	54 (12.80)	6 (5.36)	53 (12.16)	1.13 (0.72–1.76)	0.39 (0.15–1.02)
G	A	62 (14.69)	19 (16.96)	85 (19.50)	0.83 (0.56–1.23)	0.90 (0.50–1.62)
C	A	34 (8.06)	12 (10.71)	0 (0.00)	—[a]	—[a]
CYP26A1 rs4411227	CYP26B1 rs3768647					
Allele	Allele					
G	C	62 (14.69)	26 (23.21)	170 (38.99)	1.00	1.00
C	C	41 (9.72)	8 (7.14)	48 (11.01)	2.51 (1.45–4.34)[b*]	1.17 (0.48–2.82)
G	G	272 (64.45)	68 (60.71)	213 (48.85)	3.64 (2.51–5.26)*	2.14 (1.28–3.59)*
C	G	47 (11.14)	10 (8.93)	5 (1.15)	29.91 (10.75–83.23)*	11.25 (3.18–39.77)*
CYP26A1 rs4411227	CYP26B1 rs9309462					
Allele	Allele					
G	T	327 (77.49)	92 (82.14)	382 (87.61)	1.00	1.00
C	T	82 (19.43)	16 (14.29)	52 (11.93)	1.85 (1.23–2.77)*	1.07 (0.55–2.08)
G	C	7 (1.66)	2 (1.79)	1 (0.23)	9.44 (1.08–82.43)*	4.58 (0.27–77.85)
C	C	6 (1.42)	2 (1.79)	1 (0.23)	10.03 (1.05–95.60)*	12.20 (0.99–151.07)

aOR was adjusted by continuous age, ethnicity, education level, alcohol drinking, and cigarette smoking habits.
[a]Nonestimated: because the number of samples is equal to zero.
[b*]$P < 0.05$

3.2. The Distribution of Genetic Polymorphisms between the OPMDs Patients and Control Groups. There were no differences in rs4411227 polymorphism distribution between the OPMDs patients and controls (Table 2). After adjusting the covariates (age, ethnicity, education, alcohol drinking, and cigarette smoking), the subjects carrying the rs887844 A/G genotype had a marginally enhanced risk for OPMDs (aOR = 1.87; 95% CI = 1.01–3.49; P = 0.0482) compared with the G/G type. Individuals with the rs3768647 G allele had a 2.23-fold greater risk of OPMDs compared with those with the C allele (aOR = 2.23; 95% CI = 1.40–3.54). The subjects with the rs9309462 C/T genotype and C allele showed a significantly higher risk compared with the subjects with the TT and T allele genotype (aOR = 8.17; 7.87, respectively).

3.3. The Gene-Gene Joint Effects in the Risk of Oral and Pharyngeal Cancer and OPMDs. We further analyzed the gene-gene joint effects in the risk of oral and pharyngeal cancer and OPMDs (Table 3), after adjusting the covariates (age, ethnicity, education, alcohol drinking, and cigarette smoking). BQ chewers with the CYP26A1 rs4411227 C allele and CYP26B1 rs3768647 G allele had the highest risk of oral and pharyngeal cancer compared with the subjects carrying the CYP26A1 rs4411227 G allele and CYP26B1 rs3768647 C allele (aOR = 29.91; 95% CI = 10.75–83.23). Similarly, individuals carrying the CYP26A1 rs4411227 C allele and CYP26B1 rs3768647 G allele had the highest risk of OPMDs relative to the subjects carrying the CYP26A1 rs4411227 G allele and CYP26B1 rs3768647 C allele (aOR = 11.25; 95% CI = 3.18–39.77). BQ chewers with the CYP26A1 rs4411227 C allele and CYP26B1 rs9309462 C allele had the highest risk of oral and pharyngeal cancer compared with the subjects carrying the CYP26A1 rs4411227 G allele and CYP26B1 rs9309462 T allele (aOR = 10.03; 95% CI = 1.05–95.60). However, there were no significant differences on gene-gene joint effects between the presence of the CYP26A1 rs4411227 and CYP26B1 rs9309462 genetic variations regarding the risk of OPMDs.

3.4. The CYP26A1 and CYP26B1 mRNA Expression of Oral Paired Tissue and Adjacent Noncancerous Tissues. We investigated CYP26A1 and CYP26B1 quantitative mRNA in expression in eight patients (numbers 1, 2, 3, 4, 5, 6, 7, and 8) (Figure 1). Compared with their adjacent noncancerous tissues, tumor tissues exhibited the consistent downregulation mRNA of CYP26A1 and CYP26B1 in patients number 2, 3, 5, and 6 (expression >2-fold change in numbers 2, 3, and 5). In patients number 1 and 8, the upregulation of the expression of CYP26A1 and CYP26B1in cancerous tissue was observed, compared with their adjacent noncancerous tissues. In the cancer tissue of number 4, a slightly decreased expression of CYP26A1 and increased expression of CYP26B1 were found.

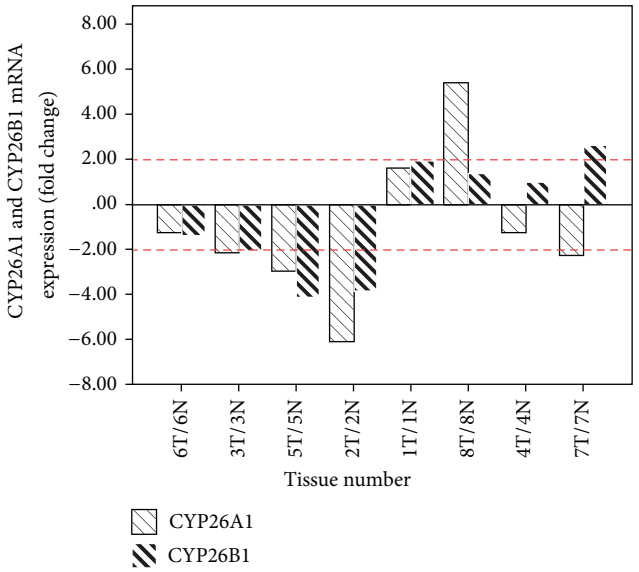

Figure 1: The induced mRNA of CYP26A1 and CYP26B1 in human oral cancer tissue (T) and its adjacent normal tissue (N). Paired tissue samples (tumor and adjacent normal tissue) without chemotherapy/radiation therapy were analyzed. Compared with human adjacent tissue ($N = 8$), the relative fold change was calculated in triplicate (columns, mean; bars, SD) using the formula $2^{-\Delta\Delta Ct}$.

CYP26A1 expression was lower in the cancer tissue of number 7 compared with its adjacent tissue, but the expression of CYP26B1 was higher in the cancer tissue than in the adjacent tissue.

4. Discussion

The International Agency for Research on Cancer (IARC) has indicated that betel quid without tobacco can cause oral cancer and has stated that, in experimental animals, there is sufficient evidence to establish the carcinogenicity of the areca nut; there is limited evidence for the carcinogenicity of arecoline [4]. The areca nut (AN) is a major ingredient of BQ, and arecoline is the most abundant AN alkaloid. In detoxifying AN or arecoline, two monooxygenase systems (cytochrome P450 and flavin-containing monooxygenases) are implicated in phase I metabolism [22]. A previous report indicated that the monooxygenase activity of CYP26B1 may be involved in the detoxification process of BQ chewing [22]. Furthermore, CYP26B1 has been demonstrated to participate in the metabolism of at-RA and has been indicated to play a major role in the protection of specific tissues for at-RA exposure [23]. A recent study demonstrated that the retinoic acid-metabolizing enzymes CYP26A1 and CYP26B1 are significantly overexpressed in colorectal cancer tissue [24].

This is the first study to indicate that the mRNA expression of CYP26 families (CYP26A1 and CYP26B1) and their SNP variants play a novel role in the occurrence or developmental mechanism of malignant oral disorders. In our analysis, we evaluated the risk effect of CYP polymorphisms among BQ chewers. These findings showed that BQ chewers with CYP26A1 risk polymorphism (rs4411227) may enhance the risk of oral and pharyngeal cancer. Also, subjects carrying CYP26B1 risk polymorphism (rs3768647/rs9309462) have an increased susceptibility to oral malignant disorders. The CYP26A1 rs4411227 and CYP26B1 rs3768647/rs9309462 may have significant joint effects in the risk of oral malignant disorders (particularly in oral and pharyngeal patients) among BQ chewers. To rule out differences in gene expression between different individuals, we collected paired oral tissues to observe the significant expression of CYP26A1 and CYP26B1. Overall, these findings seem to have strengths on the role of CYP26A1 and CYP26B1 in the etiology of oral malignant disorders.

4.1. The Susceptible Metabolic CYP26B1 Gene. The CYP26B1 gene is located on chromosome 2p13.2 and covers a total of eighteen thousand base pairs. After transcription, the CYP26B1 gene formed 6 exons and 8.57 kb introns and included an approximately 3 kb long untranslated $3'$ region [25, 26]. It is also a single-oxygenase enzyme (monooxygenase) that catalyzes many reactions, such as those involving drug metabolism and the synthesis of hormones, cholesterol, and lipids. However, the catalytic function of CYP26B1 can catalyze at-RA into a hydroxylated form; this also refers to the process of the oxidation of RA through the added oxygen in number 4 seat of the carbon skeleton, subsequently metabolizing RA into the polar and inactive form (such as 4-oxo-,4-OH-,5,6-epoxy and 18-OH-all-trans-retinoic acid) to activate it [27] while not affecting the cell physiology. A previous report suggested that CYP26B1 appears to be necessary in the physiological role of RA catabolism, whereas CYP26A1 played an important role given excessive RA in the cells [28].

4.2. The Susceptible Metabolic CYP26A1 Gene. CYP26A1 is located on chromosome 10q23-q24 [29]. CYP26A1 and CYP26B1 are at-RA hydroxylases that are responsible for the catalytic formation of similar metabolites in a cellular system; there is only 40% similarity among the CYP26A1 gene sequence and CYP26B1 gene sequence [30]. CYP26A1 is a hydroxylation enzyme for the major metabolism of RA and transforms RA into an inactive RA hydroxy derivative [31, 32]. CYP26A1 has high specificity for at-RA and oxidation RA to form 4-OH-RA, 18-OH-RA, and 4-oxo-RA [33]. Scholars found that CYP26A1 had a higher catalytic ability compared with CYP26B1 and that CYP26A1 was primarily responsible for the metabolism of at-RA and provides a protective barrier to avoid at-RA overexposure [30]. CYP26A1 may be associated with the metabolism of RA in human epidermal keratinocytes [28]. A previous report indicated that, in long term sunlight-damaged skin cells and in the increased expression of RA-metabolizing enzymes, CYP26A1 may cause a deficiency of vitamin A, which could potentially lead to the malignant transformation of keratinocytes in the early development of skin cancer [34].

A review article indicated that the inhibition of CYP26A1 expression reduces tumorigenicity through the use of RA metabolism blocking agents (RAMBAs) [15]. Previous studies demonstrated that an increased expression of CYP26A1 was found in human familial adenomatous polyposis adenomas,

sporadic colon cancers, and primary ovarian cancer [20, 35]. A report noted that RA can induce CYP26A1 expression in neuroblastoma, breast cancer, and lung cancer cell lines [36]. In breast cancer or colon cancer cells, CYP26A1 gene expression can be induced via the receptor of vitamin A [37]. In breast epithelial adenocarcinoma tissue cultures, head and neck squamous cell carcinoma cells, and acute promyelocytic leukemia (acute promyelocytic leukemia) cells, an increased expression of CYP26A1 and increased catabolic activity of RA can be detected [38–40].

Additionally, 42% (27/65) of tissue samples removed from breast cancer patients had CYP26A1 overexpression; CYP26A1 overexpression may induce intracellular RA consumption, thus pushing the cells toward tumorigenicity; CYP26A1 may be recommended as a candidate oncogene [41]. Researchers found that some CYP450 genes (e.g., CYP26A1) in primary ovarian cancer have significantly higher expressions compared with normal ovarian tissues [35]. Additionally, CYP26A1 overexpression in Barrett's esophagus adenocarcinoma may cause the consumption of intracellular vitamin A acid [42], whereas other reports found that the expression of CYP26A1 is lower in normal human epidermal cells [43, 44]. After RA treatment, at-RA turnover rates are approximately 18-fold higher in squamous head and neck cancer cell lines compared with normal oral keratinocytes; 4-oxo-RA and 4-hydroxy-RA are also generated in the former. Two squamous head and neck cancer cell lines have increased expressions of CYP26 A1 mRNA and showed the highest metabolism of RA [33]. In head and neck cancer patients, the adjacent normal oral keratinocytes showed a 15-fold higher normal oral keratinocyte turnover rate compared with noncancer patients [45]. The above results suggest that RA metabolism potentially played a role in the development of oral cancer. Similarly, recent studies indicated that the increased expression of CYP26A1 genes was related to head and neck cancer [33]. This study also suggested that increasing concentrations of endogenous RA and CYP26A1 inhibitors will be applied in the future treatment of cancer or novel therapies for skin diseases [15, 46].

4.3. Retinoic Acid (RA) and Cancer Development. Previous studies reported that the damage of normal RA homeostasis signaling was associated with the development of cancer [47]. The damage to normal RA signaling may be due to the decreased expression of the RA receptor, the decreased transcriptional response of the RA target gene, and increased RA metabolism [48]. Since 1920, vitamin A deficiency has been associated with cell carcinogenesis [49]. Vitamin A deficiency may be associated with increased susceptibility to cancer, and low amounts of vitamin A intake may increase the risk of human cancer [50].

Research data indicated that increased RA compound intake can reduce different varieties of squamous cell carcinoma (such as oral cancer, lung cancer, pharynx cancer, cervical cancer, and bladder cancer); therefore, the deficiency of RA ingestion may result in excessive cell proliferation (hyperplasia) and hyperkeratosis and cause carcinogenesis in oral cavity cells [51]. RA compounds and their isomers can be applied to treat or prevent cancer and skin diseases [48]. A series of intervention studies has indicated that vitamin A can effectively reduce the remission of betel chewers with oral leukoplakia and that it suppressed the occurrence of new oral lesions [52–54]. Previous studies recommended the use of RA treatment for the remission of malignant transformation among BQ chewers with OPMDs; this mechanism may be due to the inhibition of BQ compounds promoting carcinogenesis rather than to them inhibiting the initiation of carcinogenesis development [52, 54, 55]. Additionally, a review article suggested that the inhibition of CYP26 enzyme activity could help to increase the half-life of RA and would be clinically effective for future applications.

CYP polymorphisms related ROS provide important insight into the importance of clinical diagnostic tools (e.g., screen test of SNP) in BQ chewers for the prevention of malignant oral disorders [56]. The study limitations were a smaller sample size for evaluation of mRNA expression and lack of phenotype information among patients. In the future research, we will collect sufficient samples to confirm expression of CYP26A1 and CYP26 B1 in betel quid-related malignant oral disorders.

In conclusion, this study suggested that BQ chewers with ROS related to CYP26A1 and CYP26B1 polymorphisms are associated with an increased risk of oral and pharyngeal cancer and OPMDs. Our findings may be useful in identifying subjects who are at an increased risk for the development of oral malignant disorders.

Conflict of Interests

The authors declare that there is no conflict of interests regarding the publication of this paper.

Authors' Contribution

Shyh-Jong Wu and Yun-Ju Chen equally contributed to this work.

Acknowledgments

This study was supported by Chi-Mei Medical Center and Kaohsiung Medical University Research Foundation Grants (100CM-KMU-13 and 101CM-KMU-12), a NSC Grant from the Ministry of Science and Technology Grant (NSC 102-2314-B-037-073-), I-Shou University Grant (ISU-103-04-07A), and the Health and Welfare Surcharge of Tobacco Products Grant, the Ministry of Health and Welfare, Taiwan (MOHW103-TD-B-111-05).

References

[1] B. J. Boucher and N. Mannan, "Metabolic effects of the consumption of *Areca catechu*," *Addiction Biology*, vol. 7, no. 1, pp. 103–110, 2002.

[2] P. C. Gupta and S. Warnakulasuriya, "Global epidemiology of areca nut usage," *Addiction Biology*, vol. 7, no. 1, pp. 77–83, 2002.

[3] A. R. Winstock, C. R. Trivedy, K. A. A. S. Warnakulasuriya, and T. J. Peters, "A dependency syndrome related to areca nut use: some medical and psychological aspects among areca nut users

in the Gujarat community in the UK," *Addiction Biology*, vol. 5, no. 2, pp. 173–179, 2000.

[4] IARC, *Betel-Quid and Areca-Nut Chewing and Some Areca-Nut-Derived Nitrosamines*, vol. 85 of *IARC Monographs on the Evaluation of Carcinogenic Risks to Humans*, 2004.

[5] Y. C. Ko, Y. L. Huang, C. H. Lee et al., "Betel quid chewing, cigarette smoking and alcohol consumption related to oral cancer in Taiwan," *Journal of Oral Pathology and Medicine*, vol. 24, no. 10, pp. 450–453, 1995.

[6] C. H. Lee, Y. C. Ko, H. L. Huang et al., "The precancer risk of betel quid chewing, tobacco use and alcohol consumption in oral leukoplakia and oral submucous fibrosis in southern Taiwan," *The British Journal of Cancer*, vol. 88, no. 3, pp. 366–372, 2003.

[7] K. W. Lee, W. R. Kuo, S. M. Tsai et al., "Different impact from betel quid, alcohol and cigarette: risk factors for pharyngeal and laryngeal cancer," *International Journal of Cancer*, vol. 117, no. 5, pp. 831–836, 2005.

[8] S. L. Chiang, P. H. Chen, C. H. Lee et al., "Up-regulation of inflammatory signalings by areca nut extract and role of cyclooxygenase-2 -119G>a polymorphism reveal risk of oral cancer," *Cancer Research*, vol. 68, no. 20, pp. 8489–8498, 2008.

[9] P. H. Chen, K. W. Lee, C. H. Chen et al., "CYP26B1 is a novel candidate gene for betel quid-related oral squamous cell carcinoma," *Oral Oncology*, vol. 47, no. 7, pp. 594–600, 2011.

[10] C. Y. Yen, S. Y. Liu, C. H. Chen et al., "Combinational polymorphisms of four DNA repair genes XRCC1, XRCC2, XRCC3, and XRCC4 and their association with oral cancer in Taiwan," *Journal of Oral Pathology and Medicine*, vol. 37, no. 5, pp. 271–277, 2008.

[11] P. H. Chen, C. C. Tsai, Y. C. Lin et al., "Ingredients contribute to variation in production of reactive oxygen species by areca quid," *Journal of Toxicology and Environmental Health A: Current Issues*, vol. 69, no. 11, pp. 1055–1069, 2006.

[12] C. C. Chiu, J. W. Haung, F. R. Chang et al., "Golden berry-derived 4β-hydroxywithanolide e for selectively killing oral cancer cells by generating ROS, DNA damage, and apoptotic pathways," *PLoS ONE*, vol. 8, no. 5, Article ID e64739, 2013.

[13] T. Y. Liu, C. L. Chen, and C. W. Chi, "Oxidative damage to DNA induced by areca nut extract," *Mutation Research*, vol. 367, no. 1, pp. 25–31, 1996.

[14] C. Y. Wang, T. T. Yang, C. L. Chen, W. C. Lin, and C. F. Lin, "Reactive oxygen species-regulated glycogen synthase kinase-3beta activation contributes to all-trans retinoic acid-induced apoptosis in granulocyte-differentiated HL60 cells," *Biochemical Pharmacology*, vol. 88, no. 1, pp. 86–94, 2014.

[15] A. C. Ross and R. Zolfaghari, "Cytochrome P450s in the regulation of cellular retinoic acid metabolism," *Annual Review of Nutrition*, vol. 31, pp. 65–87, 2011.

[16] T. R. J. Evans and S. B. Kaye, "Retinoids: present role and future potential," *British Journal of Cancer*, vol. 80, no. 1-2, pp. 1–8, 1999.

[17] R. S. Guleria, R. Choudhary, T. Tanaka, K. M. Baker, and J. Pan, "Retinoic acid receptor-mediated signaling protects cardiomyocytes from hyperglycemia induced apoptosis: role of the renin-angiotensin system," *Journal of Cellular Physiology*, vol. 226, no. 5, pp. 1292–1307, 2011.

[18] M. L. Conte da Frota Jr., E. Gomes da Silva, G. A. Behr et al., "All-trans retinoic acid induces free radical generation and modulate antioxidant enzyme activities in rat sertoli cells," *Molecular and Cellular Biochemistry*, vol. 285, no. 1-2, pp. 173–179, 2006.

[19] N. Hail Jr., H. J. Kim, and R. Lotan, "Mechanisms of fenretinide-induced apoptosis," *Apoptosis*, vol. 11, no. 10, pp. 1677–1694, 2006.

[20] D. N. Shelton, I. T. Sandoval, A. Eisinger et al., "Up-regulation of CYP26A1 in adenomatous polyposis coli-deficient vertebrates via a WNT-dependent mechanism: implications for intestinal cell differentiation and colon tumor development," *Cancer Research*, vol. 66, no. 15, pp. 7571–7577, 2006.

[21] C. Y. Yen, C. H. Chen, C. H. Chang et al., "Matrix metalloproteinases (MMP) 1 and MMP10 but not MMP12 are potential oral cancer markers," *Biomarkers*, vol. 14, no. 4, pp. 244–249, 2009.

[22] S. L. Chiang, S. S. Jiang, Y. J. Wang et al., "Characterization of arecoline-induced effects on cytotoxicity in normal human gingival fibroblasts by global gene expression profiling," *Toxicological Sciences*, vol. 100, no. 1, pp. 66–74, 2007.

[23] J. A. White, H. Ramshaw, M. Taimi et al., "Identification of the human cytochrome P450, P450RAI-2, which is predominantly expressed in the adult cerebellum and is responsible for all-trans-retinoic acid metabolism," *Proceedings of the National Academy of Sciences of the United States of America*, vol. 97, no. 12, pp. 6403–6408, 2000.

[24] G. T. Brown, B. G. Cash, D. Blihoghe et al., "The expression and prognostic significance of retinoic acid metabolising enzymes in colorectal cancer," *PLoS ONE*, vol. 9, no. 3, Article ID e90776, 2014.

[25] Y. Yamamoto, R. Zolfaghari, and A. C. Ross, "Regulation of CYP26 (cytochrome P450RAI) mRNA expression and retinoic acid metabolism by retinoids and dietary vitamin A in liver of mice and rats," *The FASEB Journal*, vol. 14, no. 13, pp. 2119–2127, 2000.

[26] D. R. Nelson, "A second CYP26 P450 in humans and zebrafish: CYP26B1," *Archives of Biochemistry and Biophysics*, vol. 371, no. 2, pp. 345–347, 1999.

[27] J. Marill, T. Cresteil, M. Lanotte, and G. G. Chabot, "Identification of human cytochrome P450s involved in the formation of all-trans-retinoic acid principal metabolites," *Molecular Pharmacology*, vol. 58, no. 6, pp. 1341–1348, 2000.

[28] E. Pavez Loriè, H. Li, A. Vahlquist, and H. Törmä, "The involvement of cytochrome p450 (CYP) 26 in the retinoic acid metabolism of human epidermal keratinocytes," *Biochimica et Biophysica Acta—Molecular and Cell Biology of Lipids*, vol. 1791, no. 3, pp. 220–228, 2009.

[29] J. A. White, B. Beckett, S. W. Scherer, J. Herbrick, and M. Petkovich, "P450RAI (CYP26A1) maps to human chromosome 10q23-q24 and mouse chromosome 19C2-3," *Genomics*, vol. 48, no. 2, pp. 270–272, 1998.

[30] A. R. Topletz, J. E. Thatcher, A. Zelter et al., "Comparison of the function and expression of CYP26A1 and CYP26B1, the two retinoic acid hydroxylases," *Biochemical Pharmacology*, vol. 83, no. 1, pp. 149–163, 2012.

[31] J. D. Lutz, V. Dixit, C. K. Yeung et al., "Expression and functional characterization of cytochrome P450 26A1, a retinoic acid hydroxylase," *Biochemical Pharmacology*, vol. 77, no. 2, pp. 258–268, 2009.

[32] K. Niederreither, S. Abu-Abed, B. Schuhbaur, M. Petkovich, P. Chambon, and P. Dollé, "Genetic evidence that oxidative derivatives of retinoic acid are not involved in retinoid signaling during mouse development," *Nature Genetics*, vol. 31, no. 1, pp. 84–88, 2002.

[33] I. Klaassen, R. H. Brakenhoff, S. J. Smeets, G. B. Snow, and B. J. M. Braakhuis, "Enhanced turnover of all-trans-retinoic

acid and increased formation of polar metabolites in head and neck squamous cell carcinoma lines compared with normal oral keratinocytes," *Clinical Cancer Research*, vol. 7, no. 4, pp. 1017–1025, 2001.

[34] M. Osanai and G.-H. Lee, "Enhanced expression of retinoic acid-metabolizing enzyme CYP26A1 in sunlight-damaged human skin," *Medical Molecular Morphology*, vol. 44, no. 4, pp. 200–206, 2011.

[35] D. Downie, M. C. E. McFadyen, P. H. Rooney et al., "Profiling cytochrome P450 expression in ovarian cancer: identification of prognostic markers," *Clinical Cancer Research*, vol. 11, no. 20, pp. 7369–7375, 2005.

[36] T. Liu, A. Bohlken, S. Kuljaca et al., "The retinoid anticancer signal: mechanisms of target gene regulation," *British Journal of Cancer*, vol. 93, no. 3, pp. 310–318, 2005.

[37] E. Sonneveld, C. E. van den Brink, B. M. van der Leede et al., "Human retinoic acid (RA) 4-hydroxylase (CYP26) is highly specific for all-trans-RA and can be induced through RA receptors in human breast and colon carcinoma cells," *Cell Growth and Differentiation*, vol. 9, no. 8, pp. 629–637, 1998.

[38] J. van Heusden, W. Wouters, F. C. S. Ramaekers et al., "The antiproliferative activity of all-trans-retinoic acid catabolites and isomers is differentially modulated by liarozole-fumarate in MCF-7 human breast cancer cells," *The British Journal of Cancer*, vol. 77, no. 8, pp. 1229–1235, 1998.

[39] I. Klaassen, R. H. Brakenhoff, S. J. Smeets, G. B. Snow, and B. J. M. Braakhuis, "Metabolism and growth inhibition of four retinoids in head and neck squamous normal and malignant cells," *British Journal of Cancer*, vol. 85, no. 4, pp. 630–635, 2001.

[40] C. R. Larsen, P. B. Hansen, and N. T. Clausen, "all-trans-retinoic acid-induced expression and regulation of retinoic acid 4-hydroxylase (CYP26) in human promyelocytic leukemia," *The American Journal of Hematology*, vol. 70, no. 1, pp. 39–47, 2002.

[41] M. Osanai, N. Sawada, and G. H. Lee, "Oncogenic and cell survival properties of the retinoic acid metabolizing enzyme, CYP26A1," *Oncogene*, vol. 29, no. 8, pp. 1135–1144, 2010.

[42] C. L. Chang, E. Hong, P. Lao-Sirieix, and R. C. Fitzgerald, "A novel role for the retinoic acid-catabolizing enzyme CYP26A1 in Barrett's associated adenocarcinoma," *Oncogene*, vol. 27, no. 21, pp. 2951–2960, 2008.

[43] R. Heise, J. Mey, M. M. Neis et al., "Skin retinoid concentrations are modulated by CYP26AI expression restricted to basal keratinocytes in normal human skin and differentiated 3D skin models," *Journal of Investigative Dermatology*, vol. 126, no. 11, pp. 2473–2480, 2006.

[44] C. Popa, A. J. Dicker, A. L. Dahler, and N. A. Saunders, "Cytochrome P450, CYP26AI, is expressed at low levels in human epidermal keratinocytes and is not retinoic acid-inducible," *The British Journal of Dermatology*, vol. 141, no. 3, pp. 460–468, 1999.

[45] I. Klaassen, J. Cloos, S. J. Smeets et al., "Nonmalignant oral keratinocytes from patients with head and neck squamous cell carcinoma show enhanced metabolism of retinoic acid," *Oncology*, vol. 63, no. 1, pp. 56–63, 2002.

[46] C. H. Nelson, B. R. Buttrick, and N. Isoherranen, "Therapeutic potential of the inhibition of the retinoic acid hydroxylases CYP26A1 and CYP26B1 by xenobiotics," *Current Topics in Medicinal Chemistry*, vol. 13, no. 12, pp. 1402–1428, 2013.

[47] S. Y. Sun and R. Lotan, "Retinoids and their receptors in cancer development and chemoprevention," *Critical Reviews in Oncology/Hematology*, vol. 41, no. 1, pp. 41–55, 2002.

[48] S. J. Freemantle, M. J. Spinella, and E. Dmitrovsky, "Retinoids in cancer therapy and chemoprevention: promise meets resistance," *Oncogene*, vol. 22, no. 47, pp. 7305–7315, 2003.

[49] S. B. Wolbach and P. R. Howe, "Tissue changes following deprivation of fat-soluble a vitamin," *The Journal of Experimental Medicine*, vol. 42, no. 6, pp. 753–777, 1925.

[50] N. Wald, M. Idle, J. Boreham, and A. Bailey, "Low serum-vitamin-A and subsequent risk of cancer. Preliminary results of a prospective study," *The Lancet*, vol. 2, no. 8199, pp. 813–815, 1980.

[51] S. Graham, "Epidemiology of retinoids and cancer," *Journal of the National Cancer Institute*, vol. 73, no. 6, pp. 1423–1428, 1984.

[52] H. F. Stich, A. P. Hornby, B. Mathew, R. Sankaranarayanan, and M. K. Nair, "Response of oral leukoplakias to the administration of vitamin A," *Cancer Letters*, vol. 40, no. 1, pp. 93–101, 1988.

[53] H. F. Stich, B. Mathew, R. Sankaranarayanan, and M. K. Nair, "Remission of oral precancerous lesions of tobacco/areca nut chewers following administration of beta-carotene or vitamin A, and maintenance of the protective effect," *Cancer Detection and Prevention*, vol. 15, no. 2, pp. 93–98, 1991.

[54] H. F. Stich, M. P. Rosin, A. P. Hornby, B. Mathew, R. Sankaranarayanan, and M. K. Nair, "Remission of oral leukoplakias and micronuclei in tobacco/betel quid chewers treated with beta-carotene and with beta-carotene plus vitamin A," *International Journal of Cancer*, vol. 42, no. 2, pp. 195–199, 1988.

[55] H. F. Stich and S. S. Tsang, "Promoting activity of betel quid ingredients and their inhibition by retinol," *Cancer Letters*, vol. 45, no. 1, pp. 71–77, 1989.

[56] C. Y. Lin, T. S. Pan, C. C. Ting et al., "Cytochrome P450 metabolism of betel quid-derived compounds: implications for the development of prevention strategies for oral and pharyngeal cancers," *The Scientific World Journal*, vol. 2013, Article ID 618032, 11 pages, 2013.

Hindawi Publishing Corporation
The Scientific World Journal
Volume 2014, Article ID 183548, 8 pages
http://dx.doi.org/10.1155/2014/183548

Research Article

The Influence of Monoamine Oxidase Variants on the Risk of Betel Quid-Associated Oral and Pharyngeal Cancer

Ping-Ho Chen,[1,2,3] Bin Huang,[4,5] Tien-Yu Shieh,[3,6] Yan-Hsiung Wang,[1,7] Yuk-Kwan Chen,[1,8] Ju-Hui Wu,[9,10] Jhen-Hao Huang,[11] Chun-Chia Chen,[12,13] and Ka-Wo Lee[14,15]

[1] *School of Dentistry, College of Dental Medicine, Kaohsiung Medical University, No. 100 Shih-Chuan 1st Road, Kaohsiung 80708, Taiwan*
[2] *Cancer Center, Kaohsiung Medical University Hospital, Kaohsiung Medical University, No. 100 Shih-Chuan 1st Road, Kaohsiung 80708, Taiwan*
[3] *Global Center of Excellence for Oral Health Research and Development, No. 100 Shih-Chuan 1st Road, Kaohsiung 80708, Taiwan*
[4] *Department of Biomedical Science and Environmental Biology, College of Life Science, Kaohsiung Medical University, No. 100 Shih-Chuan 1st Road, Kaohsiung 80708, Taiwan*
[5] *Department of Biological Sciences, National Sun Yat-sen University, No. 70 Lienhai Road, Kaohsiung 80424, Taiwan*
[6] *School of Oral Hygiene, Taipei Medical University, No. 250 Wuxing Street, Taipei 11031, Taiwan*
[7] *Orthopaedic Research Center, College of Medicine, Kaohsiung Medical University, No. 100 Shih-Chuan 1st Road, Kaohsiung 80708, Taiwan*
[8] *Division of Oral Pathology & Diagnosis, Department of Dentistry, Kaohsiung Medical University Hospital, No. 100 Shih-Chuan 1st Road, Kaohsiung 80708, Taiwan*
[9] *Department of Oral Hygiene, College of Dental Medicine, Kaohsiung Medical University, No. 100 Shih-Chuan 1st Road, Kaohsiung 80708, Taiwan*
[10] *Department of Dentistry, Kaohsiung Medical University Hospital, No. 100 Shih-Chuan 1st Road, Kaohsiung 80708, Taiwan*
[11] *Institute of Biomedical Sciences, National Sun Yat-sen University, No. 70 Lienhai Road, Kaohsiung 80424, Taiwan*
[12] *Division of Traumatology & Plastic Surgery, Department of Surgery, Chi Mei Medical Center, No. 901 Zhonghua Road, Yongkang District, Tainan 710, Taiwan*
[13] *Institute of Imaging and Biomedical Photonics, College of Photonics, National Chiao Tung University, 1001 University Road, Hsinchu 30010, Taiwan*
[14] *Department of Otolaryngology, Kaohsiung Medical University Hospital, No. 100 Shih-Chuan 1st Road, Kaohsiung 807, Taiwan*
[15] *Department of Otolaryngology, College of Medicine, Kaohsiung Medical University, No. 100 Shih-Chuan 1st Road, Kaohsiung 80708, Taiwan*

Correspondence should be addressed to Chun-Chia Chen; chen.jica@msa.hinet.net and Ka-Wo Lee; kawolee@cc.kmu.edu.tw

Received 5 June 2014; Revised 26 June 2014; Accepted 26 June 2014; Published 15 October 2014

Academic Editor: Hsueh-Wei Chang

Betel quid (BQ) and areca nut (AN) (major BQ ingredient) are group I human carcinogens illustrated by International Agency for Research on Cancer and are closely associated with an elevated risk of oral potentially malignant disorders (OPMDs) and cancers of the oral cavity and pharynx. The primary alkaloid of AN, arecoline, can be metabolized *via* the monoamine oxidase (MAO) gene by inducing reactive oxygen species (ROS). The aim of this study was to investigate whether the variants of the susceptible candidate MAO genes are associated with OPMDs and oral and pharyngeal cancer. A significant trend of MAO-A mRNA expression was found in *in vitro* studies. Using paired human tissues, we confirmed the significantly decreased expression of MAO-A and MAO-B in cancerous tissues when compared with adjacent noncancerous tissues. Moreover, we determined that MAO-A single nucleotide polymorphism variants are significantly linked with oral and pharyngeal cancer patients in comparison to OPMDs patients [rs5953210 risk G-allele, odds ratio = 1.76; 95% confidence interval = 1.02-3.01]. In conclusion, we suggested that susceptible MAO family variants associated with oral and pharyngeal cancer may be implicated in the modulation of MAO gene activity associated with ROS.

1. Introduction

Oral and pharyngeal cancer is one of the most prevalent cancers in the world. In Taiwan, cancers of the oral cavity and pharynx were the fourth most prevalent cancers among males [1]. In 2010, the age-standardized incidence rate was estimated to be 40.56 per 100,000 persons (adjusted by the world population in 2000) for oral and pharyngeal cancer in Taiwanese males [1]. Also, the age-standardized mortality rate of males for oral and pharyngeal cancer in 2010 was 14.71 per 100,000, which leads to oral and pharyngeal cancer being ranked as the fourth leading cause of death due to cancer. Several studies suggested that betel quid (BQ) use may increase the risk of cancers of the oral cavity and pharynx and of oral potentially malignant disorders (OPMDs), including erythroplakia, leukoplakia, lichen planus, and oral submucous fibrosis (OSF) [2–4]. In addition, malignant transformation of OPMDs can result in the occurrence of oral and pharyngeal cancer [5].

There are approximately 600 million BQ chewers in the world [6]. Following nicotine, alcohol, and caffeine, BQ chewing is the fourth most frequently used addictive and psychoactive substance in the world [7]. BQ and AN (the major ingredients in various methods of BQ chewing) have been evaluated as group I carcinogens for humans by the International Agency for Research on Cancer [2]. In mammalian cells, arecoline was major alkaloid in AN, and it can induce cytotoxicity [8–10]. In human endothelial cells, the effects of cell cycle arrest, cytotoxicity, and apoptosis could be induced by arecoline treatment [11]. Arecoline is the major compound among the AN alkaloids, and it may be metabolized by MAO gene *via* xenobiotic metabolism, which is involved in phase I biotransformation [12]. AN extract or arecoline induces cell necrosis through increasing reactive oxygen species (ROS) [13] and ROS may be produced by MAO catalysis [14]. Microarray analysis screening data indicated that 100 μg/mL arecoline treatment in a commercial normal human gingival fibroblast (HGF) cell line may induce MAO-A gene expression [12]. Therefore, we assume that the MAO-A gene may be associated with arecoline induction in oral cells and may be implicated in the occurrence or development of oral and pharyngeal cancer. To the best of our knowledge, no study has examined the correlation between the MAO gene variations and oral and pharyngeal cancer or OPMDs. The specific aim of this paper was to investigate whether susceptible MAO genes are associated with oral and pharyngeal cancer and OPMDs.

2. Materials and Methods

2.1. Study Subjects. This study was approved by the Ethical Review Committee of the Institutional Review Board (IRB) of Kaohsiung Medical University (KMU) Chung-Ho Memorial Hospital (KMUH-IRB-950094, KMUH-IRB-950315, and KMUH-IRB-970413). A total of 260 male patients diagnosed with oral and pharyngeal cancer and 68 male patients diagnosed with OPMDs participated in the study. Males with oral and pharyngeal cancer or OPMDs were selected from the Department of Otolaryngology and Division of Oral and Maxillofacial Surgery, Department of Dentistry at KMU Hospital. In this study, all participants agreed to undersign a written informed consent. All cases of oral cancer or OPMDs were histologically confirmed by pathologists or surgeons. By signing the informed consent, all subjects agreed to answer a questionnaire administered by trained interviewers and to provide blood samples for experimental analysis. Additionally, the informed consent permitted the collection of oral cancerous tissue and noncancerous adjacent oral tissue (a safe margin) from cancer patients during necessary surgery resection. Oral cancerous tissue and adjacent noncancerous tissues were collected without radiation therapy or chemotherapy.

2.2. Isolation and Culture of Human Gingival Fibroblasts (HGF). Normal gingival tissue samples were obtained from the biopsy specimens during periodontal surgery on healthy subjects, all of whom provided informed consent. The study was approved by the hospital ethics committee (KMUH-IRB-20110031). HGF were isolated following a previously described method with some modifications [15, 16].

2.3. Cytotoxicity Assay. Normal clinical oral tissue was isolated to culture human gingival fibroblasts (HGF). Oral epidermal gingival squamous carcinoma, Ca9-22 cell line, was purchased from the Cell Bank of Japanese Collection of Research Bioresources (JCRB number JCRB0625). The details of our cell culture method were shown in our previous study [17]. Cells were treated with various concentrations (0, 50, 100, 200, 400, and 800 μM) of arecoline incubated for 24 h and 48 h. The MTT was used to evaluate the cell proliferation for 2 h in CO_2 incubator (37°C). In an ELISA reader (Bio Tek el800), cells were treated by using DMSO, and the absorbance (570 nm) was explored with the wavelength of reference (630 nm) after the removal of the culture medium. The percent of viable cells was shown in comparison with the vehicle controls.

2.4. Real-Time qRT-PCR Analysis. Following the commercial protocol of the manufacturer, the total RNA was extracted from the cells and tissues using TRIzol (Invitrogen, Carlsbad, CA, USA) as described [18]. Each cDNA pool was stored at −20°C until further qRT-PCR analysis. The primer pairs of specific oligonucleotide were selected from Roche Universal ProbeLibrary for qRT-PCR assays. The reactions of qRT-PCR using SYBR Green I kit were performed on the Roche Light-Cycler Instrument 1.5 system. The expression or repression of the target gene compared to the GAPDH gene (internal control) was calculated by the formula: $2^{-\Delta\Delta C_P}$, where $\Delta C_p = C_{P_{\text{target gene}}} - C_{P_{\text{internal control}}}$ and $\Delta\Delta C_p = \Delta C_{P_{\text{cancerous tissue}}} - \Delta C_{P_{\text{adjacent noncancerous tissue}}}$ in each sample.

2.5. Protein Extraction and Western Blotting. The cell samples were washed with wash buffer [10 mM HEPES, pH 7.4, containing 140 mM NaCl, 4 mM KCl, and 11 mM glucose]. Cell lysate samples were obtained by sonication in lysis buffer [250 mM HEPES, pH 7.7, containing 1 mM EDTA, 0.1 mM neocuproine, and 0.4% (w/v) CHAPS]. The protein

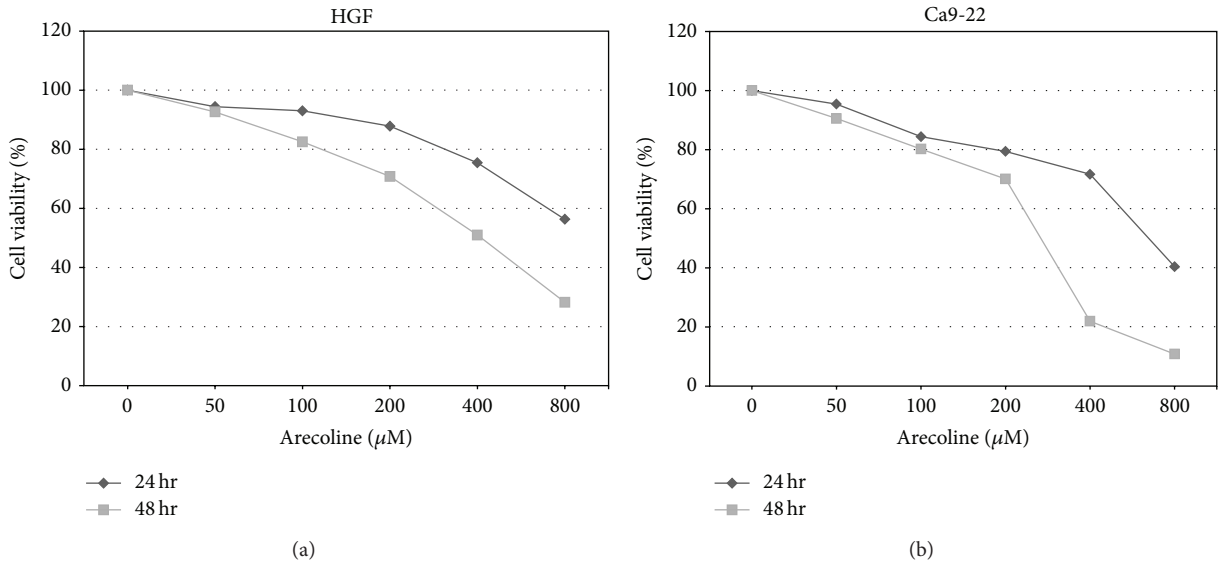

Figure 1: The effects of different arecoline concentrations on the viability of HGF and Ca9-22 cells for 24 h and 48 h. (a) HGF cells viability. (b) Ca9-22 cells viability. An asterisk (∗) indicates a statistically significant difference ($P < 0.05$).

concentration was determined using the BCA protein assay reagent (Thermo Fisher Scientific Inc., Rockford, IL, USA). The cell lysate (40 μg) was mixed with SDS-PAGE sample buffer [62.5 mM Tris-HCl, pH 6.8, 3% (w/v) SDS, 5% (v/v) 2-mercaptoethanol, and 10% (v/v) glycerol] and was then separated by SDS-PAGE. The blotted membranes were hybridized with monoclonal antibodies (Merck Millipore Corporation, Billerica, MA, USA), developed with the SuperSignal West Femto reagent (Thermo Fisher Scientific Inc.), and exposed to X-ray films. The images on X-ray films from three replicates were scanned using a digital scanner (Microtek International Inc., Hsinchu, Taiwan) and were analyzed using Progenesis Samespots v2.0 software (NonLinear Dynamics) to determine the level of protein expression.

2.6. Statistical Analysis. The assay results of MAO gene expression were presented as the mean and standard errors (SE) of the mean (mean ± SE) for each group. Between the control and treatment groups, one-way ANOVA and Tukey's honestly significant difference (HSD) test for post hoc multiple comparisons were used to evaluate statistical significance of the relative fold change. We also estimated the trend of dose-dependent effects for cell viability and MAO-A mRNA expression using a Cochran-Armitage trend test (P for trend). Because of the small sample size ($N = 8$) for the paired tissue, we conducted a nonparametric Wilcoxon signed-rank test to compare the protein expression differences between cancer tissue and its adjacent tissue.

The association between allele and diseases was estimated by chi-square (χ^2) test and an unconditional logistic regression model; odds ratio (OR), 95% confidence interval (CI), and exact P value were estimated. All statistical analysis was carried out using the IBM SPSS Statistics 19 (SPSS, Chicago, IL) and SAS Statistical Package (Version 9.1.3, SAS Institute Inc., Cary, NC, USA). Results that were considered significantly statistically different were marked with an asterisk ($P < 0.05$).

3. Results

3.1. HGF and Ca9-22 Cells Viability. MTT assay was used to estimate cell viability (%) after HGF and Ca9-22 cells exposure to six different concentrations (0, 50, 100, 200, 400, and 800 μM) of arecoline for 24 h and 48 h. After the arecoline concentration was increased, cell survival gradually decreased in a time- and dose-dependent manner (Figure 1).

3.2. The mRNA Expression of MAO-A in HGF Cells and Oral Cancer Cell Lines (Ca9-22). Figure 2 showed that, at 200, 400, and 800 μM arecoline, the expression of MAO-A was above 2-fold and was statistically significant at the 400 and 800 μM doses in HGF cells ($P < 0.05$). An increasing trend effect ($P < 0.0001$) for MAO-A expression could be observed in HGF cells when the arecoline dose increased gradually. In cancer cell lines (Ca9-22), compared with the untreated control group, mRNA expression of MAO-A was increased slightly at 50 μM. Conversely, a greater than 2-fold change in the downregulation of MAO-A was found to be statistically significant at 100, 200, 400, and 800 μM arecoline treatments compared with the control group (0 μM) ($P < 0.05$); the change in downregulation was particularly significant at 800 μM arecoline in the Ca9-22 cancer cell line (the mean fold change ± standard errors (SE) was −8.55 ± 0.33). When the arecoline dose was gradually increasing, a decreasing trend effect ($P < 0.0001$) for MAO-A expression could be observed.

3.3. The MAO-A and MAO-B mRNA and Protein Expression of Paired Tissue in Oral Cancer Patients. In comparison with their adjacent noncancerous tissues, the downregulation

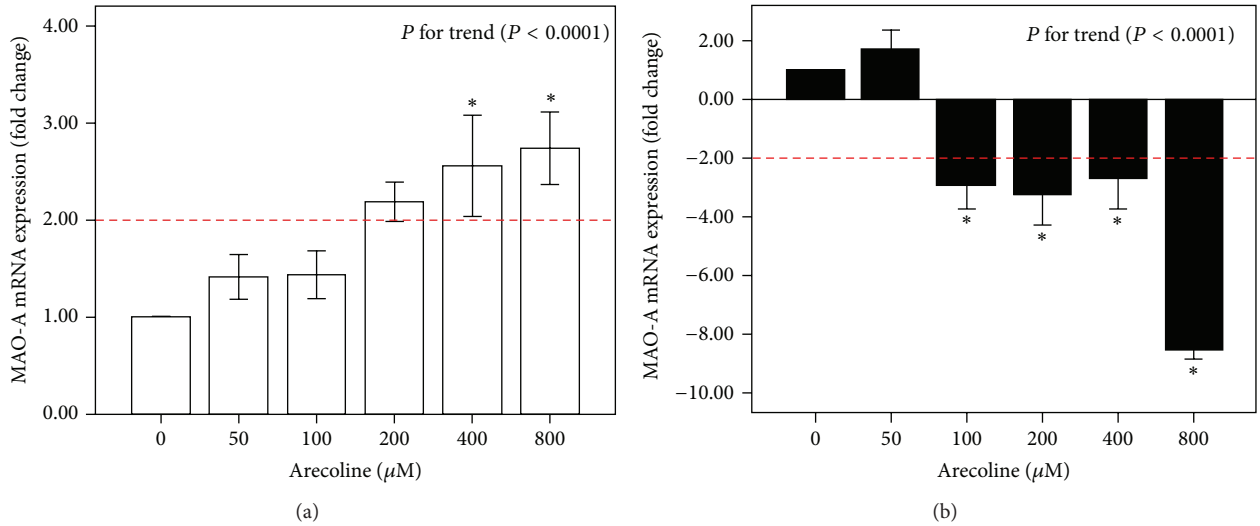

Figure 2: The mRNA expression of MAO-A after arecoline treatment at different concentrations (0, 50, 100, 200, 400, and 800 μM). (a) Normal human gingival fibroblast cells (HGF). (b) Cancer cells (Ca9-22 cell line). The average fold change (mean ± standard errors (SE)) of the MAO-A gene was measured in triplicate; error bars indicate SE of mean. Multiple comparisons of mean MAO-A expression were analyzed by one-way ANOVA, and a post hoc comparison was performed by Tukey's HSD test. The P value for the trend is presented, and an asterisk (∗) indicates a statistically significant difference ($P < 0.05$) compared with cells without treatment.

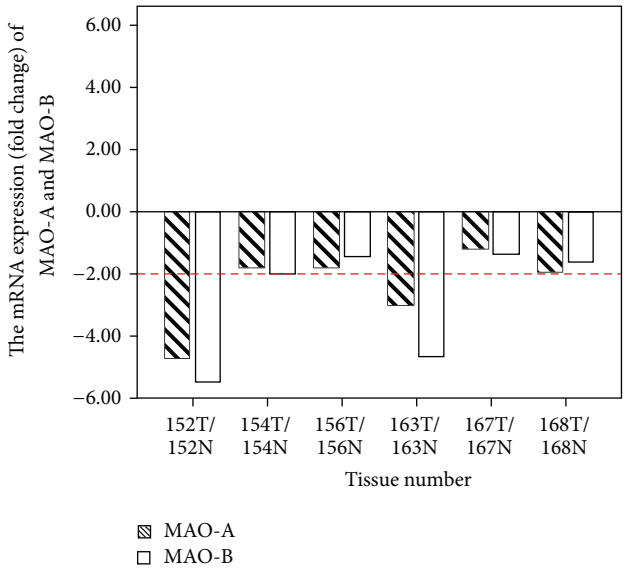

Figure 3: The mRNA expression of MAO-A and MAO-B in human oral tumor (T) tissues compared with their adjacent normal (N) tissues. The relative fold change was estimated by the formula $2^{-\Delta\Delta C_p}$ compared with adjacent tissue ($N = 6$).

mRNA of MAO-A and MAO-B for cancer tissues were observed in patients numbers 152, 154, 156, 163, 167, and 168 (Figure 3). Using Western blotting, we investigated MAO-A and MAO-B quantitative protein expression from eight patients (numbers 136, 149, 152, 156, 163, 167, 174, and 186) (Figure 4). Compared with their adjacent noncancerous tissue, downregulation of protein expression of MAO-A and MAO-B in cancerous tissue was shown in patients numbers 149, 156, 163, 167, 174, and 186, excluding number 136 and number 152. MAO-A expression was higher in number 136 cancer tissue than in its adjacent tissue, but MAO-B expression was lower in cancer tissue than in the adjacent tissue. In number 152 cancer tissue, slightly increased expression of MAO-A and decreased expression of MAO-B were found.

3.4. MAO-A Single Nucleotide Polymorphism (SNP) Analysis. We selected a total of 260 males with oral and pharyngeal cancer and 68 males with OPMDs. All of these participants have a habit of BQ chewing. Table 1 shows that compared with OPMDs patients, BQ chewers who had the MAO-A A-allele (SNP rs2283725) had an increased risk of oral cancer (OR = 1.69; 95% CI = 0.98–2.90), although at borderline significant level. BQ chewers who had the MAO-A G-allele (SNP rs5953210) had a significantly increased risk (OR = 1.76; 95% CI = 1.02–3.01) of oral cancer ($P < 0.05$).

4. Discussion

BQ chewing is an emerging health-associated issue in Asia and the South Pacific islands, as well as among diverse migrant populations in western countries. This is the first study to indicate that variants of the MAO gene may be related to BQ-related oral and pharyngeal cancer occurrence. The MAO gene is present in human blood and neuron synapses, and it catalyzes deamination effects of biogenic amines and regulates the concentration of several neurotransmitters (such as dopamine, serotonin, norepinephrine, and catecholamines) in the central nervous system, which plays an important role in physiology and behavior [19]. The MAO gene is divided into two types. The MAO-A gene is primarily responsible for the metabolism of serotonin and norepinephrine and may indirectly affect mood and impulse control; the MAO-A gene is a major determinant of

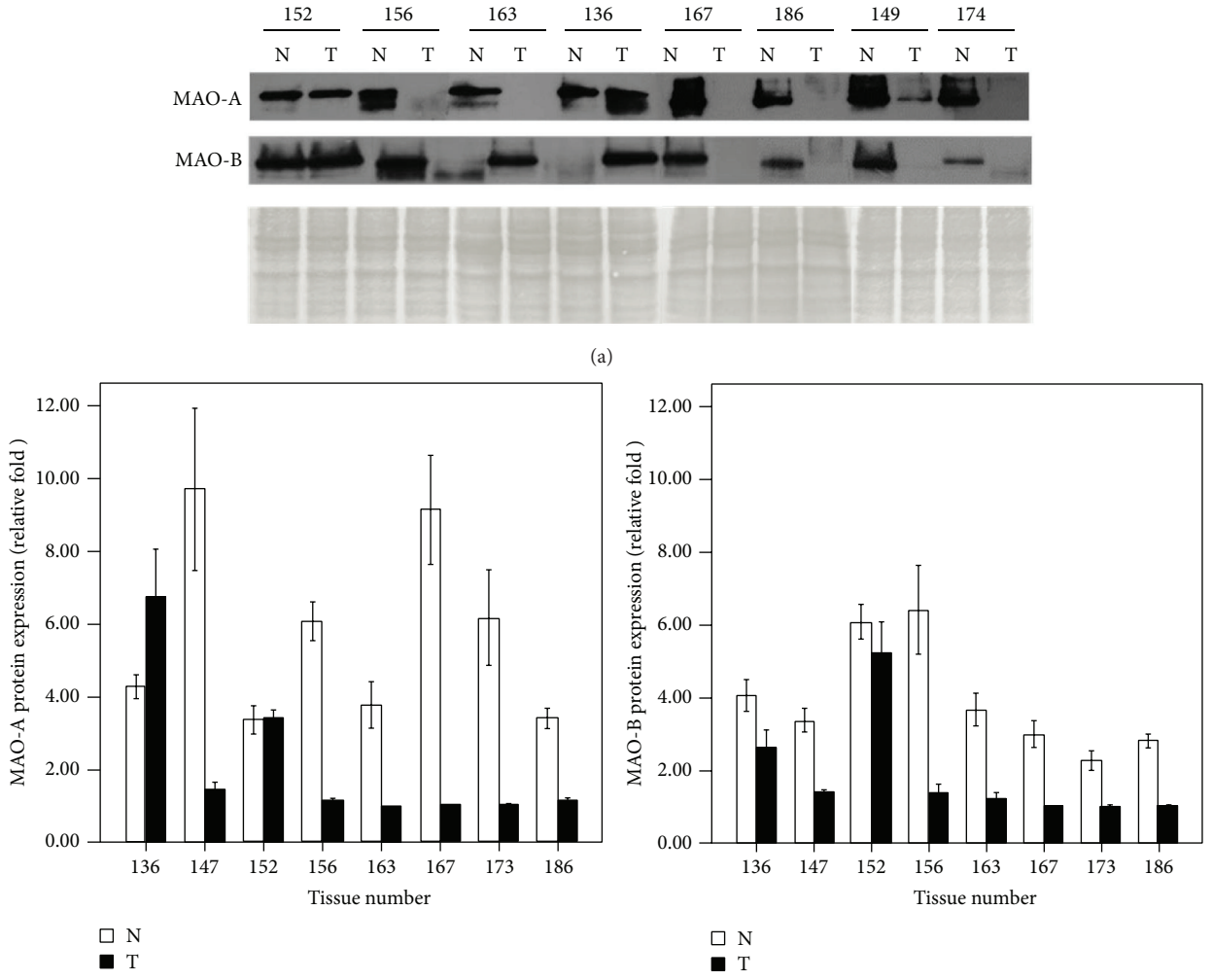

Figure 4: (a) The induced protein expression of MAO-A and MAO-B of human oral tumor (T) tissues compared with their adjacent normal (N) tissues. (b) The protein expression of MAO-A and MAO-B was presented by relative fold; the average fold (mean ± SE) was calculated in triplicate.

Table 1: Distribution of BQ chewers with MAO-A allele types between oral and pharyngeal cancer and OPMDs male patients.

	Oral and pharyngeal cancer		OPMDs		P^a	OR (95% CI)
	N	(%)[a]	*N*	(%)		
BQ chewers						
rs2283725						
Allele						
G	95	(36.5)	33	(49.3)	0.0572	1.00
A	165	(63.5)	34	(50.7)		1.69 (0.98–2.90)
rs5953210						
Allele						
A	94	(36.3)	34	(50.0)	0.0393	1.00
G	165	(63.7)	34	(50.0)		1.76 (1.02–3.01)[b*]

[a]Statistical *P* values were estimated by chi-square (χ^2) test; [b*] $P < 0.05$.
BQ: betel quid; OPMDs: oral potentially malignant disorders; OR: odds ratio; 95% CI: 95% confidence interval.

Table 2: Clinical characteristics and substance use status comparison of male BQ chewers with oral cancer ($N = 10$).

Number	Age	Tumor site	ICD 9 code	TNM	Stage	Pathological diagnosis	A[a]	B[b]	C[c]
136	45	Tongue	141	T2N1M0	III	SCC[d]	+	+	+
149	71	Oral	145.9	T2N0M0	II	Verrucous carcinoma	−	+	+
152	46	Tongue	141	T2N0M0	II	SCC	+	+	+
154	39	Buccal	145	T3N0M0	III	SCC	+	+	+
156	57	Buccal	145	T3N0M0	III	SCC, grand II	NA	+	+
163	39	Oral	145.9	T2N0M0	II	SCC, grand II	−	+	+
167	45	Tongue	141	T2N0M0	II	SCC, grand II	+	+	+
168	56	Buccal	145	T2N0M0	II	SCC	+	+	−
174	45	Buccal	145	T4N1M0	IV A	SCC	−	+	+
186	46	Buccal	145	T4N1M0	IV A	SCC	+	+	+

[a]Alcohol use.
[b]Betel use.
[c]Cigarette use.
[d]SCC: squamous cell carcinoma.
NA: no information can be available.

MAO activity [20]. The MAO-B gene is associated with the metabolism of dopamine and phenylethylamine [20].

Past studies only focused on the association of the MAO-A gene with other cancers and never explored its association with oral pharyngeal cancer, specifically. Also, the relationship between MAO-B and cancer has rarely been mentioned. Mikula et al. found that downregulation of MAO-A may be associated with the occurrence of colon cancer [21]. MAO-A gene was downregulated in lymph node status (N_0) of gastric cancer [22]. In prostate cancer, Peehl et al. noted that there is a high expression of MAO-A in patients with a high tumor grade [23]; the targeting of antidepression drugs on MAO-A may provide potential future applications in the treatment of prostate cancer [24]. Two studies have shown that MAO-A gene expression is suppressed in cholangiocarcinoma patients [25, 26]. A case-control study also found that tumor cells had high concentrations of metanephrine in patients with pheochromocytoma, which may be due to the downregulation of MAO-A [27]. Rybaczyk et al. found that MAO-A exhibited significantly lower expression in cancerous tissue than its noncancerous control tissue in human, mouse, and zebrafish studies [28].

To our knowledge, population data regarding the relationship between the MAO gene and oral and pharyngeal cancer among BQ users has not been available. Previous studies have indicated that arecoline can cause many adverse effects in cells, such as cytotoxicity, carcinogenicity, immunotoxicity, and genotoxicity [8–11]. Arecoline may be metabolized by the MAO gene *via* xenobiotic metabolism, which is involved in phase I biotransformation. To simulate the oral cells of Taiwanese men, we cultured normal HGF cells from the biopsy specimens. In the *in vitro* model, our results suggested that in primary cell culture of HGF, treatment with arecoline may increase expression of MAO-A in a dose-dependent manner. Conversely, Ca9-22 cancer cells treated with higher concentrations of arecoline may induce downregulation of MAO-A.

To exclude individual differences of gene expression in humans, paired tissues from oral cancer patients were used to explore the mRNA and protein expression of MAO-A and MAO-B. The clinical characteristics and substance use status (alcohol, betel, and cigarette use) of the oral and pharyngeal patients were shown in Table 2. Overall, in the *in vivo* model, our data indicated that patients (numbers 152, 154, 156, 163, 167, and 168) showed consistent downregulation of MAO-A and MAO-B mRNA in oral cancer tissue compared with noncancerous adjacent tissue. Decreased MAO-A and MAO-B protein expression was found to be statistically significant in cancerous tissue compared with adjacent noncancerous tissue among 8 patients using the nonparametric Wilcoxon signed-rank test ($P < 0.05$, Figure 5).

Generally, the protein expression of the MAO gene exhibited downregulation in oral cancer tissue compared with noncancerous tissue, and this performance is consistent with mRNA levels. This pattern was also observed in the cell model; the normal HFG cells with higher doses of arecoline showed higher mRNA expression, and the cancerous Ca9-22 cells with higher doses of arecoline showed lower mRNA expression. We speculated that the differences of mRNA expression observed between normal HFG cell and cancer Ca9-22 cell may be associated with the cancer type, but this phenomenon needs to be confirmed in further study.

The MAO-A gene is located on chromosome Xp11.3, and the MAO-B gene is located on the chromosome Xp11.23 region. In this study, one SNP (rs2283725, located on intron 3) of MAO-A was selected to analysis. The other one located on the 5′ intergenic region (rs5953210, located on 5′ near gene) was also included to allow ascertainment of linkage disequilibrium (LD) extent beyond the gene boundaries. Previous reports have indicated OPMDs are significant predictors for malignant transformation to oral and pharyngeal cancer [5, 29, 30]. BQ chewers with both MAO-A SNPs, rs2283725 and rs5953210, were associated with the risk of oral and pharyngeal cancer occurrence compared with OPMDs. The rs5953210 risk G-allele was significantly associated with the risk of oral and pharyngeal cancer (OR = 1.76; 95% CI = 1.02–3.01) and the rs2283725 risk A-allele at borderline significant level (OR = 1.69; 95% CI = 0.98–2.90). Overall,

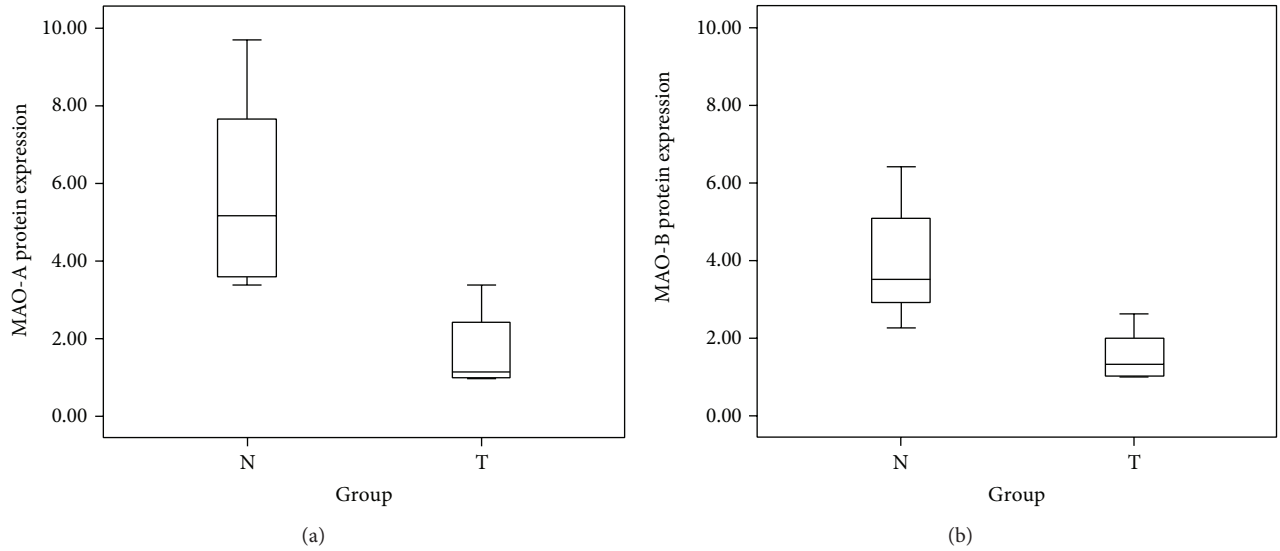

Figure 5: Boxplot of protein expression among 8 patients. (a) MAO-A protein expression between oral tumor (T) tissue and the oral normal (N) adjacent tissue; (b) MAO-B expression between oral tumor (T) tissue and the oral normal (N) adjacent tissue.

our results suggest that MAO-A variants may contribute to genetic susceptibility to oral and pharyngeal cancer in BQ chewers. In addition, BQ chewers with risk allele combined with cigarette or alcohol use significantly increased the risk of oral and pharyngeal cancer (data not shown). A case-control study of 2,572 Caucasian men suggested that a rare 5-copy variation of the MAO-A variable-number tandem repeat (VNTR) genotype may be associated with the development of prostate cancer; the frequency of the rare 5-copy variation in the case group (0.5%) was lower than the frequency in the control group (1.8%) and reduced the risk of prostate cancer (OR = 0.30; 95% CI = 0.13–0.71) [31]. A previous report indicated that, in gastric cancer, changes to the MAO-A gene may be related to the DNA copy number of cancerous tissue with a statistically significant linear correlation [32]. Limitations of this study were small sample size to present the expression of MAO-A mRNA and protein. A large size of sample was needed to confirm expression of MAO-A and MAO-B in betel quid-related oral and pharyngeal cancer. Additionally, we cannot take OPMDs specimen for further research, because it is very difficult to recruit OPMDs patients willing to undergo surgery and sign the informed consent.

In conclusion, this report is the first study to consider how downregulation of the MAO gene family (MAO-A and MAO-B) and MAO-A SNP variants play an important role in the occurrence or development mechanism of oral and pharyngeal cancer. Our previous report demonstrated that BQ chewing may significantly produce ROS, which may contribute to oxidative injury of oral tissue [33]. A screen tool of MAO at-risk variations may be useful to prevent the occurrence of oral and pharyngeal cancer among BQ chewers. In the future, these studies may provide new insight into the relationship between malignant transformation of OPMDs and oral and pharyngeal cancer in the modulation of MAO gene activity associated with ROS.

Abbreviations

BQ: Betel quid
AN: Areca nut
OPMDs: Oral potentially malignant disorders
MAO: Monoamine oxidase
SNP: Single nucleotide polymorphism.

Conflict of Interests

The authors declare that there is no conflict of interests regarding the publication of this paper.

Authors' Contribution

Chun-Chia Chen and Ka-Wo Lee contributed equally to this study.

Acknowledgments

This study was financially supported by NSC Grant (NSC 102-2314-B-037-073-) from the Ministry of Science and Technology, Taiwan; by Grant of the Health and Welfare Surcharge of Tobacco Products, the Ministry of Health and Welfare, Taiwan, (MOHW103-TD-B-111-05); and by Grants (100CM-KMU-13 and 101CM-KMU-12) from the Chi-Mei Medical Center and Kaohsiung Medical University Research Foundation.

References

[1] Ministry of Health and Welfare, *Cancer Registration System Annual Report*, Ministry of Health and Welfare, Taiwan, 2010.

[2] P. H. Chen, K. W. Lee, C. H. Chen et al., "CYP26B1 is a novel candidate gene for betel quid-related oral squamous cell carcinoma," *Oral Oncology*, vol. 47, no. 7, pp. 594–600, 2011.

[3] K. W. Lee, W. R. Kuo, S. M. Tsai et al., "Different impact from betel quid, alcohol and cigarette: risk factors for pharyngeal and laryngeal cancer," *International Journal of Cancer*, vol. 117, no. 5, pp. 831–836, 2005.

[4] C. H. Lee, Y. C. Ko, H. L. Huang et al., "The precancer risk of betel quid chewing, tobacco use and alcohol consumption in oral leukoplakia and oral submucous fibrosis in southern Taiwan," *British Journal of Cancer*, vol. 88, no. 3, pp. 366–372, 2003.

[5] P. S. Ho, P. L. Chen, S. Warnakulasuriya, T. Y. Shieh, Y. K. Chen, and I. Y. Huang, "Malignant transformation of oral potentially malignant disorders in males: a retrospective cohort study," *BMC Cancer*, vol. 9, article 260, 2009.

[6] B. J. Boucher and N. Mannan, "Metabolic effects of the consumption of Areca catechu," *Addiction Biology*, vol. 7, no. 1, pp. 103–110, 2002.

[7] P. C. Gupta and C. S. Ray, "Epidemiology of betel quid usage," *Annals of the Academy of Medicine Singapore*, vol. 33, no. 4, supplement, pp. 31–36, 2004.

[8] B. J. Dave, A. H. Trivedi, and S. G. Adhvaryu, "In vitro genotoxic effects of areca nut extract and arecoline," *Journal of Cancer Research and Clinical Oncology*, vol. 118, no. 4, pp. 283–288, 1992.

[9] S. Deb and A. Chatterjee, "Influence of buthionine sulfoximine and reduced glutathione on arecoline-induced chromosomal damage and sister chromatid exchange in mouse bone marrow cells in vivo," *Mutagenesis*, vol. 13, no. 3, pp. 243–248, 1998.

[10] L. P. Shirname, M. M. Menon, and S. V. Bhide, "Mutagenicity of betel quid and its ingredients using mammalian test systems," *Carcinogenesis*, vol. 5, no. 4, pp. 501–503, 1984.

[11] S. K. Tseng, M. C. Chang, C. Y. Su et al., "Arecoline induced cell cycle arrest, apoptosis, and cytotoxicity to human endothelial cells," *Clinical Oral Investigations*, vol. 16, no. 4, pp. 1267–1273, 2012.

[12] S. L. Chiang, S. S. Jiang, and Y. J. Wang, "Characterization of erecoline-induced effects on cytotoxicity in normal human gingival fibroblasts by global gene expression profiling," *Toxicological Sciences*, vol. 100, no. 1, pp. 66–74, 2007.

[13] W. T. Ji, C. I. Lee, J. Y. F. Chen et al., "Areca nut extract induces pyknotic necrosis in serum-starved oral cells via increasing reactive oxygen species and inhibiting GSK3β: an implication for cytopathic effects in betel quid chewers," *PLoS ONE*, vol. 8, no. 5, Article ID e63295, 2013.

[14] D. E. Edmondson, "Hydrogen peroxide produced by mitochondrial monoamine oxidase catalysis: biological implications," *Current Pharmaceutical Design*, vol. 20, no. 2, pp. 155–160, 2014.

[15] H. T. Chen, M. J. Lee, C. H. Chen et al., "Proliferation and differentiation potential of human adipose-derived mesenchymal stem cells isolated from elderly patients with osteoporotic fractures," *Journal of Cellular and Molecular Medicine*, vol. 16, no. 3, pp. 582–593, 2012.

[16] C. Y. Yen, C. H. Chen, C. H. Chang et al., "Matrix metalloproteinases (MMP) 1 and MMP10 but not MMP12 are potential oral cancer markers," *Biomarkers*, vol. 14, no. 4, pp. 244–249, 2009.

[17] S. L. Chiang, P. H. Chen, C. H. Lee et al., "Up-regulation of inflammatory signalings by areca nut extract and role of Cyclooxygenase-2 -1195G>A polymorphism reveal risk of oral cancer," *Cancer Research*, vol. 68, no. 20, pp. 8489–8498, 2008.

[18] C. Y. Yen, C. Y. Huang, M. F. Hou et al., "Evaluating the performance of fibronectin 1 (FN1), integrin α4β1 (ITGA4), syndecan-2 (SDC2), and glycoprotein CD44 as the potential biomarkers of oral squamous cell carcinoma (OSCC)," *Biomarkers*, vol. 18, no. 1, pp. 63–72, 2013.

[19] J. van Amsterdam, R. Talhout, W. Vleeming, and A. Opperhuizen, "Contribution of monoamine oxidase (MAO) inhibition to tobacco and alcohol addiction," *Life Sciences*, vol. 79, no. 21, pp. 1969–1973, 2006.

[20] G. S. Hotamisligil and X. O. Breakefield, "Human monoamine oxidase A gene determines levels of enzyme activity," *American Journal of Human Genetics*, vol. 49, no. 2, pp. 383–392, 1991.

[21] M. Mikula, T. Rubel, J. Karczmarski, K. Goryca, M. Dadlez, and J. Ostrowski, "Integrating proteomic and transcriptomic high-throughput surveys for search of new biomarkers of colon tumors," *Functional and Integrative Genomics*, vol. 11, no. 2, pp. 215–224, 2011.

[22] V. Ojetti, R. Persiani, F. C. Cananzi et al., "cDNA-microarray analysis as a new tool to predict lymph node metastasis in gastric cancer," *World Journal of Surgery*, vol. 38, no. 8, pp. 2058–2064, 2014.

[23] D. M. Peehl, M. Coram, H. Khine, S. Reese, R. Nolley, and H. Zhao, "The significance of monoamine oxidase-A expression in high grade prostate cancer," *Journal of Urology*, vol. 180, no. 5, pp. 2206–2211, 2008.

[24] V. Flamand, H. Zhao, and D. M. Peehl, "Targeting monoamine oxidase A in advanced prostate cancer," *Journal of Cancer Research and Clinical Oncology*, vol. 136, no. 11, pp. 1761–1771, 2010.

[25] L. Huang, G. Frampton, A. Rao et al., "Monoamine oxidase A expression is suppressed in human cholangiocarcinoma via coordinated epigenetic and IL-6-driven events," *Laboratory Investigation*, vol. 92, no. 10, pp. 1451–1460, 2012.

[26] G. Alpini, P. Invernizzi, E. Gaudio et al., "Serotonin metabolism is dysregulated in cholangiocarcinoma, which has implications for tumor growth," *Cancer Research*, vol. 68, no. 22, pp. 9184–9193, 2008.

[27] E. Grouzmann, M. Matter, S. Bilz et al., "Monoamine oxidase a down-regulation contributes to high metanephrine concentration in pheochromocytoma," *Journal of Clinical Endocrinology and Metabolism*, vol. 97, no. 8, pp. 2773–2781, 2012.

[28] L. A. Rybaczyk, M. J. Bashaw, D. R. Pathak, and K. Huang, "An indicator of cancer: downregulation of Monoamine Oxidase-A in multiple organs and species," *BMC Genomics*, vol. 9, article 134, 2008.

[29] S. Warnakulasuriya, N. W. Johnson, and I. van der Waal, "Nomenclature and classification of potentially malignant disorders of the oral mucosa," *Journal of Oral Pathology and Medicine*, vol. 36, no. 10, pp. 575–580, 2007.

[30] S. Warnakulasuriya, T. Kovacevic, P. Madden et al., "Factors predicting malignant transformation in oral potentially malignant disorders among patients accrued over a 10-year period in South East England," *Journal of Oral Pathology and Medicine*, vol. 40, no. 9, pp. 677–683, 2011.

[31] T. A. White, E. M. Kwon, R. Fu et al., "The Monoamine Oxidase A gene promoter repeat and prostate cancer risk," *Prostate*, vol. 72, no. 15, pp. 1622–1627, 2012.

[32] S. Yang, H. C. Jeung, H. J. Jeong et al., "Identification of genes with correlated patterns of variations in DNA copy number and gene expression level in gastric cancer," *Genomics*, vol. 89, no. 4, pp. 451–459, 2007.

[33] P. H. Chen, C. C. Tsai, Y. C. Lin et al., "Ingredients contribute to variation in production of reactive oxygen species by areca quid," *Journal of Toxicology and Environmental Health*, vol. 69, no. 11, pp. 1055–1069, 2006.

Hindawi Publishing Corporation
The Scientific World Journal
Volume 2014, Article ID 180462, 10 pages
http://dx.doi.org/10.1155/2014/180462

Research Article

Antiproliferative Effects of Methanolic Extracts of *Cryptocarya concinna* Hance Roots on Oral Cancer Ca9-22 and CAL 27 Cell Lines Involving Apoptosis, ROS Induction, and Mitochondrial Depolarization

Hurng-Wern Huang,[1] Yi-An Chung,[1] Hsun-Shuo Chang,[2,3] Jen-Yang Tang,[4,5,6] Ih-Sheng Chen,[2,3] and Hsueh-Wei Chang[6,7,8]

[1] *Institute of Biomedical Science, National Sun Yat-Sen University, Kaohsiung 80424, Taiwan*
[2] *Graduate Institute of Natural Products, College of Pharmacy, Kaohsiung Medical University, Kaohsiung 80708, Taiwan*
[3] *School of Pharmacy, College of Pharmacy, Kaohsiung Medical University, Kaohsiung 80708, Taiwan*
[4] *Department of Radiation Oncology, Faculty of Medicine, College of Medicine, Kaohsiung Medical University, Kaohsiung 80708, Taiwan*
[5] *Department of Radiation Oncology, Kaohsiung Medical University Hospital, Kaohsiung 80708, Taiwan*
[6] *Cancer Center, Translational Research Center, Kaohsiung Medical University Hospital, Kaohsiung Medical University, Kaohsiung 80708, Taiwan*
[7] *Institute of Medical Science and Technology, National Sun Yat-sen University, Kaohsiung 80424, Taiwan*
[8] *Department of Biomedical Science and Environmental Biology, Kaohsiung Medical University, Kaohsiung 80708, Taiwan*

Correspondence should be addressed to Ih-Sheng Chen; m635013@kmu.edu.tw and Hsueh-Wei Chang; changhw@kmu.edu.tw

Received 16 July 2014; Accepted 25 August 2014; Published 15 October 2014

Academic Editor: Shao-Yu Chen

Cryptocarya-derived natural products were reported to have several biological effects such as the antiproliferation of some cancers. The possible antioral cancer effect of *Cryptocarya*-derived substances was little addressed as yet. In this study, we firstly used the methanolic extracts of *C. concinna* Hance roots (MECCrt) to evaluate its potential function in antioral cancer bioactivity. We found that MECCrt significantly reduced cell viability of two oral cancer Ca9-22 and CAL 27 cell lines in dose-responsive manners ($P < 0.01$). The percentages of sub-G1 phase and annexin V-positive of MECCrt-treated Ca9-22 and CAL 27 cell lines significantly accumulated ($P < 0.01$) in a dose-responsive manner as evidenced by flow cytometry. These apoptotic effects were associated with the findings that intracellular ROS generation was induced in MECCrt-treated Ca9-22 and CAL 27 cell lines in dose-responsive and time-dependent manners ($P < 0.01$). In a dose-responsive manner, MECCrt also significantly reduced the mitochondrial membrane potential in these two cell lines ($P < 0.01$–0.05). In conclusion, we demonstrated that MECCrt may have antiproliferative potential against oral cancer cells involving apoptosis, ROS generation, and mitochondria membrane depolarization.

1. Introduction

Oral squamous cell carcinoma (OSCC) is a type of cancer that frequently occurs in oral cavity. Although it is comparatively easy to clinically inspect by a dentist or to detect by some OSCC tumor markers [1, 2], this carcinoma is usually ignored by patients especially for the early stage. Subsequently, OSCC is frequently diagnosed at advanced stages which then lead to high mortality [3]. Therefore, the drug development of antioral cancer is still necessary and remains to be a challenge.

Natural products have improved the drug discovery for anticancer therapy [4]. For example, some anticancer

drugs derived from natural products were approved by the United States Food and Drug Administration [5]. In basic researches, natural products with antioral cancer effects have increasingly being reported. This holds for the ethanolic and methanolic extracts of red alga *Gracilaria tenuistipitata* [6, 7], crude extracts of *Selaginella tamariscina* (oriental medicinal herb) [8], green tea [9], goniothalamin from *Goniothalamus* species [10], and 4β-hydroxywithanolide E from golden berry [11].

Cryptocarya plants (family Lauraceae), comprising about 350 species worldwide, are widely distributed in the tropics and subtropics [12]. This plant group is well known for its common secondary metabolites, containing alkaloids, flavonoids, and α-pyrones [12–15]. Several biological effects of *Cryptocarya*-derived natural products have been reported that include anti-dengue virus [16], anti-HIV [17], anti-tuberculosis [18], antiplasmodial [19], antitrypanosomal [20], and anti-inflammatory [21] function.

Anticancer effects of crude extracts of *Cryptocarya* plant are known as well. For example, the ethanolic extracts of fruit and trunk bark of *C. obovata* showed 56% and 23% growth inhibition of human KB cells at 10 μg/mL, respectively [22]. Methanolic extracts of the leaves of *C. griffithiana* provide cytotoxicity forhuman HL60 promyelocytic leukemia cells [23].

Recently, accumulating findings for anticancer effects of pure compounds isolated from *Cryptocarya* plants were reported, especially from methanolic extracts. For example, compounds isolated from methanol extracts of the trunk bark of *C. infectoria* [24], the trunk bark of *C. costata* [25], and the wood of *C. konishii* [26] were reported to be cytotoxic to leukemia cells. Compounds from methanolic extracts of leaves of *C. chinensis*, were shown to be cytotoxic to human lung cancer and glioblastoma cells [27]. These drugs were isolated from the trunk bark, wood, and leaves of *Cryptocarya* sp. However, the bioactivity of the roots of *Cryptocarya* plants remained little investigated, particularly with respect to antioral cancer.

Because *C. concinna* Hance is an evergreen plant commonly distributed in low-altitude forests in Taiwan [28], it is easy to prepare methanolic extracts of the roots of *C. concinna* Hance (namely, for MECCrt). We, therefore, chose two OSCC cell lines, that is, Ca9-22 and CAL 27, to evaluate the possible anticancer function of MECCrt and investigate their drug mechanisms in terms of cell viability, cell cycle distribution, apoptosis, reactive oxygen species (ROS) generation, and mitochondrial depolarization.

2. Materials and Methods

2.1. Cell Cultures and Methanolic Extracts of C. concinna. Two human OSCC cell lines Ca9-22 and CAL 27, purchased from the Cell Bank, RIKEN BioResource Center (Tsukuba, Japan) and the American Type Culture Collection (ATCC; Virginia, USA), respectively, were incubated in DMEM/F12 (3 : 2) medium (Gibco, Grand Island, NY, USA) supplemented with 10% fetal bovine serum (Gibco), 100 U/mL penicillin, 100 μg/mL streptomycin, and 0.03% glutamine. These two cell lines were humidly incubated at 37°C with 5% CO_2 in the humid atmosphere.

C. concinna was identified by one of the authors (Ih-Sheng Chen) and its roots were collected at Mudan, Pingtung County, Taiwan, in May 2004. A voucher specimen (Chen 6153) has been deposited in the Herbarium of the School of Pharmacy, College of Pharmacy, Kaohsiung Medical University. The dried roots of *C. concinna* were processed by slicing and cold methanol-extraction for three times at room temperature. Finally, the solution was evaporated under reduced pressure to yield the methanolic extract (MECCrt). MECCrt was stored at −20°C and dissolved in dimethyl sulfoxide (DMSO) before treatment.

2.2. Cell Viability. Cell viability was measured by the CellTiter 96 AQueous one solution cell proliferation assay (MTS) (Promega Corporation, Madison, WI, USA) as previously described [11]. Ca9-22 and CAL 27 cell lines were seeded at a density of 1×10^5 and 2×10^5 cells per well in a 6-well plate, respectively. After plating for 24 h, these cells were incubated with different concentrations of MECCrt for 24 h and finally subjected to a MTS assay applying an ELISA reader at 490 nm.

2.3. Cell Cycle Progression and Sub-G1 Population. Propidium iodide (PI, Sigma, St. Louis, MO, USA) was added to stain the cellular DNA content [29]. In brief, 3×10^5 cells per well in 6 well plates were plated for 24 h and then treated with vehicle (DMSO; 1 μL/2 mL culture medium) as a control or 5, 10, 15, 20, and 25 μg/mL of MECCrt for 24 h. After exposure termination, cells were centrifuged, washed twice with PBS, fixed overnight with 70% ethanol, and centrifuged. Subsequently, the cell pellets were resuspended in 50 μg/mL PI reagent and stand for 30 min at 37°C in darkness. Cell cycle distribution was evaluated by a flow cytometer (BD Accuri C6; Becton-Dickinson, Mansfield, MA, USA) and a BD Accuri C6 Software (version 1.0.264).

2.4. Apoptosis. To validate apoptosis in MECCrt-treated oral cancer cells, annexin V (Strong Biotect Corporation, Taipei, Taiwan) [30]/PI (Sigma, St Louis, MO, USA) method was used [31]. Briefly, 3×10^5 cells per well in 6 well plates were plated for 24 h and then treated with vehicle or indicated concentrations of MECCrt for 24 h. Subsequently, apoptotic cells were stained for 30 min with 100 μL binding buffer containing 2 μL of annexin-V-fluorescein isothiocyanate (FITC) stock (0.25 μg/μL) and 2 μL of PI stock (1 mg/mL). Finally, it was suspended with 400 μL PBS for analysis of a flow cytometer (BD Accuri C6; Becton-Dickinson) and its software.

2.5. Intracellular ROS. The dye 2′,7′-dichlorodihydrofluorescein diacetate (DCFH-DA) was used to detect ROS by its fluorescence change [7]. Cells at the density of 3×10^5 in 2 mL medium per well in 6 well plates were plated for 24 h. Different concentrations of MECCrt were added to Ca9-22 cells for 6 h and 12 h. After washing with PBS, 100 nM DCFH-DA in PBS was added to cells in 6 well plates at cell culture incubator for 30 min. After trypsinization, PBS washing, and

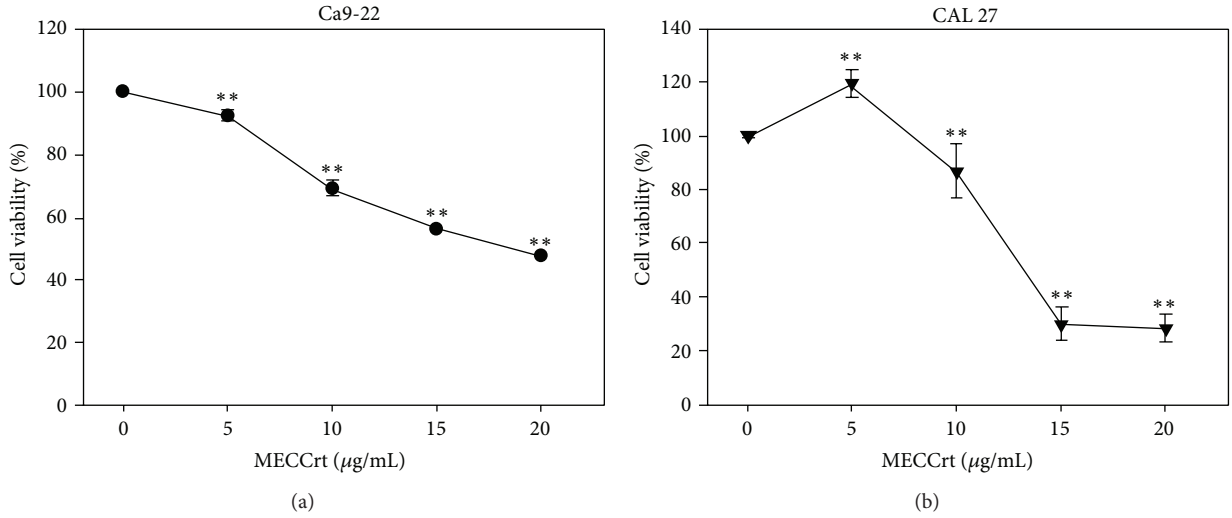

Figure 1: Cell viability of two oral cancer cells was inhibited by MECCrt. Oral cancer Ca9-22 and CAL 27 cell lines were treated with various concentrations of MECCrt (0, 5, 10, 15, and 20 μg/mL) for 24 h. The cell viability was measured by the MTS assay. Data, means ± SDs ($n = 18$). $^{**}P < 0.01$ against vehicle.

centrifugation, cell pellets were resuspended in 1 mL PBS before analyzing by a flow cytometer (BD Accuri C6; Becton-Dickinson) and its software.

2.6. Mitochondrial Membrane Potential. MitoProbe $DiOC_2(3)$ assay kit (Invitrogen, Eugene, OR, USA) was applied to analyze mitochondrial membrane potential (MMP) as described previously [10]. Briefly, 3×10^5 cells in 2 mL medium per well in 6 well plates were plated for 24 h. After MECCrt treatment, 10 μL of 10 μM $DiOC_2(3)$ was added per well and incubated in a cell culture incubator for 20 min. After being harvested, cells were washed and resuspended in 1 mL PBS for analysis using a flow cytometer (BD Accuri C6; Becton-Dickinson) and its software.

2.7. Statistical Analysis. The significance of differences was determined by Student's t-test compared with the test data with the vehicle controls. Data are expressed as means ± SDs.

3. Results

3.1. Antiproliferation in MECCrt-Treated Two Oral Cancer Cell Lines. Based on MTS assay (Figure 1), the relative cell viability (%) of oral cancer Ca9-22 cells at indicated concentrations of MECCrt (0, 5, 10, 15, and 20 μg/mL) was 100.0 ± 0.7, 93.3 ± 2.3, 71.4 ± 3.0, 57.6 ± 1.6, and 48.4 ± 1.2, after 24 h, respectively. The relative cell viability (%) of CAL 27 cells at indicated concentrations of MECCrt (0, 5, 10, 15, and 20 μg/mL) was 100.0 ± 0.8,119.3 ± 4.9, 86.9 ± 10.0, 29.8 ± 6.2, and 28.4 ± 5.5, respectively. The MTS-based cell viabilities of MECCrt-treated two oral cancer Ca9-22 and CAL 27 cell lines significantly reduced in a dose-responsive manner ($P < 0.01$ compared to the vehicle).

3.2. Sub-G1 Population in MECCrt-Treated Two Oral Cancer Cell Lines. The MECCrt-treated effects of cell cycle distribution profiles are demonstrated in Figure 2(a). After MECCrt treatment (Figure 2(b)), the sub-G1 populations (%) of MECCrt- (0, 5, 10, 15, 20, and 25 μg/mL) treated oral cancer Ca9-22 cells were 5.0 ± 0.3, 6.7 ± 0.1, 18.1 ± 0.6, 17.9 ± 0.7, 16.5 ± 0.3, and 22.4 ± 1.3 and those of MECCrt-treated CAL 27 cells were 6.7 ± 1.7, 5.1 ± 1.1, 7.9 ± 0.1, 28.3 ± 1.0, 52.6 ± 0.2, and 69.1 ± 0.1, respectively. These sub-G1 changes significantly accumulated in a dose-responsive manner ($P < 0.01$).

3.3. Apoptosis of MECCrt-Treated Two Oral Cancer Cell Lines. To validate the possible outcome of apoptosis in MECCrt-induced sub-G1 accumulation of these two oral cancer cells, annexin V/PI profiles of flow cytometry were generated (Figure 3(a)). In Figure 3(b), the percentages of annexin V-positive intensities for MECCrt (0, 5, 10, 15, 20, and 25 μg/mL) treatment of Ca9-22 cells were 9.3 ± 0.2, 8.6 ± 0.3, 11.7 ± 0.9, 22.3 ± 0.8, 40.0 ± 0.2, and 54.4 ± 1.7 and those of MECCrt-treated CAL 27 cells were 24.8 ± 0.1, 17.5 ± 0.3, 20.7 ± 0.4, 59.8 ± 1.7, 79.4 ± 0.2, and 85.3 ± 0.5, respectively. Accordingly, MECCrt treatments significantly increased in annexin V-positive intensities of two oral cancer Ca9-22 and CAL 27 cell lines in a dose-responsive manner ($P < 0.01$).

3.4. ROS Generation in MECCrt-Treated Two Oral Cancer Cell Lines. To validate the role of ROS in the MECCrt-induced apoptosis of two oral cancer cell lines, a DCFH-DA assay of flow cytometry was chosen. Figures 4(a) and 4(b) show the relative ROS-positive staining (%) of two oral cancer Ca9-22 and CAL 27 cell lines for the different concentrations of MECCrt treatment for 6 and 12 h incubation. After MECCrt treatment for 6 h, the relative ROS-positive staining (%) of 0, 5, 10, 15, 20, and 25 μg/mL MECCrt-treated Ca9-22 cells was

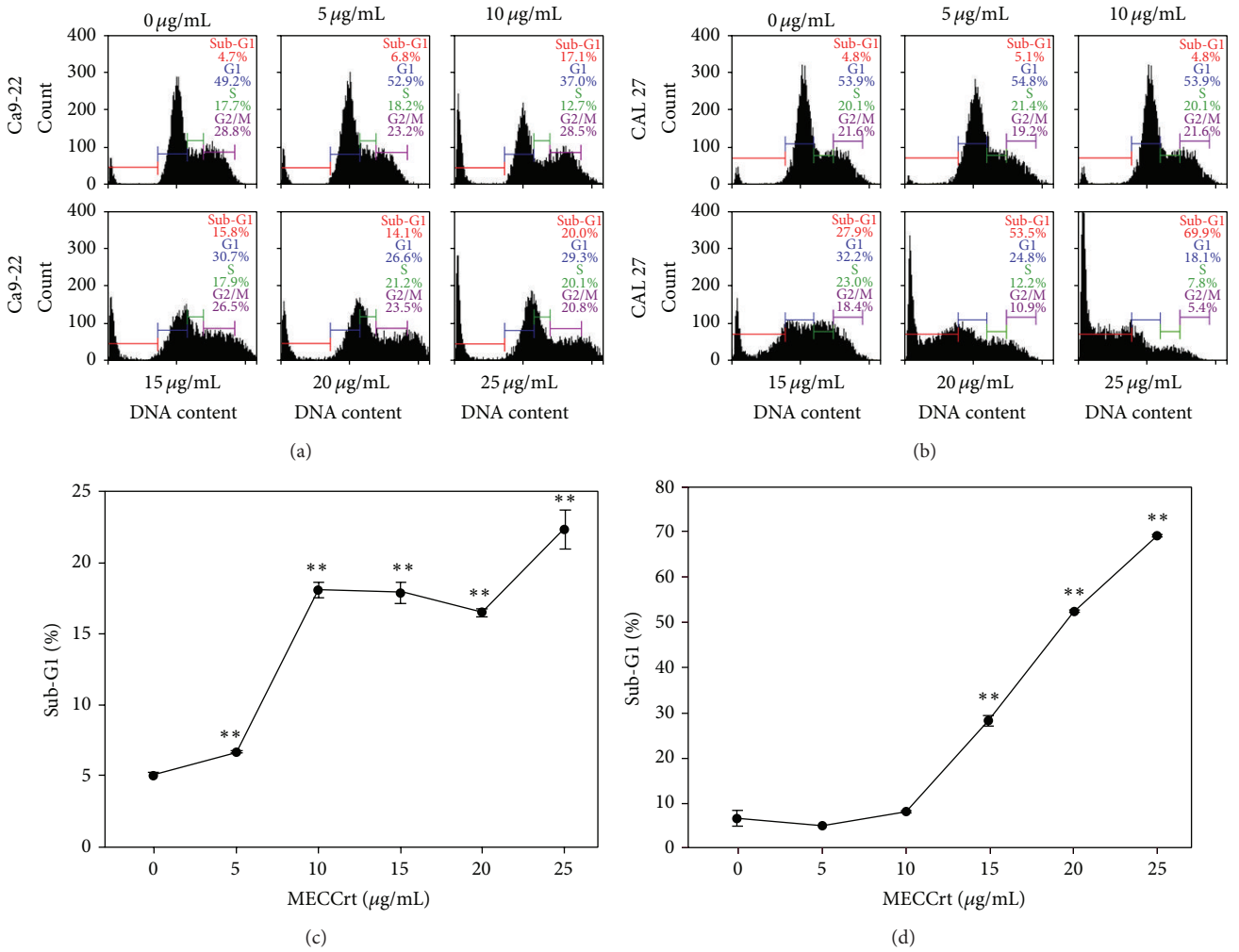

Figure 2: The sub-G1 accumulation of two oral cancer cells was induced by MECCrt. Oral cancer Ca9-22 and CAL 27 cell lines were treated with 0, 5, 10, 15, 20, and 25 μg/mL of MECCrt for 24 h. ((a) and (b)) Representative cell cycle distribution profiles of flow cytometry for MECCrt-treated oral cancer Ca9-22 and CAL 27 cells and vehicles at 24 h, respectively. ((c) and (d)) Statistics analyses for the percentages of sub-G1 population in (a) and (b), respectively. Data, means ± SDs ($n = 3$). $^{**}P < 0.01$ against vehicle.

100.0 ± 1.8, 106.7 ± 0.4, 131.2 ± 0.8, 140.6 ± 1.6, 150.6 ± 0.3, and 183.1 ± 7.8 and that of MECCrt-treated CAL 27 cells was 100.0 ± 0.8, 114.1 ± 1.4, 142.3 ± 1.5, 161.1 ± 0.7, 179.8 ± 1.1, and 185.1 ± 1.4, respectively. After MECCrt treatment for 12 h, the relative ROS-positive staining (%) of 0, 5, 10, 15, 20, and 25 μg/mL MECCrt-treated Ca9-22 cells was 100.0 ± 2.3, 124.1 ± 0.4, 166.4 ± 1.2, 184.8 ± 0.6, 193.3 ± 0.3, and 200.5 ± 0.0 and that of MECCrt-treated CAL 27 cells was 100.0 ± 0.9, 140.7 ± 1.4, 177.1 ± 0.3, 193.8 ± 0.1, 198.6 ± 0.1, and 199.4 ± 0.1, respectively. Accordingly, MECCrt treatments significantly increased in both dose-responsive and time-dependent manners in these two oral cancer cell lines ($P < 0.05$) (Figures 4(c) and 4(d)).

3.5. MMP Depolarization in MECCrt-Treated Two Oral Cancer Cell Lines. Figures 5(a) and 5(b) show the MMP profiles of $DiOC_2(3)$-positive intensities for the vehicle and MECCrt-treated oral cancer cell lines in 24-hour treatments. Treated with MECCrt (0, 5, 10, 15, 20, and 25 μg/mL) for 24 h, the $DiOC_2(3)$-positive (%) intensities of Ca9-22 cells were 100.0 ± 2.9, 96.1 ± 2.4, 94.0 ± 1.6, 76.8 ± 1.4, 45.6 ± 1.4, and 25.0 ± 1.1, respectively. Similarly, the percentages of $DiOC_2(3)$-positive (%) intensities of MECCrt-treated CAL 27 cells were 100.0 ± 1.5, 114.2 ± 0.7, 108.9 ± 1.3, 51.3 ± 0.5, 27.3 ± 0.5, and 7.5 ± 0.4, respectively. Accordingly, MECCrt significantly reduced $DiOC_2(3)$-positive intensities of two oral cancer Ca9-22 and CAL 27 cell lines in a dose-responsive manner ($P < 0.01$–0.05).

4. Discussion

We discovered for the first time that methanolic extracts of the roots of *C. concinna* Hance have an antiproliferative effect on two oral cancer cell lines. The proliferation inhibiting function of MECCrt against oral cancer Ca9-22 and CAL 27 cell lines was dose-responsive (Figure 1).

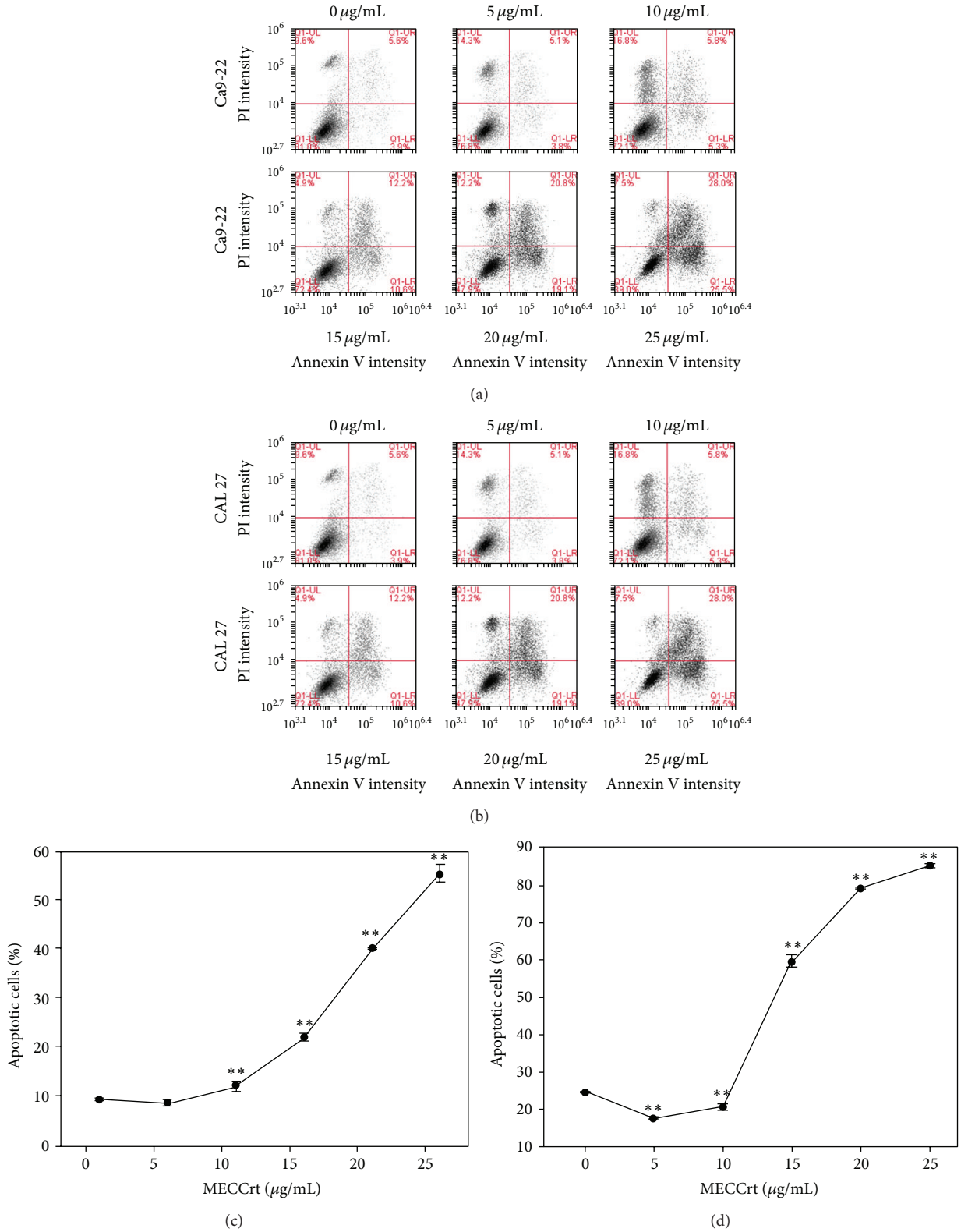

Figure 3: Apoptosis of two oral cancer cells was induced by MECCrt. Oral cancer Ca9-22 and CAL 27 cell lines were treated with 0–25 μg/mL of MECCrt for 24 h. ((a) and (b)) Representative results of annexin V/PI double staining of flow cytometry for MECCrt-treated oral cancer Ca9-22 and CAL 27 cell lines and vehicle controls at 24 h, respectively. ((c) and (d)) Quantification analysis of apoptosis for MECCrt-treated oral cancer Ca9-22 and CAL 27 cell lines in (a) and (b), respectively. Data, means ± SDs ($n = 3$). $^{**}P < 0.01$ against vehicle.

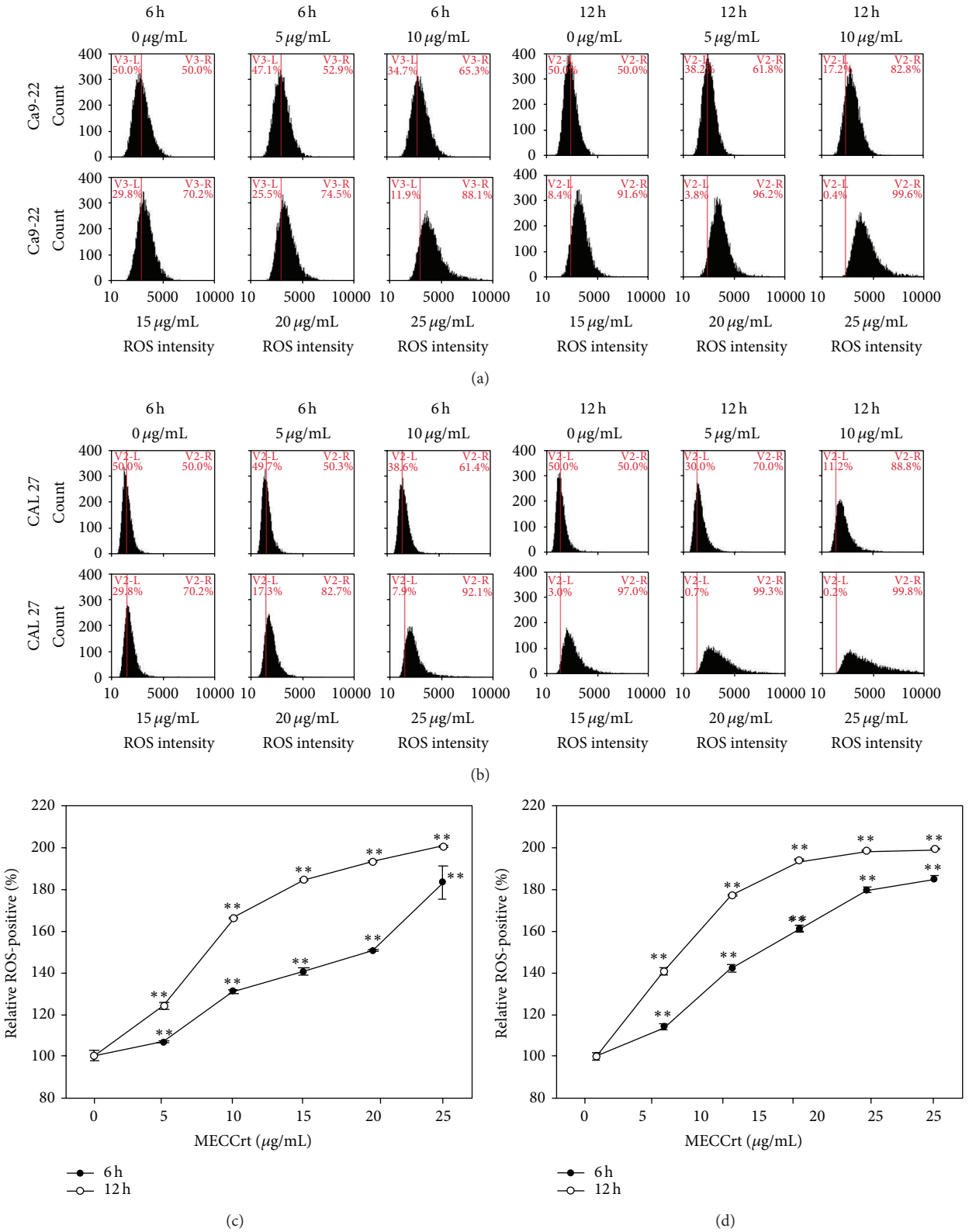

Figure 4: Reactive oxygen species (ROS) generation of two oral cancer cell lines was induced by MECCrt. Oral cancer Ca9-22 and CAL 27 cell lines were treated with different concentrations (0–25 μg/mL) of MECCrt for 6 and 12 h. ((a), (b)) Representative ROS profiles of flow cytometry for MECCrt-treated oral cancer Ca9-22 and CAL 27 cell lines. ((c) and (d)) Statistics analysis of relative ROS intensity in (a) and (b), respectively. Data, means ± SDs ($n = 3$). $^{**}P < 0.01$ against vehicle.

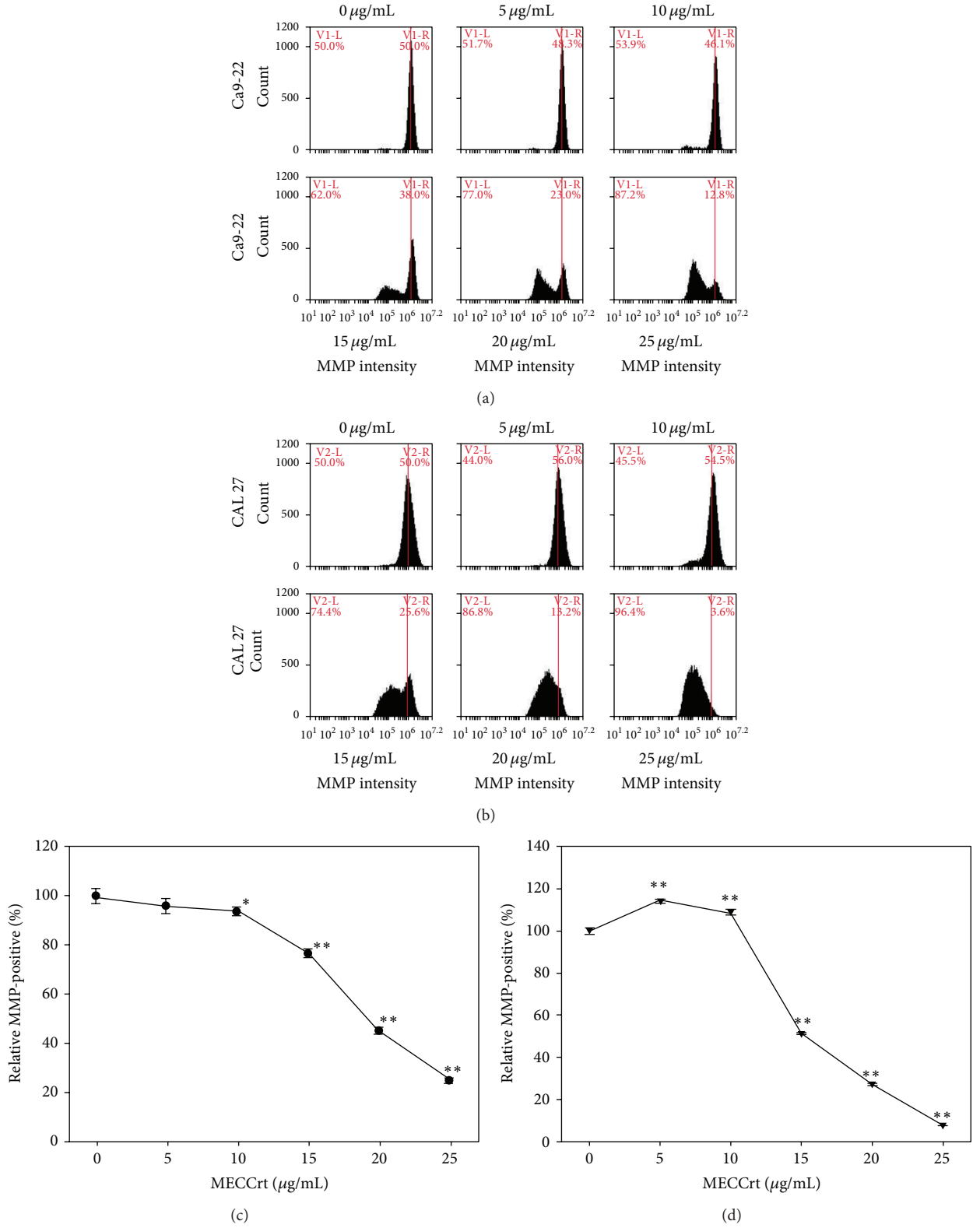

Figure 5: Depolarization of mitochondrial membrane potential (MMP) of Ca9-22 and CAL 27 oral cancer cell lines was induced by MECCrt. Oral cancer Ca9-22 and CAL 27 cell lines were treated with different concentrations (0–25 μg/mL) of MECCrt for 24 h. ((a), (b)) Representative MMP profiles of flow cytometry for MECCrt-treated oral cancer Ca9-22 and CAL 27 cells. ((c) and (d)) Quantification analysis of relative MMP intensity in (a) and (b), respectively. Data, means ± SDs ($n = 3$). $^{*}P < 0.05$ and $^{**}P < 0.01$ against vehicle.

The anticancer effects for other *Cryptocarya*-derived compounds from methanolic extracts of nonroot parts have been reported earlier. For example, for murine leukemia P-388 cells, the IC_{50} values of 2′,4′-dihydroxy-5′,6′-dimethoxychalcone, and isodidymocarpin, isolated from tree bark of *C. costata*, were 5.7 and 11.1 μM [25] and IC_{50} values of the chalcone derivative (desmethylinfectocaryone) and phenolic compound (infectocaryone), isolated from wood of *C. konishii*, were 2.17 and 0.8 μM [26] at 48 h, respectively. For compounds from leaves of *C. chinensis*, the IC_{50} values of infectocaryone and cryptocaryanone A were at the μM level for human lung cancer NCI-H460 cells and glioblastoma SF-268 cells [27]. These *Cryptocarya*-derived compounds from methanolic extracts of nonroot parts showed the IC_{50} values ranging from 0.8 to 11 μM. This is close to our preliminary result that the IC_{50} of the clinical anticancer drug cisplatin at 24 h treatment in oral cancer Ca9-22 cells is 3.06 μg/mL (10.2 μM) (data not shown). In the present study, the IC_{50} values of the MECCrt in oral cancer Ca9-22 and CAL 27 cell lines at 24 h were 18.67 and 13.22 μg/mL, respectively. Although the IC_{50} values of the MECCrt were about 3-4 folds of cisplatin for oral cancer cells, its crude extract nature has to be concerned. Therefore, it is warranted to further investigate the particular bioactive components that are included in the methanolic extracts of *Cryptocarya concinna* Hance roots.

Moreover, the anticancer effect for trunk bark of *C. infectoria*-derived methanol extracts was reported to be cytotoxic to KB cells [24]. KB cells were regarded as oral epidermal carcinoma, however, it was recently validated to have marker chromosomes and DNA finger printings of human cervical cancer HeLa cells (http://www.ncbi.nlm.nih.gov/mesh?Db=mesh&term=KB+Cells) [32]. Accordingly, the anticancer effect of oral cancer by the bioactive compounds from *Cryptocarya* plant remains unclear. Conversely, we here demonstrate the antioral cancer effect of methanolic extracts of a *Cryptocarya* species for the first time, using two OSCC cell lines Ca9-22 and CAL 27.

In several anticancer drugs [6, 7, 10, 11, 33–36], ROS generation is one of the common strategies to inhibit cancer cell proliferation. ROS plays a vital role in early stages of apoptosis [37] and leads to MMP depolarization [38, 39]. Escaping apoptosis is demonstrated to be involved in the drug resistance of cancer cells [40, 41]. To enhance apoptotic induction of anticancer drugs may interfere the drug resistance if there. In the present study, we observed that apoptosis was inducible by MECCrt in two OSCC cell lines as it was demonstrated by sub-G1 monitoring and annexin V/PI assay. We also found that MECCrt significantly induced the ROS level and reduced the MMP level in two oral cancer cell lines in dose-responsive ways. These findings suggest that oxidative stress may be involved in the MECCrt-induced antiproliferative effect in two oral cancer Ca9-22 and CAL 27 cell lines. However, the role of oxidative stress in MECCrt need to be further examined by the ROS scavenger such as N-acetylcysteine [42] to confirm if raised ROS has played a critical role in the process of apoptosis. Furthermore, the ROS may generate nonapoptotic effect like autophagy described in literature [43, 44]. Therefore, it was warranted to further investigate the role of autophagy in MECCrt-treated oral cancer cell lines in future.

5. Conclusions

We demonstrated the antiproliferative and apoptotic effects of MECCrt through ROS generation and mitochondrial depolarization in two OSCC cell lines. Therefore, these results suggest that MECCrt has anticancer potential for oral cancer therapy.

Conflict of Interests

The authors declare that there is no conflict of interests regarding the publication of this paper.

Acknowledgments

This work was supported by funds of the NSC102-2314-B-384-002, MOST103-2320-B-037-008, the 103CM-KMU-09, the National Sun Yat-sen University-KMU Joint Research Project (#NSYSU-KMU 103-p014), the kmtth-102-011, and the Health and welfare surcharge of tobacco products, the Ministry of Health and Welfare, Taiwan, Republic of China (MOHW103-TD-B-111-05). The authors also acknowledge Dr. Hans-Uwe Dahms for the English editing.

References

[1] C.-Y. Yen, C.-H. Chen, C.-H. Chang et al., "Matrix metalloproteinases (MMP) 1 and MMP10 but not MMP12 are potential oral cancer markers," *Biomarkers*, vol. 14, no. 4, pp. 244–249, 2009.

[2] C.-Y. Yen, C.-Y. Huang, M.-F. Hou et al., "Evaluating the performance of fibronectin 1 (FN1), integrin $\alpha 4\beta 1$ (ITGA4), syndecan-2 (SDC2), and glycoprotein CD44 as the potential biomarkers of oral squamous cell carcinoma (OSCC)," *Biomarkers*, vol. 18, no. 1, pp. 63–72, 2013.

[3] H. Myoung, S.-P. Hong, P.-Y. Yun, J.-H. Lee, and M.-J. Kim, "Anti-cancer effect of genistein in oral squamous cell carcinoma with respect to angiogenesis and in vitro invasion," *Cancer Science*, vol. 94, no. 2, pp. 215–220, 2003.

[4] H. K. Kim, E. G. Wilson, Y. H. Choi, and R. Verpoorte, "Metabolomics: a tool for anticancer lead-finding from natural products," *Planta Medica*, vol. 76, no. 11, pp. 1094–1102, 2010.

[5] A. D. Kinghorn, L. Pan, J. N. Fletcher, and H. Chai, "The relevance of higher plants in lead compound discovery programs," *Journal of Natural Products*, vol. 74, no. 6, pp. 1539–1555, 2011.

[6] C.-C. Yeh, C.-N. Tseng, J.-I. Yang et al., "Antiproliferation and induction of apoptosis in Ca9-22 oral cancer cells by ethanolic extract of *Gracilaria tenuistipitata*," *Molecules*, vol. 17, no. 9, pp. 10916–10927, 2012.

[7] C.-C. Yeh, J.-I. Yang, J.-C. Lee et al., "Anti-proliferative effect of methanolic extract of *Gracilaria tenuistipitata* on oral cancer cells involves apoptosis, DNA damage, and oxidative stress," *BMC Complementary and Alternative Medicine*, vol. 12, article 142, 2012.

[8] J. S. Yang, C. W. Lin, C. H. Hsin, M. J. Hsieh, and Y. C. Chang, "*Selaginella tamariscina* attenuates metastasis via Akt pathways

in oral cancer cells," *PLoS ONE*, vol. 8, no. 6, Article ID e68035, 2013.

[9] B. Narotzki, A. Z. Reznick, D. Aizenbud, and Y. Levy, "Green tea: a promising natural product in oral health," *Archives of Oral Biology*, vol. 57, no. 5, pp. 429–435, 2012.

[10] C.-Y. Yen, C.-C. Chiu, R.-W. Haung et al., "Antiproliferative effects of goniothalamin on Ca9-22 oral cancer cells through apoptosis, DNA damage and ROS induction," *Mutation Research*, vol. 747, no. 2, pp. 253–258, 2012.

[11] C.-C. Chiu, J.-W. Haung, F.-R. Chang et al., "Golden berry-derived 4β-hydroxywithanolide E for selectively killing oral cancer cells by generating ROS, DNA damage, and apoptotic pathways," *PLoS ONE*, vol. 8, no. 5, Article ID e64739, 2013.

[12] M. T. Davies-Coleman and D. E. A. Rivett, "Naturally occurring 6-substituted 5,6-dihydro-α-pyrones," *Fortschritte der Chemie Organischer Naturstoffe*, vol. 55, pp. 1–35, 1989.

[13] A. Toribio, A. Bonfils, E. Delannay et al., "Novel seco-dibenzopyrrocoline alkaloid from *Cryptocarya oubatchensis*," *Organic Letters*, vol. 8, no. 17, pp. 3825–3828, 2006.

[14] A. J. Cavalheiro and M. Yoshida, "6-[ω-arylalkenyl]-5,6-dihydro-α-pyrones from *Cryptocarya moschata* (Lauraceae)," *Phytochemistry*, vol. 53, no. 7, pp. 811–819, 2000.

[15] L. D. Juliawaty, M. Kitajima, H. Takayama, S. A. Achmad, and N. Aimi, "A new type of stilbene-related secondary metabolite, idenburgene, from *Cryptocarya idenburgensis*," *Chemical and Pharmaceutical Bulletin*, vol. 48, no. 11, pp. 1726–1728, 2000.

[16] P.-M. Allard, E. T. H. Dau, C. Eydoux et al., "Alkylated flavanones from the bark of *Cryptocarya chartacea* as dengue virus NS5 polymerase inhibitors," *Journal of Natural Products*, vol. 74, no. 11, pp. 2446–2453, 2011.

[17] T.-S. Wu, C.-R. Su, and K.-H. Lee, "Cytotoxic and anti-HIV phenanthroindolizidine alkaloids from *Cryptocarya chinensis*," *Natural Product Communications*, vol. 7, no. 6, pp. 725–727, 2012.

[18] T.-H. Chou, J.-J. Chen, C.-F. Peng, M.-J. Cheng, and I.-S. Chen, "New flavanones from the leaves of *Cryptocarya chinensis* and their antituberculosis activity," *Chemistry and Biodiversity*, vol. 8, no. 11, pp. 2015–2024, 2011.

[19] A. A. Nasrullah, A. Zahari, J. Mohamad, and K. Awang, "Antiplasmodial alkaloids from the bark of *Cryptocarya nigra* (Lauraceae)," *Molecules*, vol. 18, no. 7, pp. 8009–8017, 2013.

[20] R. A. Davis, O. Demirkiran, M. L. Sykes et al., "7′,8′-Dihydroobolactone, a typanocidal α-pyrone from the rainforest tree Cryptocarya obovata," *Bioorganic and Medicinal Chemistry Letters*, vol. 20, no. 14, pp. 4057–4059, 2010.

[21] R. Feng, Z. K. Guo, C. M. Yan, E. G. Li, R. X. Tan, and H. M. Ge, "Anti-inflammatory flavonoids from *Cryptocarya chingii*," *Phytochemistry*, vol. 76, pp. 98–105, 2012.

[22] V. Dumontet, N. Van Hung, M.-T. Adeline et al., "Cytotoxic flavonoids and α-pyrones from *Cryptocarya obovata*," *Journal of Natural Products*, vol. 67, no. 5, pp. 858–862, 2004.

[23] C. Y. Ong, S. K. Ling, R. M. Ali et al., "Systematic analysis of in vitro photo-cytotoxic activity in extracts from terrestrial plants in Peninsula Malaysia for photodynamic therapy," *Journal of Photochemistry and Photobiology B*, vol. 96, no. 3, pp. 216–222, 2009.

[24] V. Dumontet, C. Gaspard, N. van Hung et al., "New cytotoxic flavonoids from *Cryptocarya infectoria*," *Tetrahedron*, vol. 57, no. 29, pp. 6189–6196, 2001.

[25] H. Usman, E. H. Hakim, T. Harlim et al., "Cytotoxic chalcones and flavanones from the tree bark of *Cryptocarya costata*," *Zeitschrift fur Naturforschung C*, vol. 61, no. 3-4, pp. 184–188, 2006.

[26] F. Kurniadewi, L. D. Juliawaty, Y. M. Syah et al., "Phenolic compounds from *Cryptocarya konishii*: their cytotoxic and tyrosine kinase inhibitory properties," *Journal of Natural Medicines*, vol. 64, no. 2, pp. 121–125, 2010.

[27] T.-H. Chou, J.-J. Chen, S.-J. Lee, M. Y. Chiang, C.-W. Yang, and I.-S. Chen, "Cytotoxic flavonoids from the leaves of *Cryptocarya chinensis*," *Journal of Natural Products*, vol. 73, no. 9, pp. 1470–1475, 2010.

[28] J. C. Liao, "Lauraceae in flora of Taiwan," in *Editorial Committee of the Flora of Taiwan*, vol. 2, pp. 448–451, Taipei, Taiwan, 1996.

[29] B. H. Chen, H. W. Chang, H. M. Huang et al., "(-)-anonaine induces DNA damage and inhibits growth and migration of human lung carcinoma H1299 cells," *Journal of Agricultural and Food Chemistry*, vol. 59, no. 6, pp. 2284–2290, 2011.

[30] M.-Y. Lin, Y.-R. Lee, S.-Y. Chiang et al., "Cortex Moutan induces bladder cancer cell death via apoptosis and retards tumor growth in mouse bladders," *Evidence-based Complementary and Alternative Medicine*, vol. 2013, Article ID 207279, 8 pages, 2013.

[31] C.-C. Chiu, P.-L. Liu, K.-J. Huang et al., "Goniothalamin inhibits growth of human lung cancer cells through DNA damage, apoptosis, and reduced migration ability," *Journal of Agricultural and Food Chemistry*, vol. 59, no. 8, pp. 4288–4293, 2011.

[32] J. Masters, "False cell lines.," *Carcinogenesis*, vol. 23, no. 2, p. 371, 2002.

[33] H. Ding, C. Han, D. Guo et al., "Selective induction of apoptosis of human oral cancer cell lines by avocado extracts via a ROS-mediated mechanism," *Nutrition and Cancer*, vol. 61, no. 3, pp. 348–356, 2009.

[34] J.-C. Lee, M.-F. Hou, H.-W. Huang et al., "Marine algal natural products with anti-oxidative, anti-inflammatory, and anti-cancer properties," *Cancer Cell International*, vol. 13, no. 1, article 55, 2013.

[35] C. Gorrini, I. S. Harris, and T. W. Mak, "Modulation of oxidative stress as an anticancer strategy," *Nature Reviews Drug Discovery*, vol. 12, no. 12, pp. 931–947, 2013.

[36] D. Trachootham, J. Alexandre, and P. Huang, "Targeting cancer cells by ROS-mediated mechanisms: a radical therapeutic approach?" *Nature Reviews Drug Discovery*, vol. 8, no. 7, pp. 579–591, 2009.

[37] A. K. Samhan-Arias, F. J. Martín-Romero, and C. Gutiérrez-Merino, "Kaempferol blocks oxidative stress in cerebellar granule cells and reveals a key role for reactive oxygen species production at the plasma membrane in the commitment to apoptosis," *Free Radical Biology and Medicine*, vol. 37, no. 1, pp. 48–61, 2004.

[38] S.-H. Oh and S.-C. Lim, "A rapid and transient ROS generation by cadmium triggers apoptosis via caspase-dependent pathway in HepG2 cells and this is inhibited through *N*-acetylcysteine-mediated catalase upregulation," *Toxicology and Applied Pharmacology*, vol. 212, no. 3, pp. 212–223, 2006.

[39] R. A. Ehlers, A. Hernandez, L. S. Bloemendal, R. T. Ethridge, B. Farrow, and B. M. Evers, "Mitochondrial DNA damage and altered membrane potential ($\Delta\psi$) in pancreatic acinar cells induced by reactive oxygen species," *Surgery*, vol. 126, no. 2, pp. 148–155, 1999.

[40] S. McKenzie and N. Kyprianou, "Apoptosis evasion: the role of survival pathways in prostate cancer progression and therapeutic resistance," *Journal of Cellular Biochemistry*, vol. 97, no. 1, pp. 18–32, 2006.

[41] S. Fulda, "Evasion of apoptosis as a cellular stress response in cancer," *International Journal of Cell Biology*, vol. 2010, Article ID 370835, 6 pages, 2010.

[42] H. Lin, X.-B. Liu, J.-J. Yu, F. Hua, and Z.-W. Hu, "Antioxidant N-acetylcysteine attenuates hepatocarcinogenesis by inhibiting ROS/ER stress in TLR2 deficient mouse," *PLoS ONE*, vol. 8, no. 10, Article ID e74130, 2013.

[43] R. Scherz-Shouval and Z. Elazar, "ROS, mitochondria and the regulation of autophagy," *Trends in Cell Biology*, vol. 17, no. 9, pp. 422–427, 2007.

[44] R. Scherz-Shouval and Z. Elazar, "Regulation of autophagy by ROS: physiology and pathology," *Trends in Biochemical Sciences*, vol. 36, no. 1, pp. 30–38, 2011.

Hindawi Publishing Corporation
The Scientific World Journal
Volume 2014, Article ID 754721, 9 pages
http://dx.doi.org/10.1155/2014/754721

Research Article

A Proteomics Analysis to Evaluate Cytotoxicity in NRK-52E Cells Caused by Unmodified Nano-Fe_3O_4

Yi-Reng Lin,[1] Chao-Jen Kuo,[2] Hugo You-Hsien Lin,[2,3,4] Chin-Jen Wu,[5] and Shih-Shin Liang[6,7]

[1] *Department of Biotechnology, Fooyin University, 151 Jinxue Road, Kaohsiung 83102, Taiwan*
[2] *Graduate Institute of Medicine, Kaohsiung Medical University, 100 Shih-Chuan 1st Road, Kaohsiung 80708, Taiwan*
[3] *Division of Nephrology, Department of Internal Medicine, Kaohsiung Medical University Hospital, Kaohsiung Medical University, 100 Shih-Chuan 1st Road, Kaohsiung 80708, Taiwan*
[4] *Department of Internal Medicine, Kaohsiung Municipal Ta-Tung Hospital, Kaohsiung Medical University, Kaohsiung, Taiwan*
[5] *Kaiser Pharmaceutical Co., Ltd., 9 Huan-Gong Road, Tainan 71041, Taiwan*
[6] *Department of Biotechnology, College of Life Science, Kaohsiung Medical University, 100 Shih-Chuan 1st Road, Kaohsiung 80708, Taiwan*
[7] *Center for Resources, Research and Development, Kaohsiung Medical University, 100 Shih-Chuan 1st Road, Kaohsiung 80708, Taiwan*

Correspondence should be addressed to Shih-Shin Liang; liang0615@kmu.edu.tw

Received 21 April 2014; Accepted 5 June 2014; Published 17 August 2014

Academic Editor: Hsueh-Wei Chang

We synthesized unmodified Fe_3O_4 nanoparticles (NPs) with particles size from 10 nm to 100 nm. We cultured NRK-52E cell lines (rat, kidney) and treated with Fe_3O_4 NPs to investigate and evaluate the cytotoxicity of NPs for NRK-52E cells. Through global proteomics analysis using dimethyl labeling techniques and liquid phase chromatography coupled with a tandem mass spectrometer (LC-MS/MS), we characterized 435 proteins including the programmed cell death related proteins, ras-related proteins, glutathione related proteins, and the chaperone proteins such as heat shock proteins, serpin H1, protein disulfide-isomerase A4, endoplasmin, and endoplasmic reticulum resident proteins. From the statistical data of identified proteins, we believed that NPs treatment causes cell death and promotes expression of ras-related proteins. In order to avoid apoptosis, NRK-52E cell lines induce a series of protective effects such as glutathione related proteins to reduce reactive oxygen species (ROS), and chaperone proteins to recycle damaged proteins. We suggested that, in the indigenous cellular environment, Fe_3O_4 NPs treatment induced an antagonistic effect for cell lines to go to which avoids apoptosis.

1. Introduction

In general, nanoparticles (NPs) are a group of particles with diameter size between one nanometer to one hundred nanometers. NPs have properties such as a high specific surface area and have a high potential to be a good catalytic agent, and therefore NPs have been widely used in fields such as antibacterial [1], antimicrobial [2, 3], drug delivery [4], and global use in research [5, 6]. However, having high catalytic potential, NPs were modified with polysaccharide or chitosan to avoid cytotoxicity [2, 3]. Based on the response of toxicity, NPs such as those that use silver and titanium dioxide were evaluated for cytotoxicity, DNA damage, and reactive oxygen species (ROS) [7–9]. Especially in AgNPs, numerous studies showed that in cellular responses, 100 nm AgNPs induced serine/threonine protein kinase (PAK), phosphatase 2A, and mitogen-activated protein kinase (MAPK) pathways, and 20 nm AgNPs induced ROS, SUMOylation, and protein carbonylation [10]. Moreover, published papers increasingly show that proteomics analysis and LC-MS/MS were utilized

to demonstrate the effects of NPs, such as quantitative proteomics to evaluate AgNPs exert cellular responses [10], AgNPs treatment directly involved in ROS, metal detoxification according to genomics and proteomics results [11], and the toxic effects and behavior in *Caenorhabditis elegans* [12].

Previous studies reported that *in vitro* experiments and AgNPs exposure directly induced ROS, cell death, apoptosis, and inflammation [13, 14]. In animal model studies, female rats had AgNPs accumulation in kidney regions, especially in the glomerulus [15]. A variety of reports showed evidence that AgNPs treatment has cytotoxicity in proteomics and genomics; however no evaluated studies of other NPs are described with Fe_3O_4 or gold nanoparticles.

MS-based quantitative proteomics has been developed at a marvelous rate in the past two decades for biomarker discovery and drug screening. In addition, proteomics provides numerous proteins expression profiles using quantitative techniques to estimate and established the relationships using bioinformatics software. Current quantitative comparisons between specimens both with drug treatment and without treatment or normal and abnormal tissues are beneficial to identify the proteins with upregulation or downregulation and to set up biologic mechanisms and pathways [16, 17]. However in complicated tissue specimens, abundant proteins interfere with the detection of rare proteins. Multiple dimensional separation systems were used to fractionate peptides into different fractions through liquid phase chromatography (LC) to decrease the samples' complication and to increase the amount of protein identification [16, 18].

In this work, we synthesized bare Fe_3O_4 NPs and characterized the size of NPs by transmission electron microscope (TEM). After treatment with unmodified Fe_3O_4 NPs, we next utilized dimethyl labeling quantitative reagents to label the tryptic peptides of NRK-52E cell lines with treated and untreated Fe_3O_4 NPs [19]. In global proteomics research coupled with LC-MS/MS, we demonstrated 435 identified proteins in NRK-52E cell lines by Mascot and simultaneously quantitated 311 proteins through the use of Mascot Distiller bioinformatics software. We classified proteins into chaperone proteins, cell death related and apoptotic proteins, ras-related proteins, and glutathione related proteins. Using STRING for protein-protein interaction [20], we demonstrated the relationships between Fe_3O_4 NPs and multifarious proteins.

2. Materials and Methods

2.1. Chemical Reagents. Sodium acetate, ferric chloride ($FeCl_3$), ferrous chloride ($FeCl_2$), sodium cyanoborohydride ($NaBCNH_3$), and trifluoroacetic acid (TFA) were obtained from Sigma-Aldrich (St. Louis, MO, USA). Acetonitrile (MeCN) was bought from Merck (Seelze, Germany). Ammonium hydrogen carbonate (NH_4HCO_3), hydrochloric acid, sodium hydroxide, sodium dodecyl sulphate (SDS), and ethanol were purchased from J. T. Baker (Phillipsburg, NJ, USA). Formaldehyde-D_2 solution (20% solution in D_2O) was purchased from Isotec Corp. (Miamisburg, OH, USA), while formaldehyde-H_2 solution (36.5%–38% in H_2O), potassium chloride (KCl), sodium chloride (NaCl), sodium dihydrogen phosphate (NaH_2PO_4), potassium dihydrogen phosphate (KH_2PO_4), dimethyl sulfoxide (DMSO), formic acid (FA, 98%–100%), and iodoacetamide (IAM) were purchased from Sigma (St. Louis, MO, USA). Trypsin was purchased from Promega (Madison, WI, USA). The protein concentration of cell lysate was determined by Bradford assay based on the measurement BSA calibration curve (Thermo, Rockford, IL, USA). Deionized H_2O with a resistance of 18.2 MΩ was obtained using a Millipore water system.

2.2. Fabrication of Fe_3O_4 Nanoparticles (NPs) by Hydrothermal Precipitation. The nanoscale magnetic iron oxide particles were prepared by hydrothermal homogeneous coprecipitation [21–23]. Ferric chloride ($FeCl_3$, 5.2 g) and ferrous chloride ($FeCl_2$, 2.0 g) were dissolved with sonication in 50 mL clean glassware containing aqueous hydrochloric acid (2 M, 25 mL) at 50°C. Subsequently, the mixture was degassed continuously using a nitrogen gas cylinder. Sodium hydroxide (NaOH 150 mL, 2 M) was slowly injected drop by drop into the glassware. The color of the solution transformed from yellow to orange, and finally the color shifted to black through the NaOH dripping down. After incubation at 50°C for one hour, the supernatant was removed through a strong magnet absorbing NPs. The generated NPs were then washed with deionized water and removed by a centrifugal tube with 1,800 rpm for two minutes. Then finally the NPs were rinsed with 0.5 M HCl, deionized water and ethanol sequentially.

2.3. Characterization of Fe_3O_4 by Transmission Electron Microscope (TEM). The size of the synthetic Fe_3O_4 NPs was characterized by a JEOL JEM 1200-EX transmission electron microscope (TEM) with the accelerating voltage 80 keV. One μL of the nanoparticles solution was dropped on a cupric grid with stabilized carbon, and subsequently the surplus solution evaporated in the atmosphere.

2.4. NRK-52E Cell Culture, the Conditions of Fe_3O_4 NPs Treatment, and Protein Concentration. The cells, NRK-52E (CRL-1571; American Type Culture Collection, Manassas, VA), were cultured in Dulbecco's modified Eagle's medium (DMEM, Sigma-Aldrich) and supplemented with 5% fetal bovine serum (FBS) and 1% penicillin (Gibco, Grand Island, NY, USA). Cells were cultured in a 100 mm dish with a 5% CO_2 incubator at 37°C. Until cells reached 80% confluence, they were cultured with the absence of serum medium for 24 hours. After starvation cells were treated with 1 ng Fe_3O_4 NPs in each dish for 24 hours, and comparison groups were treated with dimethyl sulfoxide (DMSO). After being washed three times with phosphate-buffered saline (PBS), the cells were lysed with modified RIPA buffer containing 1% NP-40, 0.1% SDS, 150 mM NaCl, 50 mM Tris-HCl, and 1 tablet/10 mL of Roche minicomplete protease inhibitor cocktail at pH 7.5. Finally, the protein concentration of NRK-52E cell lysate was determined using the Bradford assay.

2.5. Tryptic Digestion, Dimethyl Labeling, Desalting, and Fractionation. Samples of lysated protein solution 60 μL

containing 100 μg of total proteins treated with Fe_3O_4 NPs and DMSO were reduced by reaction with 0.7 μL of 1 M DTT and 9.3 μL of 7.5% SDS at 95°C for 5 minutes. The sample bottles were put on ice and then for alkylation were treated with 8 μL of 50 mM IAM at room temperature for 30 minutes in the dark with agitation. Furthermore, sample proteins were precipitated by 52 μL of 50% trichloroacetic acid (TCA) with incubation on ice for 15 minutes. By centrifugation to remove the supernatant, the protein pellets were washed in different solutions according to priority with 150 μL of 10% TCA, 250 μL of deionized H_2O, 250 μL of acetone, and two times with 250 μL of deionized H_2O. After removing the supernatant, the protein pellets were digested in 2 μg of trypsin in 200 μL 50 mM NH_4HCO_3 (pH 8.5). An additional 2 μg of trypsin was added after 4 hours of tryptic digestion, and then the samples were digested for 14 hours at 37°C. Eventually the tryptic digestion samples were dried by vacuum centrifugation to remove the digested buffer. For labeling procedures, the lyophilized samples were redissolved in 180 μL of 100 mM sodium acetate buffer at pH 5.5. Simultaneously the treated NPs samples were labeled using 10 μL of 4% formaldehyde-D_2 and then those samples treated DMSO were labeled using 10 μL of 4% formaldehyde-H_2. Both of the samples were vortexed for 5 minutes, followed by treatment with 10 μL of 600 mM sodium cyanoborohydride for 1 hour. Finally, the labeled solutions were combined after adjusting to pH 2-3 using 10% TFA/H_2O for desalting by a homemade C18 cartridge desalting kit. After vacuum centrifugation drying, the triplicate combined samples were fractionated with a hydrophilic interaction chromatography (HILIC) separated system. HILIC system was performed using an L-7100 pump system (Hitachi, Tokyo, Japan) connecting a TSK gel Amide-80 HILIC column (2.0 mm × 150 mm, 3 μm particle size; Tosoh Biosciences, Tokyo, Japan) with a flow rate of 200 μL/min. The mobile phase system was used for gradient elution: solvent (A) was 0.1% TFA in water; solvent (B) was 0.1% TFA in 100% MeCN. The eluted fraction from the homemade C18 cartridge was dissolved in 25 μL of solution containing 85% MeCN and 0.1% TFA and then injected into the 20 μL sample loop. Furthermore, the gradient was performed as follows: 95% (B) for 2 minutes; 95%~60% (B) for 32 minutes; 60%~5% (B) for 10 minutes; 5% (B) for 5 minutes; 5%~95% (B) for 1 minute; and 95% (B) for 10 minutes. Each fraction contained 1.2 mL buffer in the total of 10 collected fractions, and finally every fraction was dried in a vacuum centrifuged system.

2.6. Protein Identification by LC-MS/MS Analysis. The vacuum dried lyophilized samples were redissolved in 10 μL of 0.1% FA in H_2O and analyzed using a Thermo LTQ Orbitrap XL (Thermo Fisher Scientific, San Jose, CA). A total of 10 μL of sample was injected onto a C18 capillary pretrapped column (0.3 mm × 5 mm, 5 μm particle size, Agilent Zorbax XDB); HPLC loading pump and separation was performed by a C18 column (i.d. 75 μm × 150 mm, 3 μm particle size, Micro Tech, Fontana, CA). A LC-MS/MS separation was performed using an Agilent 1200 series Nanoflow pump (Agilent Technologies, Santa Clara, CA). The flow rate of loading pump was set at 5 μL/min, and the gradient pump was set at 300 nL/min. The mobile phases consisted of (A) 0.1% FA in water and (B) 0.1% FA in 100% MeCN. The linear gradient was as follows: 2% (B) in 2 minutes, 2%~40% (B) in 40 minutes, 40%~95% (B) in 8 minutes, 95% (B) in 2 minutes, 95%~2% (B) in 1 minute, and 2% (B) in 7 minutes. The digested peptides were detected by a voltage of 1.8 kV in the positive detection ion mode. The separated system with full scanning mode conditions was set at m/z 400–1600 Da with resolution = 30,000. The data-dependent mode was set according to a priority to select peptides which were detected with 5 high-intensity signals in the MS mode and transferred into collision chamber for fragmentation with a collision energy of 35 eV. The fragmented ions were analyzed and detected at second MS analyzer with a mass range of m/z 100–2000 Da. To exclude ions with similar m/z and avoid interferences, the data-dependent mode was also set a repeat duration of 30 seconds.

2.7. Mascot Database Search and Mascot Distiller Quantitation. The software Xcalibur (version 2.0.7, Thermo Scientific Inc., San Jose, CA) was utilized to control Orbitrap XL and to acquire the MS and fragmentation data. The raw data including MS and MS/MS spectra were converted to a suitable file type by the Mascot Distiller software (version 2.5.1.0 (64 bits), Matrix Science Ltd., London, UK) to perform protein identification and quantitation. The parameters of the Mascot Distiller were set as follows: "Orbitrap_res_MS2" (default parameter setting) for peak list transformation; "Rattus" for the taxonomy in the Swiss-Prot databank of the Mascot search engine; zero allowable missed cleavages for tryptic digestion; dimethylation (MD) for quantitation; fixed modification was selected carbamidomethyl for cysteine modification; peptide tolerance of 10 ppm with precursor ions; and 0.8 Da tolerance for MS/MS. Peptides charge was selected when they had charges of 1^+, 2^+, and 3^+, and the instrument was set to "ESI-trap." Finally, the protein quantitative result was listed by the heavy-labeled/light-labeled (D/H) ratios from the Mascot Distiller.

3. Results and Discussion

3.1. Fe_3O_4 NPs Synthesis and Characterization. Bare and unmodified Fe_3O_4 NPs were synthesized by hydrothermal precipitation and NPs were fabricated by chemical method to have a uniform particle size. In Figure 1, TEM images showed that we took three photos of Fe_3O_4 NPs with 20 nm, 50 nm, and 100 nm scale bars. It is considered that NPs with a higher surface area are easier to aggregate with other NPs; therefore through the aggregation in Fe_3O_4 NPs there were Fe_3O_4 particles generated above 100 nm if no additional protective agent was modified onto Fe_3O_4 (Figure 1(c)). We considered that Fe_3O_4 NPs with dispersive diameter sizes are suitable for cytotoxicity evaluation due to the fact that NPs found in the environment have random sizes.

3.2. Schematic Representation of Samples Pretreatments, Fractionation, Protein Identification, and Protein Quantitation.

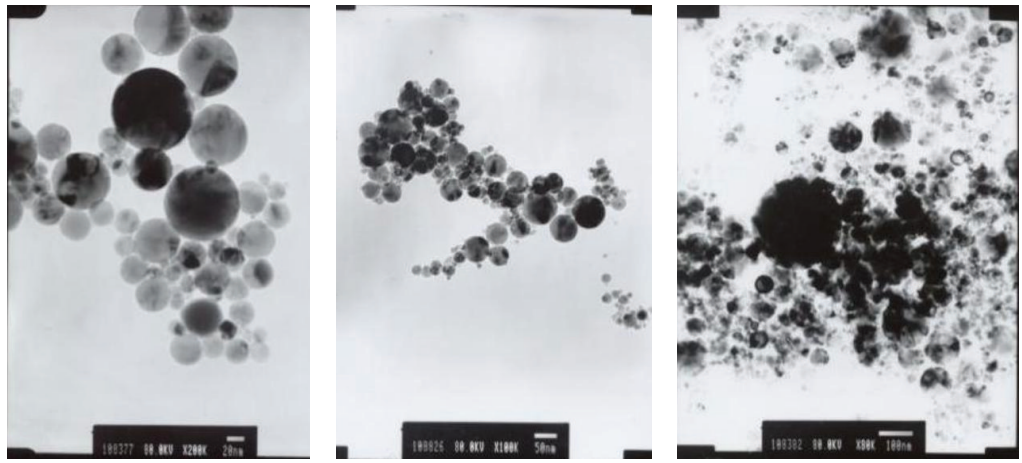

(a) (b) (c)

Figure 1: TEM images of Fe_3O_4 NPs with different sizes as follows: (a) 20 nm, (b) 50 nm, and (c) 100 nm scale bars.

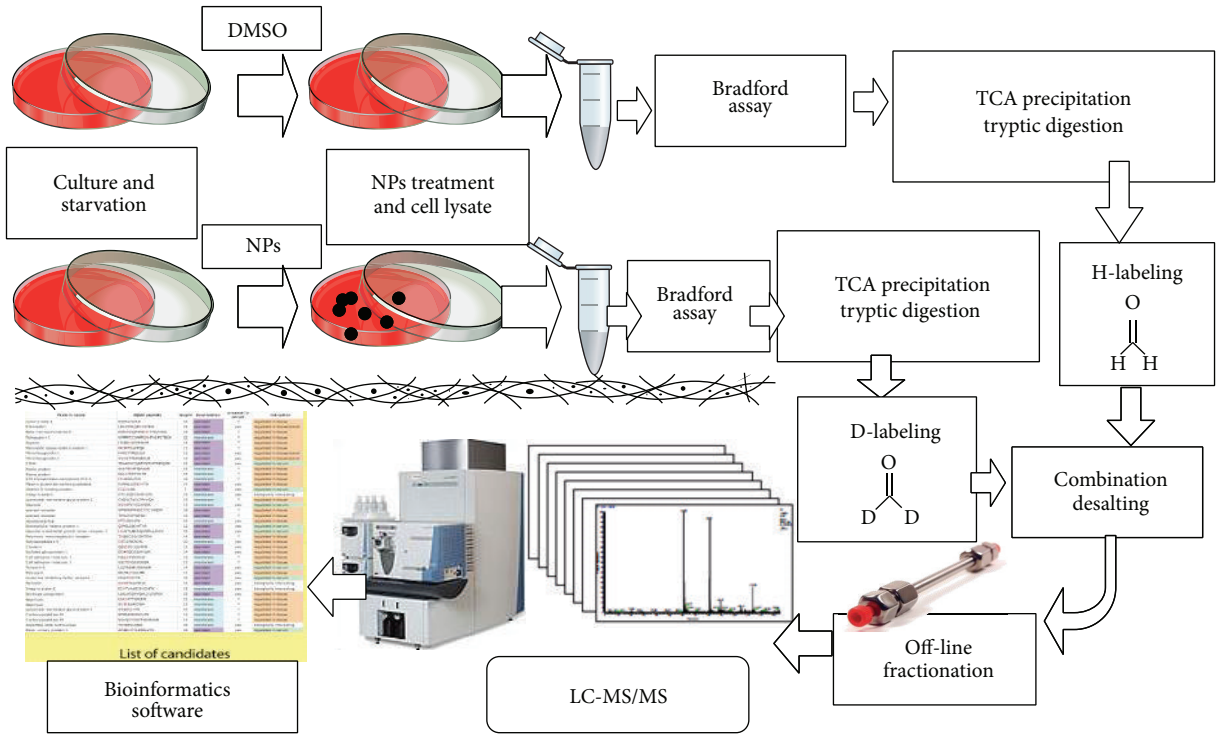

Figure 2: Simplified flow chart of sample pretreatment, fractionation, and analysis using LC-MS/MS.

For protein quantitation, the procedures and using reagents including formaldehyde-H_2, formaldehyde-D_2, and sodium cyanoborohydride ($NaBCNH_3$) were obeyed as following the previous literature [19]. By utilization of dimethyl labeling, the differences of protein expressions in treatment with and without NPs was enabled to be determined. In the mass spectrum, the proteins of NRK-52E treated NPs were labeled as formaldehyde-D_2 and proteins of untreated NPs were labeled as formaldehyde-H_2. In the same sequential peptides, however, different treatments had a mass difference 4 Da or 8 Da depending on the use of the labeling agent. Off-line HILIC fractionation was utilized to decrease the complication of the mixed samples [16, 18]. Through LC-MS/MS, the proteins identification and quantitative ratios of D/H peptides were identified and calculated using the bioinformatic Mascot Distiller software to finally generate a protein list. The

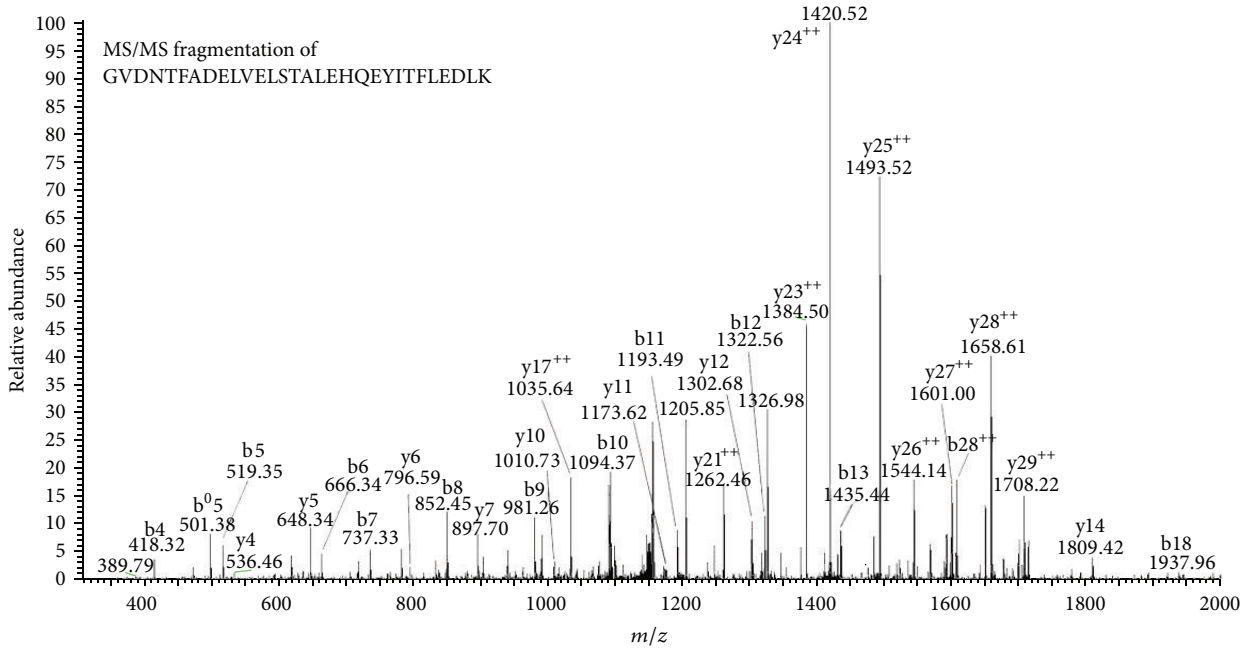

Figure 3: MS/MS spectrum of the peptide sequence GVDNTFADELVELSTALEHQEYITFLEDLK (m/z 1168.60, 3^+), which is a peptide of complement component 1 Q subcomponent-binding protein (C1qBP).

schematic flow chart of the process is shown in Figure 2 from sample pretreatment and protein identification to protein quantitation.

3.3. Quantitative Results of NRK-52E Proteins Associated with Fe_3O_4 NPs. From the statistical results we identified 435 proteins, of which 311 proteins have a D/H ratio and 124 proteins which we were unable to specific values. For example, complement component 1 Q subcomponent-binding protein (C1qBP) was identified with an arithmetic average D/H ratio of 4.23. Figure 3 showed the peptide belonging to C1qBP having sequences GVDNTFADELVELSTALEHQEYITFLEDLK which was fragmentized by collision induced dissociation (CID), and its MS/MS spectrum was illustrated by y-ions and b-ions. From a quantitative standpoint in support of the Mascot Distiller in bioinformatics software, the result of protein list showed that the D/H ratio belonging to GVDNTFADELVELSTALEHQEYITFLEDLK peptide was 4.23. Simultaneously the raw data from LC-MS/MS that we extracted from the labeled peptide of C1qBP by m/z 1165.92 (3^+, H-labeled) and 1168.60 (3^+, D-labeled) presented signals of peak area and peak height (Figure 4(a)) and showed the isotope pattern of H-labeled peptide and D-labeled peptide (Figure 4(b)) which demonstrated the changes in different labeling. The statistical results showed that peak area was 4.42-fold in D/H ratio and peak height was 4.22-fold; the statistical data was calculated and shown in Table 1.

3.4. Differentially Expressed Proteins of NRK-52E by Treatment with Fe_3O_4 NPs. In this study, we used Fe_3O_4 NPs to treat NRK-52E and used bioinformatics software to generate proteins identification and proteins quantitation

Table 1: The MS intensities of peptide GVDNTFADELVELSTALEHQEYITFLEDLK labeled H (m/z 1165.92) and labeled D (m/z 1168.60) in peak area and peak height.

m/z	Peak area	Peak height	Ratio of area	Ratio of height
1165.92	4084412	1240520	4.42	4.22
1168.60	18036323	5230797		

with a protein list (the protein list is shown in the electronic supplementary information available online in Supplementary Materials at http://dx.doi.org/10.1155/2014/754721). In the protein list, we observed that when Fe_3O_4 NPs were treated, ras-related proteins were expressed including ras-related protein Rab-7L1 (RAB7L_RAT, 3.2-folds), ras-related protein Rab-1A (RAB1A_RAT, 2.3-folds), ras-related protein Rab-2A (RAB2A_RAT, 1.6-folds), ras-related C3 botulinum toxin substrate 1 (RAC1_RAT, 1.2-folds), ras-related protein Rap-1A (RAP1A_RAT), and ras-related protein Rab-7a (RAB7A_RAT). Accor-ding to previous studies, ras-related proteins were associated with cancer cell metastasis [24, 25], and ras-related C3 botulinum toxin substrate 1 was associated with differential roles such as cell proliferation which could be inhibited by miR-101 [26] and signal transduction to upregulate in esophageal squamous cell carcinoma and esophageal adenocarcinoma [27].

We also identified related proteins in cell death and apoptosis, such as apoptotic protease-activating factor 1 (APAF_RAT, 780.9-folds), programmed cell death protein 10 (PDC10_RAT, 233.2-folds), galectin-1 (LEG1_RAT, 1.75-folds), and programmed cell death 6-interacting protein

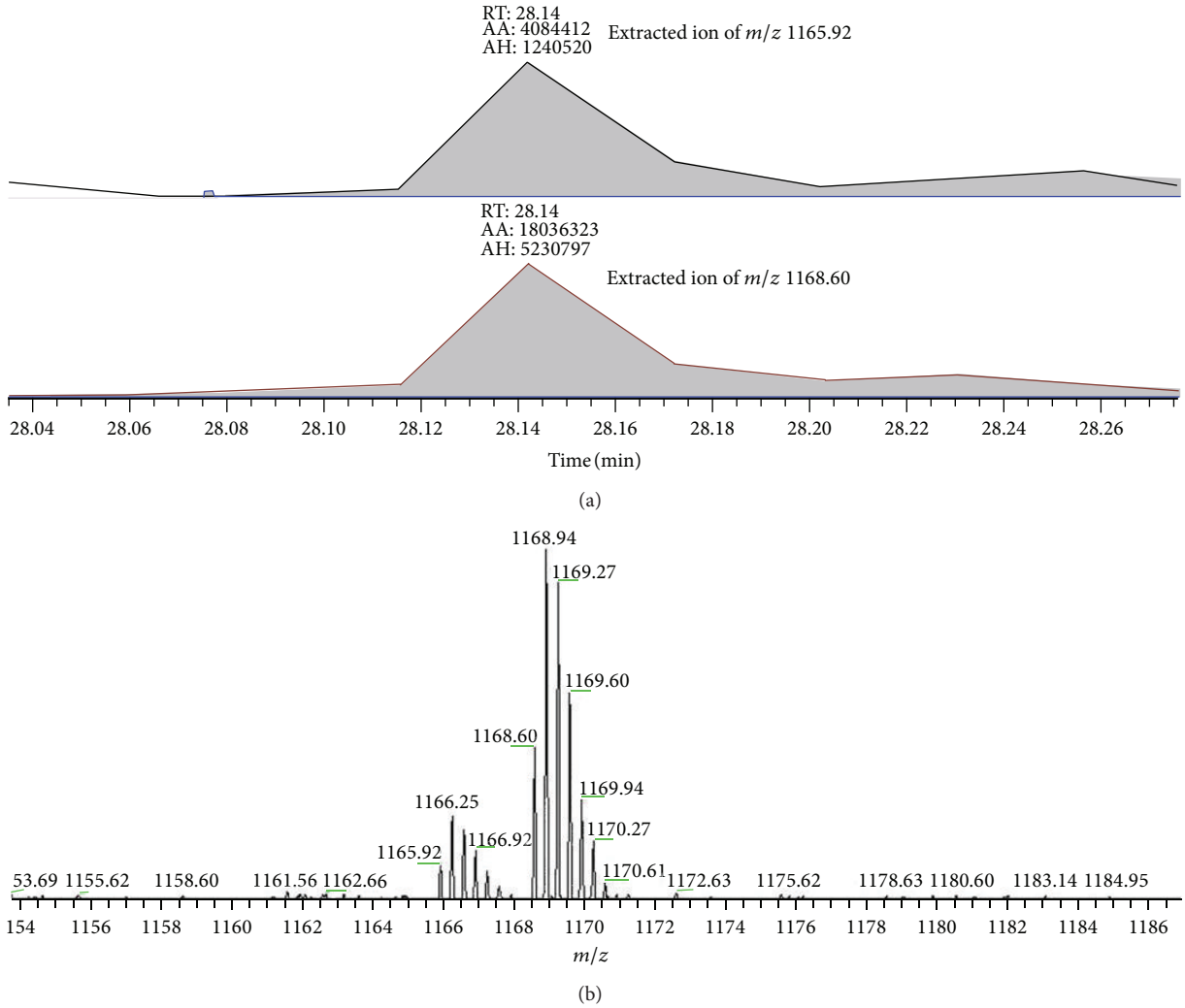

Figure 4: (a) Extracted ions of m/z 1165.92 (H-labeled) and m/z 1165.92 (D-labeled) showing signals of peak area (AA) and peak height (AH). (b) MS spectrum of GVDNTFADELVELSTALEHQEYITFLEDLK which are labeled formaldehyde-H_2 and formaldehyde-D_2. These two labeled peptides are shown in a coeluted isotopic pattern.

(PDC6I_RAT). Apoptotic protease-activating factor 1 activated procaspase-9 and modulated cellular apoptosis [28]. However, programmed cell death protein 10 promotes cell proliferation and protects malignant T cells from apoptosis [29]. The galectin family played different roles in cell apoptosis such as galectin-7 enhancing apoptosis, but galectin-1 has the opposite effect [30]. In accordance with previous studies and the proteins quantitative list, we considered that the treatment of Fe_3O_4 NPs caused an antagonistic effect. Fe_3O_4 NPs induced expression of ras-related proteins and induced programmed cell death protein 10, galectin 1 to promote cell metastasis, proliferation, and progression. However, the apoptotic protease-activating factor 1 promoted cell to go to apoptosis.

A variety of glutathione-related proteins with high expression were identified, such as glutathione reductase (Fragment), glutathione S-transferase Mu 1, glutathione S-transferase Mu 2, glutathione S-transferase P, and glutathione S-transferase alpha-3. We thought that Fe_3O_4 NPs induced reactive oxygen species (ROS) to cause overexpression of glutathione-related proteins. After one day of Fe_3O_4 NPs treatment, a strong magnet was utilized to recover the residual NPs, but there were no NPs to be recycled. We considered that the NPs had transferred into ferric ions (Fe^{3+}) and ferrous ions (Fe^{2+}) and that endogenous hydrogen peroxide (H_2O_2) reacted with ferrous ions to compose hydroxide free radicals (Fenton reaction) [31, 32]. A variety of reports show that ROS effects are exhibited when NPs were treated [7, 14]. However, ferrous ion (Fe^{2+}) is an initiator in the Fenton reaction, and ferrous ions will react with hydrogen peroxide to produce hydroxide free radicals.

3.5. Chaperone Proteins Overexpression and STRING Networks Establishment. We also characterized chaperone proteins such as heat shock proteins, serpin H1, protein disulfide-isomerase, endoplasmin, and endoplasmic reticulum resident protein.

Table 2: Statistic classification of related proteins in NRK-52E cell lines with Fe_3O_4 NPs treatment.

UNIPROT accession[a]	UNIPROT accession number[a]	Protein identification	Molecular mass (kDa)[b]	Number of peptides[b]	Ratio[c]
		Cell death and apoptosis related proteins			
APAF_RAT	Q9EPV5	Apoptotic protease-activating factor 1	146.1	2	780.9
PDC10_RAT	Q6NX65	Programmed cell death protein 10	25.0	2	233.2
LEG1_RAT	P11762	Galectin-1	15.5	5	1.75
PDC6I_RAT	Q9QZA2	Programmed cell death 6-interacting protein	99.2	n.d.	n.d.
		Ras-related proteins			
RAB7L_RAT	Q63481	Ras-related protein Rab-7L1	23.7	2	3.2
RAB1A_RAT	Q6NYB7	Ras-related protein Rab-1A	23.4	13	2.3
RAB2A_RAT	P05712	Ras-related protein Rab-2A	24.1	3	1.6
RAC1_RAT	Q6RUV5	Ras-related C3 botulinum toxin substrate 1	22.4	2	1.2
RAP1A_RAT	P62836	Ras-related protein Rap-1A	21.8	n.d.	n.d.
RAB7A_RAT	P09527	Ras-related protein Rab-7a	24.3	n.d.	n.d.
		Glutathione related proteins			
GSHR_RAT	P70619	Glutathione reductase (Fragment)	47.8	2	3.1
GSTM1_RAT	P04905	Glutathione S-transferase Mu 1	26.7	2	2.8
GSTM2_RAT	P08010	Glutathione S-transferase Mu 2	26.5	3	2.4
GSTP1_RAT	P04906	Glutathione S-transferase P	24.1	6	1.5
GSTA3_RAT	P04904	Glutathione S-transferase alpha-3	25.9	4	1.2
		Chaperone proteins			
HSBP1_RAT	Q8K3X8	Heat shock factor-binding protein 1	8.7	2	2.8
HS90B_RAT	P34058	Heat shock protein HSP 90-beta	86.0	32	2.7
SERPH_RAT	P29457	Serpin H1	47.7	30	2.5
HS90A_RAT	P82995	Heat shock protein HSP 90-alpha	87.7	31	2.4
HSP74_RAT	O88600	Heat shock 70 kDa protein 4	97.0	2	2.2
HSP7C_RAT	P63018	Heat shock cognate 71 kDa protein	72.8	40	1.9
PDIA4_RAT	P38659	Protein disulfide-isomerase A4	75.1	9	1.8
CH60_RAT	P63039	60 kDa heat shock protein, mitochondrial	62.6	29	1.6
CH10_RAT	P26772	10 kDa heat shock protein, mitochondrial	11.2	3	1.6
GRP78_RAT	P06461	78 kDa glucose-regulated protein	74.4	19	1.6
ENPL_RAT	Q66HD0	Endoplasmin	95.4	17	1.6
PDIA1_RAT	P04785	Protein disulfide-isomerase	59.1	24	1.6
ERP29_RAT	P52555	Endoplasmic reticulum resident protein 29	29.3	3	1.6
PDIA6_RAT	Q63081	Protein disulfide-isomerase A6	49.6	4	1.5
PDIA3_RAT	P11598	Protein disulfide-isomerase A3	58.6	17	1.3

[a] Protein accession and protein accession number were received from the UNIPROT database available online: http://www.uniprot.org/uniprot (accessed on May 25, 2014).
[b] Molecular weight and number of protein peptides according to the Swiss-Prot database in the Mascot search engine.
[c] Ratio values of each protein according to protein list in the Mascot Distiller.

Eventually, we used the STRING (vision 9.1, http://string-db.org/) database to establish the interactions between chaperone proteins and related proteins to demonstrate the relationships between Fe_3O_4 NPs and the associated proteins [20]. The relationships between chaperone proteins, ras-related proteins, glutathione related proteins, and cell death and apoptosis related proteins are listed in Table 2 and illustrated by STRING in Figure 5. Heat shock proteins connected

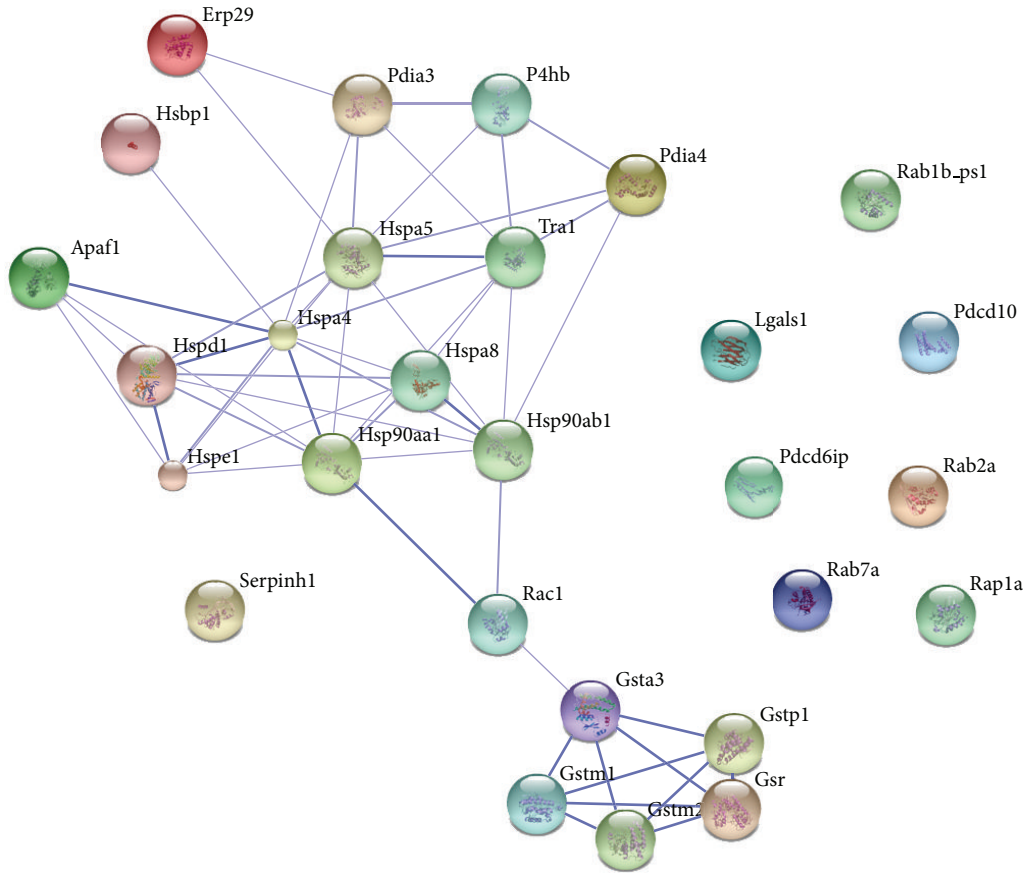

Figure 5: Schematic representation of the networks between cell death and apoptosis related proteins, ras-related proteins, glutathione related proteins, and chaperone proteins.

with each other and related ras-related C3 botulinum toxin substrate 1 and then combined to glutathione related proteins.

4. Conclusion

This is a pioneer experiment to show the cellular responses through Fe_3O_4 NPs treatment. We hypothesized an antagonistic effect in NRK-52E cell lines which is presented as cell death, apoptosis, and cancerization via programmed cell death protein and ras-related proteins; however there are protective mechanism proteins in NRK-52E such as chaperone proteins and glutathione related proteins. In future work, we shall generate or purchase Fe_3O_4 NPs in a smaller size to confirm the size effect of NPs, and we also need more evidence to prove the ROS effect induced via ferrous ions and to explain the tendency towards apoptosis or to avoid cell death.

Conflict of Interests

The all authors declare that they have no conflict of interests in this study.

Acknowledgments

This work was supported by a grant from the Kaohsiung Medical University Research Foundation (KMU-Q110023), with cooperation between the National Sun Yat-Sen University and Kaohsiung Medical University (NSYSUKMU 103-P010) and the National Science Council (NSC 102-2113-M-037-013-MY2), Taipei, Taiwan. The authors are thankful for the assistance of the Center for Resources, Research and Development of Kaohsiung Medical University.

References

[1] C. You, C. Han, X. Wang et al., "The progress of silver nanoparticles in the antibacterial mechanism, clinical application and cytotoxicity," *Molecular Biology Reports*, vol. 39, no. 9, pp. 9193–9201, 2012.

[2] A. Travan, C. Pelillo, I. Donati et al., "Non-cytotoxic silver nanoparticle-polysaccharide nanocomposites with antimicrobial activity," *Biomacromolecules*, vol. 10, no. 6, pp. 1429–1435, 2009.

[3] T. V. Mathew and S. Kuriakose, "Photochemical and antimicrobial properties of silver nanoparticle- encapsulated chitosan

functionalized with photoactive groups," *Materials Science and Engineering C*, vol. 33, no. 7, pp. 4409–4415, 2013.

[4] W. Ding and L. Guo, "Immobilized transferrin Fe_3O_4@SiO_2 nanoparticle with high doxorubicin loading for dual-targeted tumor drug delivery," *International Journal of Nanomedicine*, vol. 8, no. 1, pp. 4631–4639, 2013.

[5] H. Zhang, K. E. Burnum, M. L. Luna et al., "Quantitative proteomics analysis of adsorbed plasma proteins classifies nanoparticles with different surface properties and size," *Proteomics*, vol. 11, no. 23, pp. 4569–4577, 2011.

[6] D. Simberg, J. Park, P. P. Karmali et al., "Differential proteomics analysis of the surface heterogeneity of dextran iron oxide nanoparticles and the implications for their in vivo clearance," *Biomaterials*, vol. 30, no. 23-24, pp. 3926–3933, 2009.

[7] M. Faria, J. M. Navas, A. M. Soares, and C. Barata, "Oxidative stress effects of titanium dioxide nanoparticle aggregates in zebrafish embryos," *Science of the Total Environment*, vol. 470-471, pp. 379–389, 2014.

[8] B. Trouiller, R. Reliene, A. Westbrook, P. Solaimani, and R. H. Schiestl, "Titanium dioxide nanoparticles induce DNA damage and genetic instability in vivo in mice," *Cancer Research*, vol. 69, no. 22, pp. 8784–8789, 2009.

[9] P. Das, M. A. Xenopoulos, and C. D. Metcalfe, "Toxicity of silver and titanium dioxide nanoparticle suspensions to the aquatic invertebrate, Daphnia magna," *Bulletin of Environmental Contamination and Toxicology*, vol. 91, no. 1, pp. 76–82, 2013.

[10] T. Verano-Braga, R. Miethling-Graff, K. Wojdyla et al., *Insights into the Cellular Response Triggered by Silver Nanoparticles Using Quantitative Proteomics*, ACS Nano, 2014.

[11] F. Mirzajani, H. Askari, S. Hamzelou et al., "Proteomics study of silver nanoparticles toxicity on *Bacillus thuringiensis*," *Ecotoxicology and Environmental Safety*, vol. 100, pp. 122–130, 2014.

[12] X. Yang, C. Jiang, H. Hsu-Kim et al., "Silver nanoparticle behavior, uptake, and toxicity in *Caenorhabditis elegans*: effects of natural organic matter," *Environmental Science & Technology*, vol. 48, no. 6, pp. 3486–3495, 2014.

[13] P. V. AshaRani, G. L. K. Mun, M. P. Hande, and S. Valiyaveettil, "Cytotoxicity and genotoxicity of silver nanoparticles in human cells," *ACS Nano*, vol. 3, no. 2, pp. 279–290, 2009.

[14] R. P. Singh and P. Ramarao, "Cellular uptake, intracellular trafficking and cytotoxicity of silver nanoparticles," *Toxicology Letters*, vol. 213, no. 2, pp. 249–259, 2012.

[15] W. Kim, J. Kim, J. D. Park, H. Y. Ryu, and I. J. Yu, "Histological study of gender differences in accumulation of silver nanoparticles in kidneys of Fischer 344 rats," *Journal of Toxicology and Environmental Health A*, vol. 72, no. 21-22, pp. 1279–1284, 2009.

[16] C.-J. Kuo, S.-S. Liang, E. Hsi, S.-H. Chiou, and S.-D. Lin, "Quantitative proteomics analysis of varicose veins: Identification of a set of differentially expressed proteins related to ATP generation and utilization," *Kaohsiung Journal of Medical Sciences*, vol. 29, no. 11, pp. 594–605, 2013.

[17] M. F. Ellias, S. H. Z. Ariffin, S. A. Karsani, M. A. Rahman, S. Senafi, and R. M. A. Wahab, "Proteomic analysis of saliva identifies potential biomarkers for orthodontic tooth movement," *The Scientific World Journal*, vol. 2012, Article ID 647240, 6 pages, 2012.

[18] S. B. Ficarro, Y. Zhang, M. J. Carrasco-Alfonso et al., "Online nanoflow multidimensional fractionation for high efficiency phosphopeptide analysis," *Molecular & Cellular Proteomics*, vol. 10, no. 11, Article ID O111.011064, 2011.

[19] J. Hsu, S. Huang, N. Chow, and S. Chen, "Stable-isotope dimethyl labeling for quantitative proteomics," *Analytical Chemistry*, vol. 75, no. 24, pp. 6843–6852, 2003.

[20] A. Franceschini, D. Szklarczyk, S. Frankild et al., "STRING v9.1: protein-protein interaction networks, with increased coverage and integration," *Nucleic Acids Research*, vol. 41, no. 1, pp. D808–D815, 2013.

[21] W.-Y. Chen and Y.-C. Chen, "Functional Fe_3O_4@ZnO magnetic nanoparticle-assisted enrichment and enzymatic digestion of phosphoproteins from saliva," *Analytical and Bioanalytical Chemistry*, vol. 398, no. 5, pp. 2049–2057, 2010.

[22] H. Lin, W. Chen, and Y. Chen, "Iron oxide/tantalum oxide core-shell magnetic nanoparticle-based microwave-assisted extraction for phosphopeptide enrichment from complex samples for MALDI MS analysis," *Analytical and Bioanalytical Chemistry*, vol. 394, no. 8, pp. 2129–2136, 2009.

[23] K. Woo, J. Hong, S. Choi et al., "Easy synthesis and magnetic properties of iron oxide nanoparticles," *Chemistry of Materials*, vol. 16, no. 14, pp. 2814–2818, 2004.

[24] Y. X. Yin, F. Shen, H. Pei et al., "Increased expression of Rab25 in breast cancer correlates with lymphatic metastasis," *Tumor Biology*, vol. 33, no. 5, pp. 1581–1587, 2012.

[25] H. C. Adams III, R. Chen, Z. Liu, and I. P. Whitehead, "Regulation of breast cancer cell motility by T-cell lymphoma invasion and metastasis-inducing protein," *Breast Cancer Research*, vol. 12, no. 5, article R69, 2010.

[26] X. Lin, H. Guan, H. Li et al., "miR-101 inhibits cell proliferation by targeting Rac1 in papillary thyroid carcinoma," *Bioscience Reports*, vol. 2, no. 1, pp. 122–126, 2014.

[27] M. Bashir, D. Kirmani, H. F. Bhat et al., "P66shc and its downstream Eps8 and Rac1 proteins are upregulated in esophageal cancers," *Cell Communication and Signaling*, vol. 8, article 13, 2010.

[28] L. Mondragón, M. Orzáez, G. Sanclimens et al., "Modulation of cellular apoptosis with apoptotic protease-activating factor 1 (Apaf-1) inhibitors," *Journal of Medicinal Chemistry*, vol. 51, no. 3, pp. 521–529, 2008.

[29] B. Lauenborg, K. Kopp, T. Krejsgaard et al., "Programmed cell death-10 enhances proliferation and protects malignant T cells from apoptosis," *APMIS*, vol. 118, no. 10, pp. 719–728, 2010.

[30] B. Barkan, A. D. Cox, and Y. Kloog, "Ras inhibition boosts galectin-7 at the expense of galectin-1 to sensitize cells to apoptosis," *Oncotarget*, vol. 4, no. 2, pp. 256–268, 2013.

[31] E. W. Iyamu, H. Perdew, and G. M. Woods, "Cysteine-iron promotes arginase activity by driving the Fenton reaction," *Biochemical and Biophysical Research Communications*, vol. 376, no. 1, pp. 116–120, 2008.

[32] S. Toyokuni, "Iron and carcinogenesis: from Fenton reaction to target genes," *Redox Report*, vol. 7, no. 4, pp. 189–197, 2002.

Hindawi Publishing Corporation
The Scientific World Journal
Volume 2014, Article ID 937051, 8 pages
http://dx.doi.org/10.1155/2014/937051

Research Article

The Antiproliferative and Apoptotic Effects of Sirtinol, a Sirtuin Inhibitor on Human Lung Cancer Cells by Modulating Akt/β-Catenin-Foxo3A Axis

Yao Fong,[1] Yin-Chieh Lin,[2] Chang-Yi Wu,[3] Hui-Min David Wang,[4] Li-Li Lin,[5] Han Lin Chou,[2] Yen-Ni Teng,[6] Shyng-Shiou Yuan,[7] and Chien-Chih Chiu[2,3,7]

[1] *Department of Thoracic Surgery, Chi-Mei Medical Center, Tainan 710, Taiwan*
[2] *Department of Biotechnology, Kaohsiung Medical University, Kaohsiung 807, Taiwan*
[3] *Department of Biological Sciences, National Sun Yat-sen University, 70 Lien Hai Road, Kaohsiung 804, Taiwan*
[4] *Department of Fragrance and Cosmetics Science, Kaohsiung Medical University, Kaohsiung 807, Taiwan*
[5] *Department of Medical Research, Kaohsiung Medical University Hospital, Kaohsiung Medical University, Kaohsiung 807, Taiwan*
[6] *Department of Biological Sciences and Technology, National University of Tainan, Tainan 700, Taiwan*
[7] *Translational Research Center, Cancer Center, Department of Medical Research, and Department of Obstetrics and Gynecology, Kaohsiung Medical University Hospital, Kaohsiung Medical University, Kaohsiung 807, Taiwan*

Correspondence should be addressed to Chien-Chih Chiu; cchiu@kmu.edu.tw

Received 18 June 2014; Revised 29 June 2014; Accepted 30 June 2014; Published 12 August 2014

Academic Editor: Li-Yeh Chuang

Sirtuins, NAD^+-dependent deacetylases, could target both histones and nonhistone proteins in mammalian cells. Sirt1 is the major sirtuin and has been shown to involve various cellular processes, including antiapoptosis, cellular senescence. Sirt1 was reported to be overexpressed in many cancers, including lung cancer. Sirtinol, a specific inhibitor of Sirt1, has been shown to induce apoptosis of cancer cells by elevating endogenous level of reactive oxygen species. In the study, we investigated the effect of sirtinol on the proliferation and apoptosis of nonsmall cell lung cancer (NSCLC) H1299 cells. The results of proliferation assay and colony formation assay showed the antigrowth effect of sirtinol. The annexin-V staining further confirmed the apoptosis induction by sirtinol treatment. Interestingly, the levels of phosphorylated Akt and β-catenin were significantly downregulated with treating the apoptotic inducing doses. On the contrary, sirtinol treatment causes the significantly increased level of FoxO3a, a proapoptotic transcription factor targeted by Sirt1. These above results suggested that sirtinol may inhibit cell proliferation of H1299 cells by regulating the axis of Akt-β-catenin-FoxO3a. Overall, this study demonstrates that sirtinol attenuates the proliferation and induces apoptosis of NSCLC cells, indicating the potential treatment against NSCLC cells by inhibiting Sirt1 in future applications.

1. Introduction

Cancer is one of the leading causes of death worldwide. Lung cancer has higher mortality than other cancers in both men and women [1]. More than 80% of lung cancer patients are nonsmall cell lung cancer (NSCLC). NSCLC can be classified by the location, including adenocarcinoma, squamous cell carcinoma, and large cell lung carcinoma [2, 3]. The treatment options for patients with NSCLC include surgery, radiation therapy, chemotherapy, and targeted therapy. Chemotherapy is given as main treatment for more advanced cancers or for patients who are not healthy enough for surgery [4]. The chemotherapy for NSCLC treatment is developed and improved recently. However, the poor prognosis and drug resistance contribute to the low survival rate of NSCLC patients [5, 6].

Sirtuin (Sirt) family is a class III HDAC. In yeast, sirtuin protein plays an important role for lifespan extension in response to metabolic and other environmental stresses [7–10]. SIRT family proteins also target various nonhistone proteins including structural protein, signal intermediates, and transcription factors [11]. At least seven homologues (Sirt1–7)

have been identified in mammalian cells [12–14]. Among Sirt proteins, the physiological role of Sirt1 in mammalian cells has been reported to prevent tumorigenesis and ensure cellular longevity, and the continuous prevention of apoptosis may induce the tumorigenesis [15]. Previous studies showed that Sirt1 overexpression in cancer correlates with silencing of tumor suppressor genes [16].

Akt is a serine/threonine kinase which has been shown to be associated with proliferation and survival [17]. The overexpression and constitutively activation of Akt was observed in many cancers, including lung cancer [6] and breast cancer [5] cells, which are highly correlated with the chemoresistance of cancer cells. On the contrary, Forkhead box O3a (FoxO3a), a transcription factor, is the downstream target of Akt [17]. FoxO3a can promote anticell growth or apoptosis signaling through either inducing expression of the proapoptotic Bcl-2 such as Bim [18], stimulating the expression of death receptor ligands, including Fas ligand and tumor necrosis factor-related apoptosis-inducing ligand (TRAIL), or increasing the protein levels of cyclin-dependent kinase inhibitors [19]. Aberrant Akt-mediated phosphorylation of FoxO3a causes the survival and proliferation of cancer cells. Therefore, the signaling axis of Akt and FoxO3a regulates cell growth and survival may shed the light on developing a promising strategy for lung cancer treatment [17, 18, 20, 21].

The tumor suppressor forkhead family of transcription factors (FOXO) is one of SIRT1 substrate. The acetylation of FOXO3 increases in response to oxidative stress [22]. Therefore, FOXO3 could control the balance between stress resistance and apoptosis through its downstream targets such as GADD45 and Bim [23]. For example, Frazzi's work reported that resveratrol-induced apoptosis of Hodgkin lymphoma cells is involved in the inhibition of SIRT1 and the hyperacetylation of FoxO3 [24].

In this study, we demonstrated antigrowth and apoptosis-inducing effect of sirtinol on lung cancer cells. The sirtinol-induced antiproliferation and apoptosis of lung cancer via FoxO3a-Akt were investigated and discussed.

2. Methods

2.1. Reagents. Sirtinol was purchased from Calbiochem (Darmstadt, Germany). Sirtinol was dissolved in 100% DMSO at concentration of 10 mM and stored at −20°C until use. The following compounds were obtained from Gibco BRL (Maryland, USA): Dulbecco's modified eagle medium (DMEM), Ham's F-12 Nutrient Mixture (F-12) fetal bovine serum (FBS), trypan blue, penicillin G, and streptomycin. Dimethyl sulfoxide (DMSO), ribonuclease A (RNase A), and propidium iodide (PI) were purchased from Sigma-Aldrich (Missouri, USA). Antibodies against FoxO3a were obtained from Epitomics (California, USA). Annexin V-FITC staining kit was purchased from Strong Biotech (Taipei, Taiwan). Antibodies against phospho-Akt, β-catenin, Sirt1, and β-actin were purchased from Santa Cruz Biotechnology (California, USA). Anti-mouse and anti-rabbit IgG peroxidase-conjugated secondary antibodies were purchased from Pierce (Illinois, USA). The anti-rabbit Rhodamine-conjugated antibody was purchased from Abcam (Cambridge, UK).

2.2. Cell Culture. Human nonsmall cell lung cancer (NSCLC) cell lines H1299 were obtained from American Type Culture Collection (ATCC; Virginia, USA). All tested cells were maintained in DMEM/F-12 in 1 : 1 ratios (pH 7.4) supplemented with 10% FBS and 1% penicillin-streptomycin (100 units/mL penicillin and 100 μg/mL streptomycin). All cells were incubated in a humidified atmosphere incubator containing 5% CO_2 at 37°C.

2.3. Proliferation Assay. The cell proliferation of H1299 cells was determined by trypan blue dye exclusion assay [25] combined with Countess Automated Cell Counter performed according to the manufacturer's instruction (Invitrogen; California, USA). 1×10^5 cells were seeded in 12-well plates and treated with indicated concentrations of sirtinol (0, 10, 20, and 50 μM) for 24 h and 48 h, respectively. After incubation, the cells were stained by 0.2% trypan blue and counted by Countess.

2.4. Apoptosis Assessment. To examine the apoptosis assessment of H1299 cells after being sirtinol treated, Annexin-V/PI double staining [26] was performed to detect the externalization of phosphatidylserine (PS). 3×10^5 cells were seeded onto a 6-well plate and incubated for 24 h and treated with different concentrations of sirtinol (0, 5, 10, 20, and 50 μM) for 24 h, respectively. Afterwards, cells were harvested and stained by Annexin-V staining kit (Strong Biotech, Taipei, Taiwan) according to the manufacturer's manual. The cells were washed in 1 × Annexin-V buffer (HEPES, NaCl, $CaCl_2 \cdot 2H_2O$) and stained by Annexin-V for 30 min in 37°C water bath. The cells were analyzed by flow cytometry (FACS Calibur; Becton Dickinson; California, USA). The results of apoptosis assessment were analyzed by using the FlowJo software (Treestar, Inc.; California, USA).

2.5. Colony Formation Assay. 100 cells were planted onto a 6-well plate, and, after 24 h incubation, the cells were treated with different concentrations of sirtinol (0, 10, 20, and 50 μM). After 15 days incubation, the colonies of cells were glutaraldehyde-fixed and stained with crystal violet (0.01% w/v) for 1 h. The diameter of colonies was determined by Image-Pro Plus software (Media Cybernetics; Maryland, USA).

2.6. Cell Cycle Analysis. 3×10^5 cells were seeded in 6-well plates and incubated for 24 h. The cells were treated with different concentrations of sirtinol (0, 10, 20, and 50 μM) for 24 h. Then, the cells were harvested and fixed with ice-cold 75% ethanol for at least 24 h at −20°C. Ethanol-fixed cells were collected by centrifugation and washed with PBS. After centrifugation, the cells were resuspended in 500 μL PBS containing 2.5 μg/mL RNase A and incubated for 30 min in 37°C water bath. Then, the cells were centrifuged and stained by propidium iodide (PI) [27]. The cells were analyzed by flow

cytometry. The cell cycle distribution results were analyzed by using the FlowJo software [28].

2.7. Western Blot Analysis. 6×10^5 cells were harvested and lysed with 1 × RIPA lysis buffer. Lysates were centrifuged at 13000 rpm for 30 min and the protein concentration in the supernatant was determined. 40 μg of protein was resolved by 10% SDS-polyacrylamide gel electrophoresis (SDS-PAGE). Afterwards, the proteins were electrotransferred to the nitrocellulose membrane (PALL; Michigan, USA) and blocked with 5% fat-free milk in PBS-T buffer (1 × PBS containing 0.1% Tween 20) for 1 h. Then the membranes were incubated with primary antibodies against specific proteins overnight at 4°C. The blot was washed by PBS-T buffer and incubated with corresponding secondary antibodies for 90 min. The signals were detected by an enhanced chemiluminescence (ECL) detection kit (Amersham Piscataway; New Jersey, USA) [29].

2.8. Statistical Analysis. Differences between DMSO- and sirtinol-treated cells were analyzed in at least triplicate experiments. The significance of the differences was analyzed by Student's t-test, with $P < 0.05$ considered significantly.

3. Results

3.1. Sirtinol Exerts Antiproliferative Effect towards NSCLC Cells. We used sirtinol, a specific and direct inhibitor of the sirtuin class of deacetylase activity, to inhibit Sirt1 in H1299 cells [30]. To investigate the effect of sirtinol on cell proliferation, the NSCLC cell line H1299 was treated with different concentrations of sirtinol for 24 and 48 h, respectively. The cell viable cells were measured by trypan blue staining assay combined with automatic cell counter. The results of both cell proliferation assay and colony formation assay showed the antigrowth effect of sirtinol on NSCLC H1299 cells, especially at the dose of 20 and 50 μM sirtinol treatment (Figures 1 and 2). We also examined whether sirtinol induced NSCLC H1299 cells apoptosis. We treated the cells with different concentrations of sirtinol (0, 10, 20, and 50 μM) and then conducted the flow cytometry-based Annexin V and PI double staining assay. The cellular apoptosis was detected at high concentration of sirtinol treatment (Figure 4).

3.2. The Effect of Sirtinol on Regulating Cell Cycle Distribution of H1299 Cells. In previous study, Sirt1 has shown to exert the ability to induce cell cycle arrest and resistance to oxidative stress [31]. Therefore, we examined whether sirtinol induced NSCLC H1299 cell cycle disturbance. After sirtinol treatment, the cells were stained by PI, and detected the cell cycle distribution by flow cytometry (Figure 3). The result showed that the highest dose (50 μM) of sirtinol treatment induces G1-phase accumulation.

3.3. The Effect of Sirtinol on Modulating the Expression of Pro-survival Proteins. Sirt1 was reported to deacetylate various nonhistone protein targets, including p53, NF-κB, β-catenin, and FoxO3a [32–34]. Because H1299 cells do not express the tumor suppressor p53 protein, we used Western blot

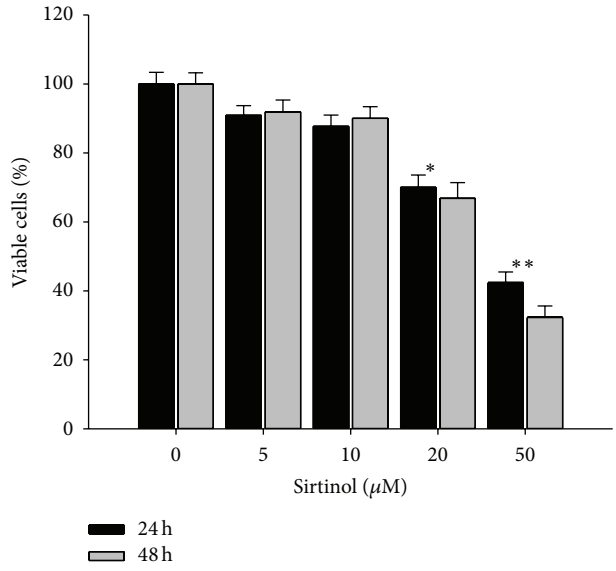

Figure 1: Effect of sirtinol on cellular proliferation of H1299 cells. H1299 cells treated with different concentrations (5, 10, 20 and 50 μM) of sirtinol for 24 h and 48 h, respectively. The cell survival was determined by the trypan blue staining assay combined with the Countess Automated Cell Counter. $^{**}P < 0.001$ against vehicle control.

to analyze the protein level of β-catenin, NF-κB p65, and FoxO3a after sirtinol treatment (Figure 5). NF-κB p65 is a critical transcription factor that regulates inflammation and cell proliferation and differentiation. NF-κB was reported to be aberrantly expressed and constitutively activated in lung cancer [35, 36]. However, the results of Western blot showed that no significant changes of NF-κB p65 protein levels were observed (data not shown), suggesting that the antiproliferative effect of sirtinol on lung cancer H1299 cells is NF-κB p65-independent. On the contrary, the previous study showed that sirt1 plays a tumor suppressive role mediated through inhibition of β-catenin [37]. The protein level of β-catenin was decreased only in cytotoxic concentrations 20 and 50 μM, suggesting that β-catenin did not involve in Sirt1-induced cells invasiveness, and Sirt1 may play a role as a tumor promoter in H1299 cells.

The transcription factor FoxO3a has a crucial role in mediating the cytostatic and cytotoxic effects of anticancer drug [38, 39]. Recent study suggested that FoxO3a may be a major mediator for the cytotoxic effect of cisplatin in lung cancer cells [40]. More recently, Zheng's work demonstrated that ectopic expression of FoxO3a enhanced $p21^{CIP1/WAF1}$ expression and berberine, a compound derived from traditional Chinese medicine-induced apoptosis in human lung adenocarcinoma cells [41], indicating the important role of FoxO3a in the initiation of apoptosis in cancer cells.

Furthermore, FoxO3a is a well-known nonhistone target of Sirt1. It has been reported that Sirt1 would deacetylate and repress FoxO3a activity and reduce forkhead-dependent

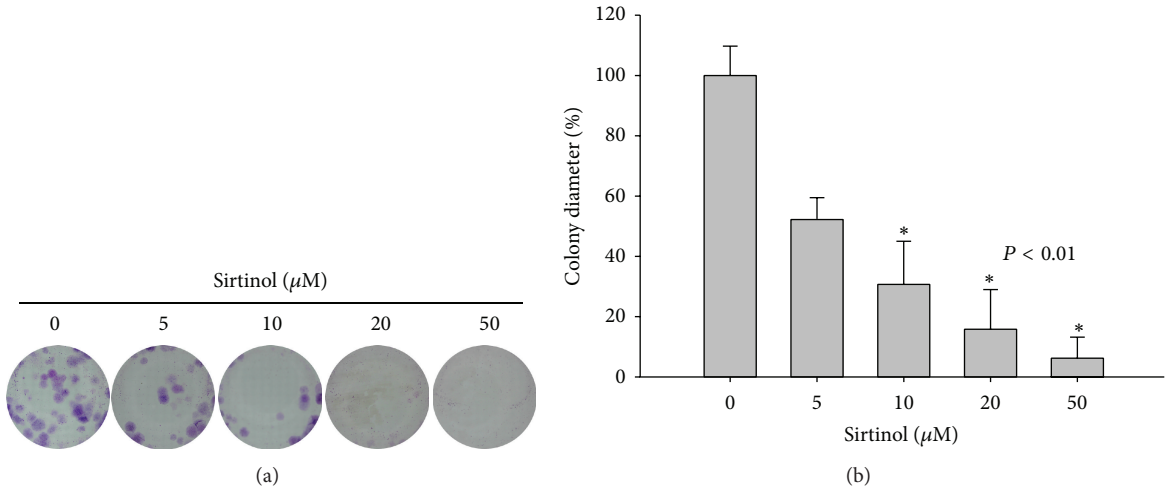

Figure 2: Sirtinol inhibits the colony formation of lung cancer cells. H1299 cells were treated with different concentrations (5, 10, 20 and 50 μM) of sirtinol for 15 days, respectively. Afterwards, the cells were glutaraldehyde-fixed and stained with Giemsa stain for 1 h. (a) The colony formation analysis of H1299 cells. (b) The quantification analysis of the colony diameter. Data are represented as mean ± SD ($n = 3$). $^{*}P < 0.01$ compared with the vehicle control.

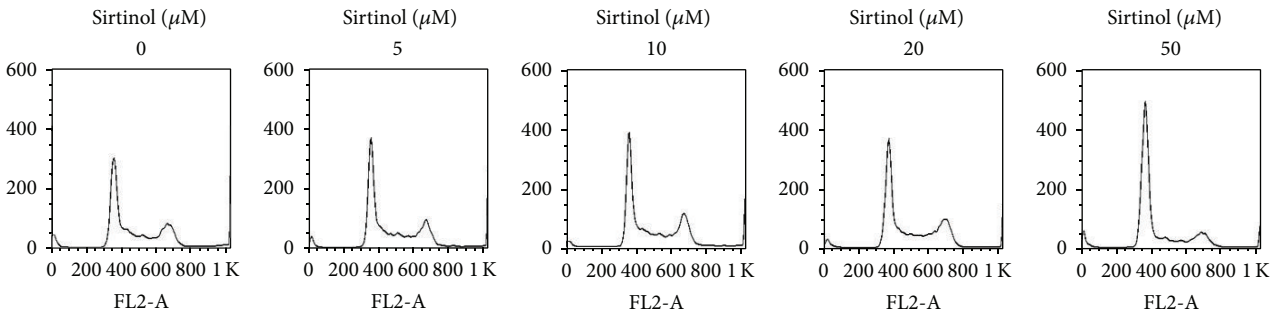

Phase (%)/dose (μM)	0	5	10	20	50
G0/G1	56.12 ± 2.98^{a}	55.32 ± 2.89^{a}	54.71 ± 1.96^{a}	54.14 ± 2.37^{a}	67.31 ± 3.48^{c}
G2/M	26.28 ± 1.85^{a}	28.38 ± 4.19^{a}	29.51 ± 2.20^{b}	29.39 ± 2.76^{b}	18.62 ± 1.95^{c}
S	14.49 ± 1.79^{a}	13.19 ± 1.18^{a}	12.76 ± 0.91^{b}	12.95 ± 0.44^{b}	8.85 ± 1.40^{c}
Sub-G1	3.11 ± 0.93^{a}	3.11 ± 0.68^{a}	3.02 ± 0.67^{a}	3.52 ± 0.09^{a}	5.23 ± 1.89^{b}

(b)

Figure 3: The effect of sirtinol on cell cycle distribution of lung cancer cells. H1299 cells treated with indicated concentrations (from 5 to 50 μM) of sirtinol for 24 h, respectively. Cells were stained with PI and detected the cell cycle distribution by flow cytometry. (a) Flow cytometry profile represents PI staining in x-axis and cell number in y-axis. (b) The quantitative analysis of cell cycle distribution. Different letter notations indicate the statistical significance between drug treatment and vehicle (a versus b and a versus c indicate the $P < 0.05$ and 0.001, resp.).

apoptosis [23]. In the result of Western blot, FoxO3a was increased after sirtinol treatment, suggesting that Sirt1 represses the protein level of FoxO3a in NSCLC H1299 cells.

We next examined the proteins that involve in cellular proliferation and metastasis protein, including the phosphorylation of Akt [42–44] (Figure 5). The phosphorylation of levels of Akt was decreased only in cytotoxic concentrations 20 and 50 μM, suggesting that Akt did not involve in sirtinol-induced inhibition of cells' invasiveness but the apoptosis pathway.

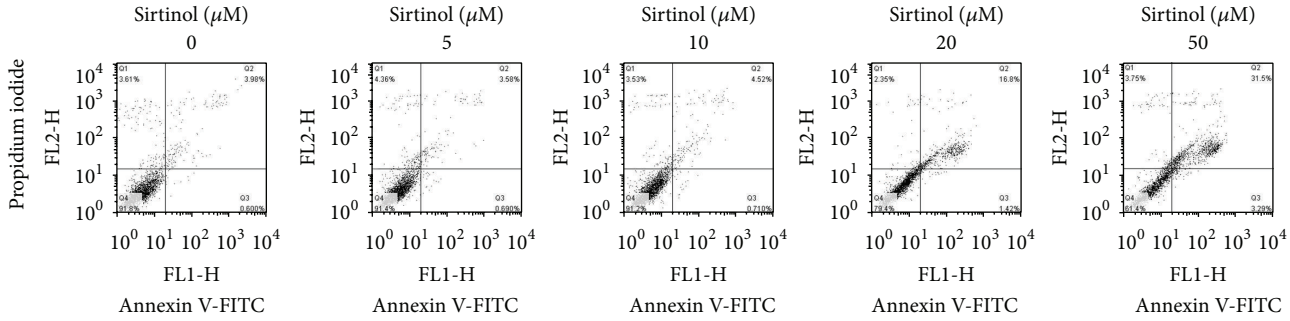

(a)

Phase (%)/dose (μM)	0	5	10	20	50
Necrosis (A^-P^+)	3.98 ± 0.33^a	4.21 ± 0.36^a	3.55 ± 0.41^a	2.47 ± 0.11^c	3.88 ± 0.14^a
Late apoptosis (A^+P^+)	3.82 ± 0.15^a	3.47 ± 0.27^a	4.02 ± 0.51^a	16.3 ± 1.04^c	30.67 ± 0.85^c
Early apoptosis (A^+P^-)	0.56 ± 0.05^a	0.71 ± 0.08^a	0.73 ± 0.02^a	1.53 ± 0.12^c	2.94 ± 0.31^c
Healthy (A^-P^-)	91.63 ± 0.21^a	91.6 ± 0.53^a	91.7 ± 0.78^a	79.7 ± 0.98^c	62.47 ± 1.05^c

(b)

Figure 4: Sirtinol induces apoptosis of H1299 cells. Cells were treated with indicated concentrations of sirtinol and stained with Annexin-V and PI at 24 h, respectively. (a) Flow cytometry profiling represents the results of Annexin-V-FITC staining. (b) The quantificative analysis of cell apoptosis. Different letter notations indicate the statistical significance between sirtinol treatment and vehicle (*a* versus *b* and *a* versus *c* indicate the $P < 0.05$ and 0.001, resp.).

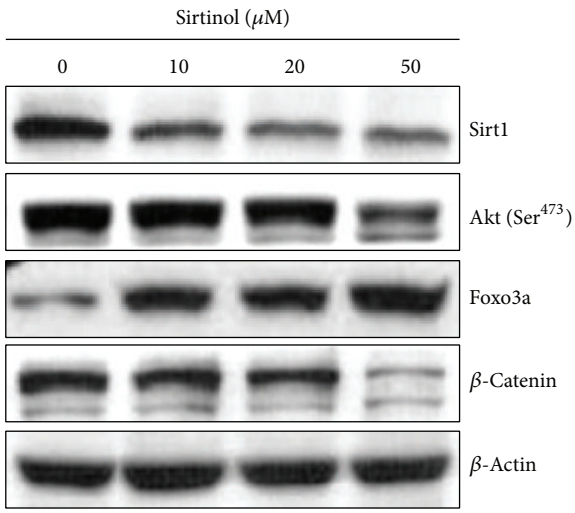

Figure 5: Modulation of protein levels in NSCLC H1299 cells after sirtinol treatment. H1299 cells treated with indicated concentrations (10, 20, and 50 μM) of sirtinol for 24 h, respectively. The results of Western blot of Sirt1 nonhistone target protein, including FoxO3a, Akt phosphorylation, and β-catenin. β-Actin as an internal control.

4. Discussion

Sirt1 has been shown to be involved in a variety of biological processes, including transcriptional silencing, stress responses, aging, apoptosis, tumorigenesis, and cellular metabolism [45, 46]. It targets diverse histone and various nonhistone proteins including structural protein, signal intermediates, and transcription factors, such as α-tubulin, p53 [47–49], FoxO [20, 23, 31], E2F1 [50], NF-κB [51, 52], and Ku70 [53]. Additionally, Sirt1 has been shown to overexpress in several cancer cells, including breast, prostate, ovarian, and colon cancer cell lines [46, 54–58]. Recent studies showed the tumorigenicity role of Sirt1. For example, Sirt1 was reported to promote cell migration and invasion of prostate cancer [59, 60]. Consistently, our preliminary result also showed that Sirt1 would overexpress in NSCLC cell lines (data not shown).

The production of ROS has been resulted in cellular damage and genomic instability [61]. Furthermore, many anticancer drugs could induce apoptosis by increasing the level of endogenous ROS in the cancer cells [62, 63]. Recent study showed that sirtinol treatment induces the apoptosis of lung carcinoma 549 cells by increasing the level of endogenous ROS [64].

Accordingly, we proposed the positive role of Sirt1 in the progression of NSCLC cells. We used sirtinol, a specific inhibitor of sirtuin, to inhibit Sirt1. Our results showed that sirtinol exerts a significant cytotoxicity towards NSCLC H1299 cells with a dose-responsive manner (20 and 50 μM). The Western results showed that sirtinol-induced inhibition of Sirt1 resulted in the increased transcription factor FoxO3a. These above results suggest a close correlation of sirtinol-induced antilung cancer and the regulation of Akt-FoxO3a signaling pathway (Figure 6).

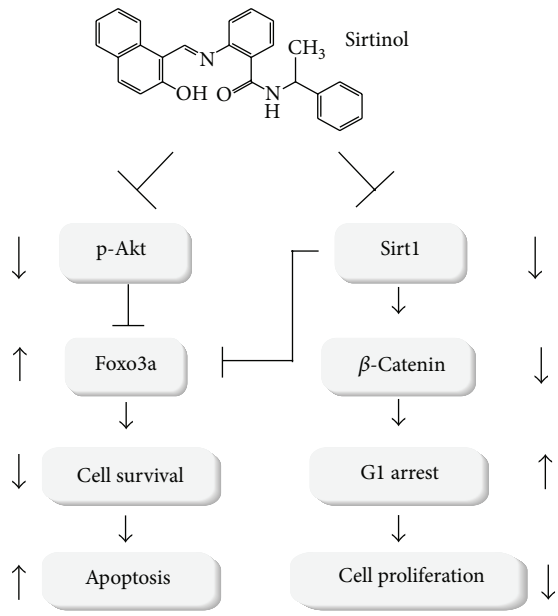

Figure 6: Possible model of sirtinol-induced antiproliferation and apoptosis in lung cancer cells. Sirtinol downregulates the activation of prosurvival Akt serine/threonine kinase and the protein level of β-catenin, a proliferation-associated transcription factor, insulting in the cell cycle G_1-phase accumulation and the growth arrest. On the contrary, sirtinol treatment causes the upregulation of the proapoptotic transcription factor FoxO3a, a target of both Akt signaling and Sirt1. This may render H1299 cells more sensitive to apoptosis. Finally, sirtinol induces the apoptosis of lung cancer cells.

5. Conclusions

In this study, we used sirtinol, a specific inhibitor of Sirt1, to investigate the role of Sirt1 in the apoptosis and proliferation of H1299 cells. Sirtinol treatment causes the cell cycle arrest and apoptosis of lung cancer cells. Furthermore, sirtinol-induced inhibition of Sirt1 activity may increase the protein levels of the transcription factor Foxoa3a whereas it downregulates the activation of Akt and the protein level of β-catenin after sirtinol treatment. Our recent work suggests that sirtinol-induced antiproliferation and apoptosis of lung cancer cells may be correlated with Akt-FoxO3a signaling pathway (Figure 6).

Conflict of Interests

The authors declare that they have no conflict of interests.

Acknowledgments

The study was financially supported by Grant no. NSC101-2320-B-037-046-MY3 from the National Science Council, Taiwan, Grant nos. 101-CM-KMU-11 and 102-CM-KMU-09 from the ChiMei-KMU Joint Research Project, Grant no. NSYSUKMU102-P031 from the NSYSU-KMU Joint Research Project, and Grant no. MOHW103-TD-B-111-05 from the Ministry of Health and Welfare, Taiwan.

References

[1] M. Heron, "Deaths: leading causes for 2008," *National Vital Statistics Reports: From the Centers for Disease Control and Prevention, National Center for Health Statistics, National Vital Statistics System*, vol. 60, no. 6, pp. 1–94, 2012.

[2] D. L. Longo, *Harrison's Principles of Internal Medicine*, McGraw-Hill, New York, NY, USA, 2011.

[3] R. Siegel, D. Naishadham, and A. Jemal, "Cancer statistics, 2012," *CA: A Cancer Journal for Clinicians*, vol. 62, no. 1, pp. 10–29, 2012.

[4] S. Burdett, R. Stephens, L. Stewart et al., "Chemotherapy in addition to supportive care improves survival in advanced non-small-cell lung cancer: a systematic review and meta-analysis of individual patient data from 16 randomized controlled trials—NSCLC Meta-Analyses Collaborative Group," *Journal of Clinical Oncology*, vol. 26, no. 28, pp. 4617–4625, 2008.

[5] R. Pirker and W. Minar, "Chemotherapy of advanced non-small cell lung cancer," *Frontiers of Radiation Therapy and Oncology*, vol. 42, pp. 157–163, 2010.

[6] T. D. Wagner and G. Y. Yang, "The role of chemotherapy and radiation in the treatment of locally advanced non-small cell lung cancer (NSCLC)," *Current Drug Targets*, vol. 11, no. 1, pp. 67–73, 2010.

[7] K. T. Howitz, K. J. Bitterman, H. Y. Cohen et al., "Small molecule activators of sirtuins extend Saccharomyces cerevisiae lifespan," *Nature*, vol. 425, no. 6954, pp. 191–196, 2003.

[8] L. Guarente and F. Picard, "Calorie restriction—the SIR2 connection," *Cell*, vol. 120, no. 4, pp. 473–482, 2005.

[9] V. D. Longo and B. K. Kennedy, "Sirtuins in aging and age-related disease," *Cell*, vol. 126, no. 2, pp. 257–268, 2006.

[10] L. Fontana, L. Partridge, and V. D. Longo, "Extending healthy life span—from yeast to humans," *Science*, vol. 328, no. 5976, pp. 321–326, 2010.

[11] Y. Olmos, J. J. Brosens, and E. W. F. Lam, "Interplay between SIRT proteins and tumour suppressor transcription factors in chemotherapeutic resistance of cancer," *Drug Resistance Updates*, vol. 14, no. 1, pp. 35–44, 2011.

[12] M. C. Haigis and D. A. Sinclair, "Mammalian sirtuins: biological insights and disease relevance," *Annual Review of Pathology: Mechanisms of Disease*, vol. 5, pp. 253–295, 2010.

[13] Y. Cen, D. Y. Youn, and A. A. Sauve, "Advances in characterization of human sirtuin isoforms: chemistries, targets and therapeutic applications," *Current Medicinal Chemistry*, vol. 18, no. 13, pp. 1919–1935, 2011.

[14] Y. Horio, T. Hayashi, A. Kuno, and R. Kunimoto, "Cellular and molecular effects of sirtuins in health and disease," *Clinical Science*, vol. 121, no. 5, pp. 191–203, 2011.

[15] C. L. Brooks and W. Gu, "How does SIRT1 affect metabolism, senescence and cancer?" *Nature Reviews Cancer*, vol. 9, no. 2, pp. 123–128, 2009.

[16] K. Pruitt, R. L. Zinn, J. E. Ohm et al., "Inhibition of SIRT1 reactivates silenced cancer genes without loss of promoter DNA hypermethylation," *PLoS Genetics*, vol. 2, no. 3, article e40, 2006.

[17] X. Zhang, N. Tang, T. J. Hadden, and A. K. Rishi, "Akt, FoxO and regulation of apoptosis," *Biochimica et Biophysica Acta*, vol. 1813, no. 11, pp. 1978–1986, 2011.

[18] Y. Lv, S. Song, K. Zhang, H. Gao, and R. Ma, "CHIP regulates AKT/FoxO/Bim signaling in MCF7 and MCF10A cells," *PLoS ONE*, vol. 8, no. 12, Article ID e83312, 2013.

[19] J. Seoane, H. Le, L. Shen, S. A. Anderson, and J. Massagué, "Integration of smad and forkhead pathways in the control of neuroepithelial and glioblastoma cell proliferation," *Cell*, vol. 117, no. 2, pp. 211–223, 2004.

[20] N. Hariharan, Y. Maejima, J. Nakae, J. Paik, R. A. Depinho, and J. Sadoshima, "Deacetylation of FoxO by Sirt1 plays an essential role in mediating starvation-induced autophagy in cardiac myocytes," *Circulation Research*, vol. 107, no. 12, pp. 1470–1482, 2010.

[21] C. Wu, B. Jin, L. Chen et al., "MiR-30d induces apoptosis and is regulated by the Akt/FOXO pathway in renal cell carcinoma," *Cellular Signalling*, vol. 25, no. 5, pp. 1212–1221, 2013.

[22] A. Brunet, L. B. Sweeney, J. F. Sturgill et al., "Stress-Dependent Regulation of FOXO Transcription Factors by the SIRT1 Deacetylase," *Science*, vol. 303, no. 5666, pp. 2011–2015, 2004.

[23] M. C. Motta, N. Divecha, M. Lemieux et al., "Mammalian SIRT1 represses forkhead transcription factors," *Cell*, vol. 116, no. 4, pp. 551–563, 2004.

[24] R. Frazzi, R. Valli, I. Tamagnini, B. Casali, N. Latruffe, and F. Merli, "Resveratrol-mediated apoptosis of hodgkin lymphoma cells involves SIRT1 inhibition and FOXO3a hyperacetylation," *International Journal of Cancer*, vol. 132, no. 5, pp. 1013–1021, 2013.

[25] C. Yen, C. Chiu, R. Haung et al., "Antiproliferative effects of goniothalamin on Ca9-22 oral cancer cells through apoptosis, DNA damage and ROS induction," *Mutation Research—Genetic Toxicology and Environmental Mutagenesis*, vol. 747, no. 2, pp. 253–258, 2012.

[26] C. Chiu, P. Liu, K. Huang et al., "Goniothalamin inhibits growth of human lung cancer cells through DNA damage, apoptosis, and reduced migration ability," *Journal of Agricultural and Food Chemistry*, vol. 59, no. 8, pp. 4288–4293, 2011.

[27] C. C. Chiu, H. W. Chang, D. W. Chuang et al., "Fern plant-derived protoapigenone leads to DNA damage, apoptosis, and g2/m arrest in lung cancer cell line H1299," *DNA and Cell Biology*, vol. 28, no. 10, pp. 501–506, 2009.

[28] L. Bonetta, "Flow cytometry smaller and better," *Nature Methods*, vol. 2, no. 10, pp. 785–794, 2005.

[29] C. Chiu, J. Haung, F. Chang et al., "Golden berry-derived 4β-hydroxywithanolide E for selectively killing oral cancer cells by generating ROS, DNA damage, and apoptotic pathways," *PLoS ONE*, vol. 8, no. 5, Article ID e64739, 2013.

[30] H. Ota, E. Tokunaga, K. Chang et al., "Sirt1 inhibitor, Sirtinol, induces senescence-like growth arrest with attenuated Ras-MAPK signaling in human cancer cells," *Oncogene*, vol. 25, no. 2, pp. 176–185, 2006.

[31] A. Brunet, L. B. Sweeney, J. F. Sturgill et al., "Stress-dependent regulation of FOXO transcription factors by the sirt1 deacetylase," *Science*, vol. 303, no. 5666, pp. 2011–2015, 2004.

[32] H. Vaziri, S. K. Dessain, E. N. Eaton et al., "hSIR2SIRT1 functions as an NAD-dependent p53 deacetylase," *Cell*, vol. 107, no. 2, pp. 149–159, 2001.

[33] C. X. Deng, "SIRT1, is it a tumor promoter or tumor suppressor?" *International Journal of Biological Sciences*, vol. 5, no. 2, pp. 147–152, 2009.

[34] S. Nemoto, M. M. Fergusson, and T. Finkel, "Nutrient availability regulates SIRT1 through a forkhead-dependent pathway," *Science*, vol. 306, no. 5704, pp. 2105–2108, 2004.

[35] Y. Saitoh, V. J. Martínez Bruyn, S. Uota et al., "Overexpression of NF-κB inducing kinase underlies constitutive NF-κB activation in lung cancer cells," *Lung Cancer*, vol. 70, no. 3, pp. 263–270, 2010.

[36] X. Tang, D. Liu, S. Shishodia et al., "Nuclear factor-κB (NF-κB) is frequently expressed in lung cancer and preneoplastic lesions," *Cancer*, vol. 107, no. 11, pp. 2637–2646, 2006.

[37] R. Firestein, G. Blander, S. Michan et al., "The SIRT1 deacetylase suppresses intestinal tumorigenesis and colon cancer growth," *PLoS ONE*, vol. 3, no. 4, Article ID e2020, 2008.

[38] A. R. Gomes, J. J. Brosens, and E. W.-F. Lam, "Resist or die: FOXO transcription factors determine the cellular response to chemotherapy," *Cell Cycle*, vol. 7, no. 20, pp. 3133–3136, 2008.

[39] S. S. Myatt and E. W.-F. Lam, "The emerging roles of forkhead box (Fox) proteins in cancer," *Nature Reviews Cancer*, vol. 7, no. 11, pp. 847–859, 2007.

[40] H. Liu, J. Yin, C. Wang, Y. Gu, M. Deng, and Z. He, "FOXO3a mediates the cytotoxic effects of cisplatin in lung cancer cells," *Anti-Cancer Drugs*, vol. 25, no. 8, pp. 898–907, 2014.

[41] F. Zheng, Q. Tang, J. Wu et al., "p38alpha MAPK-mediated induction and interaction of FOXO3a and p53 contribute to the inhibited-growth and induced-apoptosis of human lung adenocarcinoma cells by berberine," *Journal of Experimental & Clinical Cancer Research*, vol. 33, no. 1, p. 36, 2014.

[42] K. Kamitori, M. Tanaka, T. Okuno-Hirasawa, and S. Kohsaka, "Receptor related to tyrosine kinase RYK regulates cell migration during cortical development," *Biochemical and Biophysical Research Communications*, vol. 330, no. 2, pp. 446–453, 2005.

[43] M. Morales-Ruiz, D. Fulton, G. Sowa et al., "Vascular endothelial growth factor-stimulated actin reorganization and migration of endothelial cells is regulated via the serine/threonine kinase Akt," *Circulation Research*, vol. 86, no. 8, pp. 892–896, 2000.

[44] C. Huang, J. Liu, C. C. Haudenschild, and X. Zhan, "The role of tyrosine phosphorylation of cortactin in the locomotion of endothelial cells," *Journal of Biological Chemistry*, vol. 273, no. 40, pp. 25770–25776, 1998.

[45] T. Inoue, M. Hiratsuka, M. Osaki, and M. Oshimura, "The molecular biology of mammalian SIRT proteins: SIRT2 in cell cycle regulation," *Cell Cycle*, vol. 6, no. 9, pp. 1011–1018, 2007.

[46] W. Stünkel and R. M. Campbell, "Sirtuin 1 (SIRT1): the misunderstood HDAC," *Journal of Biomolecular Screening*, vol. 16, no. 10, pp. 1153–1169, 2011.

[47] J. Luo, A. Y. Nikolaev, S. Imai et al., "Negative control of p53 by Sir2α promotes cell survival under stress," *Cell*, vol. 107, no. 2, pp. 137–148, 2001.

[48] E. Langley, M. Pearson, M. Faretta et al., "Human SIR2 deacetylates p53 and antagonizes PML/p53-induced cellular senescence," *The EMBO Journal*, vol. 21, no. 10, pp. 2383–2396, 2002.

[49] J. Yi and J. Luo, "SIRT1 and p53, effect on cancer, senescence and beyond," *Biochimica et Biophysica Acta*, vol. 1804, no. 8, pp. 1684–1689, 2010.

[50] C. Wang, L. Chen, X. Hou et al., "Interactions between E2F1 and SirT1 regulate apoptotic response to DNA damage," *Nature Cell Biology*, vol. 8, no. 9, pp. 1025–1031, 2006.

[51] L. Chen, W. Fischle, E. Verdin, and W. C. Greene, "Duration of nuclear NF-κB action regulated by reversible acetylation," *Science*, vol. 293, no. 5535, pp. 1653–1657, 2001.

[52] A. Salminen, J. Ojala, J. Huuskonen, A. Kauppinen, T. Suuronen, and K. Kaarniranta, "Interaction of aging-associated signaling cascades: inhibition of NF-κB signaling by longevity factors FoxOs and SIRT1," *Cellular and Molecular Life Sciences*, vol. 65, no. 7-8, pp. 1049–1058, 2008.

[53] J. Jeong, K. Juhn, H. Lee et al., "SIRT1 promotes DNA repair activity and deacetylation of Ku70," *Experimental & Molecular Medicine*, vol. 39, no. 1, pp. 8–13, 2007.

[54] W. Stünkel, B. K. Peh, Y. C. Tan et al., "Function of the SIRTI protein deacetylase in cancer," *Biotechnology Journal*, vol. 2, no. 11, pp. 1360–1368, 2007.

[55] K. Y. Jang, K. S. Kim, S. H. Hwang et al., "Expression and prognostic significance of SIRT1 in ovarian epithelial tumours," *Pathology*, vol. 41, no. 4, pp. 366–371, 2009.

[56] N. Kabra, Z. Li, L. Chen et al., "SirT1 is an inhibitor of proliferation and tumor formation in colon cancer," *Journal of Biological Chemistry*, vol. 284, no. 27, pp. 18210–18217, 2009.

[57] K. Nosho, K. Shima, N. Irahara et al., "SIRT1 histone deacetylase expression is associated with microsatellite instability and CpG island methylator phenotype in colorectal cancer," *Modern Pathology*, vol. 22, no. 7, pp. 922–932, 2009.

[58] B. Wang, M. K. Hasan, E. Alvarado, H. Yuan, H. Wu, and W. Y. Chen, "NAMPT overexpression in prostate cancer and its contribution to tumor cell survival and stress response," *Oncogene*, vol. 30, no. 8, pp. 907–921, 2011.

[59] Y. Zhang, M. Zhang, H. Dong et al., "Deacetylation of cortactin by SIRT1 promotes cell migration.," *Oncogene*, vol. 28, no. 3, pp. 445–460, 2009.

[60] K. Nakane, Y. Fujita, R. Terazawa et al., "Inhibition of cortactin and SIRT1 expression attenuates migration and invasion of prostate cancer DU145 cells," *International Journal of Urology*, vol. 19, no. 1, pp. 71–79, 2012.

[61] J. Lee, M. Hou, H. Huang et al., "Marine algal natural products with anti-oxidative, anti-inflammatory, and anti-cancer properties," *Cancer Cell International*, vol. 13, no. 1, article 55, 2013.

[62] H.-U. Simon, A. Haj-Yehia, and F. Levi-Schaffer, "Role of reactive oxygen species (ROS) in apoptosis induction," *Apoptosis*, vol. 5, no. 5, pp. 415–418, 2000.

[63] L. Khandrika, B. Kumar, S. Koul, P. Maroni, and H. K. Koul, "Oxidative stress in prostate cancer," *Cancer Letters*, vol. 282, no. 2, pp. 125–136, 2009.

[64] S. Pal, B. S. Shankar, and K. B. Sainis, "Cytokines from the tumor microenvironment modulate sirtinol cytotoxicity in A549 lung carcinoma cells," *Cytokine*, vol. 64, no. 1, pp. 196–207, 2013.

Hindawi Publishing Corporation
The Scientific World Journal
Volume 2014, Article ID 360153, 7 pages
http://dx.doi.org/10.1155/2014/360153

Research Article

Arsenic Modulates Posttranslational S-Nitrosylation and Translational Proteome in Keratinocytes

Bin Huang,[1,2] Kuo-Hao Chiang,[3] Hsin-Su Yu,[4] Ying-Lun Chen,[5] Huey-Ling You,[6] and Wei-Ting Liao[3]

[1] *Department of Biomedical Science and Environmental Biology, College of Life Science, Kaohsiung Medical University, Kaohsiung 80708, Taiwan*
[2] *Department of Biological Sciences, National Sun Yat-sen University, Kaohsiung 80424, Taiwan*
[3] *Department of Biotechnology, College of Life Science, No. 100, Shihchuan 1st Rd., Sanming District, Kaohsiung Medical University, Kaohsiung 80708, Taiwan*
[4] *Department of Dermatology, Kaohsiung Medical University Hospital and Kaohsiung Medical University College of Medicine, Kaohsiung 80708, Taiwan*
[5] *Department of Anesthesiology, Mackay Memorial Hospital, Taipei 10449, Taiwan*
[6] *Departments of Laboratory Medicine, Chang Gung Memorial Hospital-Kaohsiung Medical Center, Kaohsiung 83301, Taiwan*

Correspondence should be addressed to Wei-Ting Liao; wtliao@kmu.edu.tw

Received 12 June 2014; Accepted 18 June 2014; Published 8 July 2014

Academic Editor: Hsueh-Wei Chang

Arsenic is a class I human carcinogen (such as inducing skin cancer) by its prominent chemical interaction with protein thio (-SH) group. Therefore, arsenic may compromise protein S-nitrosylation by competing the -SH binding activity. In the present study, we aimed to understand the influence of arsenic on protein S-nitrosylation and the following proteomic changes. By using primary human skin keratinocyte, we found that arsenic treatment decreased the level of protein S-nitrosylation. This was coincident to the decent expressions of endothelial nitric oxide synthase (eNOS) and inducible nitric oxide synthase (iNOS). By using LC-MS/MS, around twenty S-nitrosoproteins were detected in the biotin-switched eluent. With the interest that arsenic not only regulates posttranslational S-nitrosylation but also separately affects protein's translation expression, we performed two-dimensional gel electrophoresis and found that 8 proteins were significantly decreased during arsenic treatment. Whether these decreased proteins are the consequence of protein S-nitrosylation will be further investigated. Taken together, these results provide a finding that arsenic can deplete the binding activity of NO and therefore reduce protein S-nitrosylation.

1. Introduction

Protein S-nitrosylation, the covalent attachment of nitric oxide (NO) to protein thio (-SH) group, is an important post-translational modification that affects a wide variety of proteins for cellular signaling in normal physiology and a broad spectrum of human diseases [1, 2]. S-nitrosylation signaling controls a number of cellular processes, such as protein-protein interactions [3], nuclear transcriptions [4], and membrane-associated proteins activation [5, 6]. Pathophysiology is correlated with hypo- or hyper-S-nitrosylation of specific protein targets rather than a general cellular insult due to not only the loss of or enhanced nitric oxide synthase activity but also the denitrosylation by a major denitrosylase, S-nitrosoglutathione reductase (GSNOR) [1]. Abnormal protein S-nitrosylation causes many diseases such as cardiovascular, musculoskeletal, and neurological dysfunction [7]. Furthermore, autophagy, a vacuolar degradation for long-lived and aggregate-prone proteins, plays an important role in neurodegeneration. Inhibition of autophagy by S-nitrosylation results in stress-mediated protein aggregation in neurodegenerative diseases [8, 9].

S-nitrosylation is also associated with cancer [10]. Potential mechanisms of S-nitrosylation in carcinogenesis are focused on apoptosis and DNA repair [11]. Survival of tumor cell could be induced by inactivation of proapoptotic signaling

or activation of antiapoptotic pathways [12]. Inhibition of caspase protease by protein nitrosylation promotes extended survival of malignant cells [13]. For example, nitrosylation of caspase 9 inhibits the mitochondrial pathway of apoptosis in cholangiocarcinoma cell line [14]. Additionally, p53 induces apoptotic cell death and causes cell cycle arrest in response to various stresses [15]. S-nitrosylation of p53 suppresses p53-mediated apoptosis in colon carcinogenesis [16]. Bcl-2, a major anti-apoptotic regulatory protein, was regulated by S-nitrosylation in various carcinoma tissues [11, 17, 18]. S-nitrosylation is shown to modulate the activity, stability, and cellular localization of key DNA repair proteins, including O(6)-alkylguanine-DNA-alkyltransferase (AGT), 8-oxoguanine glycosylase (Ogg1), apurinic-apyrimidinic endonuclease 1 (APE1), and DNA-dependent protein kinase catalytic subunit (DNA-PKcs) [19]. Inactivation of AGT by S-nitrosylation is found in hepatocarcinogenesis [20]. Moreover, S-nitrosylated APE1 export from the nucleus to the cytoplasm is described in colon adenomas, breast cancer, and hepatocellular carcinomas [21]. Also, S-nitrosylated DNA-PKcs shows increased transcriptional expression and activity in HEK-293 [22].

It is well known that arsenic, a human carcinogen, showed its chemical carcinogenesis activity by interaction with protein -SH groups. By its -SH binding activity, therefore, arsenic may compromise protein S-nitrosylations in cells. In addition, it is reported that arsenic has a significant effect on NO production in the endothelium [23]. Arsenic remains one of the most concerned environmental toxicants, which has been classified as a group I human carcinogen by the International Agency for Research on Cancer (IARC). Epidemiological studies demonstrated that long-term exposure to inorganic arsenic through either ingestion or inhalation is associated with an increased risk of malignant cancers in the urinary bladder, lung, and especially skin, since arsenic tends to concentrate in keratinocytes [24]. However, the role of S-nitrosylation induced by arsenic in skin carcinogenesis remains unclear. In the present study, we hypothesize that arsenic can alter protein S-nitrosylation and NO production in skin keratinocyte. Our contribution is identifying interactions between arsenic and S-nitrosylation axis in keratinocytes that can provide the novel molecular and pharmacological strategies for potential clinical applications.

2. Materials and Methods

2.1. Human Keratinocyte Culture. Freshly obtained prepuce specimens were used to cultivate the primary human cultured keratinocytes. Briefly, normal human prepuce specimens were washed with PBS, then cut into small pieces, and incubated in medium containing 0.25% trypsin overnight at 4°C. The epidermal sheet was lifted from the dermis using a fine forceps. The epidermal cells were pelleted by centrifugation (500 ×g, 10 min) and dispersed into individual cells by repeated aspiration with a pipette. Isolated keratinocytes must be cultured in commercialized keratinocyte serum free medium (Invitrogen, Carlsbad, USA) at 37°C in a humidified incubator with 5% CO_2 atmosphere with or without sodium arsenite (Sigma, St. Louis, USA) treatment (10 μM). This primary keratinocyte culture protocol using human skin samples has been approved by Institutional Review Board of Kaohsiung Medical University Hospital (KMUH-IRB-960119).

2.2. Cell Lysis and Proteins Extraction. Keratinocytes after treatment were washed with cord buffer [NaCl (0.14 M), KCl (4 mM), glucose (11 mM), and HEPES (10 mM, pH 7.4)] and then lysed with 100 μL of lysis buffer [Hepes (250 mM, pH 7.7), EDTA (1 mM), neocuproine (0.1 mM), and CHAPS (0.4%, w/v)]. After centrifugation, protein supernatant is collected and protein concentrations are determined with BCA assay reagent (Thermo Fisher Scientific Inc, Rockford, IL, USA).

2.3. Biotin Switch Method for Purifying S-Nitrosoproteins. The biotin switch method was used according to previous study [22, 25]. Cells were washed with 1 × cord buffer (10 mM HEPES, pH 7.4, 0.14 M NaCl, 4 mM KCl, and 11 mM glucose). Protein lysates were obtained using ultrasound and lysis buffer (250 mM HEPES, pH 7.7, 1 mM EDTA, 0.1 mM neocuproine, and 0.4% (w/v) CHAPS). The free thiols were methylated with blocking buffer (225 mM HEPES, pH 7.7, 0.9 mM EDTA, 0.09 mM neocuproine, 2.5% (w/v) SDS, and 20 mM MMTS) at the ratio of 0.8 mg/1 mL and were incubated at 50°C for 20 min with agitation. To remove residual MMTS, the MMTS-treated lysate was precipitated with cold acetone and the resulting pellet was resuspended in HENS buffer (250 mM HEPES, pH 7.7, 1 mM EDTA, 0.1 mM neocuproine, and 1% (w/v) SDS). This was followed by addition of one-third of the HENS suspension's final volume of 4 mM N-[6-(biotinamido) hexyl]-3′-(2′-pyridyldithio) propionamide (biotin-HPDP/DMF) mixed with 1 mM ascorbate. The protein lysate/biotin-HPDP mixture was incubated at room temperature for 1 hour to allow biotinylation to occur. These mixtures were precipitated with cold acetone to remove excess biotin-HPDP and then resuspended in HENS buffer. The biotinylated proteins (i.e., the former S-nitrosoproteins) were recovered using neutravidin-agarose beads (15 μL/per mg of initiated protein input) in neutralization buffer (20 mM HEPES, pH 7.7, 100 mM NaCl, 1 mM EDTA, and 0.5% (v/v) Triton X-100). The agarose beads were rinsed with washing buffer (20 mM HEPES, pH 7.7, 600 mM NaCl, 1mMEDTA, and 0.5% (v/v) Triton X-100). The biotinylated proteins were eluted by elution buffer (20 mM HEPES, pH 7.7, 100 mM NaCl, 1 mM EDTA, and 100 mM 2-ME). We added 100 femtomole of BSA in the eluent as a standard in the subsequent MS/MS analysis. The salt and detergent in eluents were removed by SpinOUT and DetergentOUT resins (Geno Technology Inc., MO, USA).

2.4. Mass Spectrometric Assay. Around 100 ng eluents were reduced, alkylated, and trypsin digested according to the user's guideline (In-Gel Tryptic Digestion Kit, Thermo Fisher Scientific, IL, USA). The peptide lysates were further desalting with Proteomics C18 Column (Mass solution Ltd., Taipei, Taiwan) and then subjected to mass analysis by nLC/Q-TOF

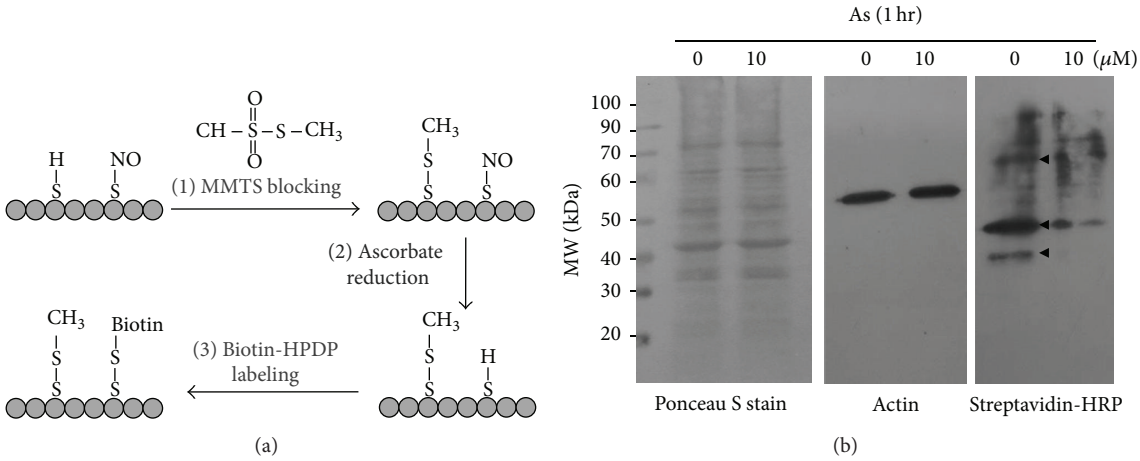

Figure 1: The arsenic decreases protein S-nitrosylation in primary keratinocytes. (a) The scheme of biotin switch showed that the NO on the cysteine residue was replaced by biotin. (b) After biotin switch, 40 μg of biotinylated lysates treated with 10 μM of arsenic for 1 h was separated by SDS-PAGE. The blotted membrane was prestained by Ponceau S and western blotted with actin (1 : 3000). Both two were applied as loading control. Streptavidin-HRP (1 : 3000) was applied to detect biotinylated proteins. The decreased S-nitrosylated proteins after arsenic treatment were indicated as triangle.

tandem mass spectrometry (Micromass, Manchester, UK). MS data were searched for against the NCBI database using an in-house MASCOT search program (Matrix Science, London, UK). Search parameters were set as mass values: monoisotopic, protein mass: unrestricted, peptide mass tolerance: ±0.4 Da, fragment mass tolerance: ±0.4 Da, max missed cleavages: 1, and the instrument type: ESI-QUAD-TOF.

2.5. Western Blot Analysis. Forty micrograms of cell lysates with various treatments was mixed with equal volume of sample buffer [Tris-HCl (62.5 mM, pH6.8), SDS (3%, w/v), 2-mercaptoethanol (5%, v/v), and glycerol (10%, v/v)] and then separated by SDS-PAGE. The gel was transferred to PVDF membranes (Millipore, MA, USA) and immunoblotted with antibodies: eNOS (1 : 3000, Cell Signaling Tech. MA, USA), iNOS (1 : 3000, Cell Signaling Tech. MA, USA). The membranes were visualized with the SuperSignal West Femto reagent (Thermo Fisher Scientific, IL, USA) on X-ray films. The images on X-ray films were scanned using a digital scanner (Microtek International Inc.) and the density was calculated by the Progenesis Samespots v2.0 software (Non-Linear Dynamics, Newcastle, UK).

2.6. Two-Dimensional Gel Electrophoresis. Extracted protein (1 mg) was precipitated with 3 volumes of cold acetone at −20°C for at least 20 min. After centrifugation, the protein pellets were air-dried for 5 min, dissolved in sample buffer [9 M urea, 2% (w/v) CHAPS, 60 mM DTT, and 2% (v/v, pH 4–7) IPG buffer (GE Healthcare BioSci., NJ, USA)], and incubated for at least 30 min to denature proteins completely. The protein solution was mixed with rehydration solution [8 M urea, 2% (w/v) CHAPS, and 0.5% (v/v, pH 4–7) IPG buffer] to reach a final volume of 340 μL and then soaked into an 18 cm DryStrip (pH 4–7, GE Healthcare BioSci.) for up to 12 h on Ettan IPGphor system (GE Healthcare BioSci.). Isoelectric focusing (IEF) was performed with the accumulated voltage set to 32 kVh. After IEF analysis, stripped gels were equilibrated with trisbuffer [50 mM Tris-HCl, pH 8.8, containing 2% (w/v) SDS, 6 M urea, 30% (v/v) glycerol, and 60 mM DL-dithiothreitol (DTT)] for 20 min. The stripped gels were then alkylated in the same buffer containing 135 mM iodoacetic acid for additional 20 min. The equilibrated IEF strip was laid on the top of a vertical SDS-PAGE system to perform the 2-DE.

2.7. Image Analysis. The gels were stained with VisPRO dye (Visual Protein Biotech., Taipei, Taiwan) and scanned with a digital scanner (Microtek International Inc.). The translational levels were calculated by ImageMaster software (GE Healthcare BioSci.). The gel slices excised from the silver-stained gel were digested with trypsin for 4 hours at 37°C (In-Gel Tryptic Digestion Kit, Thermo Fisher Scientific Inc.) and then subjected to mass spectrometric analysis.

3. Results and Discussion

3.1. Arsenic Reduces Protein S-Nitrosylation. Biotin switch is now the most popular methodology for identifying S-nitrosoproteins in various tissues [22]. In the present study, the procedure of biotin switch was simply indicated (Figure 1(a)). By treatment with 10 μM of arsenic for 1 hour, at least three groups of protein S-nitrosylation were significantly decreased in keratinocytes (Figure 1(b)). These biotinylated proteins, that is, NO-bound S-nitrosylated proteins, were purified from streptavidin conjugated agarose and then analyzed by LC-MS/MS. Totally, 20 and 13 S-nitrosoproteins were separately identified in the control and arsenic treatments. This was coincident to the decreased NO production and the reduced S-nitrosylated proteins.

3.2. Arsenic Decreases the Expressions of eNOS and iNOS. It has been reported that NO in keratinocytes was produced

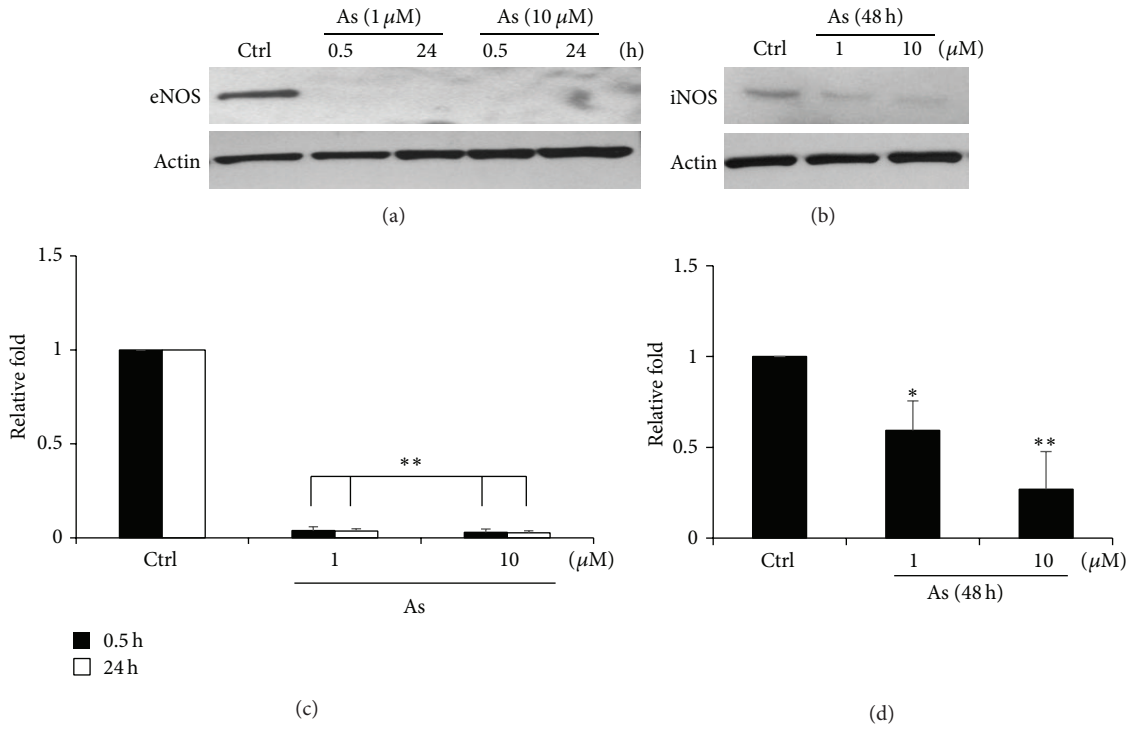

Figure 2: Arsenic attenuates the expressions of eNOS and iNOS. (a) Cells treated with 1 or 10 μM of arsenic for 0.5, 24 were used to monitor eNOS variations. (b) For investigating iNOS level, the cells were incubated with same concentration of arsenic for 48 hours. (c, d) The expression levels of eNOS and iNOS were statistically calculated from three repeats. Relative folds of protein levels shown as means ± S.E. compared to control. Statistical significance ($^{*}P < 0.05$, $^{**}P < 0.01$) analyzed using Fisher's LSD.

Table 1: Identification of arsenic-modulated proteins with nLC-MS/MS.

Spot number	Protein name[a]	Accession number[b]	MW (kDa)/pI Thero.[c]	MW (kDa)/pI Exp.[d]	Sequence coverage (%)	MOWSE score	Peptides Matched
287	Transformation upregulated nuclear protein	460789	51.0/5.1	54.5/4.9	12	268	3
631	26S proteasome non-ATPase regulatory subunit 13 isoform 1	157502193	42.9/5.5	44.3/5.2	19	380	8
720	60S acidic ribosomal protein P0	4506667	34.2/5.7	39.2/5.0	18	326	7
735	60S acidic ribosomal protein P0	4506667	34.2/5.7	39.2/6.2	29	422	7
749	60S acidic ribosomal protein P0	4506667	34.2/5.7	38.9/6.5	36	636	9
858	Cathepsin D preproprotein	4503143	44.5/6.1	30.4/5.3	25	422	9
899	NADH-Ubiquinone reductase	4758788	30.2/6.9	26.4/5.8	40	575	8
905	Enoyl-CoA hydratase	1922287	31.3/8.3	26.4/6.1	16	180	3

[a]Function of the protein obtained via the MASCOT software (http://www.matrixscience.com) search program by querying the NCBI database. The parameters were set at peptide mass tolerance ±0.4 Da and allowed missed cleavage 1.

[b]Accession number from NCSI database.

[c]Theoretic protein molecular weight and pI annotated in NCBI database.

[d]Experimental protein molecular weight and pI calculated from 2-DE gel.

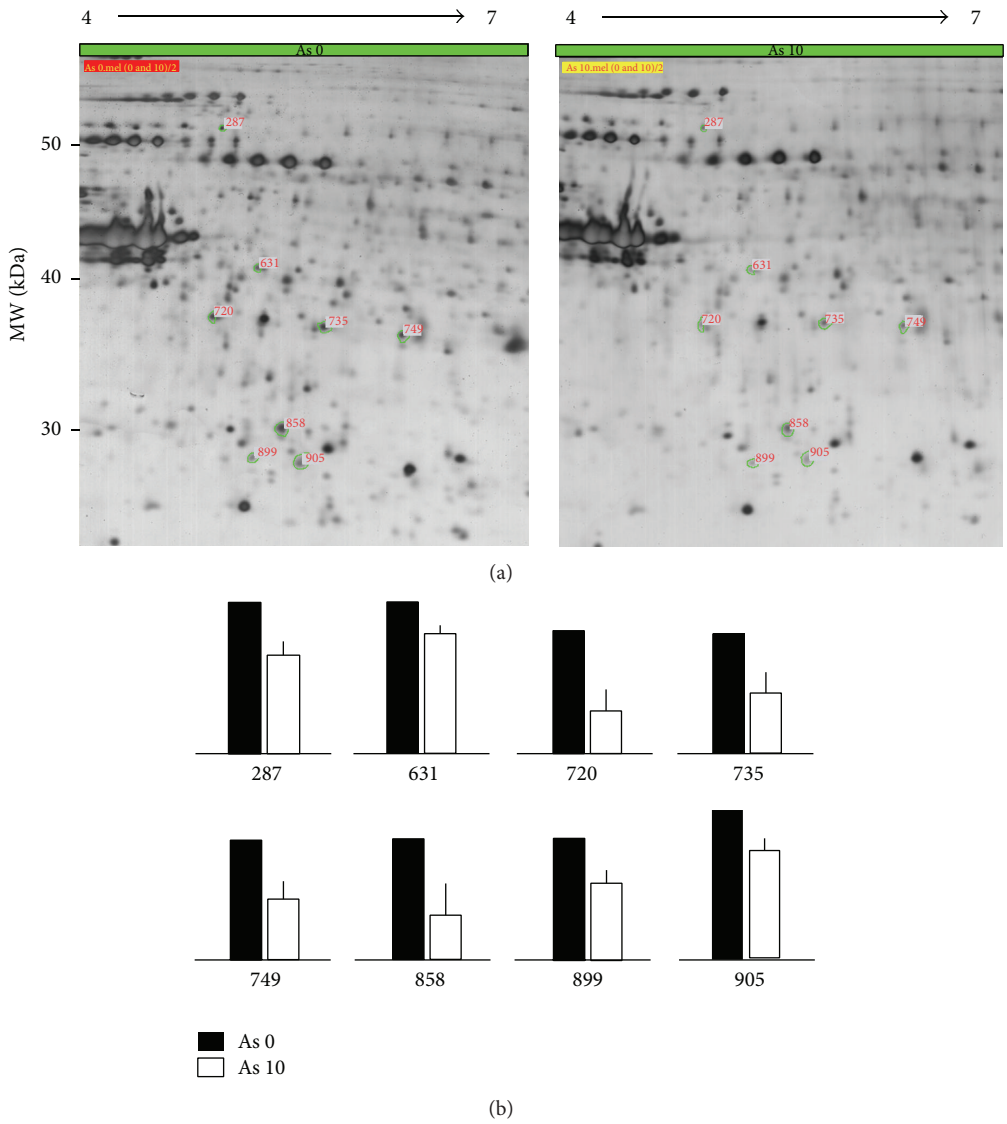

FIGURE 3: Translational proteome regulated by arsenic. The cell lysates (1 mg) treated with 10 μM of arsenic for 1 h were separated by 2-DE (pH4–7). By using ImageMaster software, the proteins with decreased expression (<0.7 fold) were indicated. (b) The relative expression levels of these decreased proteins were statistically calculated from three repeats.

through the activation of eNOS and iNOS [23]. Therefore, in the present study, we examined the expressions of both enzymes in the existence of arsenic. As shown in Figures 2(a) and 2(b), the significant decreases of their expressions were observed.

3.3. Arsenic Modulates Translational Proteome in Keratinocytes. In addition to elucidating those posttranslational S-nitrosylated proteins, we further investigated the proteins changed in their expression levels. By using 2-DE, 8 proteins showed a dramatic decrease in the expression level (Figures 3(a) and 3(b)). These identified proteins are annotated function in (Table 1). More specifically, HNRNPK is a pre-mRNA-binding protein, which has been identified to be involved in arsenic-induced apoptosis in acute myeloid leukemia cells [26]. PSMD13 is proteasome protein regulating the degradation of ubiquitinated proteins, which has been identified in fetal fibroblasts from glutathione deficient mouse using arsenic-induced apoptosis model by cDNA microarray [27]. RPLP0 is a ribosomal protein, in general conditions, constantly expressed in cells (house-keeping gene). The functional interactions between arsenic and RPLP0 required further investigations. CTSD is a protease active in intracellular protein breakdown. Increased CTSD has been identified in arsenic-treated human lymphoblastoid cell lines correlated with autophagy [28]. However, here, we found arsenic treatment decreased CTSD in human keratinocytes. NDUFS3 is a subunit of the mitochondrial membrane respiratory chain NADH dehydrogenase (Complex I). Decreased NDUFS3 has been identified in hepatoma cell line [29]. Indeed, our previous study has identified the dose response between arsenic and NDUFS3 in human keratinocytes. Low concentrations

(0.1–1.0 μM) of arsenic increased NDUFS3 associated with keratinocyte proliferation. High concentration (5.0 μM) of arsenic decreased NDUFS3 correlated with cell death [30]. This decreased NDUFS3 was represented in our current data. ECHS1 is a catalytic enzyme in mitochondrial fatty acid betaoxidation pathway; however, direct evidence between ECHS1 and arsenic is not yet clarified. To summarize, from our proteomic data, altered apoptosis and mitochondrial metabolic functions were the dominant effects of arsenic on human keratinocytes.

4. Conclusion

In the current study, we concluded that arsenic can compete with nitric oxide in binding cysteine residues so that the protein S-nitrosylation is inhibited. Whether the decreased S-nitrosylation is correlated to arsenic-induced pathology attracts a great attention in the further study. In addition, the homeostasis of cellular apoptosis and mitochondrial dysfunctions is worthy of further study.

Conflict of Interests

The authors declare that there is no conflict of interests regarding the publication of this paper.

Acknowledgments

The authors thank Dr. Hans-Uwe Dahms for critical reading of the paper. This study was supported by a grant from the National Science Council (NSC100-2314-B-037-053 and NSC101-2320-B-037-041). They are grateful to the Center for Resources, Research & Development of Kaohsiung Medical School for the support of fluorescent imaging.

References

[1] M. W. Foster, D. T. Hess, and J. S. Stamler, "Protein S-nitrosylation in health and disease: a current perspective," *Trends in Molecular Medicine*, vol. 15, no. 9, pp. 391–404, 2009.

[2] D. T. Hess, A. Matsumoto, S. O. Kim, H. E. Marshall, and J. S. Stamler, "Protein *S*-nitrosylation: purview and parameters," *Nature Reviews Molecular Cell Biology*, vol. 6, no. 2, pp. 150–166, 2005.

[3] N. V. Marozkina and B. Gaston, "S-Nitrosylation signaling regulates cellular protein interactions," *Biochimica et Biophysica Acta: General Subjects*, vol. 1820, no. 6, pp. 722–729, 2012.

[4] H. E. Marshall and J. S. Stamler, "Inhibition of NF-κB by S-nitrosylation," *Biochemistry*, vol. 40, no. 6, pp. 1688–1693, 2001.

[5] W. Kim, Y. Choi, P. V. Rayudu et al., "Attenuation of NMDA receptor activity and neurotoxicity by nitroxyl anion, NO^-," *Neuron*, vol. 24, no. 2, pp. 461–469, 1999.

[6] S. A. Lipton, Y. B. Choi, Z. H. Pan et al., "A redox-based mechanism for the neuroprotective and neurodestructive effects of nitric oxide and related nitroso-compounds," *Nature*, vol. 364, no. 6438, pp. 626–632, 1993.

[7] T. Nakamura and S. A. Lipton, "Redox modulation by S-nitrosylation contributes to protein misfolding, mitochondrial dynamics, and neuronal synaptic damage in neurodegenerative diseases," *Cell Death and Differentiation*, vol. 18, no. 9, pp. 1478–1486, 2011.

[8] S. Sarkar, V. I. Korolchuk, M. Renna et al., "Complex inhibitory effects of nitric oxide on autophagy," *Molecular Cell*, vol. 43, no. 1, pp. 19–32, 2011.

[9] S. M. Haldar and J. S. Stamler, "S-Nitrosylation at the interface of autophagy and disease," *Molecular Cell*, vol. 43, no. 1, pp. 1–3, 2011.

[10] E. Aranda, C. López-Pedrera, J. R. de la Haba-Rodríguez, and A. Rodríguez-Ariza, "Nitric oxide and cancer: the emerging role of S-nitrosylation," *Current Molecular Medicine*, vol. 12, no. 1, pp. 50–67, 2011.

[11] A. K. Iyer, N. Azad, L. Wang, and Y. Rojanasakul, "Role of S-nitrosylation in apoptosis resistance and carcinogenesis," *Nitric Oxide*, vol. 19, no. 2, pp. 146–151, 2008.

[12] S. Ghavami, M. Hashemi, S. R. Ande et al., "Apoptosis and cancer: mutations within caspase genes," *Journal of Medical Genetics*, vol. 46, no. 8, pp. 497–510, 2009.

[13] J. B. Mannick, A. Hausladen, L. Liu et al., "Fas-induced caspase denitrosylation," *Science*, vol. 284, no. 5414, pp. 651–654, 1999.

[14] N. J. Török, H. Higuchi, S. Bronk, and G. J. Gores, "Nitric oxide inhibits apoptosis downstream of cytochrome c release by nitrosylating caspase 9," *Cancer Research*, vol. 62, no. 6, pp. 1648–1653, 2002.

[15] A. Vazquez, E. E. Bond, A. J. Levine, and G. L. Bond, "The genetics of the p53 pathway, apoptosis and cancer therapy," *Nature Reviews Drug Discovery*, vol. 7, no. 12, pp. 979–987, 2008.

[16] J. L. Williams, P. Ji, N. Ouyang, L. Kopelovich, and B. Rigas, "Protein nitration and nitrosylation by NO-donating aspirin in colon cancer cells: Relevance to its mechanism of action," *Experimental Cell Research*, vol. 317, no. 10, pp. 1359–1367, 2011.

[17] N. Azad, V. Vallyathan, L. Wang et al., "*S*-nitrosylation of Bcl-2 inhibits its ubiquitin-proteasomal degradation: a novel anti-apoptotic mechanism that suppresses apoptosis," *The Journal of Biological Chemistry*, vol. 281, no. 45, pp. 34124–34134, 2006.

[18] P. Chanvorachote, U. Nimmannit, C. Stehlik et al., "Nitric oxide regulates cell sensitivity to cisplatin-induced apoptosis through S-nitrosylation and inhibition of Bcl-2 ubiquitination," *Cancer Research*, vol. 66, no. 12, pp. 6353–6360, 2006.

[19] W. Xu, L. Liu, G. C. M. Smith, and L. G. Charles, "Nitric oxide upregulates expression of DNA-PKcs to protect cells from DNA-damaging anti-tumour agents," *Nature Cell Biology*, vol. 2, no. 6, pp. 339–345, 2000.

[20] W. Wei, B. Li, M. A. Hanes, S. Kakar, X. Chen, and L. Liu, "S-nitrosylation from GSNOR deficiency impairs DNA repair and promotes hepatocarcinogenesis," *Science Translational Medicine*, vol. 2, no. 19, Article ID 19ra13, 2010.

[21] J. Jones Larry E., L. Ying, A. B. Hofseth et al., "Differential effects of reactive nitrogen species on DNA base excision repair initiated by the alkyladenine DNA glycosylase," *Carcinogenesis*, vol. 30, no. 12, pp. 2123–2129, 2009.

[22] M. T. Forrester, J. W. Thompson, M. W. Foster, L. Nogueira, M. A. Moseley, and J. S. Stamler, "Proteomic analysis of S-nitrosylation and denitrosylation by resin-assisted capture," *Nature Biotechnology*, vol. 27, no. 6, pp. 557–559, 2009.

[23] Y. Kumagai and J. Pi, "Molecular basis for arsenic-induced alteration in nitric oxide production and oxidative stress: implication of endothelial dysfunction," *Toxicology and Applied Pharmacology*, vol. 198, no. 3, pp. 450–457, 2004.

[24] C. J. Chen, Y. C. Chuang, T. M. Lin, and H. Y. Wu, "Malignant neoplasms among residents of a blackfoot disease-endemic area

in Taiwan: high-arsenic artesian well water and cancers," *Cancer Research*, vol. 45, no. 11, pp. 5895–5899, 1985.

[25] B. Huang, C. L. Liao, Y. P. Lin, S. C. Chen, and D. L. Wang, "S-nitrosoproteome in endothelial cells revealed by a modified biotin switch approach coupled with western blot-based two-dimensional gel electrophoresis," *Journal of Proteome Research*, vol. 8, no. 10, pp. 4835–4843, 2009.

[26] F. Gao, Y. Wu, M. Zhao, C. Liu, L. Wang, and G. Chen, "Protein Kinase C-delta mediates down-regulation of heterogeneous nuclear ribonucleoprotein K protein: involvement in apoptosis induction," *Experimental Cell Research*, vol. 315, no. 19, pp. 3250–3258, 2009.

[27] S. Kann, C. Estes, J. F. Reichard et al., "Butylhydroquinone protects cells genetically deficient in glutathione biosynthesis from arsenite-induced apoptosis without significantly changing their prooxidant status," *Toxicological Sciences*, vol. 87, no. 2, pp. 365–384, 2005.

[28] A. M. Bolt, R. M. Douglas, and W. T. Klimecki, "Arsenite exposure in human lymphoblastoid cell lines induces autophagy and coordinated induction of lysosomal genes," *Toxicology Letters*, vol. 199, no. 2, pp. 153–159, 2010.

[29] D. R. Yoo, S. A. Chong, and M. J. Nam, "Proteome profiling of arsenic trioxide-treated human hepatic cancer cells," *Cancer Genomics and Proteomics*, vol. 6, no. 5, pp. 269–274, 2009.

[30] C. Lee, S. Wu, C. Hong et al., "Aberrant cell proliferation by enhanced mitochondrial biogenesis via mtTFA in arsenical skin cancers," *The American Journal of Pathology*, vol. 178, no. 5, pp. 2066–2076, 2011.

Hindawi Publishing Corporation
The Scientific World Journal
Volume 2014, Article ID 810561, 8 pages
http://dx.doi.org/10.1155/2014/810561

Research Article

Expression of a Splice Variant of CYP26B1 in Betel Quid-Related Oral Cancer

Ping-Ho Chen,[1,2] Ka-Wo Lee,[3,4] Cheng-Chieh Hsu,[5] Jeff Yi-Fu Chen,[6] Yan-Hsiung Wang,[1,7] Ker-Kong Chen,[1,8] Hui-Min David Wang,[9] Hurng-Wern Huang,[5] and Bin Huang[10,11]

[1] *School of Dentistry, College of Dental Medicine, Kaohsiung Medical University, No. 100 Shih-Chuan 1st Road, Kaohsiung 80708, Taiwan*
[2] *Cancer Center, Kaohsiung Medical University Hospital, No. 100 Shih-Chuan 1st Road, Kaohsiung 80708, Taiwan*
[3] *Department of Otolaryngology, Kaohsiung Medical University Hospital, No. 100 Shih-Chuan 1st Road, Kaohsiung 80708, Taiwan*
[4] *Department of Otolaryngology, College of Medicine, Kaohsiung Medical University, No. 100 Shih-Chuan 1st Road, Kaohsiung 80708, Taiwan*
[5] *Institute of Biomedical Sciences, National Sun Yat-sen University, No. 70 Lienhai Road, Kaohsiung 80424, Taiwan*
[6] *Department of Biotechnology, Kaohsiung Medical University, No. 100 Shih-Chuan 1st Road, Kaohsiung 80708, Taiwan*
[7] *Orthopaedic Research Center, College of Medicine, Kaohsiung Medical University, No. 100 Shih-Chuan 1st Road, Kaohsiung 80708, Taiwan*
[8] *Division of Conservative Dentistry, Department of Dentistry, Kaohsiung Medical University Hospital, No. 100 Shih-Chuan 1st Road, Kaohsiung 80708, Taiwan*
[9] *Department of Fragrance and Cosmetic Science, Kaohsiung Medical University, No. 100 Shih-Chuan 1st Road, Kaohsiung 80708, Taiwan*
[10] *Department of Biomedical Science and Environmental Biology, College of Life Science, Kaohsiung Medical University, No. 100 Shih-Chuan 1st Road, Kaohsiung 80708, Taiwan*
[11] *Department of Biological Sciences, National Sun Yat-sen University, No. 70 Lienhai Road, Kaohsiung 80424, Taiwan*

Correspondence should be addressed to Hurng-Wern Huang; sting@mail.nsysu.edu.tw and Bin Huang; huangpin2@yahoo.com.tw

Received 1 May 2014; Accepted 1 June 2014; Published 7 July 2014

Academic Editor: Li-Yeh Chuang

Betel quid (BQ) is a psychostimulant, an addictive substance, and a group 1 carcinogen that exhibits the potential to induce adverse health effects. Approximately, 600 million users chew a variety of BQ. Areca nut (AN) is a necessary ingredient in BQ products. Arecoline is the primary alkaloid in the AN and can be metabolized through the cytochrome P450 (CYP) superfamily by inducing reactive oxygen species (ROS) production. Full-length CYP26B1 is related to the development of oral pharyngeal cancers. We investigated whether a splice variant of CYP26B1 is associated with the occurrence of ROS related oral and pharyngeal cancer. Cytotoxicity assays were used to measure the effects of arecoline on cell viability in a dose-dependent manner. *In vitro* and *in vivo* studies were conducted to evaluate the expression of the CYP26B1 splice variant. The CYP26B1 splice variant exhibited lower expression than did full-length CYP26B1 in the human gingival fibroblast-1 and Ca9-22 cell models. Increased expression of the CYP26B1 splice variant was observed in human oral cancer tissue compared with adjacent normal tissue, and increased expression was observed in patients at a late tumor stage. Our results suggested that the CYP26B1 splice variant is associated with the occurrence of BQ-related oral cancer.

1. Introduction

Betel quid (BQ) chewing is an emerging health-associated problem in Asia and among diverse migrant populations in western countries. Approximately, 600 million people worldwide chew BQ [1]. BQ is a psychostimulant and an addictive carcinogenic substance [2, 3]. The areca nut (AN) is the primary ingredient in various BQ products, and the International Agency for Research on Cancer (IARC) has classified the AN as a group I human carcinogen based

on findings indicating that it is associated with an elevated risk for oral potentially malignant disorders (OPMDs, such as leukoplakia, oral submucous fibrosis, erythroplakia, and lichen planus) and cancers of the oral cavity, pharynx, and esophagus [3–7].

In Taiwan, the quantity of BQ production increased approximately 44-fold from 1961 to 2001 [3]. In Taiwan alone, 2 million people are habitual BQ users, accounting for 10% of the island's Han Chinese population. BQ is typically used by men (men: 16.5%; women: 2.9%) [8], aboriginal people, blue-collar workers, people with low levels of education, and smokers and drinkers. A recent intercountry ABC study indicated that chewing rates among men (15.6%) were significantly higher than those among women (3.0%) in Taiwan [9]. In 2010, the age-standardized incidence rate of oral and pharyngeal cancer in Taiwanese men, adjusted based on the 2000 world population, was 40.56 per 100 000, ranking as the fourth most prevalent cancer [10]. The age-standardized mortality rate for oral and pharyngeal cancer was 14.71 per 100 000, indicating that this cancer also ranks as the fourth highest cause of cancer deaths.

BQ, the fourth most frequently consumed psychoactive substance worldwide (after caffeine, nicotine, and alcohol), is a masticatory mixture combining the AN, betel leaf, slaked lime, and locally varied flavorings [11]. Our previous results indicated that chewing BQ may generate significantly reactive oxygen species, such as the hydroxyl radical, which may result in oxidative damage in the oral mucosa [12]. In serum-starved oral cells, the AN extract induces pyknotic necrosis by increasing reactive oxygen species (ROS) levels [13]. Arecoline is the most abundant alkaloid in the AN and is known to induce cytotoxicity *in vivo* and *in vitro* in mammalian cells [14–16]. A previous study indicated that arecoline can induce cell cytotoxicity, cycle arrest, and apoptosis in human endothelial cells [17]. In human cells, arecoline was reported to induce the production of ROS [18], which are capable of inducing nucleotide modification and the generation of cellular 8-hydroxy-2′-deoxyguanosine-induced oxidative DNA damage [19]. A previous report indicated that all-trans retinoic acid (at-RA) induces NADPH oxidase-mediated ROS generation in granulocyte-differentiated HL60 cells [20]. In rat Sertoli cells, at-RA can generate apoptosis [21] by inducing ROS production [21, 22].

Previous studies have indicated that CYP26B1, a member of the cytochrome P450 (CYP) superfamily, is a primary at-RA metabolizing enzyme. The at-RA is a structure of retinoic acid (RA), which is an active derivative of vitamin A. Dietary retinol (vitamin A) has been metabolized into at-RA. Numerous reports have suggested that RA deficiency may be associated with carcinogenesis [23–26]. Insufficient retinol intake is related to hyperkeratosis and hyperplasia of the oral mucosa [25]. A report indicated that remission in OPMD patients with BQ chewing habits treated with RA may result from suppression of the promoting action of AN ingredients rather than inhibition of tumor initiation [27].

Our previous studies indicating that arecoline induces both *in vivo* and *in vitro* suggest that the CYP26B1 variants play a vital role in BQ-related oral and pharyngeal cancers [7, 28]. We investigated whether susceptible CYP26B1 genes and, particularly, their splicing variants are associated with oral and pharyngeal cancer.

2. Methods

2.1. Cytotoxicity Assay. Detailed information on the cell culturing procedure is provided previously [29, 30]. We obtained normal human gingival fibroblasts (HGF-1) from the American Type Culture Company (ATCC number CRL-2014) and Ca9-22 cells (a cell line of oral epidermal gingival squamous carcinoma) from the Japanese Collection of Research Bioresources Cell Bank (JCRB number JCRB0625). The arecoline-conditioned medium (0.05–0.8 mM) was freshly prepared from arecoline hydrobromide (Sigma) in a growth medium (DMEM/F12). Cells were seeded into 96-well plates at a density of 10^4 cells per well for 1 day and were then treated with various concentrations (0, 0.05, 0.1, 0.2, 0.4, and 0.8 mM) of arecoline for 24 h in a CO_2 incubator. MTT (Sigma) solution (5 mg/mL) was added to the cells and incubated for 2 h at 37°C. After the culture medium was removed, the cells were dissolved using DMSO, and absorbance was detected at 570 nm in an ELISA reader (Bio Tek el800), with a reference wavelength of 630 nm. The data are presented as the percentage of viable cells compared with the controls.

2.2. Western Blotting Analysis. Details on the method used for western blotting are provided in our previous report [7]. Mouse antihuman CYP26B1 monoclonal antibodies (Abnova, Taipei City, Taiwan) were used as the first antibody at a 1 : 1000 dilution, and a horseradish-peroxidase conjugated antimouse antibody (Cell signaling Co.) was used as the second antibody at a 1 : 1000 dilution. Both antibodies were dissolved in 3% nonfat dry milk (GE Healthcare, Uppsala, Sweden) in 0.05% TBST (8 g NaCl, 0.2 g KCl, 3 g Tris, 0.5% Tween 20, dd H_2O to 1 L, and pH 7.4). Peroxidase activity was detected using an ECL detection kit (GE Healthcare) and recorded using the HyperFilm TMMP (GE Healthcare).

2.3. Study Participants. The Department of Otorhinolaryngology and the Dentistry Department of Kaohsiung Medical University (KMU) Hospital recruited 10 male oral cancer patients. This study was approved by the institutional review board (IRB) of the Human Experiment and Ethics Committee of KMU (KMU-IRB-950070 and KMU-IRB-950072). The volunteers agreed to provide written informed consent, provide oral cancerous tissue (necessary for resection), and complete questionnaires. Pairs of cancer tissue and adjacent noncancerous oral tissue were collected from patients with oral cancer for use in a CYP26B1 gene expression assay. Pathologists or surgeons histologically confirmed that all cases were cases of oral cancer. Demographic data, information regarding previous substance use, and clinical information on the participants were collected by administering a questionnaire and analyzed.

2.4. Identification of CYP26B1 and CYP26B1 Splice Variant mRNA Expression in HGF-1 and Ca9-22 Cells. The mRNA levels of CYP26B1 and expression levels of the CYP26B1 splice

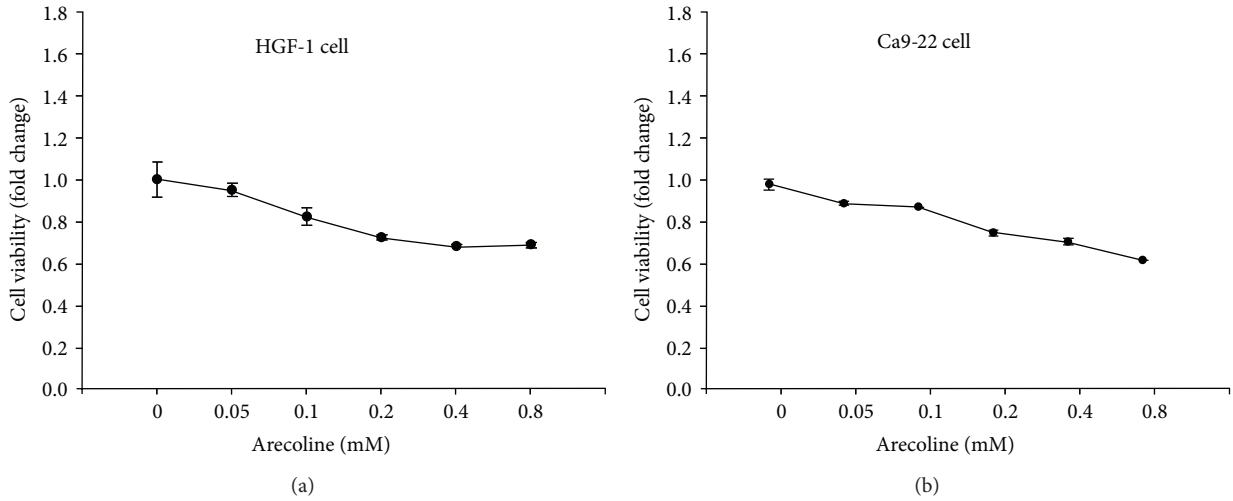

Figure 1: Effect of arecoline on the viability of HGF-1 and Ca9-22 cells. Different concentrations of arecoline were incubated with HGF and Ca9-22 cells for 24 h. Cell viability was determined using an MTT assay. (a) Arecoline induced cell death in various concentrations of arecoline in HGFs. (b) Arecoline induced cell death in various concentrations of arecoline in Ca9-22 cells.

variant in HGF-1 and Ca9-22 cells treated with arecoline were determined using semiquantitative PCR. Briefly, total RNA was isolated using a Trizol kit (Roche). The integrity and quality of total RNA were determined using DU 800 (Beckman Coulter). Total RNA was subjected to High-Capacity cDNA Reverse Transcription Kits (Applied Biosystems) to obtain complementary DNA (cDNA). PCRs were performed to investigate the expression of the genes. We designed the PCR primers in CYP26B1 gene exon 1 and exon 3 positions with oligonucleotide primers directed against cDNA sequences of CYP26B1 (forward 5′-TCTTTGAGGGCTTGGATCTG-3′, reverse 5′-GGATCACCAGCTGGATCTTG-3′). The PCRs were performed as follows: initial denaturation at 94°C for 5 min; 35 cycles of denaturation at 94°C for 30 s; annealing at 53°C for 30 s; extension temp. 72°C for 1 min; and holding at 72°C for 7 min to complete the reaction. The RT-PCR products were electrophorized in 2% agarose gel and then stained with ethidium bromide. The semiquantitation of mRNA expression was determined by subjecting the RT-PCR products to densitometry (Epson 1640 U). The cDNA (about 0.2 μg) was used as a template in a PCR amplification reaction to obtain gene products of 2 lengths: full-length CYP26B1 composed of 464 nucleotides and a CYP26B1 splice variant composed of 244 nucleotides.

The results of sequencing the 2 gene products by using NCBI BLAST indicated that the products were 99% to 100% similar (Figures 2(a) and 2(b)). The excitation intensity of the band from the agarose gel revealed that, even when the same cDNA concentration and number of cDNA reaction cycles were applied, CYP26B1 gene expression in the normal HGF-1 cell line was much lower than that of oral cancerous Ca9-22 cells.

2.5. Statistical Analysis. The one-way ANOVA and Bonferroni multiple comparison test were applied to analyze the relative fold change in the treatment groups compared with the control (HGF-1 or Ca9-22 without arecoline treatment), and a statistically significant difference ($P < 0.05$) is indicated using an asterisk. All statistical analyses were performed using the IBM SPSS Statistics 19, and the results were considered statistically significant when $P < 0.05$.

3. Results

3.1. Cell Viability of HGF-1 and Ca9-22 Cells. We used the MTT assay to evaluate cell viability following exposure to 6 concentrations (0, 0.05, 0.1, 0.2, 0.4, and 0.8 mM) of arecoline for 24 h. Cell survival gradually decreased after increasing the arecoline concentration in a dose-dependent manner. Figure 1(a) shows that arecoline reduced cell survival predominantly in a dose-dependent manner, and cell survival approached approximately 70% at arecoline concentrations of 0.4 mM and 0.8 mM. When the HGF-1 cells were treated with 0.05, 0.1, 0.2, 0.4, and 0.8 mM arecoline for 24 h, cell survival was 94%, 82%, 72%, 68%, and 68% compared with the control group, which did not receive arecoline treatment. This result was also observed in cultured Ca9-22 cells, of which viability remarkably decreased and reached about 60% at the concentration of 0.8 mM (Figure 1(b)). When the Ca9-22 cells were treated with 0.05, 0.1, 0.2, 0.4, and 0.8 mM arecoline for 24 h, cell survival was 90%, 89%, 76%, 72%, and 63% compared with the control group.

3.2. Expression of the Full-Length (57 kDa) CYP26B1 and CYP26B1 Splice Variant (49 kDa) in Cells. In normal HGF-1 cultures treated with various concentrations of arecoline, the expression of the full-length CYP26B1 protein and the splice variant exhibited significant upregulation compared with the control according to western blot analysis (Figure 3(a)). In normal HGF-1 cultures treated with doses of 0.4 and 0.8 mM arecoline, the expression of the full-length CYP26B1 protein

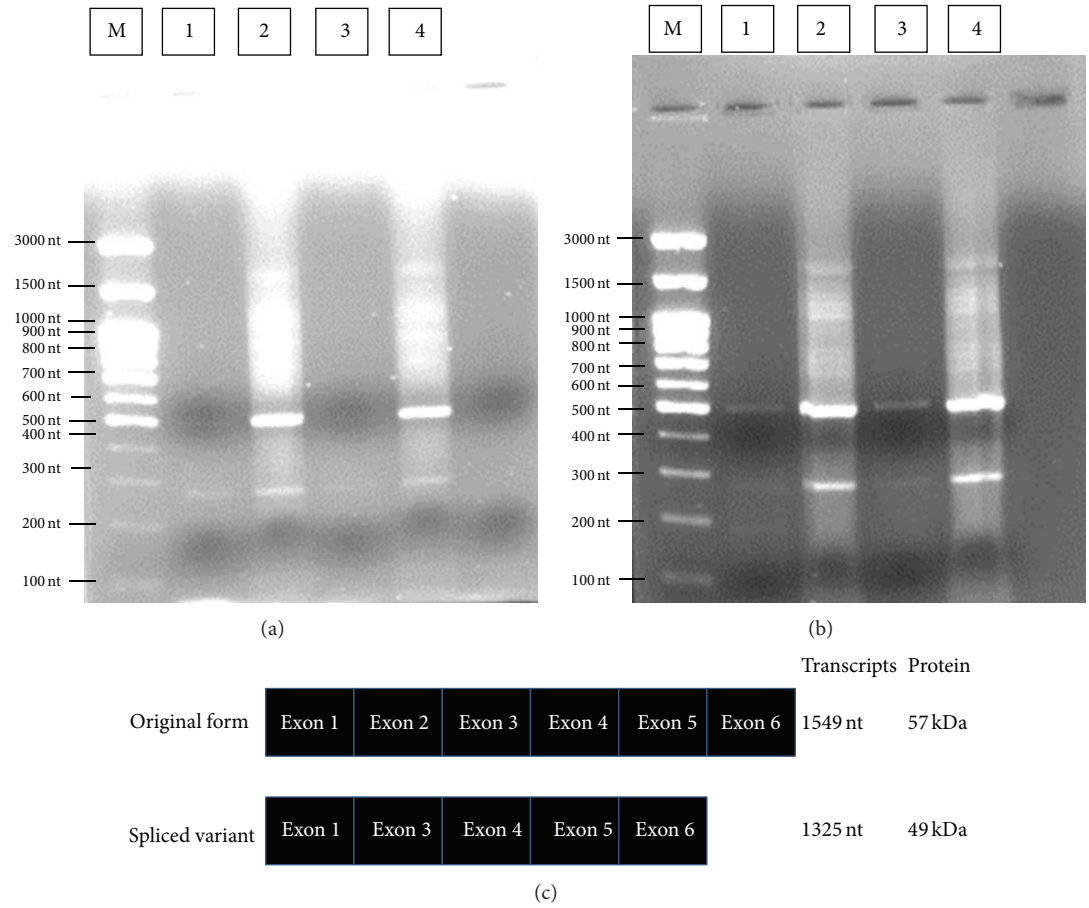

Figure 2: Expression of full-length CYP26B1 (57 kDa) and the CYP26B1 splice variant (49 kDa) in HGF-1 and Ca9-22 cell lines. CYP26B1 and the CYP26B1 splice variant were examined using RT-PCR. (a) Expression of the CYP26B1 gene in nontreated HGF-1 cells. (b) Expression of the CYP26B1 gene in nontreated Ca9-22 cells. (c) Full-length CYP26B1 and the splice variant. M: marker; lane 1: template 2 μg; lane 2: template 20 μg; lane 3: template 2 μg; lane 4: template 20 μg.

exhibited significant upregulation (2.4-fold and 2.7-fold, separately) compared with the control (Figure 3(b)). Expression of the CYP26B1 splice variant exhibited significant minor upregulation (1.6-fold and 1.5-fold, separately) at doses of 400 and 800 μM arecoline in normal HGF cultures compared with the control (Figure 3(c)).

Similarly, in cancerous oral Ca9-22 cell cultures, the expression of full-length CYP26B1 and the splice variant exhibited significant upregulation compared with the control (Figure 3(d)). In cancerous oral Ca9-22 cell cultures treated with arecoline (0.2 mM, 0.4 mM, and 0.8 mM), we observed significantly increased expression of full-length CYP26B1 (the fold changes were 2.7-fold, 3.1-fold, and 3.1-fold, resp.; Figure 3(e)). Expression of the CYP26B1 splice variant significantly increased only in cancerous oral Ca9-22 cell cultures treated with 800 μM arecoline (Figure 3(f)).

3.3. Expression of the CYP26B1 Splice Variant (49 kDa) in the Study Population. The oral cancer tissue exhibited consistent upregulation in the protein levels of the CYP26B1 splice variant. Figure 4(a) shows that the protein expression of the CYP26B1 splice variant ($N = 8$ paired sample) was an average of 6.44-fold higher in human oral squamous cell carcinoma (OSCC) tissue than in the adjacent noncancerous tissue. When a 2.0-fold change was defined as the threshold, 6 of 8 (75%) paired samples were considered significantly upregulated (>2-fold) in a range from 2.32-fold to 24.72-fold. The cases that did not exhibit significant upregulation were cases 151 (1.74-fold) and 158 (1.11-fold). The clinical characteristics of the patients are shown in Figure 4(b). The results indicated that patients with late-stage (stage III or stage IV) carcinoma exhibited a greater than 2-fold change in expression of the CYP26B1 splice variant.

4. Discussion

BQ chewing is a popular habit among Taiwanese men. Although BQ ingredients vary among regions worldwide, the AN is the primary component. Our previous study indicated that variants of full-length CYP26B1 may be associated with the occurrence of BQ-related OSCC [7]. In addition, a previous study indicated that RA metabolizing enzymes CYP26B1 are overexpressed significantly in colorectal cancer and that CYP26B1 is significantly associated with the

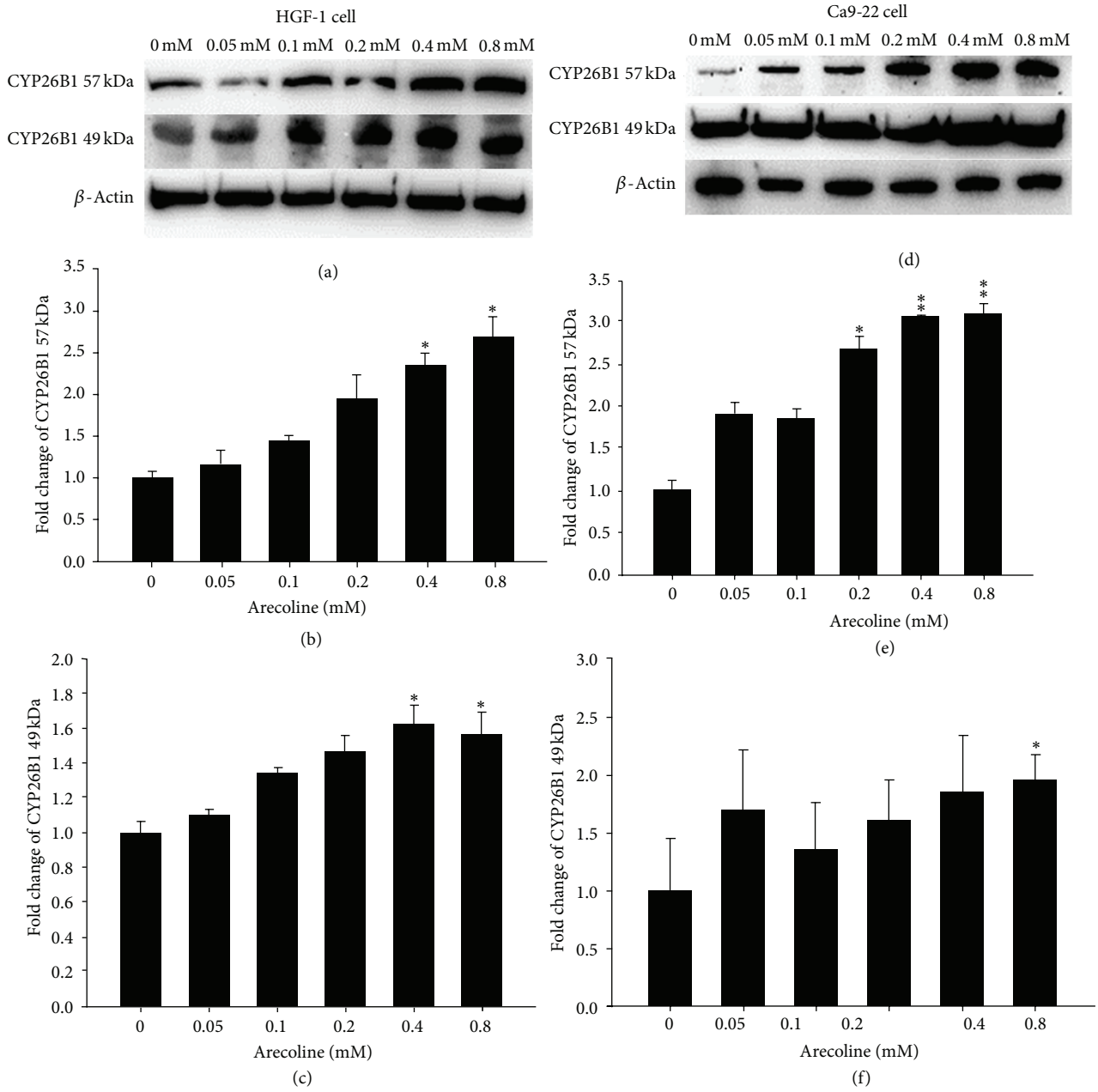

Figure 3: Expression of CYP26B1 induced by arecoline for 24 h in cultured HGF-1 and Ca9-22 cells. (a) Expression of full-length CYP26B1 (57 kDa) and the splice variant (49 kDa) in HGF-1 cells exposed to arecoline at various concentrations compared with the control, which did not receive arecoline treatment; (b) densitometric analysis of the expression of full-length CYP26B1 bands in HGF cells; (c) densitometric analysis of the expression of the CYP26B1 splice variant in HGF-1 cells; (d) expression of full-length CYP26B1 (57 kDa) and the splice variant (49 kDa) in Ca9-22 cells exposed to arecoline at various concentrations compared with the control; (e) densitometric analysis of the expression of full-length CYP26B1 bands in Ca9-22 cells; (f) densitometric analysis of the expression of the CYP26B1 splice variant in Ca9-22 cells. Mean ± SD; $^{*}P < 0.05$; $^{**}P < 0.01$; $n = 3$.

prognosis of colorectal cancer patients [31]. According to our thorough review of relevant research, no previous study has explored the relationship between the expression activity of the CYP26B1 splice variant and oral cancer.

Arecoline is a primary alkaloid in the AN. The IARC stated that evidence obtained from animal experiments strongly indicates that the AN is carcinogenic and that limited evidence indicating that arecoline is carcinogenic has been obtained from animal experiments [3]. In this experiment, normal oral cells (HGF-1) and oral cancer cells (Ca9-22) were used as cell models to explore whether arecoline treatment causes cell toxicity and affects cell survival. At 0.8 mM arecoline, the cell viability of HGF-1 cells was 68% and Ca9-22 cell survival was 63% compared with the control group.

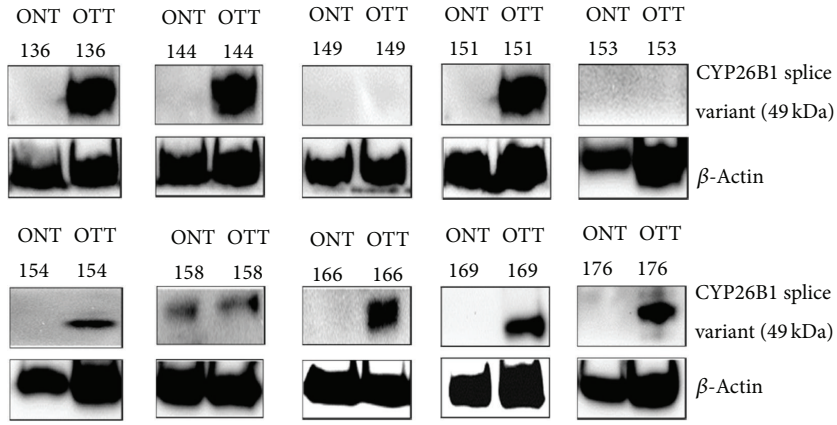

(a)

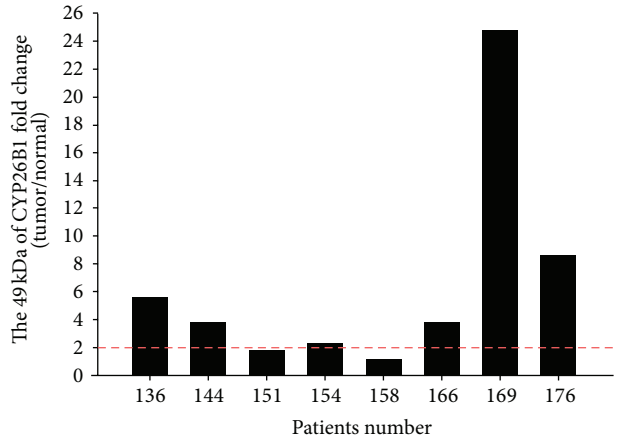

Number	136	144	149	151	153	154	158	166	169	176
Sex	Male	Male	Male	Female	Male	Male	Male	Male	Male	Male
Tumor site[a]	Tongue	Palate	Buccal	Tongue	—	Buccal	Oral	Tongue	Oral	Tongue
Age	45	51	71	53	45	39	69	55	55	56
Stage	III	IVC	II	I	—	III	IVA	III	III	IVA

[a]ONT: oral adjacent normal tissue; OTT: oral tumor tissue.

—: no information can be available.

(b)

Figure 4: Protein level of the CYP26B1 splice variant (49 kDa) in human OSCC tissue (T) and adjacent normal tissue (N). (a) Level of CYP26B1 splice variant protein expression in 10 pairs of oral tumor tissue and adjacent tissue; β-actin was used as a control for protein loading and detection. (b) Expression protein fold change level of CYP26B1 in 10 pairs of oral tumor tissue compared with the adjacent normal tissue.

Using a cell viability curve, we observed that increasing the concentration of arecoline resulted in declining cell survival. Previous studies have shown that arecoline can cause carcinogenicity, cytotoxicity, immunotoxicity, and genotoxicity [32–34]. Stimulated human peripheral blood mononuclear cells and human keratinocytes can secrete and release cytokines, causing arecoline to regulate inflammatory processes [35, 36]. A previous report indicated that arecoline induced ROS generation, suggesting that oxidative stress plays a role in arecoline-mediated cell death, gene regulation, and inflammatory procedures in human keratinocytes [34].

CYP systems are considered to contribute to detoxification of arecoline and the AN during phase I metabolism [37]. A metabolic map of arecoline in mice revealed that CYP or a flavin-containing monooxygenase might create 3 forms of *N*-oxide metabolites or arecoline [38]. Although the CYP26B1 splice variant lacks exon 2 in the coding region, it still has the ability to downgrade at-RA [39]. A previous study indicated that full-length CYP26B1 plays a crucial role in the catabolism of at-RA and regulation signaling [40], whereas the splice variant of CYP26B1 exerts slight or no influence on at-RA regulation [39].

The expression levels of CYP26B1 and its splice variant were examined according to both mRNA and protein levels in HGF-1 and Ca9-22 cells, which represented normal and cancerous oral cells. We observed that arecoline can induce

expression of both forms of CYP26B1 and that this induction rate is greater for full-length CYP26B1 in cancer cells (i.e., Ca9-22). The expression of full-length CYP26B1 was higher than that of the splice variant of CYP26B1 in HGF-1 and Ca9-22 cells treated with arecoline. Our arecoline cell toxicity data obtained from the MTT assay indicated that, when the quantity of CYP26B1 is higher, Ca9-22 cells are more susceptible to arecoline. This *in vitro* observation revealed that the expression of full-length CYP26B1 plays a greater role than does that of the CYP26B1 splice variant and is consistent with a previous report [39]. Using paired human oral cancer tissues with long-term chewing habits, we confirmed that the expression of the CYP26B1 splice variant was consistently higher in oral cancerous tissues than in adjacent noncancerous tissues. Expression of the CYP26B1 splice variant was 2-fold higher in 6 of 8 cancer tissues (75%) than in adjacent noncancerous tissues. Our results indicated that the protein expression of cases 136, 144, 154, 166, 169, and 176 was more than 2-fold (the greatest fold change was 24.7), and their stages were late (stage III or stage IV).

Arecoline, which is known to exert adverse effects, is correlated with BQ exposure [41] and can produce cytotoxicity, possibly causing the monooxygenase enzyme system (such as CYP26B1) to continue the oxidative metabolism of arecoline. The 6-ring structure of at-RA, which is metabolized by CYP26B1, is similar to that of arecoline. The mechanism through which CYP26B1 metabolizes arecoline remains unknown. We speculate that CYP26B1 plays a role in arecoline catalysis during phase I metabolism. Arecoline can stimulate the high expression of CYP26B1 or cellular at-RA, causing cancer cells to carry on the apoptosis pathway and to maintain balance and survival, resulting in CYP26B1 overexpression. However, the physiologic importance of the increased induction rate and quantity of CYP26B1 by arecoline, accompanied by ROS generation in oral cancer cells, requires further investigation.

A limitation of this study was the relatively small sample size. Because this research was more difficult to get paired tissue specimen, we suggested that the future research needs a larger number of samples to confirm expression of a splice variant of CYP26B1 in betel quid-related oral cancer.

5. Conclusion

We observed an association between a splice variant of CYP26B1 and BQ-related oral cancer, thus providing insight into the molecular mechanism of full-length CYP26B1 and a splice variant of CYP26B1 as well as their joint effects in the development of BQ-related oral cancer. This research may provide a valuable contribution into the importance of screening tests for the chemoprevention strategies and effective treatments for BQ-related oral cancers.

Conflict of Interests

The authors declare no conflict of interests regarding the publication of this paper.

Authors' Contribution

Hurng-Wern Huang and Bin Huang made equal contributions to this work.

Acknowledgments

This study was supported by a Grant from the Ministry of Science and Technology (NSC Grants NSC 102–2314-B-037-073-), a Grant from the Health and Welfare Surcharge of Tobacco Products, the Ministry of Health and Welfare, Taiwan (MOHW103-TD-B-111-05), and Grants from the Chi-Mei Medical Center and Kaohsiung Medical University Research Foundation (100CM-KMU-13 and 101CM-KMU-12).

References

[1] B. J. Boucher and N. Mannan, "Metabolic effects of the consumption of Areca catechu," *Addiction Biology*, vol. 7, no. 1, pp. 103–110, 2002.

[2] A. R. Winstock, C. R. Trivedy, K. A. A. S. Warnakulasuriya, and T. J. Peters, "A dependency syndrome related to areca nut use: some medical and psychological aspects among areca nut users in the Gujarat community in the UK," *Addiction Biology*, vol. 5, no. 2, pp. 173–179, 2000.

[3] *IARC Betel-Quid and Areca-Nut Chewing and Some Areca-Nut-Derived Nitrosamines*, vol. 85 of *IARC Monogr Eval Carcinog Risks Hum*, 2004.

[4] C.-H. Lee, Y.-C. Ko, H.-L. Huang et al., "The precancer risk of betel quid chewing, tobacco use and alcohol consumption in oral leukoplakia and oral submucous fibrosis in southern Taiwan," *British Journal of Cancer*, vol. 88, no. 3, pp. 366–372, 2003.

[5] "Betel quid chewing, cigarette smoking and alcohol consumption related to oral cancer in Taiwan," *Journal of Oral Pathology and Medicine*, vol. 24, no. 10, pp. 450–453, 1995.

[6] K. W. Lee, W. R. Kuo, S. M. Tsai et al., "Different impact from betel quid, alcohol and cigarette: risk factors for pharyngeal and laryngeal cancer," *International Journal of Cancer*, vol. 117, no. 5, pp. 831–836, 2005.

[7] P. H. Chen, K. W. Lee, C. H. Chen et al., "CYP26B1 is a novel candidate gene for betel quid-related oral squamous cell carcinoma," *Oral Oncology*, vol. 47, no. 7, pp. 594–600, 2011.

[8] Y. C. Ko, T. A. Chiang, S. J. Chang, and S. F. Hsieh, "Prevalence of betel quid chewing habit in Taiwan and related sociodemographic factors," *Journal of Oral Pathology and Medicine*, vol. 21, no. 6, pp. 261–264, 1992.

[9] C. Lee, A. M. Ko, S. Warnakulasuriya et al., "Intercountry prevalences and practices of betel-quid use in south, southeast and eastern asia regions and associated oral preneoplastic disorders: an international collaborative study by asian betel-quid consortium of south and east Asia," *International Journal of Cancer*, vol. 129, no. 7, pp. 1741–1751, 2011.

[10] "Cancer registration system annual report," Department of Health, 2010.

[11] P. C. Gupta and C. S. Ray, "Epidemiology of betel quid usage," *Annals of the Academy of Medicine Singapore*, vol. 33, no. 4, supplement, pp. 31–36, 2004.

[12] P. Chen, C. Tsai, Y. Lin et al., "Ingredients contribute to variation in production of reactive oxygen species by areca quid," *Journal*

of Toxicology and Environmental Health A, vol. 69, no. 11, pp. 1055–1069, 2006.

[13] W. T. Ji, C. I. Lee, J. Y. Chen, Y. Cheng, S. Yang, and H. Chen, "Areca nut extract induces pyknotic necrosis in serum-starved oral cells via increasing reactive oxygen species and inhibiting GSK3β: an implication for cytopathic effects in betel quid chewers," *PLoS ONE*, vol. 8, no. 5, Article ID e63295, 2013.

[14] B. J. Dave, A. H. Trivedi, and S. G. Adhvaryu, "*In vitro* genotoxic effects of areca nut extract and arecoline," *Journal of Cancer Research and Clinical Oncology*, vol. 118, no. 4, pp. 283–288, 1992.

[15] S. Deb and A. Chatterjee, "Influence of buthionine sulfoximine and reduced glutathione on arecoline-induced chromosomal damage and sister chromatid exchange in mouse bone marrow cells in vivo," *Mutagenesis*, vol. 13, no. 3, pp. 243–248, 1998.

[16] L. P. Shirname, M. M. Menon, and S. V. Bhide, "Mutagenicity of betel quid and its ingredients using mammalian test systems," *Carcinogenesis*, vol. 5, no. 4, pp. 501–503, 1984.

[17] S. K. Tseng, M. C. Chang, C. Y. Su et al., "Arecoline induced cell cycle arrest, apoptosis, and cytotoxicity to human endothelial cells," *Clinical Oral Investigations*, vol. 16, no. 4, pp. 1267–1273, 2012.

[18] T. C. Hung, L. W. Huang, S. J. Su et al., "Hemeoxygenase-1 expression in response to arecoline-induced oxidative stress in human umbilical vein endothelial cells," *International Journal of Cardiology*, vol. 151, no. 2, pp. 187–194, 2011.

[19] T. Liu, C. Chen, and C. Chi, "Oxidative damage to DNA induced by areca nut extract," *Mutation Research*, vol. 367, no. 1, pp. 25–31, 1996.

[20] C. Y. Wang, T. T. Yang, C. L. Chen, W. C. Lin, and C. F. Lin, "Reactive oxygen species-regulated glycogen synthase kinase-3beta activation contributes to all-trans retinoic acid-induced apoptosis in granulocyte-differentiated HL60 cells," *Biochemical Pharmacology*, vol. 88, no. 1, pp. 86–94, 2014.

[21] M. L. C. da Frota Jr., E. G. da Silva, G. A. Behr et al., "All-trans retinoic acid induces free radical generation and modulate antioxidant enzyme activities in rat sertoli cells," *Molecular and Cellular Biochemistry*, vol. 285, no. 1-2, pp. 173–179, 2006.

[22] N. Hail Jr., H. J. Kim, and R. Lotan, "Mechanisms of fenretinide-induced apoptosis," *Apoptosis*, vol. 11, no. 10, pp. 1677–1694, 2006.

[23] J. S. Bertram, "Inhibition of chemically induced neoplastic transformation by carotenoids: Mechanistic studies," *Annals of the New York Academy of Sciences*, vol. 686, pp. 161–175, 1993.

[24] C.-L. Chang, E. Hong, P. Lao-Sirieix, and R. C. Fitzgerald, "A novel role for the retinoic acid-catabolizing enzyme CYP26A1 in Barrett's associated adenocarcinoma," *Oncogene*, vol. 27, no. 21, pp. 2951–2960, 2008.

[25] S. Graham, "Epidemiology of retinoids and cancer," *Journal of the National Cancer Institute*, vol. 73, no. 6, pp. 1423–1428, 1984.

[26] E. Sonneveld and P. T. van der Saag, "Metabolism of retinoic acid: Implications for development and cancer," *International Journal for Vitamin and Nutrition Research*, vol. 68, no. 6, pp. 404–410, 1998.

[27] H. F. Stich, A. P. Hornby, B. Mathew, R. Sankaranarayanan, and M. K. Nair, "Response of oral leukoplakias to the administration of vitamin A," *Cancer Letters*, vol. 40, no. 1, pp. 93–101, 1988.

[28] S. S. Chiang, S. S. Jiang, Y. J. Wang et al., "Characterization of erecoline-induced effects on cytotoxicity in normal human gingival fibroblasts by global gene expression profiling," *Toxicological Sciences*, vol. 100, no. 1, pp. 66–74, 2007.

[29] S. Chiang, P. Chen, C. Lee et al., "Up-regulation of inflammatory signalings by areca nut extract and role of Cyclooxygenase-2 -1195G>a polymorphism reveal risk of oral cancer," *Cancer Research*, vol. 68, no. 20, pp. 8489–8498, 2008.

[30] C. Chiu, J. Haung, F. Chang et al., "Golden berry-derived 4β-hydroxywithanolide E for selectively killing oral cancer cells by generating ROS, DNA damage, and apoptotic pathways," *PLoS ONE*, vol. 8, no. 5, Article ID e64739, 2013.

[31] G. T. Brown, B. G. Cash, D. Blihoghe et al., "The expression and prognostic significance of retinoic acid metabolising enzymes in colorectal cancer," *PloS ONE*, vol. 9, no. 3, Article ID e90776, 2014.

[32] R. Dasgupta, I. Saha, S. Pal et al., "Immunosuppression, hepatotoxicity and depression of antioxidant status by arecoline in albino mice," *Toxicology*, vol. 227, no. 1-2, pp. 94–104, 2006.

[33] Y. S. Tsai, K. W. Lee, J. L. Huang et al., "Arecoline, a major alkaloid of areca nut, inhibits p53, represses DNA repair, and triggers DNA damage response in human epithelial cells," *Toxicology*, vol. 249, no. 2-3, pp. 230–237, 2008.

[34] G. S. Thangjam and P. Kondaiah, "Regulation of oxidative-stress responsive genes by arecoline in human keratinocytes," *Journal of Periodontal Research*, vol. 44, no. 5, pp. 673–682, 2009.

[35] H.-J. Hsu, K.-L. Chang, Y.-H. Yang, and T.-Y. Shieh, "The effects of arecoline on the release of cytokines using cultured peripheral blood mononuclear cells from patients with oral mucous diseases," *The Kaohsiung Journal of Medical Sciences*, vol. 17, no. 4, pp. 175–182, 2001.

[36] J. Jeng, Y. Wang, B. Chiang et al., "Roles of keratinocyte inflammation in oral cancer: regulating the prostaglandin E2, interleukin-6 and TNF-α production of oral epithelial cells by areca nut extract and arecoline," *Carcinogenesis*, vol. 24, no. 8, pp. 1301–1315, 2003.

[37] T. A. Patterson and J. W. Kosh, "Elucidation of the rapid in vivo metabolism of arecoline," *General Pharmacology*, vol. 24, no. 3, pp. 641–647, 1993.

[38] S. Giri, J. R. Idle, C. Chen, T. M. Zabriskie, K. W. Krausz, and F. J. Gonzalez, "A metabolomic approach to the metabolism of the areca nut alkaloids arecoline and arecaidine in the mouse," *Chemical Research in Toxicology*, vol. 19, no. 6, pp. 818–827, 2006.

[39] A. A. Elmabsout, A. Kumawat, P. Saenz-Méndez et al., "Cloning and functional studies of a splice variant of CYP26B1 expressed in vascular cells," *PLoS ONE*, vol. 7, no. 5, Article ID e36839, 2012.

[40] P. A. Ocaya, A. A. Elmabsout, P. S. Olofsson, H. Törmä, A. C. Gidlöf, and A. Sirsjö, "CYP26B1 plays a major role in the regulation of all-*trans*-retinoic acid metabolism and signaling in human aortic smooth muscle cells," *Journal of Vascular Research*, vol. 48, no. 1, pp. 23–30, 2011.

[41] I. C. Wu, P. H. Chen, C. J. Wang et al., "Quantification of blood betel quid alkaloids and urinary 8-hydroxydeoxyguanosine in humans and their association with betel chewing habits," *Journal of Analytical Toxicology*, vol. 34, no. 6, pp. 325–331, 2010.

Hindawi Publishing Corporation
The Scientific World Journal
Volume 2014, Article ID 217525, 7 pages
http://dx.doi.org/10.1155/2014/217525

Research Article

A Chinese Herbal Medicine, Jia-Wei-Xiao-Yao-San, Prevents Dimethylnitrosamine-Induced Hepatic Fibrosis in Rats

Shu-Chen Chien,[1,2] Wei-Chiao Chang,[1,3,4,5,6] Pu-Hua Lin,[7] Wei-Pin Chang,[8] Shih-Chung Hsu,[9] Jung-Chen Chang,[10] Ya-Chieh Wu,[11] Jin-Kuo Pei,[12] and Chia-Hsien Lin[12]

[1] *Department of Clinical Pharmacy, School of Pharmacy, Taipei Medical University, No. 250, Wuxing Street, Xinyi District, Taipei 110, Taiwan*
[2] *Department of Pharmacy, Taipei Medical University Hospital, No. 252, Wuxing Street, Xinyi District, Taipei 110, Taiwan*
[3] *Department of Pharmacy, Taipei Medical University-Wan Fang Hospital, No. 111, Section 3, Xinglong Road, Wenshan District, Taipei 116, Taiwan*
[4] *Master Program for Clinical Pharmacogenomics and Pharmacoproteomics, School of Pharmacy, Taipei Medical University, No. 250, Wuxing Street, Xinyi District, Taipei 110, Taiwan*
[5] *Graduate Institute of Clinical Medicine, College of Medicine, Kaohsiung Medical University, No. 100, Shiquan 1st Road, Sanmin District, Kaohsiung 807, Taiwan*
[6] *Cancer Center, Kaohsiung Medical University Hospital, No. 100, Tzyou 1st Road, Kaohsiung 807, Taiwan*
[7] *Food and Drug Administration, Ministry of Health and Welfare, No. 161-2, Kunyang Street, Nangang District, Taipei 115, Taiwan*
[8] *Department of Healthcare Management, Yuanpei University, No. 306, Yuanpei Street, Hsinchu 300, Taiwan*
[9] *Department of Early Childhood Care and Education, Kang-Ning Junior College of Medical Care and Management, No. 137, Lane 75, Section 3, Kangning Road, Neihu District, Taipei 114, Taiwan*
[10] *Department of Nursing, School of Medicine, National Taiwan University, No. 1, Section 1, Jen Ai Road, Zhongzheng District, Taipei 100, Taiwan*
[11] *Department of Nursing, Ching-Kuo Institute of Management and Health, No. 336, Fu-Hsing Road, Zhongshan District, Keelung 203, Taiwan*
[12] *Department of Health Industry Management, School of Health Care Management, Kainan University, No. 1, Kainan Road, Luzhu Shiang, Taoyuan 338, Taiwan*

Correspondence should be addressed to Chia-Hsien Lin; g870615@gmail.com

Received 7 April 2014; Revised 12 May 2014; Accepted 12 May 2014; Published 3 June 2014

Academic Editor: Li-Yeh Chuang

Jia-wei-xiao-yao-san (JWXYS) is a traditional Chinese herbal medicine that is widely used to treat neuropsychological disorders. Only a few of the hepatoprotective effects of JWXYS have been studied. The aim of this study was to investigate the hepatoprotective effects of JWXYS on dimethylnitrosamine- (DMN-) induced chronic hepatitis and hepatic fibrosis in rats and to clarify the mechanism through which JWXYS exerts these effects. After the rats were treated with DMN for 3 weeks, serum glutamic oxaloacetic transaminase (SGOT) and serum glutamic pyruvic transaminase (SGPT) levels were significantly elevated, whereas the albumin level decreased. Although DMN was continually administered, after the 3 doses of JWXYS were orally administered, the SGOT and SGPT levels significantly decreased and the albumin level was significantly elevated. In addition, JWXYS treatment prevented liver fibrosis induced by DMN. JWXYS exhibited superoxide-dismutase-like activity and dose-dependently inhibited DMN-induced lipid peroxidation and xanthine oxidase activity in the liver of rats. Our findings suggest that JWXYS exerts antifibrotic effects against DMN-induced chronic hepatic injury. The possible mechanism is at least partially attributable to the ability of JWXYS to inhibit reactive-oxygen-species-induced membrane lipid peroxidation.

1. Introduction

The benefits of Chinese herbal medicines in treating chronic diseases, including chronic liver disease, have recently attracted the attention of Western practitioners. Jia-wei-xiao-yao-san (Kami-shoyo-san; TJ-24, JWXYS) is a traditional complex Chinese herbal medicine consisting of 10 medicinal herbal preparations. JWXYS is an officially approved prescription drug in China and Taiwan. Although some reports have addressed the neuropsychological activities of JWXYS, its hepatoprotective effects have not been adequately clarified [1, 2]. The aim of this study was to investigate the hepatoprotective effects of JWXYS and to evaluate the mechanism through which JWXYS exerts these effects.

To investigate the hepatoprotective effect of JWXYS, chronic liver injury was induced by dimethylnitrosamine (DMN) [3–6]. Studies have reported that DMN can induce lipid peroxidation in the liver, thereby reducing hepatic tissue blood flow and leading to acute liver damage and even fulminant hepatitis [7, 8].

In the present study, we examined the hepatoprotective effect of JWXYS by determining the levels of serum glutamic oxaloacetic transaminase (SGOT), serum glutamic pyruvic transaminase (SGPT), albumin in the serum, and histopathological changes in rat hepatic tissues. The antioxidative effects of JWXYS on liver tissues and the superoxide-dismutase-(SOD-) like activity of JWXYS were evaluated to determine the possible mechanism.

2. Methods

2.1. Drugs and Chemicals. JWXYS (Kami-shoyo-san; TJ-24) was provided by Koda Pharmaceutical (Taoyuan, Taiwan). It consists of 10 medicinal herb preparations, namely, *Angelica sinensis* radix (3.0 g), *Bupleurum falcatum* radix (3.0 g), *Paeonia albiflora* (3.0 g), glycyrrhizae radix (2.0 g), *Moutan Radicis* cortex (2.0 g), *Gardenia fructus* (2.0 g), *Zingiber officinale* rhizome (1.0 g), *Atractylodis macrocephalae* rhizome (3.0 g), *Poria cocos* (3.0 g), and *Mentha arvensis* (1.0 g). JWXYS was dissolved in 0.9% NaCl at concentrations of 100, 300, and 1000 mg/2 mL before use.

DMN and silymarin were purchased from Sigma (St. Louis, MO, USA). Before use, DMN was dissolved in 0.9% NaCl at a concentration of 1%, and silymarin was dissolved in 1% carboxymethylcellulose at a concentration of 200 mg/2 mL.

2.2. Animals. Male Wistar rats (110–130 g; BioLasco Taiwan, Taiwan) were used. The Institutional Review Board at China Medical University (Taichung, Taiwan) reviewed and approved the study protocols. The animals were allowed to acclimate for at least 7 days on a standard laboratory diet (Fu-So, Taipei, Taiwan) under environmentally controlled conditions ($25 \pm 1^{\circ}$C and $55\% \pm 5\%$ humidity) with free access to food and tap water. A 12 h light/dark cycle was maintained, and hardwood chips were used as bedding.

In this study, 60 rats weighing 160–240 g were randomly divided into 6 groups: control (normal saline-treated), DMN-treated, DMN-treated + silymarin (200 mg/kg), and DMN-treated + JWXYS (100, 300, and 1000 mg/kg) groups.

2.3. Dimethylnitrosamine-Induced Liver Injury and Treatments. Dimethylnitrosamine (DMN) can induce hepatic sinusoidal endothelial injury and coagulation necrosis primarily in the central and periportal regions of the lobule [9, 10]. It is usually used to induce experimental liver fibrosis [4]. In our study, DMN was dissolved in normal saline and then intraperitoneally (i.p.) administered to rats 3 times per week at doses of 10 mg/mL/kg. After 3 weeks of inducing liver damage, DMN was continually i.p. administered to the 5 experimental groups, but not to the normal saline control group (1 mL/kg), for the following 3 weeks. From the beginning of the subsequent 3-week period, JWXYS (100, 300, and 1000 mg/2 mL/kg) was orally administered 3 times per day on 3 days in each week to 3 experimental groups. Before the rats were sacrificed, they were starved for 24 h after the final oral administration of JWXYS. Silymarin (200 mg/2 mL/kg) was orally administered to the silymarin group 3 times per day for 3 weeks.

2.4. Serum Biochemical and Pathological Evaluation. The protective effect of JWXYS against DMN-induced liver injury was evaluated by assessing the SGOT, SGPT, and serum albumin levels and by examining histopathological sections of the liver of all experimental animals [7].

2.5. Antioxidative Effect of Jia-Wei-Xiao-Yao-San. A study reported that (+)-alpha-tocopherol (vitamin E) can scavenge DMN-induced superoxide-free radical production [11]. Therefore, vitamin E was used as a positive control in this study.

To compare the antioxidative effects of JWXYS and vitamin E (0.5 mM) (as a positive control) in rat liver homogenates, $FeCl_2$-induced lipid peroxidation was determined based on the formation of a malonic dialdehyde-(MDA-) thiobarbituric acid (TBA) product according to a modified method described by Yuda et al. [12].

Furthermore, to evaluate the inhibitory activity of JWXYS against DMN-induced lipid peroxidation, MDA-TBA products of JWXYS- (100, 300, and 1000 mg/kg) treated rat livers were measured using the method described by Yuda et al. [12].

2.6. Superoxide-Dismutase-Like Activity Test. To evaluate the superoxide-scavenging activity of JWXYS, a cytochrome C reduction method developed by McCord and Fridovich was used [13]. Each data point represents the percent of superoxide inhibition (SI, %), and each assay was conducted in triplicate. Xanthine oxidase (XOD) converts xanthine to uric acid, yielding superoxide anions as a byproduct and subsequently converting ferricytochrome C directly to ferrocytochrome C, which exhibits absorbance at 550 nm. When a compound exhibits superoxide-scavenging activity, a reduction in ferricytochrome C occurs. Inhibition of XOD can reduce the production of superoxide anions, and XOD inhibition was measured according to the method described by Frederiks and Bosch [14].

Table 1: Effects of JWXYS and silymarin on the body weights of rats with DMN-induced chronic liver injury.

Group		Time after DMN treatment (day)			
		0	14	28	42
A	Normal control	148.0 ± 12.2	214.0 ± 13.3	282.0 ± 33.9	348.8 ± 35.5
B	DMN (10 mg/kg)	143.7 ± 23.3	190.7 ± 19.3	225.7 ± 10.5	265.7 ± 11.0*
C	DMN (10 mg/kg) + silymarin (200 mg/kg)	145.0 ± 20.0	193.2 ± 16.8	273.2 ± 22.0	325.2 ± 28.7
D	DMN (10 mg/kg) + JWXYS (100 mg/kg)	144.7 ± 17.3	190.7 ± 16.9	272.7 ± 16.3	324.8 ± 16.2
E	DMN (10 mg/kg) + JWXYS (300 mg/kg)	145.0 ± 16.9	190.2 ± 16.9	273.0 ± 16.4	325.6 ± 17.2
F	DMN (10 mg/kg) + JWXYS (1000 mg/kg)	145.0 ± 20.0	195.2 ± 16.9	277.0 ± 17.2	331.8 ± 18.2#

Each value is presented as the mean ± SE ($n = 10$).
*$P < 0.05$, significantly different from Group A.
#$P < 0.05$, significantly different from Group B.

2.7. Statistical Analysis. Statistical significance was calculated by conducting a one-way analysis of variance coupled with Dunnett's test. P values less than 0.05 indicated statistical significance.

3. Results

3.1. Body Weight. As shown in Table 1, after treatment with DMN for 42 days, the body weights of rats significantly decreased ($P < 0.05$). By contrast, the body weights of the rats significantly increased ($P < 0.05$) after they were treated with JWXYS (1000 mg/kg) in the second 3-week period compared with those of the group treated with only DMN.

3.2. Histological Observations. Histological observations confirmed the hepatoprotective effect of JWXYS. Figure 1(a) shows a normal control rat liver, in which no necrosis or inflammation was observed. By contrast, the liver of rats treated with 10 mg/kg of DMN exhibited marked widening, inflammation, and a fibrotic portal area, with irregular borders forming a spiked appearance and portal-bridging fibrosis. Nodular transformation was apparent (Figure 1(b)). In the liver of silymarin- (200 mg/kg) treated rats, only moderate widening and a fibrotic portal area with bridging fibrosis were observed (Figure 1(c)).

The protective effect of JWXYS (100, 300, and 1000 mg/kg) against DMN-induced chronic liver injury was determined by examining histological changes in rat livers. The livers of the rats in the JWXYS (100 mg/kg) group exhibited moderate widening and a fibrotic portal area with bridging and mild inflammatory cell infiltration, which were also observed in the silymarin- (200 mg/kg) treated group (Figure 1(d)). By contrast, in the livers of rats treated with 300 and 1000 mg/kg of JWXYS, only mild focal fibrotic changes of the portal area and mild bridging were noted (Figures 1(e) and 1(f)). Thus, histological improvements in the livers of rats treated with 300 and 1000 mg/kg of JWXYS were obviously more substantial than those in the livers of rats treated with 100 mg/kg of JWXYS or 200 mg/kg of silymarin.

3.3. Serum Biochemical Assay. As shown in Table 2, the SGOT and SGPT levels of the experimental groups were significantly elevated, whereas the albumin level decreased after DMN treatment compared with those of the normal control group. The results indicated that DMN can induce chronic active hepatitis and diffuse liver injury.

By contrast, treatment with JWXYS (100, 300, and 1000 mg/2 mL/kg) or silymarin (200 mg/2 mL/kg) during the second 3-week period significantly prevented further DMN-induced elevations in serum GOT and GPT levels and a further decrease in the serum albumin level (Table 2). According to these results, JWXYS exhibited strong hepatoprotective effects against DMN-induced chronic hepatic injury in rats. The hepatoprotective ability of 300 and 1000 mg/kg of JWXYS was greater than that of silymarin alone.

3.4. $FeCl_2$-Stimulated Lipid Peroxidation In Vitro. Although JWXYS (10 mg/kg) significantly inhibited 51.71% of $FeCl_2$-stimulated lipid peroxidation *in vitro*, 0.5 mM vitamin E inhibited 71.10% of $FeCl_2$-stimulated lipid peroxidation. JWXYS (0.1, 1.0, and 10 mg/kg) significantly and dose-dependently inhibited $FeCl_2$-stimulated lipid peroxidation *in vitro*. Nevertheless, we proved that JWXYS (100, 300, and 1000 mg/kg) dose-dependently inhibited DMN-induced lipid peroxidation in rat livers (*in vivo*). No significant difference was observed between treatments with 1000 mg/kg of JWXYS (69.00%) and 0.69 mM vitamin E (71.16%) (Table 3).

3.5. Superoxide-Dismutase-Like Activity. The SOD-like activity (SI%) of JWXYS (0.01, 0.1, and 1.0 mg/mL) was examined to clarify the superoxide-scavenging ability. The activity of vitamin E (8 mg/kg) was set to 100% of SOD-like activity. The results indicated that the SOD-like activity levels of JWXYS at 0.01, 0.1, and 1.0 mg/mL were 33.77%, 68.83%, and 94.81%, respectively. JWXYS at 1.0 mg/mL exhibited the strongest superoxide-scavenging activity (94.81%) (Table 4).

XOD converts xanthine to uric acid, thus yielding superoxide anions as a byproduct [15]. Therefore, inhibition of XOD can reduce the production of superoxide anions. As shown in Table 4, the levels of XOD inhibition (SI%) induced by JWXYS at 0.01, 0.1, and 1.0 mg/mL were 11.90%, 14.29%, and 83.33%, respectively. These results showed that JWXYS dose-dependently inhibited XOD activity.

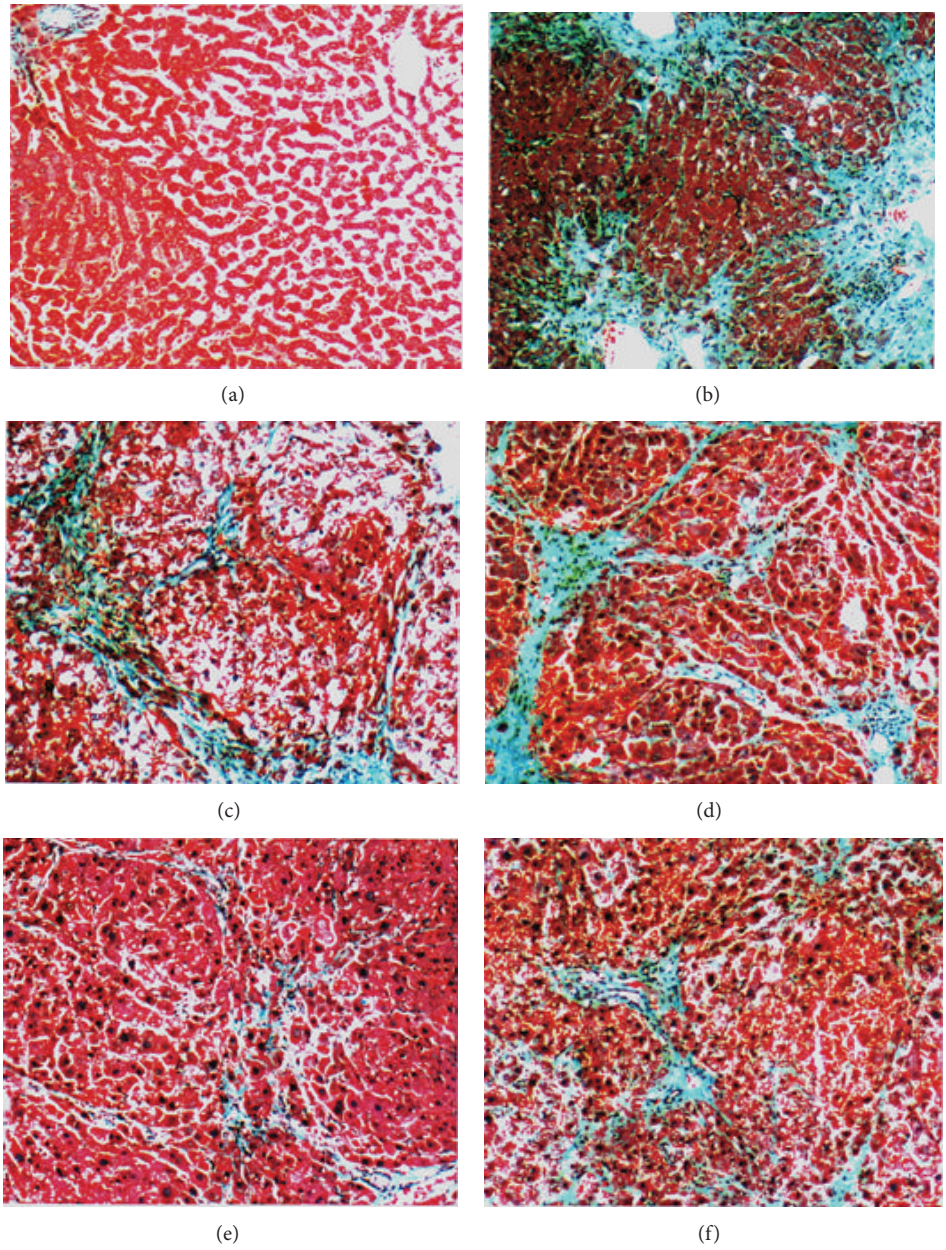

Figure 1: Histological examination performed by conducting Masson trichrome staining, 100x of JWXYS-treated and untreated rat liver. (a) vehicle, normal saline; control, normal liver; (b) DMN alone with marked widening, inflammation, and fibrotic portal tracts with bridging fibrosis. Nodular transformation was apparent. (c) DMN + 200 mg/kg of silymarin with moderate widening and fibrotic portal tracts with occasional bridging fibrosis; (d) DMN + 100 mg/kg of JWXYS with moderate widening and fibrotic portal tracts with bridging fibrosis and mild inflammatory cell infiltration; (e) DMN + 300 mg/kg of JWXYS with focal mild fibrotic change of the portal tracts and bridging fibrosis; (f) DMN + 1000 mg/kg of JWXYS with mild to moderate fibrotic portal tracts with bridging fibrosis.

4. Discussion

Chronic hepatitis B, hepatitis C, and alcoholism are the major risk factors for developing liver cirrhosis and hepatocellular carcinoma. The pathway for the progression to liver cirrhosis is the fibrotic process in the liver of patients with the aforementioned risk factors [16, 17]. Therefore, antifibrotic therapy for chronic hepatitis is a crucial topic. A previous study revealed that the combination of interferon and ribavirin exerted an antifibrotic effect in treating chronic hepatitis C. However, the effect was limited, and concerns have been raised regarding the costs and side effects [18–20]. Studies have suggested that alternative agents such as silymarin, sho-saiko-to, halofuginone, imatinib mesylate, phosphodiesterase inhibitors, and endothelin-A-receptor and angiotensin antagonists have antifibrotic effects in chronic hepatitis [20, 21].

Shimizu et al. reported that the traditional Chinese herbal medicine sho-saiko-to (as it is called in Japanese), which

Table 2: Effects of JWXYS on the SGOT, SGPT, and albumin levels in rats with DMN-induced chronic liver injury.

Group		SGOT (IU/L)	SGPT (IU/L)	Albumin (g/dL)
A	Normal control	105.3 ± 13.9	24.2 ± 3.3	4.45 ± 0.02
B	DMN (10 mg/kg)	320.1 ± 42.3$^{\#\#}$	80.3 ± 11.8$^{\#\#}$	3.24 ± 0.04$^{\#}$
C	DMN (10 mg/kg) + silymarin (200 mg/kg)	200.4 ± 17.6**	66.7 ± 11.1**	3.87 ± 0.14**
D	DMN (10 mg/kg) + JWXYS (100 mg/kg)	211.3 ± 15.6**	70.1 ± 7.6*	3.76 ± 0.15
E	DMN (10 mg/kg) + JWXYS (300 mg/kg)	193.6 ± 11.8**	63.3 ± 7.3**	3.86 ± 0.16**
F	DMN (10 mg/kg) + JWXYS (1000 mg/kg)	168.3 ± 9.9**	47.3 ± 6.8**	3.96 ± 0.18**

Values are presented as the mean ± SE ($n = 10$).
$^{\#,\#\#}P < 0.05$ and 0.01, significantly different from Group A.
$^{*,**}P < 0.05$ and 0.01, significantly different from Group B.
One-way analysis of variance coupled with Dunnett's test.
P values < 0.05 indicated significance.

Table 3: Inhibitory effects of various doses of JWXYS on $FeCl_2$-induced (*in vitro*) and DMN-induced (*in vivo*) lipid peroxidation in rat livers.

Group		MDA (nmole/mg protein)	Inhibition rate (%)
A	Normal control	1.69 ± 0.11	
	In vitro		
B	$FeCl_2$	2.63 ± 0.08**	
C	$FeCl_2$ + vitamin E (0.5 mM)	0.76 ± 0.05$^{\#\#}$	71.10
D	$FeCl_2$ + JWXYS (0.1 mg/kg)	2.10 ± 0.05$^{\#\#}$	20.15
E	$FeCl_2$ + JWXYS (1.0 mg/kg)	1.44 ± 0.06$^{\#\#}$	45.25
F	$FeCl_2$ + JWXYS (10 mg/kg)	1.27 ± 0.03$^{\#\#\#}$	51.71
	In vivo		
G	DMN	3.71 ± 0.05**	
H	DMN + vitamin E (0.69 mM)	1.07 ± 0.05$^{\triangle\triangle\triangle}$	71.16
I	DMN + JWXYS (100 mg/kg)	2.79 ± 0.05$^{\triangle\triangle}$	24.80
J	DMN + JWXYS (300 mg/kg)	2.21 ± 0.06$^{\triangle\triangle}$	40.43
K	DMN + JWXYS (1000 mg/kg)	1.15 ± 0.03$^{\triangle\triangle\triangle}$	69.00

Each value is presented as the mean ± SE ($n = 6$). Vitamin E was used as the positive control.
$^{**}P < 0.01$, significantly different from Group A.
$^{\#\#,\#\#\#}P < 0.01$ and 0.001, significantly different from Group B.
$^{\triangle\triangle,\triangle\triangle\triangle}P < 0.01$ and 0.001, significantly different from Group G.
One-way analysis of variance coupled with Dunnett's test.
P values < 0.05 indicated significance.

Table 4: Effects of JWXYS on SOD-like activity and XOD inhibition.

Group		SOD-like activity (SI%)*	XOD inhibition (SI%)$^{\#}$
A	Vitamin E (8 mg/kg)	100.00	
B	JWXYS (0.01 mg/mL)	33.77	11.90
C	JWXYS (0.1 mg/mL)	68.83	14.29
D	JWXYS (1.0 mg/mL)	94.81	83.33

*Measured using the cytochrome C reduction test.
$^{\#}$Measured using the XOD inhibition test.
Vitamin E was used as the positive control.
SI: superoxide inhibition.

features effects similar to those of silibinin, exhibited radical-scavenging ability and antifibrotic properties in activated hepatic stellate cells *in vitro* and in porcine serum-induced fibrosis *in vivo* [22]. Like sho-saiko-to, JWXYS is an option for treating patients with chronic hepatitis in China and other Asian countries.

As shown in Table 1, JWXYS eliminated the effect of DMN-induced body weight loss in rats. In addition, we observed that JWXYS treatment inhibited DMN-induced hepatic injury and fibrosis in a dose-dependent manner. The effects of JWXYS were stronger than that of silymarin (Figures 1(e) and 1(f)). As shown in Table 2, JWXYS significantly diminished the DMN-induced hepatitis and severe diffuse liver injury, thereby disrupting the sequence of events leading to liver fibrosis.

Recent research has indicated that chronic liver injury and hepatic fibrosis are related to oxidative stress, including that caused by reactive oxygen species (ROS) and lipid peroxidation [23, 24]. Studies have suggested that antioxidants such as SOD, catalase, and estradiol significantly prevent lipid peroxidation and exacerbation of liver fibrosis [25–27]. Indeed, as shown in Table 4, JWXYS inhibited XOD activity in a dose-dependent manner. XOD converts xanthine to uric acid, yielding superoxide anions as a byproduct [15], and the inhibition of XOD can substantially reduce the production of superoxide anions, thus reducing superoxide-induced lipid peroxidation and subsequent liver fibrosis.

Furthermore, our study revealed that the Chinese herbal medicine, JWXYS, significantly inhibited $FeCl_2$-stimulated (*in vitro*) and DMN-induced (*in vitro*) lipid peroxidation in a dose-dependent manner (Table 3). In the cytochrome C test, we confirmed that JWXYS exhibits a dose-dependent antioxidative activity (Table 4). Furthermore, in another experiment we performed, JWXYS exhibited no hepatotoxic effect in Wistar rats even at a dose of 2000 mg/kg orally administered for 6 weeks (data not shown).

Our study has limitations because, to extrapolate conclusions regarding humans from experimental data on rats, the dose must be validated in clinical trials. The mechanism through which JWXYS acts in cellular pathways remains

undetermined. Immunohistochemical analysis of markers such as alpha-smooth muscle actin in activated hepatic stellate cells and sets of *in vitro* culture studies on parenchymal cells and nonparenchymal cells might provide additional evidence supporting the molecular mechanisms through which JWXYS exerts antifibrotic effects. Moreover, in an ongoing follow-up study conducted in our laboratory, JWXYS exhibited strong free-radical-scavenging and antioxidant activity and inhibited free-radical-induced hepatic fibrosis. We will continue to conduct research on this topic.

5. Conclusions

We reported that JWXYS exhibits obvious dose-dependent antifibrotic effects against chronic hepatic injury that are similar to those exhibited by sho-saiko-to. This protective effect was noted even in a condition in which DMN was continually administered. The mechanism may at least partially be due to the inhibitory effect of JWXYS on lipid peroxidation and its superoxide-scavenging activities. We hope that, after additional evidence has been accumulated, JWXYS will be applied as an alternative clinical medication for chronic hepatitis and hepatic antifibrotic therapy because of its efficiency, low cost, and fewer side effects.

Abbreviations

DMN: Dimethylnitrosamine
JWXYS: Jia-wei-xiao-yao-san
MDA: Malonic dialdehyde
SGOT: Serum glutamic oxaloacetic transaminase
SGPT: Serum glutamic pyruvic transaminase
SI: Superoxide inhibition
SOD: Superoxide dismutase
TBA: Thiobarbituric acid
XOD: Xanthine oxidase.

Conflict of Interests

The authors declare that there is no conflict of interests regarding the publication of this paper.

Authors' Contribution

Shu-Chen Chien and Wei-Chiao Chang contributed to this work equally.

Acknowledgment

This work was supported by grants (NSC101-2320-B-424-001) provided by the National Science Council, Taiwan, and Health and welfare surcharge of tobacco products, Taiwan.

References

[1] T. Ishikawa, T. Funahashi, and J. Kudo, "Effectiveness of the Kampo kami-shoyo-san (TJ-24) for tremor of antipsychotic-induced parkinsonism," *Psychiatry & Clinical Neurosciences*, vol. 54, no. 5, pp. 579–582, 2000.

[2] K. Yamada and S. Kanba, "Herbal medicine (Kami-shoyo-san) in the treatment of premenstrual dysphoric disorder," *Journal of Clinical Psychopharmacology*, vol. 22, no. 4, p. 442, 2002.

[3] J.-Y. Chen, H.-L. Chen, J.-C. Cheng et al., "A Chinese herbal medicine, Gexia-Zhuyu Tang (GZT), prevents dimethylnitrosamine-induced liver fibrosis through inhibition of hepatic stellate cells proliferation," *Journal of Ethnopharmacology*, vol. 142, no. 3, pp. 811–818, 2012.

[4] J. Fujimoto, "Gene therapy for liver cirrhosis," *Journal of Gastroenterology & Hepatology*, vol. 15, pp. D33–D36, 2000.

[5] M. Kusunose, B. Qiu, T. Cui et al., "Effect of Sho-saiko-to extract on hepatic inflammation and fibrosis in dimethylnitrosamine induced liver injury rats," *Biological and Pharmaceutical Bulletin*, vol. 25, no. 11, pp. 1417–1421, 2002.

[6] Y. Matsuda, K. Matsumoto, T. Ichida, and T. Nakamura, "Hepatocyte growth factor suppresses the onset of liver cirrhosis and abrogates lethal hepatic dysfunction in rats," *Journal of Biochemistry*, vol. 118, no. 3, pp. 643–649, 1995.

[7] S. C. Lin, C. C. Lin, Y. H. Lin, and C. H. Chen, "Protective and therapeutic effects of ban-zhi-lian on hepatotoxin-induced liver injuries," *American Journal of Chinese Medicine*, vol. 22, no. 1, pp. 29–42, 1994.

[8] A. Suzuki, M. Hagino, N. Yasuda et al., "Inhibitory effects of prostaglandin E1·α-cyclodextrin (PGE1·CD) on dimethylnitrosamine-induced acute liver damage in rats," *Folia Pharmacologica Japonica*, vol. 105, no. 4, pp. 221–229, 1995.

[9] A. M. Jézéquel, R. Mancini, M. L. Rinaldesi, G. Macarri, C. Venturini, and F. Orlandi, "A morphological study of the early stages of hepatic fibrosis induced by low doses of dimethylnitrosamine in the rat," *Journal of Hepatology*, vol. 5, no. 2, pp. 174–181, 1987.

[10] X. Lu, P. Liu, C. Liu et al., "Role of hepatic sinusoidal endothelium injury in hepatic fibrogenesis induced by dimethylnitrosamine in rats," *Zhonghua Gan Zang Bing Za Zhi*, vol. 10, no. 6, pp. 441–444, 2002.

[11] D. Wu and A. I. Cederbaum, "Ethanol cytotoxicity to a transfected HepG2 cell line expressing human cytochrome P4502E1," *Journal of Biological Chemistry*, vol. 271, no. 39, pp. 23914–23919, 1996.

[12] Y. Yuda, J. Tanaka, F. Hirano, K. Igarashi, and T. Satoh, "Participation of lipid peroxidation in rat pertussis vaccine pleurisy. III. Thiobarbituric acid (TBA) reactant and lysosomal enzyme," *Chemical and Pharmaceutical Bulletin*, vol. 39, no. 2, pp. 505–506, 1991.

[13] J. M. McCord and I. Fridovich, "The reduction of cytochrome c by milk xanthine oxidase," *Journal of Biological Chemistry*, vol. 243, no. 21, pp. 5753–5760, 1968.

[14] W. M. Frederiks and K. S. Bosch, "The role of xanthine oxidase in ischemia/reperfusion damage of rat liver," *Histology & Histopathology*, vol. 10, no. 1, pp. 111–116, 1995.

[15] E. C. Viel, K. Benkirane, D. Javeshghani, R. M. Touyz, and E. L. Schiffrin, "Xanthine oxidase and mitochondria contribute to vascular superoxide anion generation in DOCA-salt hypertensive rats," *American Journal of Physiology: Heart and Circulatory Physiology*, vol. 295, no. 1, pp. H281–H288, 2008.

[16] T. Poynard, P. Bedossa, and P. Opolon, "Natural history of liver fibrosis progression in patients with chronic hepatitis C," *The Lancet*, vol. 349, no. 9055, pp. 825–832, 1997.

[17] Y. Wang, M.-Y. Xu, R.-D. Zheng et al., "Prediction of significant fibrosis and cirrhosis in hepatitis B e-antigen negative patients with chronic hepatitis B using routine parameters," *Hepatology Research*, vol. 43, no. 5, pp. 441–451, 2013.

[18] G. S. Baroni, L. D'Ambrosio, P. Curto et al., "Interferon gamma decreases hepatic stellate cell activation and extracellular matrix deposition in rat liver fibrosis," *Hepatology*, vol. 23, no. 5, pp. 1189–1199, 1996.

[19] G. Giannelli, C. Bergamini, F. Marinosci et al., "Antifibrogenic effect of IFN-α2b on hepatic stellate cell activation by human hepatocytes," *Journal of Interferon & Cytokine Research*, vol. 26, no. 5, pp. 301–308, 2006.

[20] D. Schuppan, A. Krebs, M. Bauer, and E. G. Hahn, "Hepatitis C and liver fibrosis," *Cell Death & Differentiation*, vol. 10, no. 1, pp. S59–S67, 2003.

[21] H. Yoshiji, R. Noguchi, S. Kuriyama et al., "Imatinib mesylate (STI-571) attenuates liver fibrosis development in rats," *American Journal of Physiology: Gastrointestinal & Liver Physiology*, vol. 288, no. 5, pp. G907–G913, 2005.

[22] I. Shimizu, Y.-R. Ma, Y. Mizobuchi et al., "Effects of Sho-saiko-to, a Japanese herbal medicine, on hepatic fibrosis in rats," *Hepatology*, vol. 29, no. 1, pp. 149–160, 1999.

[23] P. Bedossa, K. Houglum, C. Trautwein, A. Holstege, and M. Chojkier, "Stimulation of collagen α1(I) gene expression is associated with lipid peroxidation in hepatocellular injury: a link to tissue fibrosis?" *Hepatology*, vol. 19, no. 5, pp. 1262–1271, 1994.

[24] G. Vendemiale, I. Grattagliano, M. L. Caruso et al., "Increased oxidative stress in dimethylnitrosamine-induced liver fibrosis in the rat: effect of N-acetylcysteine and interferon-α," *Toxicology and Applied Pharmacology*, vol. 175, no. 2, pp. 130–139, 2001.

[25] G. Lu, I. Shimizu, X. Cui et al., "Antioxidant and antiapoptotic activities of idoxifene and estradiol in hepatic fibrosis in rats," *Life Sciences*, vol. 74, no. 7, pp. 897–907, 2004.

[26] K. S. Lee, M. Buck, K. Houglum, and M. Chojkier, "Activation of hepatic stellate cells by TGFα and collagen type I is mediated by oxidative stress through c-myb expression," *The Journal of Clinical Investigation*, vol. 96, no. 5, pp. 2461–2468, 1995.

[27] R. H. Shi, T. X. Chen, and X. Z. Lu, "Protective effects of free radical scavengers superoxide dismutase and catalase on experimental liver fibrosis," *Zhonghua Xiaohua Zazhi*, vol. 13, pp. 84–86, 1993.

Hindawi Publishing Corporation
The Scientific World Journal
Volume 2014, Article ID 480387, 8 pages
http://dx.doi.org/10.1155/2014/480387

Research Article

Hydrogen Sulfide Increases Nitric Oxide Production and Subsequent S-Nitrosylation in Endothelial Cells

Ping-Ho Chen,[1] Yaw-Syan Fu,[2] Yun-Ming Wang,[3] Kun-Han Yang,[4] Danny Ling Wang,[5] and Bin Huang[2,6]

[1] *School of Dentistry, College of Dental Medicine, Kaohsiung Medical University, Kaohsiung 80708, Taiwan*
[2] *Department of Biomedical Science and Environmental Biology, College of Life Science, Kaohsiung Medical University, No. 100, Shihchuan 1st Road, San Ming District, Kaohsiung 80708, Taiwan*
[3] *Department of Biological Science and Technology, Institute of Molecular Medicine and Bioengineering, National Chiao Tung University, Hsinchu 30068, Taiwan*
[4] *Institute of Biotechnology, National Cheng Kung University, Tainan 70101, Taiwan*
[5] *Institute of Medical Science, College of Medicine, Tzu Chi University, Hualien County 97004, Taiwan*
[6] *Department of Biological Sciences, National Sun Yat-Sen University, Kaohsiung 80424, Taiwan*

Correspondence should be addressed to Bin Huang; huangpin2@yahoo.com.tw

Received 21 April 2014; Accepted 5 May 2014; Published 21 May 2014

Academic Editor: Li-Yeh Chuang

Hydrogen sulfide (H_2S) and nitric oxide (NO), two endogenous gaseous molecules in endothelial cells, got increased attention with respect to their protective roles in the cardiovascular system. However, the details of the signaling pathways between H_2S and NO in endothelia cells remain unclear. In this study, a treatment with NaHS profoundly increased the expression and the activity of endothelial nitric oxide synthase. Elevated gaseous NO levels were observed by a novel and specific fluorescent probe, 5-amino-2-(6-hydroxy-3-oxo-3H-xanthen-9-yl)benzoic acid methyl ester (FA-OMe), and quantified by flow cytometry. Further study indicated an increase of upstream regulator for eNOS activation, AMP-activated protein kinase (AMPK), and protein kinase B (Akt). By using a biotin switch, the level of NO-mediated protein S-nitrosylation was also enhanced. However, with the addition of the NO donor, NOC-18, the expressions of cystathionine-γ-lyase, cystathionine-β-synthase, and 3-mercaptopyruvate sulfurtransferase were not changed. The level of H_2S was also monitored by a new designed fluorescent probe, 4-nitro-7-thiocyanatobenz-2-oxa-1,3-diazole (NBD-SCN) with high specificity. Therefore, NO did not reciprocally increase the expression of H_2S-generating enzymes and the H_2S level. The present study provides an integrated insight of cellular responses to H_2S and NO from protein expression to gaseous molecule generation, which indicates the upstream role of H_2S in modulating NO production and protein S-nitrosylation.

1. Introduction

Gas molecules that are produced by cells have been discussed for several decades regarding their protective role in the vascular system. Recently, the diverse physiologic actions of carbon monoxide (CO), nitric oxide (NO), and hydrogen sulfide (H_2S) and their role in preventing diseases through the mediation of gas-regulating and -sensing mechanisms have attracted a great deal of interest [1]. For example, NO plays an important role in the regulation of the cardiovascular function through a posttranslational protein S-nitrosylation on the cysteine residue [2]. In our previous study, a mechanical shear flow is regarded as protective for endothelial cells (ECs), leading to a series S-nitrosylation of proteins [3]. Investigating the reported mechanisms of NO on EC protection, the NO-mediated S-nitrosylated proteins, such as F1F0-ATPase, reduced the generation of Ca^{2+} and ROS in mitochondria during ischemia/reperfusion injury [4]. NO was also reported to be essential in the prevention of irreversible oxidative stress and finally provided protection from several diseases including cancer, diabetes, and neuron degeneration [5–7].

The toxic effects of hydrogen sulfide (H_2S) on living organisms have been recognized for nearly 300 years.

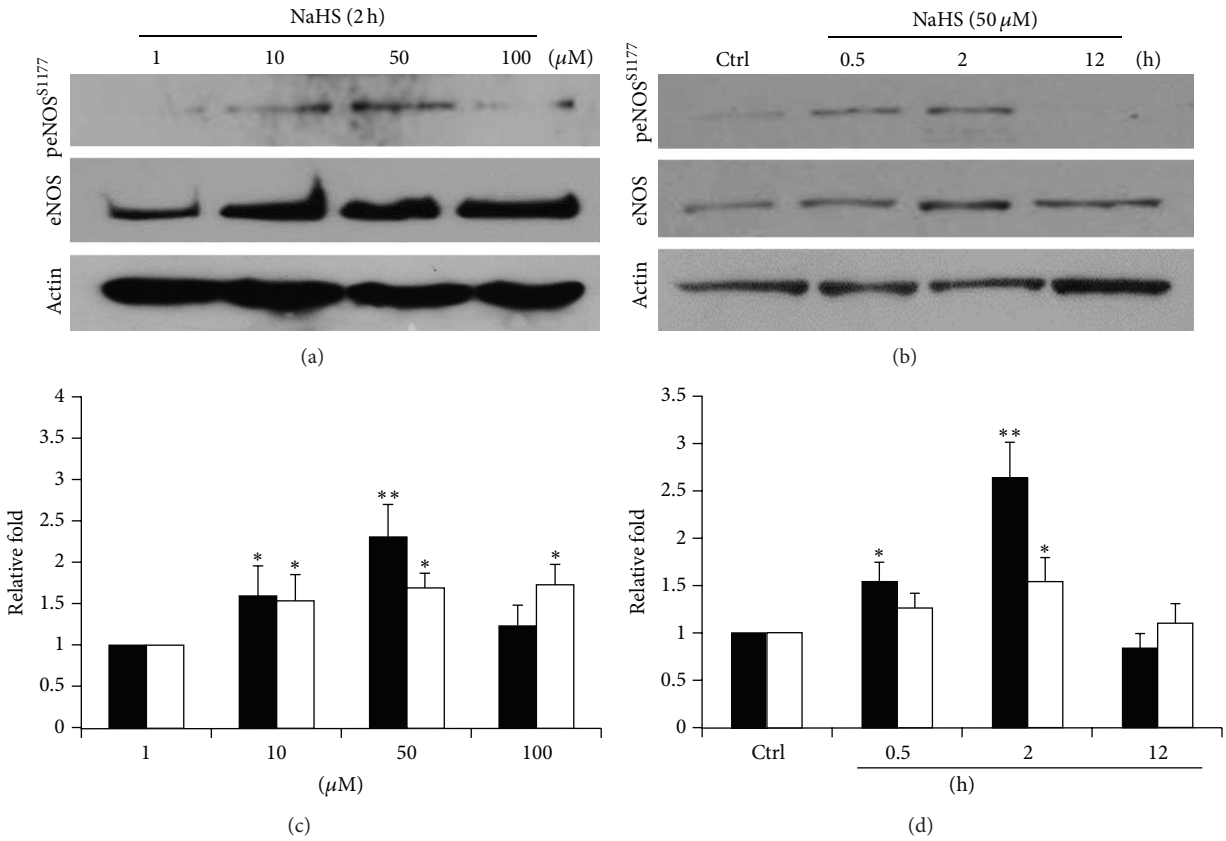

Figure 1: NaHS increases the expression and serine 1177 phosphorylation of eNOS. (a) ECs pretreated by diluting concentrations of NaHS (1 μM, 10 μM, 50 μM, and 100 μM) for 2 h. (b) ECs treated with NaHS (50 μM) for 0.5, 2, and 12 h. Blotted membranes were separately hybridized with eNOS and peNOSS1177 antibodies. ((c) and (d)) Relative folds of protein levels shown as means ± S.E. compared to control. Statistical significance ($^{*}P < 0.05$; $^{**}P < 0.01$) analyzed using Fisher's LSD.

In recent years, however, interest has been directed towards H_2S as the third gaseous mediator, which has been shown to exhibit potent vasodilatory activity both *in vitro* and *in vivo*. This is assumed to be realized by opening vascular smooth muscle K_{ATP} channels [8]. Of the three enzymes, cystathionine-γ-lyase (CSE), cystathionine-β-synthase (CBS), and 3-mercaptopyruvate sulfurtransferase (3-MST) can utilize L-cysteine as a substrate to produce H_2S. Deficiency of H_2S-producing enzymes results in some disorders such as homocystinuria, which is characterized by mental retardation, skeletal abnormalities, increased urine homocysteine, increased risks of thromboembolism, and early onset of atherosclerosis [9–11]. H_2S was also reported to protect against vascular remodeling from endothelial damage [12]. Recently, a signaling molecule for H_2S was shown to regulate vascular relaxation and angiogenesis via potassium channel S-sulfhydration [13–15].

With a similar physiological function, it is interesting to discuss the interactions between H_2S and NO in responding stimuli. In the reports cited above, H_2S and NO in synergy might regulate smooth muscle relaxation and also mitochondrial integration [16, 17]. H_2S triggers late-phase preconditioning in the postischemic small intestine by an NO- and p38 MAPK-dependent pathway [18]. Despite H_2S inhibiting NO production in lipopolysaccharide-stimulated macrophages, the H_2S can also stimulate NO production from other cells [19, 20].

Because of the technical difficulty in detecting gaseous molecules, in the current study, not only monitoring the regulations of theses enzymes but also quantifying the molecules of H_2S and NO specifically with the new designed fluorescent probes. Therefore, we question here if H_2S has any upstream role in the regulation of endothelial NO production.

2. Materials and Methods

2.1. Cell Culture and Drug Treatments. The EAhy 926 cell line was kindly donated by Cora-Jean S. Edgell, University of North Carolina, Chapel Hill. EAhy 926 cells were cultured in DMEM supplemented with fetal bovine serum (FBS, 10%), streptomycin (100 μg/mL), and penicillin (100 U/mL). ECs were replaced by the same medium containing 2% FBS and incubated overnight prior to the experimental NaHS and NOC-18 treatments.

2.2. Cell Lysis and Protein Extraction. ECs were washed with cord buffer after treatment [NaCl (0.14 M), KCl (4 mM),

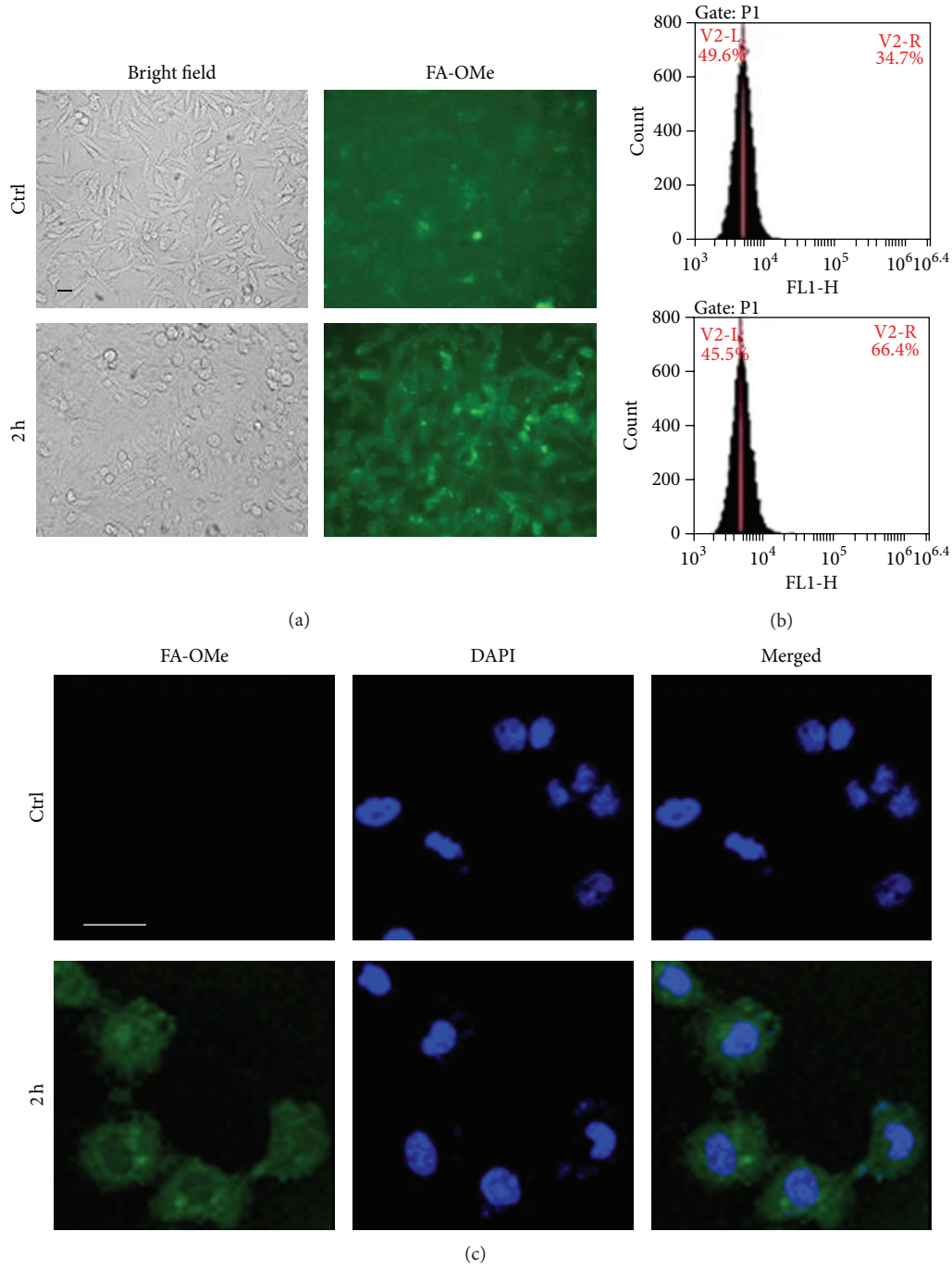

Figure 2: Elevated NO levels monitored by specific fluorescent probes. (a) ECs treated with NaHS (50 μM) for 2 h stained by FA-OMe and observed by fluorescent microscopy. (b) FA-OMe signals calculated by flow cytometry. (c) FA-OMe signals observed by confocal microscopy. Bar = 20 μm.

glucose (11 mM), and HEPES (10 mM, pH 7.4)] and then lysed with 100 μL of lysis buffer [HEPES (250 mM, pH 7.7), EDTA (1 mM), neocuproine (0.1 mM), and CHAPS (0.4%, w/v)]. After centrifugation, protein supernatant was collected and protein concentrations were determined with BCA assay reagent (Thermo Fisher Scientific Inc., Rockford, IL, USA).

2.3. Western Blot Analysis. Forty micrograms of cell lysates with various treatments were mixed with an equal volume of sample buffer [Tris-HCl (62.5 mM, pH 6.8), SDS (3%, w/v), 2-mercaptoethanol (5%, v/v), and glycerol (10%, v/v)] and then separated by SDS-PAGE. The gel was transferred to PVDF membranes (Millipore, MA, USA) and immunoblotted with antibodies: eNOS (1 : 3000; Cell Signaling Tech., MA,

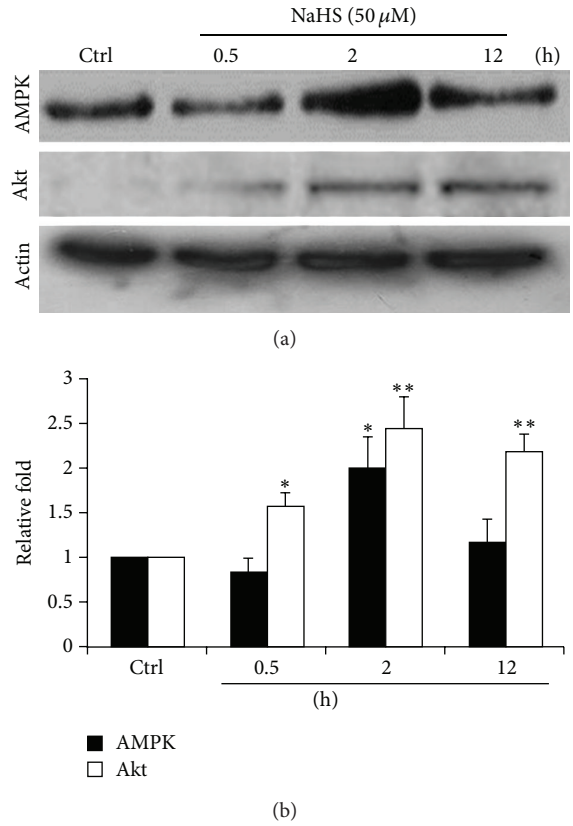

Figure 3: The expression levels of AMPK and Akt in the presence of NaHS. (a) ECs treated with NaHS (50 μM) for 0.5, 2, and 12 h. The blotted membranes hybridized with AMPK antibody. (b) Relative folds of protein levels shown as means ± S.E. compared to control. Statistical significance ($^{*}P < 0.05$; $^{**}P < 0.01$) analyzed using Fisher's LSD.

USA), peNOS^{S1177} (1 : 2000; Cell Signaling Tech.), AMPK (1 : 3000; Cell Signaling Tech.), Akt (1 : 2000; Cell Signaling Tech.), cystathionine-γ-lyase (CSE, 1 : 1000; Abnova, Taipei, Taiwan), cystathionine-β-synthase (CBS, 1 : 1000; Abnova), and 3-mercaptopyruvate sulfurtransferase (3-MST, 1 : 1000; Abcam, Cambridge, UK). The membranes were visualized with the SuperSignal West Femto reagent (Thermo Fisher Scientific, IL, USA) on X-ray films. The images from X-ray films were scanned using a digital scanner (Microtek International Inc.) and the density was calculated by the Progenesis Samespots v2.0 software (NonLinear Dynamics, Newcastle, UK).

2.4. Application of Fluorescent Probes and Imaging Conditions. For NO detection, 5-amino-2-(6-hydroxy-3-oxo-3H-xanthen-9-yl)benzoic acid methyl ester (FA-OMe) was designed [21]. ECs with NaHS treatment were coincubated with 10 μM of FA-OMe for 4 h prior to imaging. The ECs were washed three times with PBS buffer and then bathed in 2 mL of PBS. The images were obtained by the fluorescence microscope (λex 460 nm, λem 524 nm; Axiovert 40 CFL, Zeiss). As for 4-nitro-7-thiocyanatobenz-2-oxa-1,3-diazole (NBD-SCN) that was used for detecting H_2S, the cells were incubated with 5 μM NBD-SCN for 30 min and then subjected to fluorescence microscope (λex 460 nm, λem 550 nm) [22]. For confocal fluorescence images study, ECs were seeded at a density of 2×10^5 cells/well on cover glasses (24×24 mm^2) and grown for 24 h. The cells with 10 μM of FA-OMe incubation were fixed with 4% formaldehyde solution for 20 min at room temperature. Cell nuclei were stained with 40,6-diamidino-2-phenylindole (DAPI). Cover glasses containing fixed ECs were mounted in a mixture of PBS and glycerol (1 : 1) on a microscopic slide. The cells were observed using a laser scanning confocal imaging system (Olympus FluoView 300) consisting of Olympus BX51 microscope and a 20 mW output argon ion laser.

2.5. Flow Cytometry Assay. After fluorescence microscope observation, the ECs were washed twice with PBS and detached by tryptic reaction. ECs were collected by centrifugation and then resuspended in PBS. The fluorescence was immediately measured by the Accuri C6 flow cytometer (BD, NJ, USA) with excitation and emission settings of 488 and 530 nm, respectively. The fluorescence strength was obtained from 1×10^4 cells and statistically calculated from three repeats.

2.6. Evaluation of Protein S-Nitrosylation. The cell lysates (200 μg) after NaHS treatment were blocked by methyl methanethiosulfonate (MMTS), reduced by ascorbate, and labelled by biotin according to reported guideline [23]. The biotinylated lysates were then subjected to a reductant-free SDS-PAGE and western blotted with streptavidin-HRP (1 : 3000) following a previous study [24].

3. Results and Discussion

3.1. NaHS Increased the Protein Level of eNOS and the Phosphorylation on Serine 1177 Residue. Endothelial nitric oxide synthase (eNOS) is responsible for endothelial nitric oxide (NO) production and the enzyme activity is reported to be highly affected by posttranslational phosphorylation on serine 1177 residue (S1177) [25]. In this study, with the treatment of different concentrations of NaHS (1~100 μM), we found that 50 μM of NaHS can significantly enhance both the eNOS expression and the phosphorylation of the serine 1177 residue (peNOS^{S1177}) (Figures 1(a) and 1(c)). This concentration conforms well with several vascular research articles [26]. At this concentration, the highest expression level of eNOS and peNOS^{S1177} was observed at 2 hours (Figures 1(b) and 1(d)).

3.2. Cellular NO Was Precisely Determined by Specific Fluorescent Probes. In addition to the expression of eNOS, the levels of NO molecules were further measured by the specific fluorescent probe FA-OMe. This can distinguish NO and other reactive oxygen species (ROS) from reactive nitrogen species (RNS) [21]. After NaHS treatment, the NO level was increased from 34.7 ± 2.9% to 66.4 ± 3.8% at 2 hours

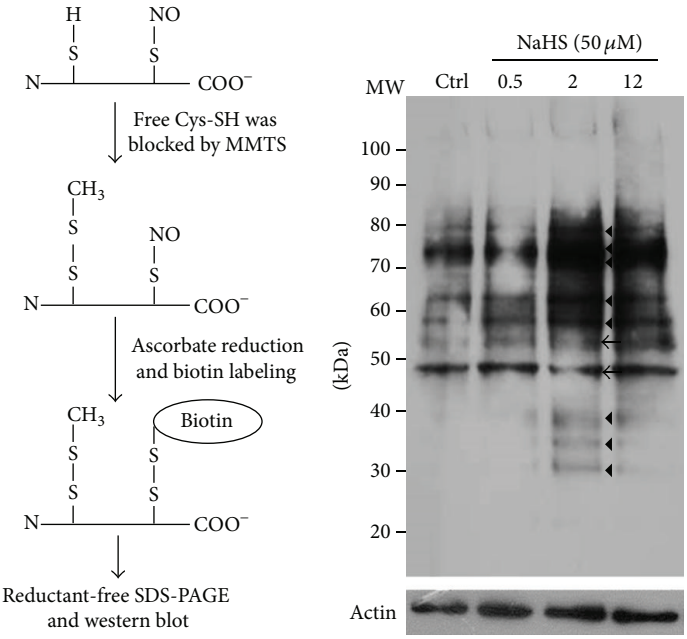

(a) (b)

Figure 4: Detection of protein S-nitrosylation. (a) Scheme representing the procedures of modified biotin switch. Biotin-labeled lysates were subjected to SDS-PAGE without any reducing agents in the buffers. (b) ECs lysate (100 μg) treated with NaHS (50 μM) for 0.5, 2, and 12 h separated by SDS-PAGE and the blotted membranes were hybridized with streptavidin-HRP. Triangle indicates proteins with increased S-nitrosylation. Arrow head indicates proteins with decreased S-nitrosylation.

(Figures 2(a) and 2(b)). By using confocal microscopy, despite the fact that the basal fluorescence in the control treatment was difficult to see, the broadly distributed NO was observed in the cytosol and also in the nuclei (Figure 2(c)).

3.3. The Expression Profiles of AMPK and Akt in the Presence of H_2S. 5′ AMP-activated protein kinase (AMPK) is an enzyme that plays a role in cellular energy homeostasis. Besides protein kinase B (Akt), AMPK is also reported to activate eNOS by phosphorylating Ser1177 in response to various stimuli [27]. In the current study, H_2S increased the protein level of AMPK at 2 h and returned to a basal level at 12 h. However, sustainable expressions of Akt were observed from 0.5 to 12 h (Figures 3(a) and 3(b)). This indicated that H_2S can stimulate eNOS activity through AMPK and Akt pathways. Similar findings were also reported recently [28, 29].

3.4. H_2S-Increased Bioavailability of NO That Can Enhance Protein S-Nitrosylation. According to previous data, we confirmed that NO level got elevated by H_2S. Since protein S-nitrosylation/denitrosylation is regarded as important in cardioprotection, its investigation of protein S-nitrosylation is, hence, important for applied medical purposes [2, 3, 30]. By using a modified biotin switch, we could identify at least 8 groups of increased S-nitrosoproteins and 2 groups of decreased S-nitrosoproteins (Figure 4). With the excellent performance in analyzing S-nitrosoproteins, mass spectrometry will be introduced in further identification of these proteins [24].

3.5. NO Did Not Reciprocally Increase the Expression of H_2S-Generating Enzymes and the H_2S Level. After confirming that H_2S can increase NO at the cellular level, we also examined whether NO can be synchronized at elevated H_2S levels. As shown in Figure 5, three key enzymes are involved in the cellular H_2S synthesis: CSE, CBS, and 3-MST. These were not changed by NOC-18 treatment (Figures 5(a) and 5(b)). Although several studies indicated that H_2S-generating enzymes can also be exerted by NO [31], we could not find differences in our microscopic and flow cytometric analysis (46.0 ± 3.1% and 43.3 ± 4.8% separately) using NBD-SCN fluorescence probe (Figures 5(c) and 5(d)). The reported study demonstrated that H_2S promotes NO production in ECs via the activation of a cascade of phosphorylation events, starting from p38 MAPK and Akt to eNOS, and this can be through NO-dependent or NO-independent mechanisms cascade. Thus, H_2S may be a key regulator for angiogenic signalling pathways, whether they required NO or not [32]. This might indicate that NO works as a downstream gaseous transmitter in the endothelium.

4. Conclusion

In the present study, hydrogen sulfide increased nitric oxide production. This was not only concluded by studying related enzymes, but also confirmed directly by detecting the final products where NO levels were observed by a novel and specific fluorescent probe, FA-OMe, and quantified by flow cytometry. The level of H_2S was also monitored by a new

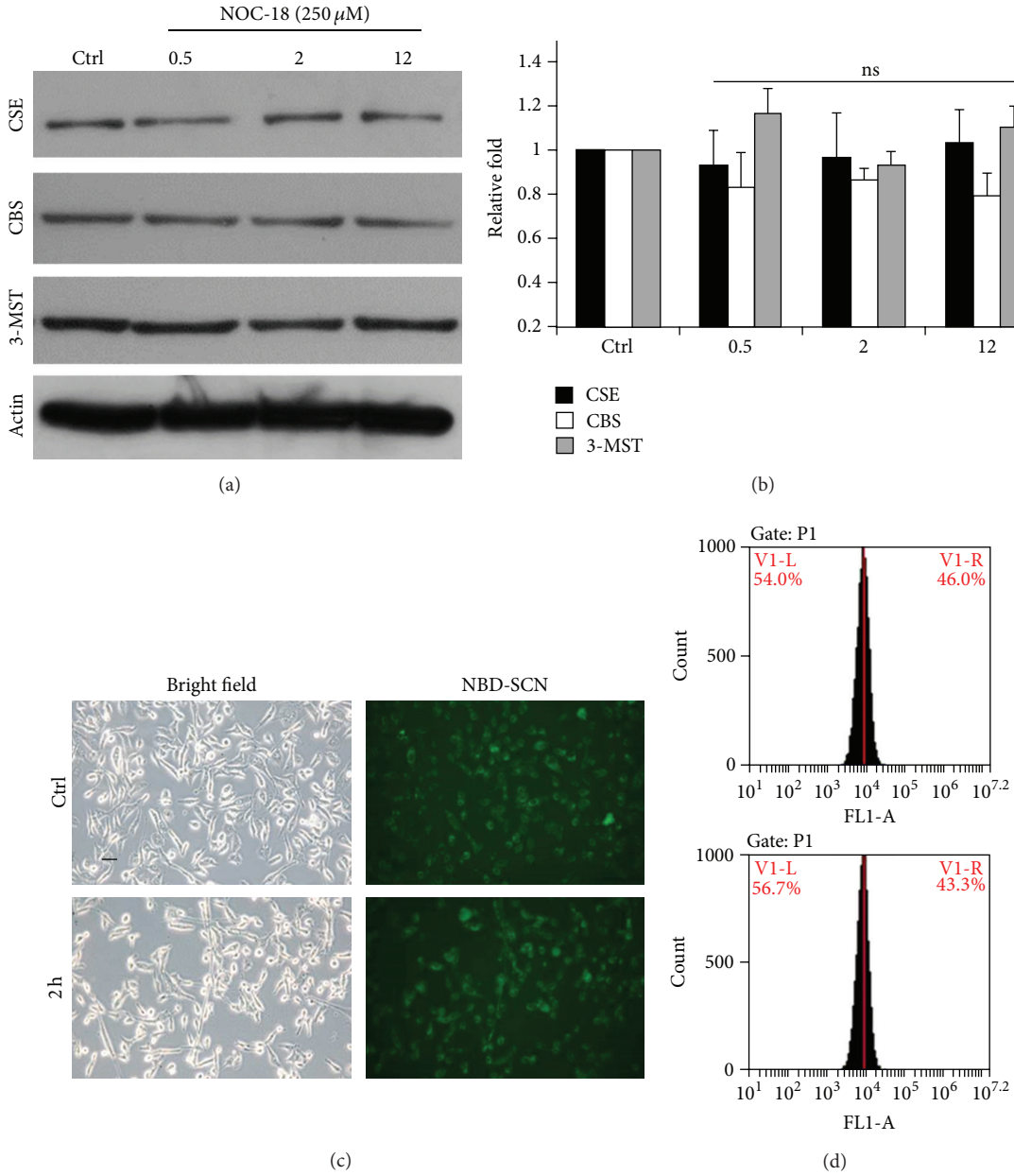

FIGURE 5: Investigation of H_2S biosynthesis under the treatment of NO. (a) ECs which treated NO donor, NOC-18 (250 μM), for 0.5, 2, and 12 h were subjected to western blot analysis with CSE, CBS, and 3-MST antibodies. (b) The statistic data showed that no significance (P = ns) was observed between treatments. (c) NBD-SCN was applied to detect cellular H_2S level specifically. (d) Fluorescent signals were calculated by flow cytometry.

designed fluorescent probe, NBD-SCN, with high specificity. The present study provides an integrated insight of cellular responses to two gaseous molecules from protein expression to gaseous molecule generation, which indicates the upstream role of H_2S in modulating NO production and protein S-nitrosylation.

Conflict of Interests

The authors declare no conflict of interests.

Authors' Contribution

Ping-Ho Chen and Yaw-Syan Fu contributed equally to this paper.

Acknowledgments

The authors thank Dr. Hans-Uwe Dahms for critical reading of the paper. This study was supported by a Grant from the National Science Council (NSC 101-2320-B-037-041).

They are grateful to the Center for Resources, Research & Development of Kaohsiung Medical School for the support of fluorescent imaging.

References

[1] M. Kajimura, R. Fukuda, R. M. Bateman, T. Yamamoto, and M. Suematsu, "Interactions of multiple gas-transducing systems: hallmarks and uncertainties of CO, NO, and H_2S Gas Biology," *Antioxidants & Redox Signaling*, vol. 13, no. 2, pp. 157–192, 2010.

[2] J. Sun and E. Murphy, "Protein S-nitrosylation and cardioprotection," *Circulation Research*, vol. 106, no. 2, pp. 285–296, 2010.

[3] B. Huang, S. C. Chen, and D. L. Wang, "Shear flow increases S-nitrosylation of proteins in endothelial cells," *Cardiovascular Research*, vol. 83, no. 3, pp. 536–546, 2009.

[4] S. Shiva, M. N. Sack, J. J. Greer et al., "Nitrite augments tolerance to ischemia/reperfusion injury via the modulation of mitochondrial electron transfer," *The Journal of Experimental Medicine*, vol. 204, no. 9, pp. 2089–2102, 2007.

[5] Y.-Y. Chen, H.-M. Chu, K.-T. Pan et al., "Cysteine S-nitrosylation protects protein-tyrosine phosphatase 1B against oxidation-induced permanent inactivation," *The Journal of Biological Chemistry*, vol. 283, no. 50, pp. 35265–35272, 2008.

[6] T. Nakamura and S. A. Lipton, "Emerging roles of S-nitrosylation in protein misfolding and neurodegenerative diseases," *Antioxidants & Redox Signaling*, vol. 10, no. 1, pp. 87–101, 2008.

[7] B. Lima, M. T. Forrester, D. T. Hess, and J. S. Stamler, "S-nitrosylation in cardiovascular signaling," *Circulation Research*, vol. 106, no. 4, pp. 633–646, 2010.

[8] S. Mani, A. Untereiner, L. Wu, and R. Wang, "Hydrogen sulfide and the pathogenesis of atherosclerosis," *Antioxidants & Redox Signaling*, vol. 20, no. 5, pp. 805–817, 2014.

[9] C. A. Wagner, "Hydrogen sulfide: a new gaseous signal molecule and blood pressure regulator," *Journal of Nephrology*, vol. 22, no. 2, pp. 173–176, 2009.

[10] G. Yang, L. Wu, B. Jiang et al., "H_2S as a physiologic vasorelaxant: hypertension in mice with deletion of cystathionine γ-lyase," *Science*, vol. 322, no. 5901, pp. 587–590, 2008.

[11] Y. Wang, X. Zhao, H. Jin et al., "Role of hydrogen sulfide in the development of atherosclerotic lesions in apolipoprotein e knockout mice," *Arteriosclerosis, Thrombosis, and Vascular Biology*, vol. 29, no. 2, pp. 173–179, 2009.

[12] T. P. Vacek, W. Gillespie, N. Tyagi, J. C. Vacek, and S. C. Tyagi, "Hydrogen sulfide protects against vascular remodeling from endothelial damage," *Amino Acids*, vol. 39, no. 5, pp. 1161–1169, 2010.

[13] A. Papapetropoulos, A. Pyriochou, Z. Altaany et al., "Hydrogen sulfide is an endogenous stimulator of angiogenesis," *Proceedings of the National Academy of Sciences of the United States of America*, vol. 106, no. 51, pp. 21972–21977, 2009.

[14] A. K. Mustafa, M. M. Gadalla, N. Sen et al., "H_2S signals through protein S-Sulfhydration," *Science Signaling*, vol. 2, no. 96, Article ID ra72, 2009.

[15] A. K. Mustafa, G. Sikka, S. K. Gazi et al., "Hydrogen sulfide as endothelium-derived hyperpolarizing factor sulfhydrates potassium channels," *Circulation Research*, vol. 109, no. 11, pp. 1259–1268, 2011.

[16] R. Hosoki, N. Matsuki, and H. Kimura, "The possible role of hydrogen sulfide as an endogenous smooth muscle relaxant in synergy with nitric oxide," *Biochemical and Biophysical Research Communications*, vol. 237, no. 3, pp. 527–531, 1997.

[17] F. Bouillaud and F. Blachier, "Mitochondria and sulfide: a very old story of poisoning, feeding, and signaling?" *Antioxidants & Redox Signaling*, vol. 15, no. 2, pp. 379–391, 2011.

[18] M. Yusof, K. Kamada, T. Kalogeris, F. Spencer Gaskin, and R. J. Korthuis, "Hydrogen sulfide triggers late-phase preconditioning in postischemic small intestine by an NO- and p38 MAPK-dependent mechanism," *American Journal of Physiology—Heart and Circulatory Physiology*, vol. 296, no. 3, pp. H868–H876, 2009.

[19] G.-S. Oh, H.-O. Pae, B.-S. Lee et al., "Hydrogen sulfide inhibits nitric oxide production and nuclear factor-κB via heme oxygenase-1 expression in RAW264.7 macrophages stimulated with lipopolysaccharide," *Free Radical Biology & Medicine*, vol. 41, no. 1, pp. 106–119, 2006.

[20] L. Grossi, "Hydrogen sulfide induces nitric oxide release from nitrite," *Bioorganic and Medicinal Chemistry Letters*, vol. 19, no. 21, pp. 6092–6094, 2009.

[21] T.-W. Shiue, Y.-H. Chen, C.-M. Wu et al., "Nitric oxide turn-on fluorescent probe based on deamination of aromatic primary monoamines," *Inorganic Chemistry*, vol. 51, no. 9, pp. 5400–5408, 2012.

[22] Y.-H. Chen, J.-C. Tsai, T.-H. Cheng, S.-S. Yuan, and Y.-M. Wang, "Sensitivity evaluation of NBD-SCN towards cysteine/homocysteine and its bioimaging applications," *Biosensors & Bioelectronics*, vol. 56, pp. 117–123, 2014.

[23] S. R. Jaffrey and S. H. Snyder, "The biotin switch method for the detection of S-nitrosylated proteins," *Science's STKE: Signal Transduction Knowledge Environment*, vol. 2001, no. 86, article Pl1, 2001.

[24] B. Huang, C. L. Liao, Y. P. Lin, S. C. Chen, and D. L. Wang, "S-nitrosoproteome in endothelial cells revealed by a modified biotin switch approach coupled with western blot-based two-dimensional gel electrophoresis," *Journal of Proteome Research*, vol. 8, no. 10, pp. 4835–4843, 2009.

[25] P. M. Bauer, D. Fulton, Y. C. Boo et al., "Compensatory phosphorylation and protein-protein interactions revealed by loss of function and gain of function mutants of multiple serine phosphorylation sites in endothelial nitric-oxide synthase," *The Journal of Biological Chemistry*, vol. 278, no. 17, pp. 14841–14849, 2003.

[26] C. Szabó and A. Papapetropoulos, "Hydrogen sulphide and angiogenesis: mechanisms and applications," *British Journal of Pharmacology*, vol. 164, no. 3, pp. 853–865, 2011.

[27] S. Dimmeler, I. Fleming, B. Fisslthaler, C. Hermann, R. Busse, and A. M. Zeiher, "Activation of nitric oxide synthase in endothelial cells by Akt-dependent phosphorylation," *Nature*, vol. 399, no. 6736, pp. 601–605, 1999.

[28] B. L. Predmore, D. Julian, and A. J. Cardounel, "Hydrogen sulfide increases nitric oxide production from endothelial cells by an Akt-dependent mechanism," *Frontiers in Physiology*, vol. 2, article 104, 2011.

[29] P. Manna and S. K. Jain, "L-cysteine and hydrogen sulfide increase PIP3 and AMPK/PPARγ expression and decrease ROS and vascular inflammation markers in high glucose treated human U937 monocytes," *Journal of Cellular Biochemistry*, vol. 114, no. 10, pp. 2334–2345, 2013.

[30] B. Huang, F. A. Li, C. H. Wu, and D. L. Wang, "The role of nitric oxide on rosuvastatin-mediated S-nitrosylation and translational proteomes in human umbilical vein endothelial cells," *Proteome Science*, vol. 10, no. 1, article 43, 2012.

[31] C. Coletta, A. Papapetropoulos, K. Erdelyi et al., "Hydrogen sulfide and nitric oxide are mutually dependent in the regulation of angiogenesis and endothelium-dependent vasorelaxation," *Proceedings of the National Academy of Sciences of the United States of America*, vol. 109, no. 23, pp. 9161–9166, 2012.

[32] Z. Altaany, G. Yang, and R. Wang, "Crosstalk between hydrogen sulfide and nitric oxide in endothelial cells," *Journal of Cellular and Molecular Medicine*, vol. 17, no. 7, pp. 879–888, 2013.

Hindawi Publishing Corporation
The Scientific World Journal
Volume 2014, Article ID 567148, 11 pages
http://dx.doi.org/10.1155/2014/567148

Research Article

Progesterone Increases Apoptosis and Inversely Decreases Autophagy in Human Hepatoma HA22T/VGH Cells Treated with Epirubicin

Wen-Tsan Chang,[1,2,3] Hsiao-Ling Cheng,[4] Bau-Shan Hsieh,[4] Chien-Chih Chiu,[5] King-Teh Lee,[1,2,3] and Kee-Lung Chang[1,4]

[1] *Graduate Institute of Medicine, College of Medicine, Kaohsiung Medical University, Kaohsiung 80708, Taiwan*
[2] *Division of Hepatobiliary and Pancreatic Surgery, Department of Surgery, Kaohsiung Medical University Hospital, Kaohsiung 80756, Taiwan*
[3] *Department of Surgery, School of Medicine, College of Medicine, Kaohsiung Medical University, Kaohsiung 80708, Taiwan*
[4] *Department of Biochemistry, School of Medicine, College of Medicine, Kaohsiung Medical University, Kaohsiung 80708, Taiwan*
[5] *Department of Biotechnology, College of Life Science, Kaohsiung Medical University, Kaohsiung 80708, Taiwan*

Correspondence should be addressed to King-Teh Lee; ktlee@kmu.edu.tw and Kee-Lung Chang; keeluch@kmu.edu.tw

Received 20 March 2014; Accepted 1 May 2014; Published 19 May 2014

Academic Editor: Hsueh-Wei Chang

Hepatocellular carcinoma (HCC) is the leading cause of cancer-related deaths worldwide. Epirubicin can induce intracellular reactive oxygen species and is widely used to treat unresectable HCC. Progesterone has been found to inhibit the proliferation of hepatoma cells. This study was designed to test the combined effects of epirubicin and progesterone on human hepatoma cell line, HA22T/VGH. These cells were treated with different concentrations of epirubicin with or without the coaddition of 30 μM progesterone and then analyzed for apoptosis, autophagy, and expressions of apoptotic-related proteins and multidrug-resistant gene. Epirubicin treatment dose-dependently inhibited the growth of HA22T/VGH cells. Addition of 30 μM progesterone, which was inactive alone, augmented the effect of epirubicin on the inhibition of growth of HA22T/VGH cells. Cotreatment with progesterone enhanced epirubicin-induced apoptosis, as evidenced by greater increase in caspase-3 activity and in the ratio of the apoptosis-regulating protein, Bax/Bcl-X_L. The combination also caused a decrease in autophagy and in the expression of multidrug resistance-related protein 1 mRNA compared to epirubicin alone. This study shows the epirubicin/progesterone combination was more effective in increasing apoptosis and inversely decreasing autophagy on HA22T/VGH cells treated with epirubicin alone, suggesting that this combination can potentially be used to treat HCC.

1. Introduction

Hepatocellular carcinoma (HCC) is the fifth most common cancer in men and the seventh in women, and it is the third most common cause of cancer-related deaths worldwide [1, 2]. Liver resection, local ablation therapy, and liver transplantation are the suggested curative therapies for HCC, while transarterial chemoembolization (TACE) has been used to treat unresectable HCC with some clinical efficacy [3–5].

Anthracyclines, such as doxorubicin or epirubicin, have been widely used to treat advanced HCC, to prevent or treat postoperative recurrence, and to downstage the disease before liver transplantation by systemic infusion or by transarterial route [6, 7]. Acting as topoisomerase-II inhibitors, anthracycline drugs induce DNA damages and acute oxidative stress in cells [8, 9]. And the quinine group of anthracyclines can cause one electron reduction to produce a semiquinone [9, 10]. The free radical semiquinone consequently produces reactive oxygen species (ROS), including superoxide anions, hydrogen peroxide, and hydroxyl radicals [9, 10]. ROS are reported to be involved in epirubicin-induced apoptosis in hepatoma cell lines [10]. Furthermore, epirubicin

is less cardiotoxic than doxorubicin [6]. Therefore, epirubicin is widely used in Europe and Asia in the treatments of cancers, including HCC [6, 8].

However, the side effects of anthracyclines include cardiomyopathy, immunosuppression, and the development of primary or secondary drug resistance, which may sometimes adversely affect survival, recurrence, and extrahepatic metastases in HCC patients [11–13]. And HCC cells themselves are usually resistant to chemotherapeutic agents, the response rates of chemotherapy in HCC are reported to be only 10.5%–20.6%, and, generally, overall survivals have been less than 12 months for advanced HCC patients [6, 12].

Autophagy, a survival mechanism of some cancer cells, can be induced during starvation, chemotherapy, radiation, hypoxia, and some endocrine therapies [14, 15]. Sun et al reported that autophagy could protect breast cancer cells from epirubicin-induced apoptosis and facilitate the development of epirubicin resistance [16]. Progesterone can reverse multidrug resistance gene expression in epirubicin-treated urethral cancer cell lines via p-glycoprotein pathway [17]. And megestrol (a progestin drug) treatment has produced some efficacy in advanced HCC in some clinical studies [18, 19]. Therefore, combining epirubicin with progesterone might be a potential strategy for treating HCC, as it might allow for the smaller doses of epirubicin, which is generally toxic, while increasing its effectiveness against HCC and decreasing epirubicin-related side effects.

Our previous study showed HA22T/VGH cells are susceptible to changes in redox status and oxidative stresses also induce apoptosis in these cells [20]. This study tested the effect of combining epirubicin with progesterone to treat a metastatic, poorly differentiated HCC cell line, HA22T/VGH. To evaluate the therapeutic effect of this combination, we analyzed occurrence of apoptosis and autophagy, expressions of their related proteins, and the expression of multidrug resistance-related protein 1 (MRP-1) gene.

2. Materials and Methods

2.1. Reagents and Antibodies. Epirubicin hydrochloride (Pharmorubicin) was purchased from Pfizer Italia S.R.L. (Milano, Italy), progesterone from Sigma-Aldrich (St. Louis, MO, USA), acridine orange from Molecular Probes (Eugene, OR, USA), protein assay reagents from Bio-Rad Laboratories (Hercules, CA, USA), and TRIzol reagent from Invitrogen Life Technologies (Carlsbad, CA, USA). All other chemicals were of analytical grade and purchased from Sigma-Aldrich (St. Louis, MO, USA). Mouse monoclonal antibodies against light chain-3 (LC-3), Beclin-1, or Bax, rabbit polyclonal antibodies against Bcl-X_L, and goat polyclonal antibodies against β-actin were purchased from Santa Cruz Biotechnology (Santa Cruz, CA, USA). Horseradish peroxidase-conjugated anti-mouse, -goat, and -rabbit IgG antibodies were purchased from BD Pharmingen Inc. (San Diego, CA, USA).

2.2. Cell Line, Cell Culture, and Drug Treatments. HA22T/VGH cell line was obtained from the Food Industry Research and Development Institute in Hsinchu, Taiwan (BCRC number: 60168) and was cultured in Dulbecco's modified Eagle's medium (DMEM) (Gibco BRL, Grand Island, NY, USA) containing 10% fetal bovine serum (FBS) (Hyclone, Auckland, NZ), 2 mM L-glutamine (Gibco BRL, Grand Island, NY, USA), 0.1 mM nonessential amino acids (Gibco BRL, Grand Island, NY, USA), 100 units/mL of penicillin, and 100 μg/mL of streptomycin (Gibco BRL, Grand Island, NY, USA) at 37°C in a humidified chamber with 5% CO_2. To investigate the effects of epirubicin and progesterone, various concentrations of epirubicin and progesterone were added to the culture medium for an indicated time period and then the cells were harvested and analyzed.

2.3. Cell Growth. After epirubicin and progesterone treatment, the cells were harvested and viable cells were counted using a dye exclusion technique as described previously [21]. Briefly, the cell suspension was centrifuged at 5,000 ×g; the supernatant was discarded, and the cell pellet was resuspended in serum-free medium. One volume of 0.4% Trypan blue (Gibco BRL, Grand Island, NY, USA) was added to one volume of cell suspension, and then cells were counted in a hemocytometer after incubation at room temperature for 3 min. All counts were done in triplicate.

2.4. TUNEL Assay. Terminal deoxynucleotidyl transferase-mediated dUTP nick-end labeling (TUNEL) assays were performed using an APO-BrdU TUNEL Assay Kit (Molecular Probes, Eugene, OR, USA) according to the manufacturer's directions as described previously [21]. Briefly, the cells were incubated for the indicated time before being trypsinized, washed with phosphate-buffered saline (PBS), and fixed in 2% paraformaldehyde (pH 7.4) for 15 min. The fixed cells were washed twice in PBS and stored at −20°C in 70% ethanol for 12–18 h prior to performing the TUNEL assay. After removing the 70% ethanol by centrifugation, the cells were washed twice in wash buffer and then incubated at 37°C for 60 min with DNA-labeling solution containing terminal deoxynucleotidyl transferase and BrdUTP. After washing twice with rinse buffer, the cells were resuspended for 30 min in the dark at room temperature in antibody solution containing Alexa Fluor 488-labeled anti-BrdU antibody. Flow cytometric analysis was subsequently performed using a Coulter Epics XL cytometer (Beckman Coulter, Miami, FL, USA) to quantify the fluorescence intensity for determination of apoptotic status. The data were analyzed using WINMDI software version 2.8 (Scripps Research Institute, La Jolla, CA, USA), with a minimum of 1×10^4 cells per sample being evaluated in each case.

2.5. Caspase-3 Colorimetric Protease Assay. The activity of caspase-3 was detected using an ApoTarget caspase-3 colorimetric protease assay kit (Invitrogen Corp., Camarillo, CA, USA) according to the manufacturer's instructions as described previously [21]. Briefly, we induced apoptosis in cells by epirubicin and/or progesterone treatments while concurrently incubating a control culture without induction. We then counted cells as pellet 3–5×10^6 cells per sample.

The cells were resuspended in 50 μL of chilled Cell Lysis Buffer, incubated on ice for 10 min, and then centrifuged for 1 min in a microcentrifuge (10000 ×g). Supernatant (cytosol extract) was transferred to a fresh tube and put on ice and protein assay reagents (Bio-Rad Laboratories, Hercules, CA, USA) were used. Each cytosol extract was diluted to a concentration of 50–200 μg protein per 50 μL Cell Lysis Buffer (1–4 mg/mL). A 50 μL of 2 × reaction buffer (containing 10 mM DTT) was added to each sample followed by 5 μL of the 4 mM DEVD-pNA substrate (200 μM of final concentration). The samples were incubated in the dark at 37°C for 2 h. Samples were read in a microplate reader set at 405 nm. Fold increase in caspase-3 activity was determined compared to that in untreated controls.

2.6. Detection of Autophagy with Acridine Orange Staining. Formation of acidic vesicular organelles (AVOs), a morphological characteristic of autophagy, was quantified by acridine orange staining as described previously [22]. In brief, acridine orange (1 μg/mL) was added 30 min prior to collection, and after being washed with PBS, cells were analyzed using the Coulter Epics XL cytometer (Beckman Coulter, Miami, FL, USA). Green (510–530 nm) and red (>650 nm) fluorescence emission from 1×10^4 cells illuminated with blue (488 nm) excitation light was measured. The data were analyzed using WINMDI software version 2.8 (Scripps Research Institute, La Jolla, CA, USA), with a minimum of 1×10^4 cells per sample being evaluated in each case.

2.7. Western Blotting. Sample preparation and Western blotting procedures were performed as described previously [21]. Briefly, cells were harvested and cytosolic extracts were prepared using lysis buffer (20 mM Tris-HCl (pH 7.2), 2 mM EGTA, 5 mM EDTA, 500 μM sodium orthovanadate, 10 mM sodium fluoride, 1% Triton X-100, 0.1% SDS, and protease inhibitor cocktail). Protein concentrations were determined using protein assay reagents. Forty to sixty micrograms of protein lysate was analyzed by SDS-polyacrylamide gel electrophoresis. After transfer of the proteins from the gel to a nitrocellulose membrane (Amersham Pharmacia Biotech, Freiburg, Germany), the membranes were blocked for 1 h at room temperature in PBS with 0.05% Tween 20 (PBS-T) containing 5% nonfat dry milk, and then they were incubated with specific primary antibodies and horseradish peroxidase-conjugated secondary antibodies. The immunoreactive bands were visualized using an enhanced chemiluminescence kit (Perkin-Elmer Life Sciences, Boston, MA, USA).

2.8. Reverse Transcription-Polymerase Chain Reaction (RT-PCR). Total RNA was extracted from cells with TRIzol reagent (Invitrogen Life Technologies, CA, USA) according to the manufacturer's instructions as described previously [23]. The complementary DNA (cDNA) was synthesized from random hexadeoxynucleotide primed reverse transcription from 2 μg of total RNA using M-MLV reverse transcriptase (Promega Corporation, WI, USA) according to the manufacturer's directions. Polymerase chain reaction (PCR) was then performed using the Dream Taq DNA polymerase (Thermo scientific, MA, USA) on an Applied Biosystems Gene Amp9700 PCR system (Applied Biosystems, Foster, CA, USA). The thermocycling began with 94°C for 5 min followed by 30 cycles of 94°C for 1 min, 60°C for 1 min, and 72°C for 1 min, and then followed by 70°C for 10 min. PCR primers sequences were as follows: multidrug resistance-related protein 1 (MRP-1) forward, 5′-AGG TGGACCTGT TTC GTG AC-3′; reverse, 5′-ACCCTGTGATCCACCAGAAG-3′, and GAPDH forward, 5′-GAC ATC AAG AAG GTG GTG AAG CAG-3′; reverse, 5′-GCG TCA AAG GTG GAG GAG TGG-3′. The amplified PCR products were analyzed on 2% agarose gels and photographs were taken. The intensity of each band was calculated by densitometry analysis and the results were expressed as a percentage of the optical density of the corresponding GAPDH band.

2.9. Statistical Analysis. Comparisons among the groups of cells, one-way analysis of variance (ANOVA), and Fisher's least significant difference test were performed using the SPSS 17.0 statistical software (SPSS, Chicago, IL). All experiments were performed at least thrice. All data are expressed as the mean ± standard deviation (S.D.). Value differences were considered significant if $P < 0.05$.

3. Results and Discussions

3.1. Inhibition of Cell Growth. To gain initial insight into the effects of epirubicin alone or in combination with progesterone on cell growth of hepatoma cell line, HA22T/VGH cells were treated for 24 or 48 h without or with different doses of epirubicin in the absence or presence of 30 μM progesterone. The IC_{50} of progesterone was 100 μM and almost not cytotoxic to HA22T/VGH cells at concentrations <50 μM (data not shown). Therefore, a concentration of 30 μM progesterone was the dosage chosen for the cotreatment with epirubicin. During the 24 h incubation period, the untreated HA22T/VGH cells proliferated, while the growth of the cells treated with epirubicin ≥0.3 μM was significantly inhibited. The addition of 30 μM progesterone significantly augmented epirubicin's inhibition of growth at concentration of ≥0.1 μM (Figure 1(a)). During 48 h incubation, epirubicin inhibited cell growth in a dose-dependent manner and the coaddition of progesterone augmented its effect (Figure 1(b)).

3.2. Induction of Apoptosis and Expressions of Apoptosis-Related Proteins. Apoptotic cells were measured by flow cytometric analysis after TUNEL staining (Figure 2(a)). After 24 h treatment with epirubicin, a significant increase in the percentage of TUNEL-positive apoptotic cells was seen as compared with controls at concentrations ≥0.1 μM epirubicin. Although progesterone alone did not cause a significant change in the number of apoptotic cells, using it in combination with epirubicin at concentrations ≥0.3 μM had a stronger effect. The fluorescence intensities of apoptotic cells of HA22T/VGH cells treated with 30 μM progesterone, 0.3 μM epirubicin, or combination therapy were 102.2 ± 20.3%, 193.8 ± 20.0%, and 264.0 ± 38.0%, respectively, compared with those of controls (Figure 2(a)). Figure 2(b) shows

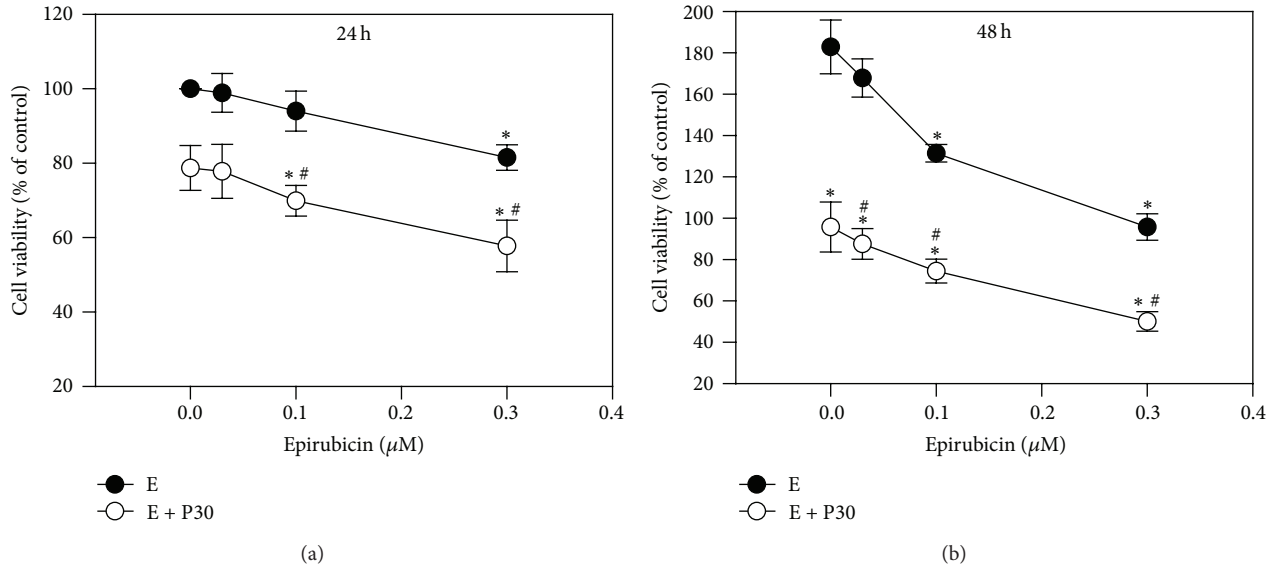

Figure 1: Effects of epirubicin on cell growth without or with progesterone addition. HA22T/VGH cells were treated with different concentrations of epirubicin without or with 30 μM progesterone for 24 h (a) or 48 h (b). Results are expressed as the mean ± standard deviation (S.D.) for three separate experiments. E: epirubicin; P30: 30 μM progesterone. $^{*}P < 0.05$ compared to the corresponding untreated controls. $^{\#}P < 0.05$ compared to the corresponding epirubicin-treated group.

that adding 30 μM progesterone to 0.3 μM epirubicin treatment produced more caspase-3 activity (212.5 ± 10.6%) than using 0.3 μM epirubicin alone (126.0 ± 5.7%). These results showed epirubicin at concentration of 0.3 μM activated caspase-3 and induced apoptosis, and combining the two drugs had a significant effect on apoptosis in HA22T/VGH cells.

To determine whether the treatment-induced apoptosis was associated with altered expression of apoptosis-relating proteins, HA22T/VGH cells were treated for 24 h with 0.3 μM epirubicin in the presence or absence of 30 μM progesterone and analyzed by Western blotting. Figure 3 shows that progesterone alone had no significant effect (94.8 ± 10.6% versus 100 ± 0.0%) on the antiapoptotic protein, Bcl-X_L levels, whereas epirubicin caused a decrease (71.1 ± 13.6% versus 100 ± 0.0%; $P < 0.05$), compared with those of controls. The combination of epirubicin and progesterone caused a marked decrease in expression of Bcl-X_L compared to 0.3 μM epirubicin alone (13.9 ± 4.8% versus 71.1 ± 13.6; $P < 0.05$). Meanwhile, progesterone alone had no effect on the proapoptotic protein, Bax levels; epirubicin alone decreased Bax levels. The coaddition of progesterone and epirubicin significantly lessened the decrease of Bax levels compared to epirubicin alone (84.7 ± 31.3% versus 38.0 ± 7.1%; $P < 0.05$). Thus, the ratio of proapoptotic/antiapoptotic factor, Bax/Bcl-X_L, was extremely enhanced by the combination therapy, which can partly explain why apoptosis was increased by the combination (Figure 3).

Activation of caspase-3 is an essential step in apoptosis. Our results demonstrated progesterone augmented caspase-3 activity of epirubicin-treated HA22T/VGH cells significantly. Epirubicin or doxorubicin can induce intracellular ROS [8, 9]. ROS production may interact with Fas-associated death domain (FADD) pathway and FADD sequence can result in activation of caspase-3 which has been reported in various cancer cell lines [24, 25]. This study also found that progesterone interfered with the expression of apoptosis-regulating proteins, upregulating Bax and downregulating Bcl-X_L, in the epirubicin-treated HA22T/VGH cells. It is currently unknown whether progesterone initially triggers apoptosis upstream from caspase-3 or not. Bcl-X_L expression is important for the inhibition of apoptosis initiated by various cellular stresses in human HCC cells [26, 27]. We, therefore, propose that the Bcl-2 family may contribute to the improved efficacy of treating HA22T/VGH cells with a combination of epirubicin and progesterone. On the other hand, the expression of the progesterone receptor and its potential role in HA22T/VGH cells have not been reported till now; however, some studies have evaluated the role of the progesterone receptor-mediated apoptosis in other human hepatoma cells. Cheng et al. demonstrated that treatment with RU486, a progesterone receptor antagonist, inhibits the progesterone-mediated response to estradiol pretreatment in tumor necrosis factor-induced apoptotic Huh-7 cells [28]. On the contrary, Zhang and Chow reported that the progesterone receptor is not involved in the action of megestrol-induced apoptosis in HepG2 cells [29]. Thus, further studies on the potential role of the progesterone receptor in HA2T/VGH cells are necessary.

3.3. Autophagy Reduction by Combination. It has been reported that autophagy can be induced during chemotherapy [30, 31]. To determine whether the treatments had an effect on autophagy induction, HA22T/VGH cells were treated for 24 h with 0.3 μM epirubicin in the presence or absence of 30 μM progesterone, then subjected to acridine

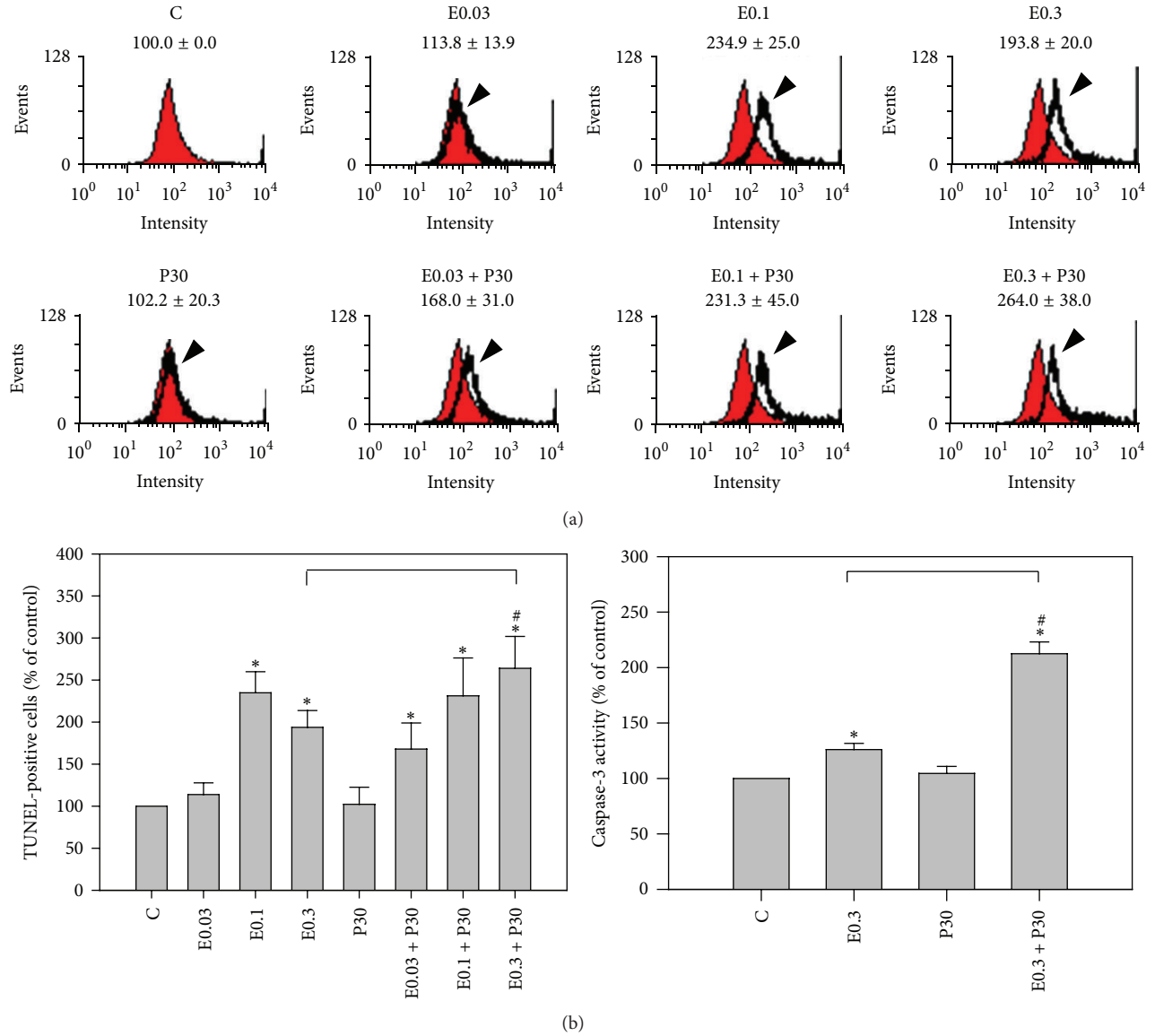

Figure 2: Apoptosis induction by epirubicin without or with progesterone addition. HA22T/VGH cells were treated with indicated concentrations of epirubicin without or with 30 μM progesterone for 24 h and evaluated by (a) TUNEL staining or (b) caspase-3 activity. Results are expressed as the mean ± standard deviation (S.D.) for three separate experiments. C: untreated cells, E0.03: 0.03 μM epirubicin, E0.1: 0.1 μM epirubicin, E0.3: 0.3 μM epirubicin, and P30: 30 μM progesterone. $^{*}P < 0.05$ compared to the untreated controls. $^{\#}P < 0.05$ compared to the corresponding epirubicin-treated group.

orange staining, and analyzed by flow cytometry. Figure 4 shows both epirubicin and progesterone increased autophagy compared to controls by AVOs analysis, though epirubicin was more effective than progesterone. Surprisingly, coaddition of progesterone significantly reduced the epirubicin-induced increase of autophagy. To further explore the expression of autophagy-related proteins, HA22T/VGH cells were treated for 24 h with 0.3 μM epirubicin in the presence or absence of 30 μM progesterone and then subjected to Western blotting. As shown in Figure 5, neither epirubicin nor progesterone had an effect on Beclin-1 levels, but the combination of the two significantly reduced Beclin-1 levels. The expressions of proteins of Beclin-1 of HA22T/VGH cells treated with 0.3 μM epirubicin, 30 μM progesterone, or combination therapy for 24 h were 119.9 ± 19.5%, 113.6 ± 1.4%, and 77.4 ± 2.6%, respectively, compared with those of controls. Figure 5 also shows progesterone had no effect on LC3-I levels, whereas epirubicin markedly reduced LC3-I levels, indicating that it may convert LC3-I to LC3-II. Interestingly, coaddition of progesterone to epirubicin treatment significantly reversed LC3-I levels. The expressions of proteins of LC3-I of HA22T/VGH cells treated with 0.3 μM epirubicin, 30 μM progesterone, or combination therapy for 24h were 21.5 ± 16.2%, 76.6 ± 17.3%, and 99.8 ± 25.6%, respectively, compared with those of controls. This is compatible with the results of AVOs formation shown in Figure 4.

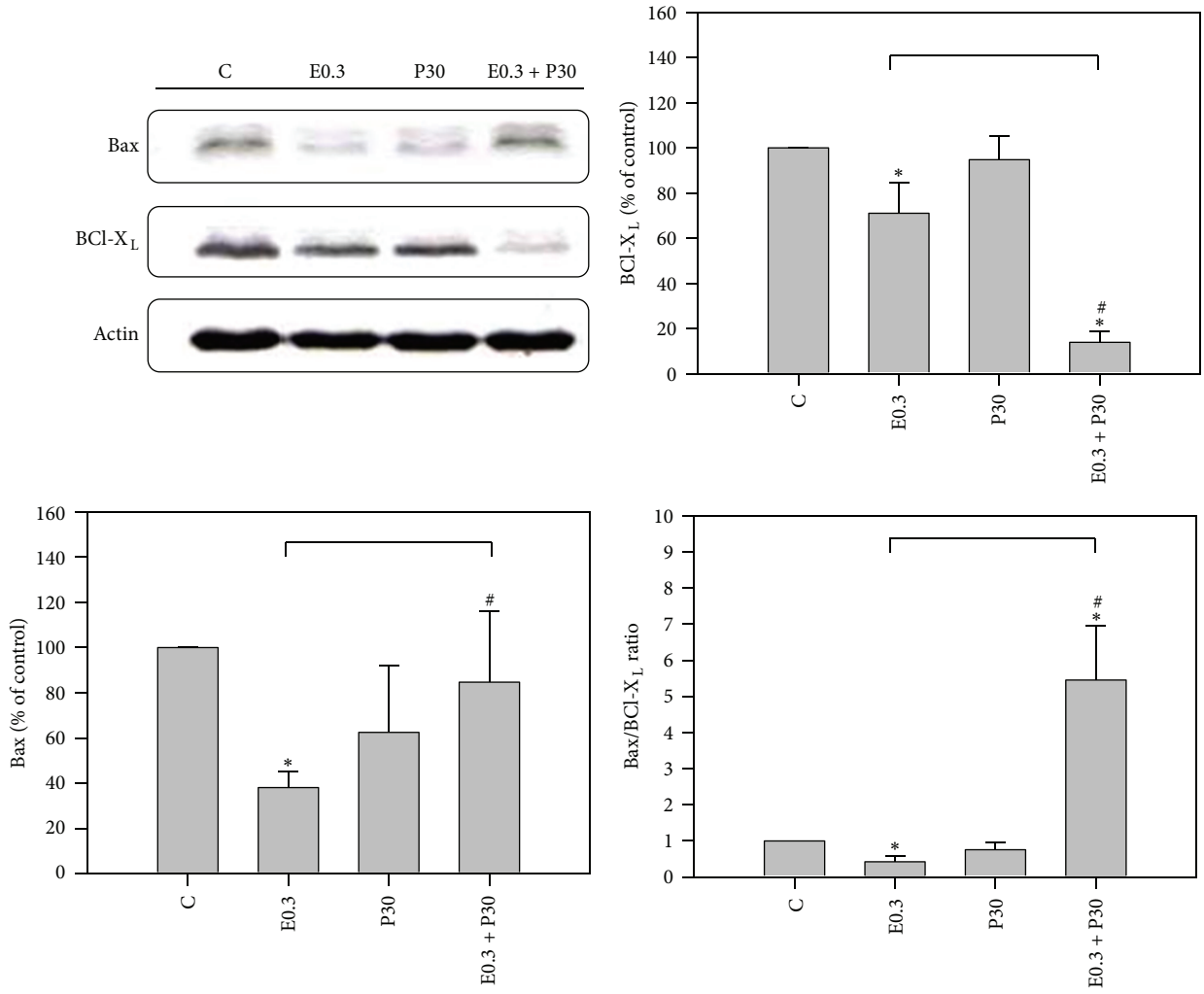

Figure 3: Western blotting shows Bax and Bcl-X_L expressions of HA22T/VGH cells after epirubicin and/or progesterone treatment for 24 h. Results are expressed as the mean ± standard deviation (S.D.) for three separate experiments. C: untreated cells, E0.3: 0.3 μM epirubicin, and P30: 30 μM progesterone. $^{*}P < 0.05$ compared to the untreated controls. $^{\#}P < 0.05$ compared to epirubicin-treated group.

Many studies have indicated that autophagy can serve as a survival mechanism for cancer cells and suggested that autophagy inhibitor might enhance the antitumor effects of chemotherapy or target therapy agents *in vivo* [30, 31]. In addition, Shen et al. reported inhibition of autophagy could enhance proapoptotic effects of ZD6474 in glioblastoma cells [31]. Greene et al. also reported inhibition of late-stage autophagy synergistically enhanced pyrrolo-1, 5-benzoxazepine-6-induced apoptotic cell death in human colon cancer cells [32]. In this study, progesterone was found to be able to reduce epirubicin-induced autophagy in HA22T/VGH cells. There are some interactions between autophagy and apoptosis mediated by Beclin-1 and Bcl-X_L proteins [32–34]. Beclin-1 is an autophagy-related protein, while Bcl-X_L is an anti-apoptosis-related protein. However, Bcl-X_L and Bcl-2 have been reported to be negative regulators of Beclin-1 [33–35]. Bcl-X_L can inhibit Beclin-1 activity by stabilizing Beclin-1 homodimerization [34]. Akar et al. reported that doxorubicin induced autophagy through the upregulation of Beclin-1, which was further enhanced by siRNA-mediated Bcl-2 silencing MCF-7 cells [36]. The expressions of Beclin-1 and AVOs were compatible in Figures 4 and 5, indicating that 30 μM progesterone could decrease the expression of AVOs in HA22T/VGH cells treated with 0.3 μM epirubicin and these effects may be induced by suppression of expression of Beclin-1. In contrast, the present study found that after progesterone was added, the expressions of Bcl-X_L and Beclin-1 both were reduced. Our results proved that progesterone in combination with epirubicin could increase the epirubicin-induced apoptosis and decrease epirubicin-induced autophagy in HA22T/VGH cells. Therefore, the decreased expression of Beclin-1 could not be explained by the interactions between Beclin-1 and Bcl-X_L described above.

Thus, Figure 4 displays progesterone increased autophagy compared to controls maybe due to the fact that 30 μM progesterone does not augment the expression of Bcl-X_L shown in Figure 3. It has been demonstrated that

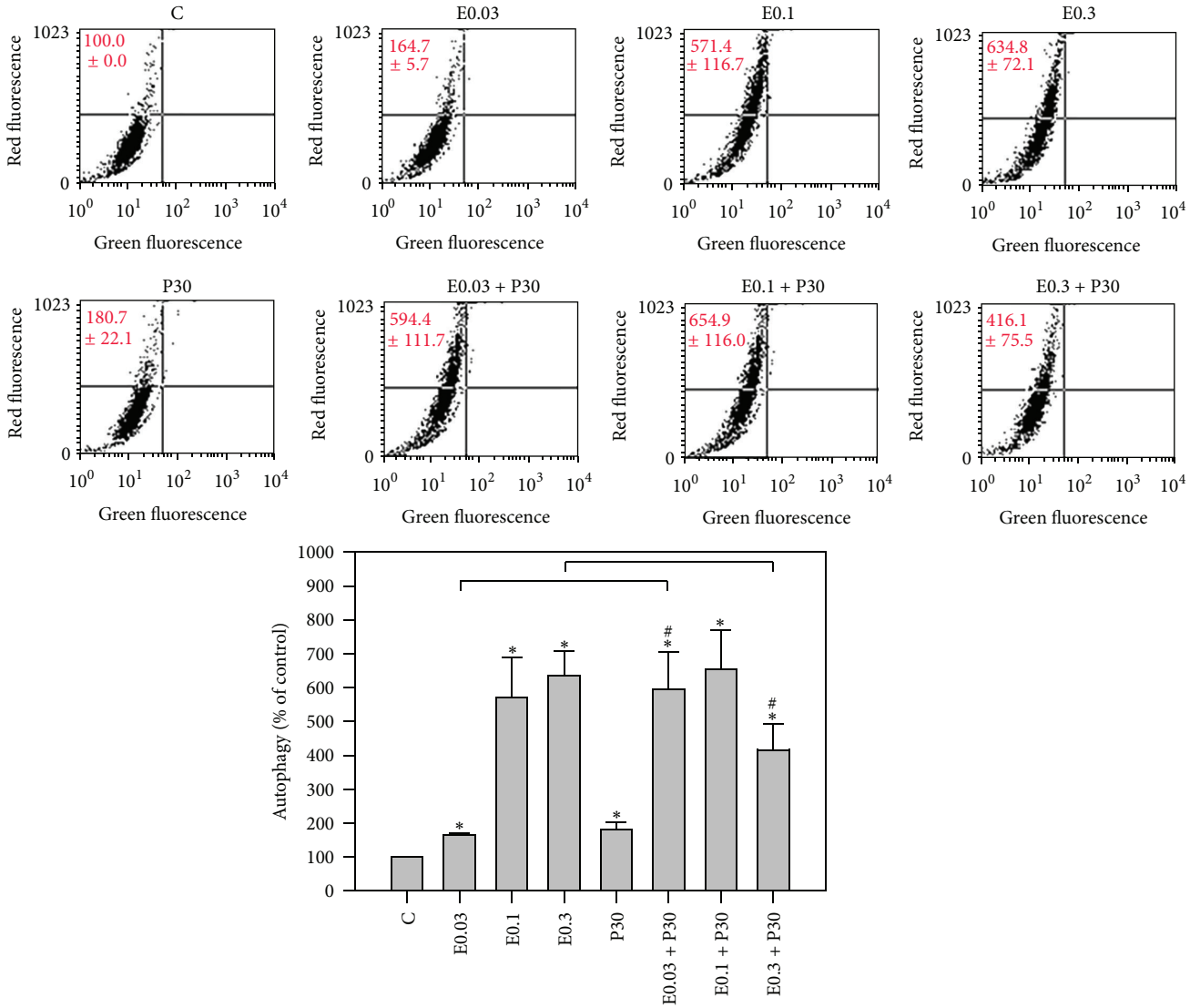

FIGURE 4: Epirubicin and/or progesterone effect on autophagy induction. HA22T/VGH cells were treated with epirubicin and/or progesterone for 24 h then stained with acridine orange and followed by flow cytometric analysis of autophagy. Results are expressed as the mean ± standard deviation (S.D.) for three separate experiments. C: untreated cells, E0.03: 0.03 μM epirubicin, E0.1: 0.1 μM epirubicin, E0.3: 0.3 μM epirubicin, and P30: 30 μM progesterone. $^{*}P < 0.05$ compared to the untreated controls. $^{\#}P < 0.05$ compared to epirubicin-treated group.

the Toll-like receptor 4 (TLR4)—myeloid differentiation factor 88 (MyD88) pathway can mediate lipopolysaccharide (LPS)—induced autophagy by reducing the binding of Beclin-1 and Bcl-2 and thus triggers autophagy activation in human and murine macrophages [37, 38]. Su et al. reported progesterone inhibited TLR4-mediated innate immune response in murine macrophages [39]. Hepatocytes also express TLR4 receptors and are responsive to LPS [38, 40]. Our preliminary study also shows combination of progesterone and epirubicin can decrease epirubicin-induced expression of TLR4 and MyD88 and sequent production of interlukin-6 in HA22T/VGH cells (unpublished data). Thus, coaddition of progesterone significantly reduced the epirubicin-induced autophagy in HA22T/VGH cells which may be caused by inhibition of TLR4-MyD88 pathway by progesterone. However, further studies on the potential role of TLR4 and MyD88 pathway in HA22T/VGH cells are necessary.

The microtubule-associated protein 1-light chain-3 (LC3) is an ubiquitin-like molecule which is a mammalian homologue of the autophagy-related Atg8 encoded product in yeast [41]. During the fusion of autophagosomal membranes, cytosolic LC3 (LC3-I) is conjugated to phosphatidylethanolamine (PE) through two consecutive ubiquitylation-like reactions catalyzed by the E1-like enzyme (Atg7) and E2-like enzyme (Atg3) to form the LC3-phospholipid conjugate (LC3-II) [42, 43]. During the fusion of autophagosomes with lysosomes, intra-autophagosomal LC3-II is also degraded by lysosomal proteases [41, 43]. In this study, we found epirubicin alone enhanced

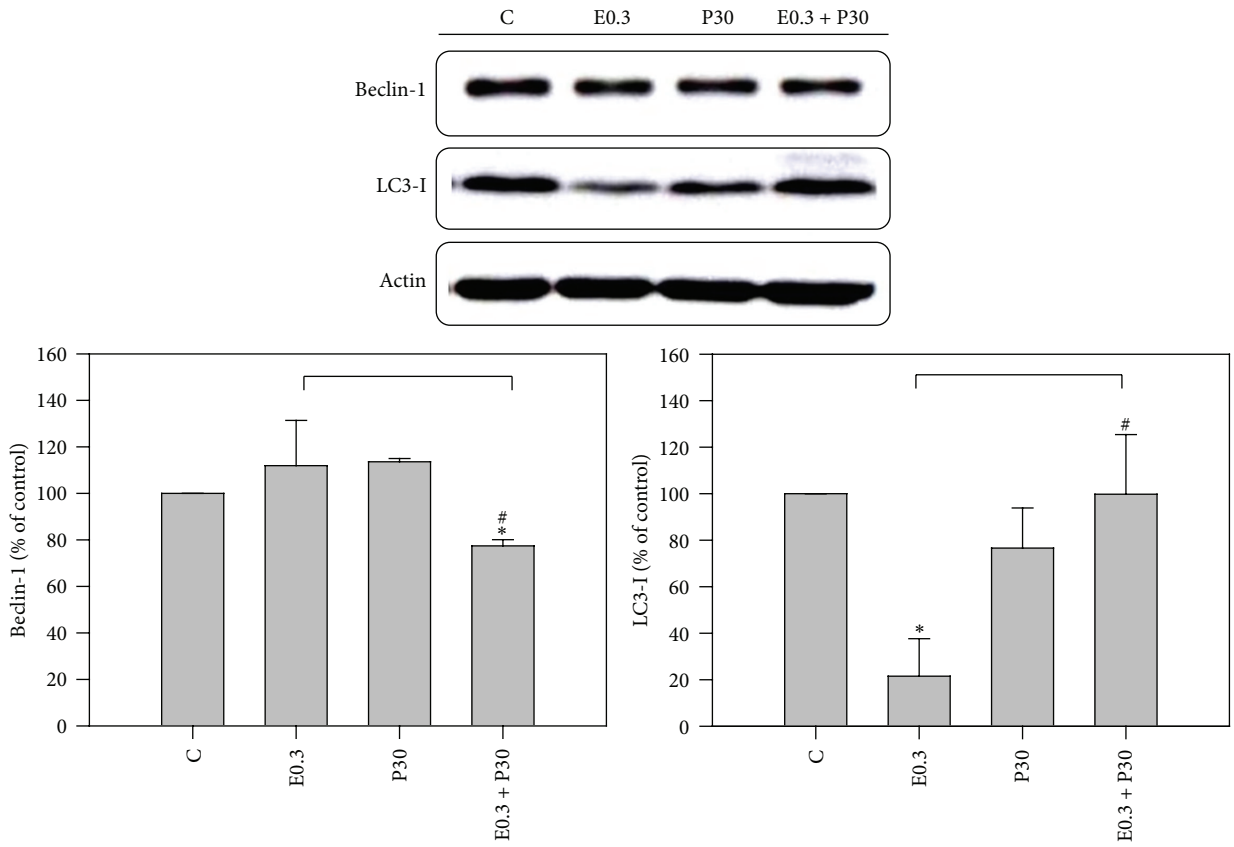

Figure 5: Western blotting shows Beclin-1 and LC3-I expressions in HA22T/VGH cells after epirubicin and/or progesterone treatment for 24 h. Results are expressed as the mean ± standard deviation (S.D.) for three separate experiments. C: untreated cells, E0.3: 0.3 μM epirubicin, and P30: 30 μM progesterone. $^{*}P < 0.05$ compared to the untreated controls. $^{\#}P < 0.05$ compared to epirubicin-treated group.

the formation of AVOs but decreased the expression of LC3-I, whereas coaddition of progesterone decreased the formation of AVOs and reversed the expression of LC3-I. These results indicate that epirubicin may promote the turnover of LC3-I to LC3-II, a possibility that is compatible with epirubicin-induced formation of AVOs during the same incubation period (24 h). And addition of progesterone to epirubicin to treat HA22T/VGH cells significantly decreased epirubicin-induced autophagy.

3.4. Decrease of Multidrug Resistance-Related Protein 1 (MRP-1) mRNA Expression by Combination. We examined the MRP-1 mRNA expression in 0.3 μM epirubicin and/or 30 μM progesterone treated HA22T/VGH cells for 6, 12, or 24 h by RT-PCR analysis. As Figure 6 shows, there was no significant difference in MRP-1 mRNA expression by epirubicin and/or progesterone treatment for 6 h or 12 h, whereas cotreatment of epirubicin and progesterone produced lower MRP-1 mRNA expression after 24 h treatment, suggesting that the combination might lessen drug resistance in HA22T/VGH cells. The expressions of MRP-1 mRNA HA22T/VGH cells treated with 0.3 μM epirubicin, 30 μM progesterone, or combination therapy for 24 h were 120.1 ± 19.0%, 109.6 ± 21.0%, and 69.0 ± 12.0%, respectively, compared with those of controls. There are many studies indicating that chemotherapy can evoke drug resistance and that this resistance may be related to the expression of multidrug resistance-related protein gene, MRP-1 [44, 45]. Expression of multidrug resistance protein 1 (MRP-1) has been commonly observed in liver tissue and HCC cell lines treated with doxorubicin [46, 47]. It also has been reported that enhanced autophagy can induce drug-resistance in epirubicin-treated breast cancer cells [16] and increase of autophagy can induce production of MRP-1 [48]. This study found that the addition of progesterone to epirubicin-treated HA22T/VGH cells significantly decreased the expression of multidrug resistance-related protein 1 (MRP-1) gene, a decrease that might be related to the reduction of autophagy. Because the mechanisms underlying this possibility are not fully clarified in this study, more *in vitro* and *in vivo* studies are required.

4. Conclusions

Epirubicin is an anthracycline drug that can induce intracellular ROS [8, 9]. This study showed that epirubicin treatment inhibited the growth of HA22T/VGH cells in a dose-dependent manner. The addition of 30 μM progesterone, which was inactive by itself, augmented epirubicin's inhibition of growth of cancer cells. Cotreatment with progesterone resulted in enhancement of the epirubicin-induced apoptosis,

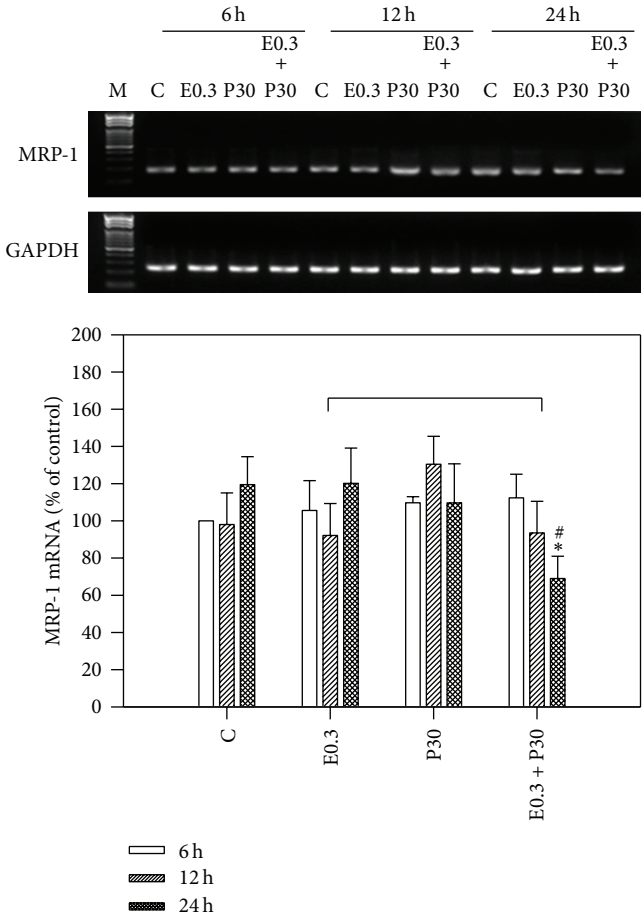

Figure 6: Epirubicin and/or progesterone effect on MRP-1 expression. HA22T/VGH cells were treated with epirubicin and/or progesterone for 6, 12, or 24 h, and then MRP-1 mRNA was analyzed by RT-PCR. The MRP-1 mRNA expression was normalized to GAPDH mRNA. The density of band was expressed as the relative density compared to that in untreated cells (control), taken as 100%. Results are expressed as the mean ± standard deviation (S.D.) for three separate experiments. C: untreated cells, E0.3: 0.3 μM epirubicin, and P30: 30 μM progesterone. $^{*}P < 0.05$ compared to the untreated controls. $^{\#}P < 0.05$ compared to epirubicin-treated group.

as evidenced by greater increase in caspase-3 activity and in the ratio of the apoptosis-regulating protein, Bax/Bcl-X_L. The cotreatment also caused a decrease in autophagy, but decreased Beclin-1 and reversed LC3-I expressions. Furthermore, this combination reduced mRNA expression of the multidrug resistance-related protein 1 (MRP-1) gene.

However, clinical results of systemic single-epirubicin chemotherapy for palliative treatment of advanced HCC or prevention of postoperative recurrence in HCC have not been suggested [3, 6, 11, 12]. However, local embolization of unresectable or advanced HCC with epirubicin or doxorubicin through hepatic artery (TACE) has been suggested as a palliative treatment in west and east countries [3, 4]. Therefore, the present study shows the coadministration of epirubicin and progesterone might be a feasible and rational choice of therapy for clinical HCC treatment and this combination is worth further evaluation. However, more *in vitro* and *in vivo* studies are required.

Abbreviations

HCC: Hepatocellular carcinoma
AVOs: Acidic vesicular organelles
FADD: Fas-associated death domain
MRP-1: Multidrug resistance-related protein 1
ROS: Reactive oxygen species
LC-3: Light chain-3
TLR-4: Toll-like receptor 4
MyD88: Myeloid differentiation factor 88.

Conflict of Interests

The authors declare that there is no conflict of interests regarding the publication of this paper.

Authors' Contribution

Wen-Tsan Chang contributed to conception and design, analysis and interpretation, data collection, and writing of the paper. Hsiao-Ling Cheng and Bau-Shan Hsieh contributed to analysis and interpretation and data collection. Chien-Chih Chiu contributed to analysis and interpretation of data and critical revision of the paper. King-Teh Lee and Kee-Lung Chang contributed to conception and design, analysis and interpretation, critical revision of the paper, and obtaining funding.

Acknowledgments

This work was supported by National Science Council of Taiwan Grants NSC98-2314-B-037-028-MY1 and NSC98-2314-B-037-028-MY2, the Kaohsiung Medical University Grant KMU-Q101025, and the Kaohsiung Medical University Hospital Grant KMUH-96-6R33.

References

[1] H. B. El-Serag, "Hepatocellular carcinoma," *New England Journal of Medicine*, vol. 365, no. 12, pp. 1118–1127, 2011.

[2] J. Ferlay, H. R. Shin, F. Bray, D. Forman, C. Mathers, and D. M. Parkin, "Estimates of worldwide burden of cancer in 2008: GLOBOCAN 2008," *International Journal of Cancer*, vol. 127, no. 12, pp. 2893–2917, 2010.

[3] J. Bruix and M. Sherman, "American Association for the Study of Liver Diseases. Management of hepatocellular carcinoma: an update," *Hepatology*, vol. 53, no. 3, pp. 1020–1022, 2011.

[4] M. Omata, L. A. Lesmana, R. Tateishi et al., "Asian pacific association for the study of the liver consensus recommendations on hepatocellular carcinoma," *Hepatology International*, vol. 4, no. 2, pp. 439–474, 2010.

[5] W. T. Chang, W. Y. Kao, G. Y. Chau et al., "Hepatic resection can provide long-term survival of patients with non-early-stage hepatocellular carcinoma: extending the indication for resection?" *Surgery*, vol. 152, no. 5, pp. 809–820, 2012.

[6] S. J. Kim, H. Y. Seo, J. G. Choi et al., "Phase II study with a combination of epirubicin, cisplatin, UFT, and leucovorin in advanced hepatocellular carcinoma," *Cancer Chemotherapy and Pharmacology*, vol. 57, no. 4, pp. 436–442, 2006.

[7] T. J. Green, P. J. Rochon, S. Chang et al., "Downstaging disease in patients with hepatocellular carcinoma outside of milan criteria: strategies using drug-eluting bead chemoembolization," *Journal of Vascular and Interventional Radiology*, vol. 24, no. 11, pp. 1613–1622, 2013.

[8] M. Kebieche, Z. Lakroun, M. Lahouel, J. Bouayed, Z. Meraihi, and R. Soulimani, "Evaluation of epirubicin-induced acute oxidative stress toxicity in rat liver cells and mitochondria, and the prevention of toxicity through quercetin administration," *Experimental and Toxicologic Pathology*, vol. 61, no. 2, pp. 161–167, 2009.

[9] E. Salvatorelli, S. Guarnieri, P. Menna et al., "Defective one- or two-electron reduction of the anticancer anthracycline epirubicin in human heart: relative importance of vesicular sequestration and impaired efficiency of electron addition," *Journal of Biological Chemistry*, vol. 281, no. 16, pp. 10990–11001, 2006.

[10] A. Ozkan and K. Fişkin, "Epirubicin HCl toxicity in human liver-derived hepatoma G2 cells," *Polish Journal of Pharmacology*, vol. 56, no. 4, pp. 435–444, 2004.

[11] A. X. Zhu, C. S. Fuchs, J. W. Clark et al., "A phase II study of epirubicin and thalidomide in unresectable or metastatic hepatocellular carcinoma," *Oncologist*, vol. 10, no. 6, pp. 392–398, 2005.

[12] W. Yeo, T. S. Mok, B. Zee et al., "A randomized phase III study of doxorubicin versus cisplatin/interferon α-2b/doxorubicin/fluorouracil (PIAF) combination chemotherapy for unresectable hepatocellular carcinoma," *Journal of the National Cancer Institute*, vol. 97, no. 20, pp. 1532–1538, 2005.

[13] C. Duvoux, T. Kiuchi, B. Pestalozzi, R. Busuttil, and R. Miksad, "What is the role of adjuvant therapy after liver transplantation for hepatocellular carcinoma?" *Liver Transplantation*, vol. 17, supplement 2, pp. S147–S158, 2011.

[14] J. H. Ahn and M. Lee, "Autophagy-dependent survival of mutant B-Raf melanoma cells selected for resistance to apoptosis induced by inhibitors against oncogenic B-Raf," *Biomolecules & Therapeutics*, vol. 21, no. 2, pp. 114–120, 2013.

[15] Z. Yang and D. J. Klionsky, "Mammalian autophagy: core molecular machinery and signaling regulation," *Current Opinion in Cell Biology*, vol. 22, no. 2, pp. 124–131, 2010.

[16] W. L. Sun, J. Chen, Y. P. Wang, and H. Zheng, "Autophagy protects breast cancer cells from epirubicin-induced apoptosis and facilitates epirubicin-resistance development," *Autophagy*, vol. 7, no. 9, pp. 1035–1044, 2011.

[17] J. Lewin, A. Cooper, and B. Birch, "Progesterone: a novel adjunct to intravesical chemotherapy," *BJU International*, vol. 90, no. 7, pp. 736–741, 2002.

[18] E. Villa, I. Ferretti, A. Grottola et al., "Hormonal therapy with megestrol in inoperable hepatocellular carcinoma characterized by variant oestrogen receptors," *British Journal of Cancer*, vol. 84, no. 7, pp. 881–885, 2001.

[19] A. Giacomin, A. Sergio, V. Vanin et al., "Megestrol and embryonic extracts in the treatment of advanced hepatocellular carcinoma: a prospective randomized trial in the pre-sorafenib era," *Hepatology Research*, vol. 40, no. 2, pp. 153–160, 2010.

[20] B. S. Hsieh, L. W. Huang, S. J. Su et al., "Combined arginine and ascorbic acid treatment induces apoptosis in the hepatoma cell line HA22T/VGH and changes in redox status involving the pentose phosphate pathway and reactive oxygen and nitrogen species," *Journal of Nutritional Biochemistry*, vol. 22, no. 3, pp. 234–241, 2011.

[21] H. L. Cheng, S. J. Su, L. W. Huang et al., "Arecoline induces HA22T/VGH hepatoma cells to undergo anoikis—involvement of STAT3 and RhoA activation," *Molecular Cancer*, vol. 9, article 126, 2010.

[22] S. Paglin, T. Hollister, T. Delohery et al., "A novel response of cancer cells to radiation involves autophagy and formation of acidic vesicles," *Cancer Research*, vol. 61, no. 2, pp. 439–444, 2001.

[23] Y. C. Hu, H. L. Cheng, B. S. Hsieh, L. W. Huang, T. C. Huang, and K. L. Chang, "Arsenic trioxide affects bone remodeling by effects on osteoblast differentiation and function," *Bone*, vol. 50, no. 6, pp. 1406–1415, 2012.

[24] H. L. Huang, L. W. Fang, S. P. Lu, C. K. Chou, T. Y. Luh, and M. Z. Lai, "DNA-damaging reagents induce apoptosis through reactive oxygen species-dependent Fas aggregation," *Oncogene*, vol. 22, no. 50, pp. 8168–8177, 2003.

[25] W. H. Liu and L. S. Chang, "Arachidonic acid induces Fas and FasL upregulation in human leukemia U937 cells via Ca^{2+}/ROS-mediated suppression of ERK/c-Fos pathway and activation of p38 MAPK/ATF-2 pathway," *Toxicology Letters*, vol. 191, no. 2-3, pp. 140–148, 2009.

[26] K. T. Ng, D. Y. Guo, Q. Cheng et al., "A garlic derivative, S-allylcysteine (SAC), suppresses proliferation and metastasis of hepatocellular carcinoma," *PLoS ONE*, vol. 7, no. 2, Article ID e31655, 2012.

[27] J. Zhao, L. Dong, B. Lu et al., "Down-regulation of osteopontin suppresses growth and metastasis of hepatocellular carcinoma via induction of apoptosis," *Gastroenterology*, vol. 135, no. 3, pp. 956–968, 2008.

[28] X. Cheng, I. Shimizu, Y. Yuan et al., "Effects of estradiol and progesterone on tumor necrosis factor alpha-induced apoptosis in human hepatoma HuH-7 cells," *Life Sciences*, vol. 79, no. 21, pp. 1988–1994, 2006.

[29] K. Zhang and P. K. H. Chow, "The effect of megestrol acetate on growth of HepG2 cells in vitro and in vivo," *Clinical Cancer Research*, vol. 10, no. 15, pp. 5226–5232, 2004.

[30] E. Donohue, A. Thomas, N. Maurer et al., "The autophagy inhibitor verteporfin moderately enhances the antitumor activity of gemcitabine in a pancreatic ductal adenocarcinoma model," *Journal of Cancer*, vol. 4, no. 7, pp. 585–596, 2013.

[31] J. Shen, H. Zheng, J. Ruan et al., "Autophagy inhibition induces enhanced proapoptotic effects of ZD6474 in glioblastoma," *British Journal of Cancer*, vol. 109, no. 1, pp. 164–171, 2013.

[32] L. M. Greene, D. P. Nolan, D. Regan-Komito, G. Campiani, D. C. Williams, and D. M. Zisterer, "Inhibition of late-stage autophagy synergistically enhances pyrrolo-1,5-benzoxazepine-6-induced apoptotic cell death in human colon cancer cells," *International Journal of Oncology*, vol. 43, no. 3, pp. 927–935, 2013.

[33] R. Kang, H. J. Zeh, M. T. Lotze, and D. Tang, "The Beclin 1 network regulates autophagy and apoptosis," *Cell Death and Differentiation*, vol. 18, no. 4, pp. 571–580, 2011.

[34] D. Lama and R. Sankararamakrishnan, "Molecular dynamics simulations of pro-apoptotic BH3 peptide helices in aqueous medium: relationship between helix stability and their binding affinities to the anti-apoptotic protein Bcl-X_L," *Journal of Computer-Aided Molecular Design*, vol. 25, no. 5, pp. 413–426, 2011.

[35] L. L. Fu, Y. Cheng, and B. Liu, "Beclin-1: autophagic regulator and therapeutic target in cancer," *The International Journal of Biochemistry & Cell Biology*, vol. 45, no. 5, pp. 921–924, 2013.

[36] U. Akar, A. Chaves-Reyez, M. Barria et al., "Silencing of Bcl-2 expression by small interfering RNA induces autophagic cell death in MCF-7 breast cancer cells," *Autophagy*, vol. 4, no. 5, pp. 669–679, 2008.

[37] C. S. Shi and J. H. Kehrl, "MyD88 and Trif target Beclin 1 to trigger autophagy in macrophages," *Journal of Biological Chemistry*, vol. 283, no. 48, pp. 33175–33182, 2008.

[38] A. Mencin, J. Kluwe, and R. F. Schwabe, "Toll-like receptors as targets in chronic liver diseases," *Gut*, vol. 58, no. 5, pp. 704–720, 2009.

[39] L. Su, Y. Sun, F. Ma, P. Lü, H. Huang, and J. Zhou, "Progesterone inhibits Toll-like receptor 4-mediated innate immune response in macrophages by suppressing NF-κB activation and enhancing SOCS1 expression," *Immunology Letters*, vol. 125, no. 2, pp. 151–155, 2009.

[40] M. J. Scott and T. R. Billiar, "β2-integrin-induced p38 MAPK activation is a key mediator in the CD14/TLR4/MD2-dependent uptake of lipopolysaccharide by hepatocytes," *Journal of Biological Chemistry*, vol. 283, no. 43, pp. 29433–29446, 2008.

[41] S. Barth, D. Glick, and K. F. Macleod, "Autophagy: assays and artifacts," *Journal of Pathology*, vol. 221, no. 2, pp. 117–124, 2010.

[42] I. Tanida, M. Yamasaki, M. Komatsu, and T. Ueno, "The FAP motif within human ATG7, an autophagy-related E1-like enzyme, is essential for the E2-substrate reaction of LC3 lipidation," *Autophagy*, vol. 8, no. 1, pp. 88–97, 2012.

[43] S. E. Kaiser, K. Mao, A. M. Taherbhoy et al., "Noncanonical E2 recruitment by the autophagy E1 revealed by Atg7-Atg3 and Atg7-Atg10 structures," *Nature Structural & Molecular Biology*, vol. 19, no. 12, pp. 1242–1249, 2012.

[44] Y. L. Lo, Y. Liu, and J. C. Tsai, "Overcoming multidrug resistance using liposomal epirubicin and antisense oligonucleotides targeting pump and nonpump resistances in vitro and in vivo," *Biomedicine & Pharmacotherapy*, vol. 67, no. 4, pp. 261–267, 2013.

[45] V. H. Villar, O. Vogler, J. Martinez-Serra et al., "Nilotinib counteracts P-glycoprotein-mediated multidrug resistance and synergizes the antitumoral effect of doxorubicin in soft tissue sarcomas," *PLoS ONE*, vol. 7, no. 5, Article ID e37735, 2012.

[46] F. Wu, Z. Y. Shao, B. J. Zhai, C. L. Zhao, and D. M. Shen, "Ultrasound reverses multidrug resistance in human cancer cells by altering gene expression of ABC transporter proteins and bax protein," *Ultrasound in Medicine and Biology*, vol. 37, no. 1, pp. 151–159, 2011.

[47] E. M. Leslie, R. G. Deeley, and S. P. C. Cole, "Multidrug resistance proteins: role of P-glycoprotein, MRP1, MRP2, and BCRP (ABCG2) in tissue defense," *Toxicology and Applied Pharmacology*, vol. 204, no. 3, pp. 216–237, 2005.

[48] S. C. Lim, K. S. Hahm, S. H. Lee, and S. H. Oh, "Autophagy involvement in cadmium resistance through induction of multidrug resistance-associated protein and counterbalance of endoplasmic reticulum stress WI38 lung epithelial fibroblast cells," *Toxicology*, vol. 276, no. 1, pp. 18–26, 2010.

Hindawi Publishing Corporation
The Scientific World Journal
Volume 2014, Article ID 568145, 5 pages
http://dx.doi.org/10.1155/2014/568145

Clinical Study

Interval between Intra-Arterial Infusion Chemotherapy and Surgery for Locally Advanced Oral Squamous Cell Carcinoma: Impacts on Effectiveness of Chemotherapy and on Overall Survival

Chih-Fung Wu,[1] Chien-Hsing Lee,[2] Edward Hsi,[3] Chung-Ho Chen,[4,5] and Jen-Yang Tang[4,6,7,8]

[1] *Department of Surgery, Faculty of Medicine, College of Medicine, Kaohsiung Medical University Hospital, Kaohsiung 807, Taiwan*
[2] *Department of Nursing, Min-Hwei Junior College of Health Care Management, Tainan 736, Taiwan*
[3] *Department of Medical Research, Kaohsiung Medical University Hospital, Kaohsiung 807, Taiwan*
[4] *Cancer Center, Kaohsiung Medical University Hospital, Kaohsiung 807, Taiwan*
[5] *Department of Oral Maxillofacial Surgery, Kaohsiung Medical University Hospital, Kaohsiung 807, Taiwan*
[6] *Department of Radiation Oncology, Faculty of Medicine, College of Medicine, Kaohsiung Medical University, Kaohsiung 807, Taiwan*
[7] *Department of Radiation Oncology, Kaohsiung Medical University Hospital, Kaohsiung 807, Taiwan*
[8] *Department of Radiation Oncology, Kaohsiung Municipal Ta-Tung Hospital, Kaohsiung 801, Taiwan*

Correspondence should be addressed to Jen-Yang Tang; reyata@kmu.edu.tw

Received 20 March 2014; Accepted 30 April 2014; Published 18 May 2014

Academic Editor: Hsueh-Wei Chang

Background. The interval between intra-arterial infusion chemotherapy (IAIC) and surgery was investigated in terms of its effects on survival in patients with locally advanced oral squamous cell carcinoma (OSCC). *Methods.* This retrospective study analyzed 126 patients who had completed treatment modalities for stage IV OSCC. All patients were followed up for 3 years. Kaplan-Meier and Cox regression methods were used to determine how survival was affected by general factors, primary tumor volume, TNM stage, and duration of neoadjuvant chemotherapy. *Results.* In 126 patients treated for locally advanced OSCC by preoperative induction IAIC using methotrexate, multivariate analysis of relevant prognostic factors showed that an IAIC duration longer than 90 days was significantly associated with poor prognosis (hazard ratio, 1.77; $P = 0.0259$). *Conclusions.* Duration of IAIC is a critical factor in the effectiveness of multimodal treatment for locally advanced OSCC. Limiting the induction course to 90 days improves overall survival.

1. Introduction

Invasive oral squamous cell carcinoma (OSCC) accounts for most malignant disorders of the oral cavity. In Taiwan, oral cancer is currently the fourth most common cancer in males [1]. Although 80–90% of patients with early stage OSCC are cured, outcomes remain poor in those with advanced stage tumors [2, 3]. In OSCC stages IVA and IVB, short-induction chemotherapy achieves high primary remission rate with possible organ preservation and acceptable toxicity [4]. For controlling the progression of cancer, intravenous systemic or regional intra-arterial infusion chemotherapy (IAIC) via superselective catheterization has varying success [5–7]. Kaohsiung Medical University Hospital (KMUH) and many other centers have used IAIC for decades to treat head and neck cancers, and preoperative superselective infusion generally obtains a good response with minimal toxicity [8–13]. For patients in early stages of OSCC, the main curative modality is either surgery or radiotherapy [14]. For patients in advanced stages, however, a multidisciplinary approach is usually applied; for example, dissection of the primary tumor and selected regional lymph nodes is combined with

salvage treatments such as radiotherapy and chemotherapy, which have a high therapeutic ratio [14, 15]. For OSCC in an advanced stage but still operable, the typical treatment modality is radical ablative surgery followed by radiotherapy or radiochemotherapy, which is the same treatment applied in laryngeal and pharyngeal squamous cell carcinoma [16, 17].

However, no clinical trials have compared the beneficial effects between IAIC and surgery. At our hospital, systemic intravenous chemotherapy is not the typical neoadjuvant therapy for OSCC. The standard therapy is IAIC followed by surgical intervention and postoperative concurrent chemoradiotherapy. Therefore, this retrospective study investigated how the IAIC-surgery interval affects outcomes of treatment for locally advanced OSCC.

2. Materials

2.1. Patient Characteristics. This study retrospectively analyzed 126 consecutive patients who had received IAIC treatment for OSCC at KMUH from 2005 to 2010. Inclusion criteria included histologically confirmed primary OSCC originating from cheek mucosa, no distant metastasis at presentation, and no previous treatment of a malignancy at any oral cavity site. The analysis excluded patients who did not complete the therapeutic protocol and those who had incomplete medical records. The remaining patients who had locally advanced IVA or IVB lesions (without distant metastasis) and who met the enrollment criteria were enrolled for further analysis. Patients who had received a multidisciplinary therapeutic treatment regimen of regional chemotherapy, surgery, and irradiation were retrospectively analyzed. Institutional review board approval was obtained before beginning data collection. Due to the small number of female patients, only male patients were enrolled. The 126 enrolled patients had a median age of 50.6 years. The AJCC TNM staging system was applied retrospectively in all patients (Table 1). The mean follow-up period was 29.2 months (range 4.6–84.8 months). The date of the last follow-up was recorded as the date of the last admission, the date of the last outpatient visit, or the date of death.

2.2. Pretreatment Evaluation. The pretreatment evaluation included history, clinical examination, hematological evaluation, and primary tumor biopsy. Before beginning treatment, the extent of the spread was determined by bone scan, chest X-ray, contrast-enhanced computed tomography (CT) of the head and neck, and ultrasound scan of the abdomen. All patients were restaged according to 7th edition of the AJCC cancer-staging manual for the oral cavity.

2.3. Treatment Protocol. A totally implantable port-catheter system (Jet Port Plus Allround; PFM, Cologne, Germany) was used for continuous IAIC as described previously [11]. Briefly, the catheter tip was placed on a branch of the feeding artery proximal to the tumor. The tumorous area and the proper position of the catheter tip were confirmed by staining with patent blue V (Guerbet Co, France).

Table 1: Patients' characteristics.

Characteristics	Number of patients who completed treatment (%)	Number of all patients (%)
Number of patients	126	1,459
Median age (years)	50.6	52.5
Age range (years)	28–82	22–87
Differentiation		
I	74 (72.5)	760 (64.0)
II	26 (25.5)	394 (33.2)
III	2 (2)	33 (2.7)
T stage		
1	1 (0.8)	341 (23.4)
2	12 (9.5)	420 (28.8)
3	8 (6.3)	122 (8.4)
4	1 (0.8)	3 (0.2)
4A	104 (82.5)	563 (38.6)
4B	0 (0)	8 (0.5)
N stage		
0	21 (16.7)	633 (43.4)
1	55 (43.7)	505 (34.6)
2	49 (38.9)	308 (21.1)
3	1 (0.8)	11 (0.8)
IAIC-OP interval		
Range (months)	0.4–14	0–14.8
≥90 days	54 (42.9)	132 (45.2)
<90 days	72 (57.1)	160 (54.8)

Methotrexate 50 mg was infused intra-arterially every 24 hrs with leucovorin 6 mg given intramuscularly every 6 hrs during the course of methotrexate infusion. Methotrexate was given continuously for a mean period of 7.5 days and the regimen was changed to weekly bolus of 25 mg via intra-arterial route. The patients received IAIC for 2-3 months before surgery.

No patients had received other treatments before undergoing IAIC. Surgical resection including the primary site with neck dissection was performed 2 weeks after completion of intra-arterial chemotherapy when the mucositis had subsided. After surgical resection, OSCC risk factors identified by pathology were evaluated before performing radiotherapy.

2.4. Treatment Evaluation. Each patient was clinically evaluated in follow-up examinations performed at 1- to 3-month intervals. Disease-free survival was defined as the date of treatment to the date that evidence of recurrence was noted.

2.5. Statistical Analysis. The association between IAIC duration and treatment response was analyzed by Pearson chi-square test. Survival rates were calculated by Kaplan-Meier method and compared by Cochran-Mantel-Haenszel test. Overall survival (OS) was calculated from the time of initial diagnosis to the time of death of any cause. Patients who had survived or who were disease-free at the end of the follow-up

Table 2: Tumor distribution in the oral cavity.

Tumor site	*N* (%)
Buccal mucosa	68 (54)
Gum	27 (21.4)
Tongue	20 (15.9)
Other	11 (8.7)
Total	126 (100)

were censored. Potential confounding factors were adjusted and analyzed by Cox proportional hazard regression analysis. The statistical analysis was performed with JMP version 9. All statistical tests were performed at a 0.05 significance level. Estimated results were reported with the hazard ratio (HR) and 95% confidence interval (CI).

3. Results

3.1. Characteristics of Prognostic Factors. In this retrospective review of Taiwan population of consecutive patients who had received IAIC for OSCC, the inclusion criteria were the following: histologically confirmed primary OSCC originating from cheek mucosa, no distant metastasis at presentation, and no history of treatment for a malignancy at an oral cavity site. Patients were excluded if they did not complete the therapeutic protocol or if their medical records did not contain the data required for the analysis in this study. After the exclusions, 126 patients who had locally advanced lesions in OSCC stages IVA or IVB (without distant metastasis) and who met all enrollment requirements were enrolled for further analysis (Table 1). The sites of locally advanced OSCC in the enrolled patients included the tongue (15.9%), gums (21.4%), buccal mucosa (54%), and other (8.7%) (Table 2).

3.2. Contribution of Prognostic Characteristics to Mortality in Locally Advanced Buccal Cancer. Since the review of medical records for the enrolled patients revealed varying durations of IAIC, this study determined the optimal duration of IAIC in terms of overall survival. A receiver operating characteristic (ROC) curve analysis of the sensitivity and specificity of various IAIC durations in predicting 3-year overall survival in the 126 patients with locally advanced OSCC indicated that the optimal duration of IAIC was 90 days. Univariate Cox regression analysis indicated that longer durations of IAIC (>90 days) (hazard ratio [HR], 1.95; 95% confidence interval [CI] 1.19–3.24; $P < 0.0085$), mucosa sites compared to gum sites (HR, 2.27; 95% CI, 1.11–5.25; $P = 0.0235$), tongue sites compared to gum sites (HR, 2.50; 95% CI, 1.01–6.47; $P = 0.0477$), and other sites comparing to gum sites (HR, 2.93; 95% CI, 1.07–7.96; $P = 0.0360$) were each associated with OS in patients with OSCC (Table 3).

Age and differentiation were not significantly associated with survival. Multivariate analysis was used to assess the effect of long duration of IAIC (>90 days) on OS, independently of other factors. The results showed that >90 days IAIC retained a statistically significant association with OS (HR, 1.77; 95% CI, 1.07–2.97; $P = 0.0259$). According to the multivariate analysis, mucosa comparing to gum was the only other significant risk factor with regard to OS (HR, 2.08; 95% CI, 1.02–4.84; $P = 0.0451$). Kaplan-Meier survival curves showed that prolonged (>90 days) neoadjuvant chemotherapy (Figure 1) was associated with poor survival (Log-Rank $P = 0.0077$).

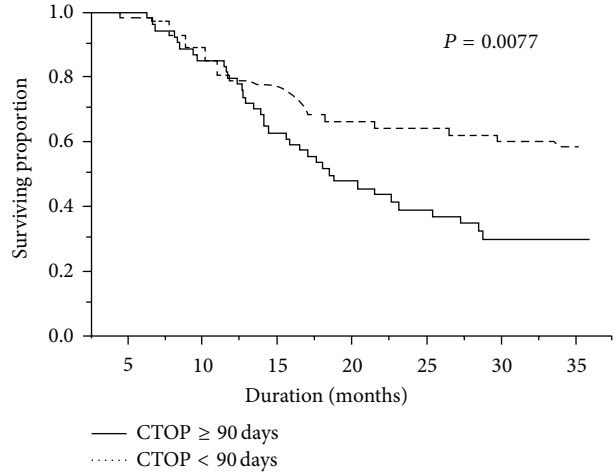

Figure 1: Interval between intra-arterial infusion chemotherapy (IAIC) and surgical resection: effect on overall survival. Kaplan-Meier plots of overall survival in patients with locally advanced oral squamous cell carcinoma: IAIC-surgery intervals ≥90 days versus IAIC-surgery intervals <90 days. CTOP: duration of induction chemotherapy before surgical resection.

4. Discussion

After excluding patients with early stage OSCC, female patients, and patients with incomplete medical records, the final analysis included 126 patients registered at KMU Hospital for treatment of locally advanced OSCC. Multivariate analysis of relevant prognostic factors showed that a long duration of IAIC was significantly associated with a poor prognosis. The maximum benefit of IAIC was observed when IAIC was limited to 90 days. To the best of our knowledge, this study is the first to report survival rates and prognostic factors in patients who have received induction IAIC for locally advanced OSCC.

The use of IAIC to treat locally advanced cancers began in the 1980s [13]. Since then, it has been widely used as a palliative modality to treat various conditions, particularly head and neck cancer. Compared to intravenous systemic chemotherapy, the theoretical advantage of IAIC is its capability to deliver higher drug concentrations to the tumor site but with lower systemic toxicity [18]. However, no guidelines have been established for selecting the optimal duration of induction chemotherapy before surgical resection (CTOP) for locally advanced OSCC, and no guidelines are available for predicting how the duration of induction chemotherapy affects the oncologic outcome. Our study showed that the duration of IAIC correlated with overall survival, and the ROC assay showed that patients who had received 90 days

Table 3: Univariate and multivariate analysis of prognostic factors in locally advanced OSCC receiving neoadjuvant IAIC.

	Survival					
	Univariate			Multivariate		
	HR	95% CI	*P* value	HR	95% CI	*P* value
Age	0.98	0.95–1.00	0.0890			
Differentiation						
I	1.00					
II + III	1.78	0.97–3.14	0.0616			
Sites						
Gum	1.00			1.00		
Mucosa	2.27	1.11–5.25	0.0235	2.08	1.02–4.84	0.0451
Tongue	2.50	1.01–6.47	0.0477	2.24	0.90–5.83	0.0826
Others	2.93	1.07–7.96	0.0360	2.41	0.88–6.66	0.0865
IAIC-OP interval ≥90	1.95	1.19–3.24	0.0085	1.77	1.07–2.97	0.0259

of IAIC presented with the best survival. However, Kaplan-Meier survival analysis showed that hazard ratios varied in a time-dependent fashion (Figure 1). The IAIC revealed a protective effect in the early stage of a multiple treatment modality and apparently improved survival (Figure 1, dotted line). However, treatment outcomes worsened as the duration of chemotherapy increased and as the delay in surgical intervention increased. The probable explanation is that prolonged IAIC causes selective killing of certain strains of malignant cells and causes fibrosis of locoregional tissue. Indicators of a poor outcome of subsequent salvage treatment, radiotherapy, or adjuvant chemotherapy include the presence of a radiotherapy-resistant strain and a hypoxic environment.

The Cox regression assay of age, differentiation, and CTOP duration revealed one statistically significant factor. The Cox regression results were consistent with the hypothesis based on chi-square analysis. Despite recent advances in aggressive combined treatment regimens, for example, radical surgery, chemoradiation, neoadjuvant chemotherapy, and target therapy, the long-term survival of OSCC patients has not substantially improved and responses to different treatment modalities are still difficult to predict. However, high morbidity and mortality rates are expected in patients who present with an advanced stage of the disease, low Karnofsky status, or bad habits [19]. Despite advances in the diagnosis and therapeutic treatment of OSCC, the prognosis for advanced stages of the disease remains poor.

5. Conclusion

This study revealed that when followed by appropriate surgical resection, selective lymph node dissection, and adjuvant radiotherapy, IAIC has an important contributing role in improving survival of OSCC by reducing systemic toxicities. However, the maximal benefit of IAIC is conferred when chemotherapy is limited to 90 days. Prolonged neoadjuvant IAIC obtains adverse outcomes.

Conflict of Interests

The authors declare that they have no competing interests in the publication of this study.

Authors' Contribution

Chih-Fung Wu and Chien-Hsing Lee contributed equally to this work.

Acknowledgment

This work was supported by a Grant from the Excellence for Cancer Research Center through funding by the Department of Health, Executive Yuan, Taiwan (TAIWAN) (DOH102-TD-C-111-002).

References

[1] T. Y. Hsieh, K. P. Chang, S. S. Lee et al., "Free flap reconstruction in patients with advanced oral squamous cell carcinoma: analysis of patient survival and cancer recurrence," *Microsurgery*, vol. 32, no. 8, pp. 598–604, 2012.

[2] H. T. Eich, M. Löschcke, M. Scheer et al., "Neoadjuvant radiochemotherapy and radical resection for advanced squamous cell carcinoma of the oral cavity: outcome of 134 patients," *Strahlentherapie und Onkologie*, vol. 184, no. 1, pp. 23–29, 2008.

[3] M. Kreppel, U. Drebber, H.-T. Eich et al., "Combined-modality treatment in advanced oral squamous cell carcinoma: primary surgery followed by adjuvant concomitant radiochemotherapy," *Strahlentherapie und Onkologie*, vol. 187, no. 9, pp. 555–560, 2011.

[4] S. Semrau, F. Waldfahrer, M. Lell et al., "Feasibility, toxicity, and efficacy of short induction chemotherapy of docetaxel plus cisplatin or carboplatin (TP) followed by concurrent chemoradio—therapy for organ preservation in advanced cancer of the hypopharynx, larynx, and base of tongue: early results," *Strahlentherapie und Onkologie*, vol. 187, no. 1, pp. 15–22, 2011.

[5] M. Nakanishi, Y. Demura, Y. Umeda et al., "Multi-arterial infusion chemotherapy for non-small cell lung carcinoma—significance of detecting feeding arteries and tumor staining," *Lung Cancer*, vol. 61, no. 2, pp. 227–234, 2008.

[6] L. Andreana, G. Isgro, L. Marelli et al., "Treatment of hepatocellular carcinoma (HCC) by intra-arterial infusion of radio-emitter compounds: trans-arterial radio-embolisation of HCC," *Cancer Treatment Reviews*, vol. 38, no. 6, pp. 641–649, 2012.

[7] J.-K. Burkhardt, H. A. Riina, B. J. Shin, J. A. Moliterno, C. P. Hofstetter, and J. A. Boockvar, "Intra-arterial chemotherapy for malignant gliomas: a critical analysis," *Interventional Neuroradiology*, vol. 17, no. 3, pp. 286–295, 2011.

[8] C. R. N. Rasch, M. Hauptmann, and A. J. M. Balm, "Intra-arterial chemotherapy for head and neck cancer: is there a verdict?" *Cancer*, vol. 117, no. 4, p. 874, 2011.

[9] A. Ishii, Y. Korogi, T. Hirai et al., "Intraarterial infusion chemotherapy and conformal radiotherapy for cancer of the mouth: prediction of the histological response to therapy with magnetic resonance imaging," *Acta Radiologica*, vol. 48, no. 8, pp. 900–906, 2007.

[10] W. Kobayashi, B. G. Teh, H. Sakaki et al., "Superselective intra-arterial chemoradiotherapy with docetaxel-nedaplatin for advanced oral cancer," *Oral Oncology*, vol. 46, no. 12, pp. 860–863, 2010.

[11] C.-F. Wu, C.-M. Chen, Y.-S. Shen et al., "Effective eradication of oral verrucous carcinoma with continuous intraarterial infusion chemotherapy," *Head and Neck*, vol. 30, no. 5, pp. 611–617, 2008.

[12] C.-H. Chen, G.-T. Lin, Y.-C. Fu et al., "Comparison of deltopectoralis flap and free radial forearm flap in reconstruction after oral cancer ablation," *Oral Oncology*, vol. 41, no. 6, pp. 602–606, 2005.

[13] C.-F. Wu, C.-J. Huang, K.-P. Chang, and C.-M. Chen, "Continuous intra-arterial infusion chemotherapy as a palliative treatment for oral squamous cell carcinoma in octogenarian or older patients," *Oral Oncology*, vol. 46, no. 7, pp. 559–563, 2010.

[14] S. A. Bhide, K. L. Newbold, K. J. Harrington, and C. M. Nutting, "Clinical evaluation of intensity-modulated radiotherapy for head and neck cancers," *The British Journal of Radiology*, vol. 85, no. 1013, pp. 487–494, 2012.

[15] D. G. Pfister, K.-K. Ang, D. M. Brizel et al., "Head and neck cancers: clinical practice guidelines in oncology," *Journal of the National Comprehensive Cancer Network*, vol. 9, no. 6, pp. 596–650, 2011.

[16] J. T. Parsons, W. M. Mendenhall, S. P. Stringer, N. J. Cassisi, and R. R. Million, "An analysis of factors influencing the outcome of postoperative irradiation for squamous cell carcinoma of the oral cavity," *International Journal of Radiation Oncology, Biology, Physics*, vol. 39, no. 1, pp. 137–148, 1997.

[17] J. S. Cooper, T. F. Pajak, A. A. Forastiere et al., "Postoperative concurrent radiotherapy and chemotherapy for high-risk squamous-cell carcinoma of the head and neck," *The New England Journal of Medicine*, vol. 350, no. 19, pp. 1937–2019, 2004.

[18] C.-F. Wu, C.-M. Chen, C.-H. Chen, T.-Y. Shieh, and M.-C. Sheen, "Continuous intraarterial infusion chemotherapy for early lip cancer," *Oral Oncology*, vol. 43, no. 8, pp. 825–830, 2007.

[19] L. Olasz, E. Orsi, T. Markó, and J. Szalma, "Induction chemotherapy response and recurrence rates in correlation with N0 or N+ stage in oral squamous cell cancer (OSCC)," *Cancer and Metastasis Reviews*, vol. 29, no. 4, pp. 607–611, 2010.